THÈSE DE DOCTORAT

présentée et soutenue publiquement à

Université de Lille

École doctorale Sciences pour l'Ingénieur

Pour obtenir le grade de **DOCTEUR**

Spécialité: ***Mécanique des solides, des matériaux, des structures et des surfaces***

Par **Xiang YAN**

Design of biphasic polymeric fiber from melt-spinning charged with nanoparticles-Effects of the formulation and the fillers localization, to obtain a functionalized fiber at surface level

Conception de fibres polymères biphasiques chargées en nanoparticules via le filage à l'état fondu - Effet de la formulation, et de la localisation des nanoparticules afin d'obtenir une fibre fonctionnalisée en surface

Soutenue le 21 novembre 2019 devant la Commission d'Examen :

Prof. Frederic PROCHAZKA	**Rapporteur**
Dr. Aurélie TAGUET	**Rapporteur**
Prof. Sophie DUQUESNE	**Examinateur**
Dr. Samira BENALI	**Examinateur**
Dr. Cédric SAMUEL	**Invitée**
Dr. Carole AUBRY	**Invitée**
Prof. Fabien SALAUN	**Directeur de thèse**
Prof. Eric DEVAUX	**Co-directeur de thèse**
Dr. Aurélie CAYLA	**Co-encadrant de thèse**

Acknowledgement

Time flies. 3 years of study is going to be finished. It was hard to imagine to go abroad for such a long time, since I had already stayed in Chengdu, China for 26 years without going to any other countries.

Fortunately, I have gained a lot of experience and happy stories, instead of gaining weight. First of all, I would like to thank my great mother country China as well as Chinese Scholarship Council (CSC) to offer me this opportunity to continue my study in a foreign country. I would also like to thank France, the country with Liberté, Égalité, Fraternité. Thank myself to choose France as my destination of PhD study.

I would like to be grateful for becoming the PhD student of Prof. Fabien SALAUN, Eric DEVAUX as well as Aurélie CAYLA. Thanks a lot to Prof. SALAUN for welcoming me to ENSAIT. It's him who recognized my academic level, and gave me the key for opening the door to the academic world. After I went to ENSAIT, he always makes his efforts to guide me and inspire me. His meticulous spirit and enthusiasm about the scientific research will always embrave me. Without his instruction, this thesis could not be reached to present level.

I would also like to show my sincere gratitude to Prof. DEVAUX, who is the headmaster of ENSAIT. In each meeting, he is always patient to offer me the guidance. He is very elegant and wise as a leader and a professor. I am very appreciated to be his PhD student.

Last but not the least, I would like to show my great gratitude to my supervisor Aurélie CAYLA. She participates the most with me in my research experiments. She also taught me a lot of textile knowledge. The time with her is always happy and unforgettable. She is not only the supervisor, but also my comrade in the research "battle".

In addition, I would like to thank the other teachers in ENSAIT as well as in Sichuan University: Stephane Giraud, Peng Wang, etc. (ENSAIT); Pengqing Liu, Mengjin Jiang, etc. (Sichuan University).

I would like thank my colleagues and friends for sharing their previous time with me, including the Chinese friends and international friends (such as our officemate, Maneesh). I also miss the friends in China, who also give me support in their heart.

Personally, I would also thank my dearest parents，衷心感谢爸爸妈妈的养育之恩，希望你们健康开心。I would like to thank my girlfriend Yanni，感谢在法国的相遇与陪伴，回去吃遍中华美食。

This is not the end of the story, but just the beginning… Let's continue to write the story. Take care, each of my friends. I hope see you again in the near bright future.

Sincerely Yours,

Cordialement,

此致敬礼，

Xiang YAN （翔仔）

Table of Contents

List of Figures

List of Tables

Introduction

Polymer blending is a common method to endow the materials with synergetic properties. The blending strategy also offers the possibility of manufacturing porous materials, if one of the phases can be removed. The method is carried out in two consecutive steps, i.e., (i) target and sacrificial polymers are mixed at melting state without adding any solvent, and (ii) the sacrificial polymer is extracted with the solvent to obtain a porous material. With the development of nanotechnology, more and more nanoparticles are being utilized to tailor the microstructure. Apart from regulating the structure, nanoparticles can endow the material with additional properties. In the case that the nanoparticles are localized at the interface, after the etching of sacrificial phase, surface modified scaffold with nanoparticles can be obtained. It provides a possibility to prepare surface functionalized material. This strategy can be also extended to textile area with the aid of melt spinning technology.

Polypropylene (PP) is a non-polar polymer with a good fiber-forming ability for textile use. Thermoplastic polyvinyl alcohol (PVA), as polar polymer, is immiscible with PP, and it can be removed in warm water as sacrificial phase. PVA is biodegradable and water-soluble, and also has important fiber-forming properties. Melt spinning is one of the main routes to produce upstream polymeric fibers for textile use. The related technology (e.g., twisting, knitting, weaving) can be applied with melt-spun fibers.

This PhD work is funded by China Scholarship Council (CSC), and performed in Laboratoire de Génie et Matériaux Textiles (GEMTEX, ENSAIT, France). The objective is to fabricate the (nano)particle-tailored high-specific-area polypropylene textile products.

In Chapter 1, a literature survey was conducted. The application of polypropylene and the meltable water-soluble polymers were introduced. Some important factors concerning the biphasic morphology prediction and control were investigated. Afterwards, the information about the (nano)particles as compatiblizers was also

reported, including the homogenously modified and the Janus particles. The related survey of transformation of biphasic blends to multifilament yarns was presented, for fabricating porous fibers/microfibers.

In Chapter 3, blends with three different mass ratios of PP/PVA (70/30, 60/40, 50/50 (wt.%/wt.%)) were compounded and manufactured into fibers. The purpose of this research is to study the morphological evolution from extrudates to multifilament yarns of PP-PVA, through different tests along the whole textile production process. Different PP/PVA ratios have been studied to optimize the appropriate formulation to obtain porous PP-PVA blend fibers by melt spinning followed by phase extraction.

In Chapter 4, efforts were made to use silica nanoparticles with different surface chemistries into the biphasic fibers, of which their mass ratio was 70/30 (PP to PVA). Efforts were made to develop blends with interface distributed silicas, and the feasibility of fabricating surface-modified porous PP fibers was also demonstrated.

In Chapter 5, the Janus kaolinite particles were firstly used in PP-PVA biphasic systems with the mass ratio of 70/30. The Janus particles have a stronger affinity towards the biphasic interface compared with the conventional homogenously modified particles. Therefore, the materials were manufactured into multifilament yarns by melt spinning technology to fabricate the surface-tailored PP porous fibers.

In Chapter 6, the mass ratio of PP to PVA was reversed to 30/70 in order to fabricate the PP matrix/PVA disperse fiber. Therefore, the PP microfibers were expected to obtained after the removal of PVA. In addition, the incorporation of Janus kaolinite particles was also attempted.

In the research, emphasis was put on both of the extrudates and the fibers of the polymer blends, as well as the knitted fabrics. The melt flow index (MFI) was determined to ensure the spinnability of the polymer mixture within an appropriate temperature range. To evaluate the morphology change including the biphasic structure and filler localization, the scanning microscopy analyses (SEM) and transmission electron scanning microscopy (TEM) were carried out. The measurement of PVA accessibility degree and the rheological analyses were also combined. The mechanical

measurement of the obtained fibers and fabrics was also a key investigation. In addition, the thermal properties and aggregation structures of the blends were examined.

Chapter I:

State of the Art

Chapter 1 State of the Art

In this chapter, a literature survey is started with the introduction of polypropylene, one of the most conventional thermoplastic polymers in people's life. It demonstrates that the functionality of PP is difficult to be achieved, sometimes PP material should be paired with some other polymers to be given more possibilities for derived use.

Afterward, the basic concept, processing methods as well as prediction methods are illustrated. Water-soluble polymers are an essential branch, can also accompany with other polymers to form polymer pairs. For the lack of compatibility, the surfactant is often required to make up with the drawbacks.

Furthermore, the melt spinning technology in order to fabricate the biphasic fibers is introduced. If one of the phases is removed, the porous fibers or microfibers may be obtained.

1.1 Application of polypropylene

Polypropylene (PP) was discovered in 1954 by the Nobel prize winner, an Italian scientist Giulio Natta and became popular very quickly. It is a classical non-polar polymer from inexpensive petroleum derivative with excellent resistant properties against chemical reagent as well as mechanical abuse. Furthermore, the thermal stability of PP provides the feasibility in many fields, compared with polyethylene. PP belongs to a vinyl polymer, of which the structure is shown in Figure 1-1 (omnexus.specialchem.com., 2019). There are mainly three kinds of molecular configuration, including atactic, syndiotactic and isotactic polypropylene, which is displayed in Figure 1-2 (Krassig, 1984). In addition, the hemiisotactic polypropylene is also an interesting kind in macromolecular stereochemistry, as a coexistence of order and disorder with the even monomeric units of the same configuration and odd units of a random configuration (Karger-Kocsis and Bárány, 2019).

One of the important uses is to be manufactured into fibers. The PP polymer candidate is normally isotactic, of which the commercial products were available in

1957, and its fibrous products appeared immediately since the late 1950s (Cook, 1968). In addition, syndiotactic polypropylene can be also manufactured into fibers revealed by a patent (Gownder and Nguyen, 2006), and they were found have a higher tenacity compared with the isotactic polypropylene.

Meanwhile, the PP material lacks reactive groups for being functionalized. However, the melt processing temperature span of PP is relatively wide, which provides feasibility to be paired with another polymer with functionality in the melt manufacturing process.

In addition, the PP fibers are composed of aliphatic hydrocarbon polymers, therefore, the surface energies are relatively lower than those of other thermoplastic fibers from the polar polymer (Ugbolue, 2017).

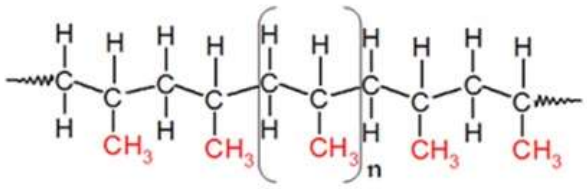

Figure 1-1 Chemical structure of polypropylene (omnexus.specialchem.com., 2019).

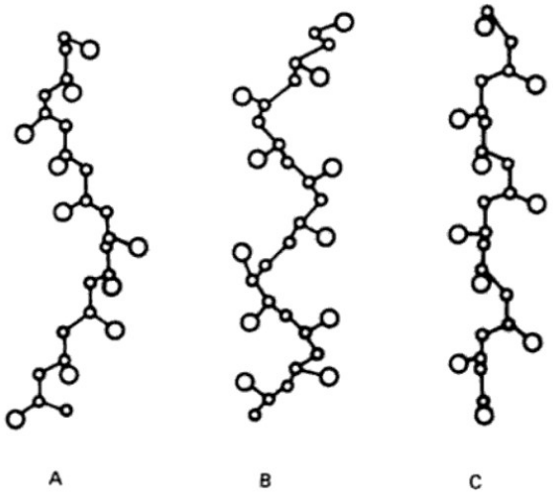

Figure 1-2 Molecular configurations of the polypropylene (a) atactic; (b) syndiotactic; (c) isotactic (Left-handed Helix) (Krassig, 1984).

PP is one of the cheapest synthetic polymers, and it has an outstanding fiber-forming ability for potential textile domains. Its low density offers the possibility of being float as robs, nets or other forms of technical textiles (Pritchard *et al.*, 2000). The specific gravity of some kinds of fibers in the textile industry are listed in Table 1-1 (Galanti and Mantell, 1965). It is found that polypropylene fibers have an outstanding advantage of specific gravity as 0.90-0.92 compared with other industrialized fibers. In addition, the PP fibers have an exceptionally low thermal conductivity, which can be used in for insulating applications. PP can also be a very good electronic insulator with low power loss even in the condition of radio frequencies. The crystallinity of PP is from 40% to 60% (Maddah, 2016). The mechanical properties of the PP fibers are dominantly influenced by the crystallinity degree, crystalline morphology, molar mass and chains orientation.

Table 1-1 Specific gravity of various fibers.

Fiber	Specific Gravity
Polypropylene	0.90-0.92
Cotton	1.50-1.55
Wool	1.30-1.32
Cellulose	1.52
Cellulose acetate	1.32
Polyamides	1.14
Polyacrylonitrile	1.14-1.17
Polyethylene terephthalate (PET)	1.38-1.39
Copolymer of acrylonitrile and vinyl chloride	1.30
Polyvinylidene chloride (PVDC)	1.72
Glass fiber	2.54

1.2 Immiscible polymer blends

When two polymers are mixed, the polymer blends can be miscible, partially miscible or immiscible (molecular level). Immiscible polymer blending is an ideal strategy for endowing the materials with additional as well as combined properties. The phase behaviors of polymer blends (macromolecules) are different from those of the small molecules, for the entropy of mixing the small molecules provides the driving force for miscibility, but the that of mixing the macromolecules can be negligible. Quantitative calculation starts with the free energy ΔG_m, which determines the miscibility of the polymer blends as shown in Equation 1-1.

$$\Delta G_m = \Delta H_m - T\Delta S_m \quad \textbf{Equation 1-1}$$

where ΔG_m, ΔH_m and ΔS_m represent the Gibbs energy, enthalpy as well as entropy of mixing, respectively.

Two conditions concerning ΔG_m are required to be fulfilled with regard to miscibility:

$$\Delta G_m < 0$$

$$\left(\frac{\partial^2(\Delta G_m)}{\partial \phi_i^2}\right)_{T,p} > 0$$

where ΔGm represents the molar Gibbs free energy of mixing, ϕ is the volume fraction of the component i.

Polymers have low entropic gain, and ΔS_m is small and positive. In most of the conditions, the mixing is commitment with endothermic process, which indicates that ΔH_m is positive. It results in the positive values of ΔG_m, representing the immiscibility. Therefore, in most of the cases, the blends exhibit immiscible.

On occasion, the immiscible polymers and miscible polymers can be converted to each other, due to the change of the environment, including temperature, pressure or the polymer fractions (Thomas *et al.*, 2014).

Most of the polymer pairs are thermodynamically immiscible due to the low mixing entropy (Chen *et al.*, 2005; Schmidt *et al.*, 2002). The morphology control of the immiscible blends is of great significance.

There are several possibilities of the biphasic morphology of the blends, including dispersed structure, matrix-fiber-structure, lamellar structure and co-continuous structure, displayed in Figure 1-3 (Pötschke and Paul., 2003), sometimes the structure can be complicated and multifarious due to different raw materials and manufacturing conditions.

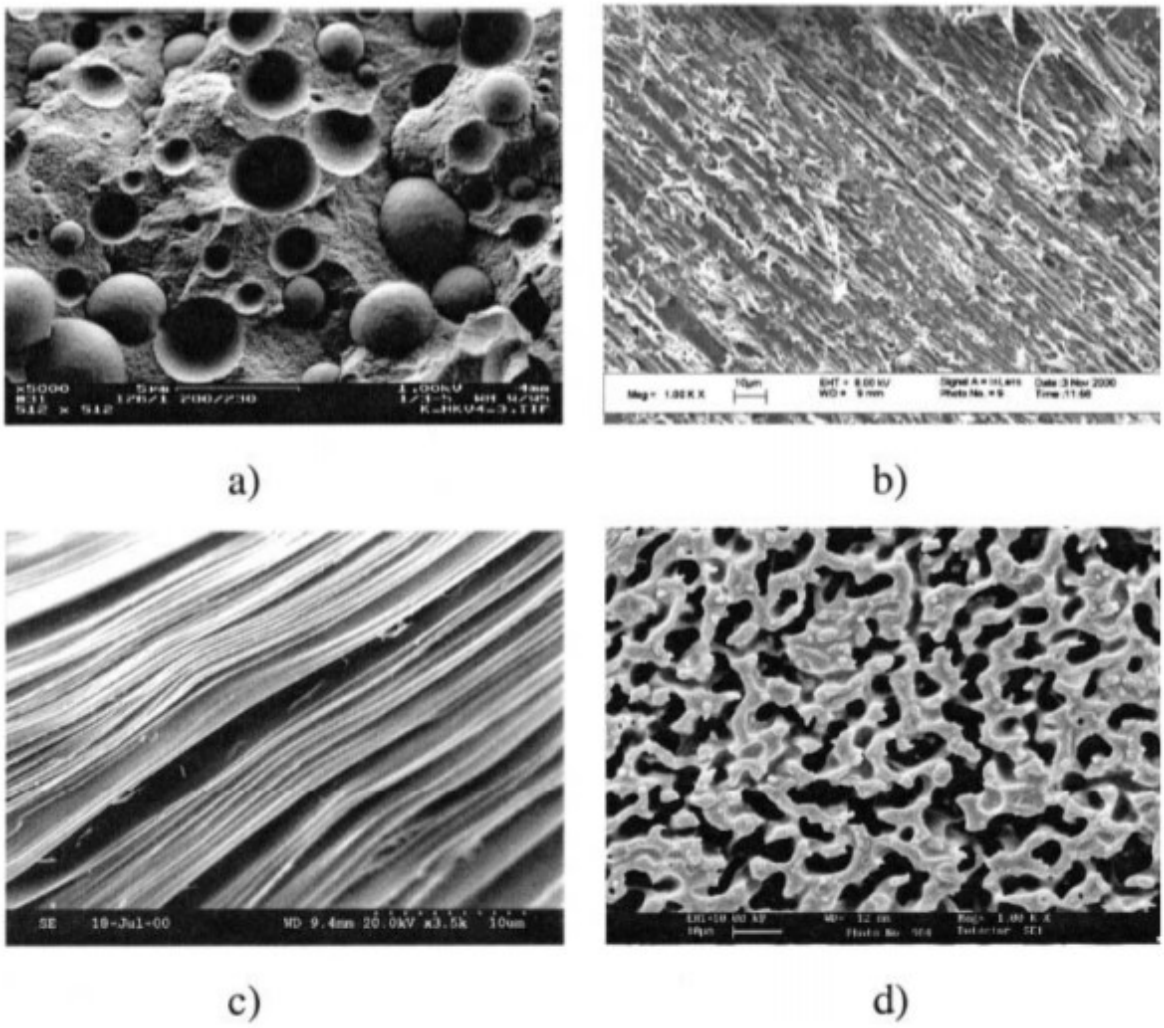

Figure 1-3 Different kinds of morphology observed by SEM analyses (a) Dispersed structure; (b) matrix-fiber-structure; (c) lamellar structure; (d) co-continuous structure (Pötschke and Paul., 2003).

1.3 Prediction of biphasic morphology

Many factors determine the morphology of the blends, and many researchers have proposed several practical models to make related predictions.

1.3.1 Viscosity and elasticity ratios

The biphasic morphology is correlated with their viscoelasticity, which has been introduced in detail by Mekhilef and Verhoogt (1996). Avgeropoulos *et al.* (1976) gave

a semi-empirical formula concerning the relationship between torque ratio and the polymer volume fraction of phase inversion. Non-uniform stress fields exist in the same processing device; therefore, the result only serves as an approximation (Pötschke and Paul., 2003). The related equation is illustrated in Equation 1-2.

$$\frac{T_1}{T_2} = \frac{\phi_1}{\phi_2} \quad \textbf{Equation 1-2}$$

where the T_i represents the torque of polymer i, and ϕ_i represents the volume fraction of polymer i. Torque symbolizes the shearing and elongational forces during the manufacturing inside the compounding device.

This formula was evolved towards the relationship between viscosity and volume fraction of phase inversion, completed by Miles and Zurek (1988), shown in Equation 1-3.

$$\frac{\eta_1(\dot{\gamma})}{\eta_2(\dot{\gamma})} = \frac{\phi_1}{\phi_2} = \mu \quad \textbf{Equation 1-3}$$

where the $\eta_i(\dot{\gamma})$ represents the viscosity of phase i at a certain low shear rate. In addition, the viscosity ratio can also determine the feasibility of the fibrillation of the minor phase, if phase 1 is regarded as the minor phase. Tsebrenko *et al.* (1980) and White and Min (1985) found that if μ was close to or lower than 1, the fibrillar distribution of minor phase appeared in the blends. If μ is low, the drops are easy to be elongated due to the shear flow, and with the increment of μ values, the droplet is easier to break up into short fibrils. If μ is higher than 1 the deformation in the extrudate was more insignificant. Furthermore, with tremendously high viscosity ratios, the droplets do not deform in the shear flow, but still possibly occurred in the extensional flow (Bentley and Leal, 1986).

Metelkhin and Blekht (1984) proposed a formula concerning the phase inversion and viscosity ratio, evolved from Tomotika's theory (thread instability) (Tomotika, 1935). A thread-like dispersed phase around another liquid has the tendency of breaking up due to the interfacial tension. The related equation is shown in Equation 1-4 to predict the critical volume fraction for biphasic phase inversion.

$$\phi_2=[1+F(\lambda)\times\lambda]^{-1} \quad \textbf{Equation 1-4}$$

Where $F(\lambda)=1+2.25\log(\lambda)+1.81[\log(\lambda)]^2$, in which λ represents the viscosity ratio.

Based on the previous discussion, Utracki established an updated formula as Equation 1-5.

$$\frac{\eta_2}{\eta_1}=\left(\frac{\phi_m-\phi_{2i}}{\phi_m-\phi_{1i}}\right)^{[\eta]\phi_m} \quad \textbf{Equation 1-5}$$

where [η] represents the intrinsic viscosity, ϕ_m represents the maximum packing volume fraction, and ϕ_{1i} and ϕ_{2i} represent the volume fraction of the continuous and dispersed phases at the phase inversion point.

The elasticity ratio is also a determining factor, especially when the viscosity ratio of the dispersed phase to the matrix phase is too high. Bourry and Favis (1998) proposed a formula connecting the volume fraction to the storage module (G') and the loss tangent (tan δ), respectively illustrated in Equation 1-6 and Equation 1-7.

$$\frac{\phi_1}{\phi_2}=\frac{G'_1}{G'_2} \quad \textbf{Equation 1-6}$$

$$\frac{\phi_1}{\phi_2}=\frac{\tan\delta_1}{\tan\delta_2} \quad \textbf{Equation 1-7}$$

Where G'_i represents the storage modulus of polymer i, and tan δ_i represents the loss tangent of polymer i. The prediction is not accurate but can give a main trend influenced by the elasticity ratios.

1.3.2 Surface tension

The surface tension of the components is also of significant importance for the final morphology of the blends. Low interfacial stresses promote droplet rupture rather than the formation of the elongated fibrous phase (White and Min, 1985). Willemse *et al.* (1999) demonstrated that the interfacial tension determines the region of the co-continuity. They proposed a formula concerning the geometrical requirements for the co-continuity as in Equation 1-8.

$$\frac{1}{\phi_{d,cc}} = 1.38 + 0.0213\left(\frac{\eta_m \dot{\gamma}}{\gamma} R_0\right)^{4.2} \quad \textbf{Equation 1-8}$$

The lower limit of the minor phase volume fraction can be calculated, of which the co-continuous morphologies can be reached, for the specific polymeric system and blending conditions. The limit for co-continuity ($\phi_{d,cc}$) can be estimated in terms of interfacial tension γ, the viscosity of matrix phase η_m, the shear rate $\dot{\gamma}$, the equivalent sphere radius of the minor phase R_0.

Compared with miscible systems, the linear viscoelasticity is strongly influenced by the microstructures of the biphasic phases. Palierne (1990) made the connection of the morphology with the viscoelastic response in an emulsion system, well known as Palierne's Model. Graebling *et al.* (1993) simplified the model and regarded the particle size distribution is narrow with the R_v/R_n value not exceeding 2, where R_v is the volume average radius and R_n is the number average radius. Thus, the complex modulus is in relationship with the interfacial tension γ and the droplet sizes D_i, which is given in Equation 1-9.

$$G^*(w)=G'(w)+iG''(w)=G_m^*(w)\left[\frac{1+3\sum_i \phi_i H_m^*(w)}{1-2\sum_i \phi_i H_m^*(w)}\right] \quad \textbf{Equation 1-9}$$

Where

$$H_i^*(w)=\frac{\frac{4\gamma}{D_i}\left(2G_m^*(w)+5G_d^*(w)\right)+\left(G_d^*(w)-G_m^*(w)\right)\left(16G_m^*(w)+19G_d^*(w)\right)}{\frac{40\gamma}{D_i}\left(G_m^*(w)+G_d^*(w)\right)+\left(2G_d^*(w)+3G_m^*(w)\right)\left(16G_m^*(w)+19G_d^*(w)\right)}$$

Many researchers simulated this formula from the rheological tests to calculate the surface tension, and different blending systems exhibit varied surface tension. For example, the surface tension of poly(trimethylene terephthalate) PTT/polyamide-12 (PA12) blends can reach as high as 7 mN/m (Asadinezhad *et al.*, 2005), while that of poly (butylene succinate) (PBS)/polylactide (PLA) is significantly lower as 1.12 mN/m (Wu *et al.*, 2012).

In addition, there are also Yu's, Bousmina's models as well as Gramespacher and Meissner Model (G-M Model) to calculate the dynamic moduli (Yu *et al.*, 2002; Bousmina, 1999; Gramespacher and Meissner, 1992). One of the most typical ones is G-M Model, evolved from the emulsion system developed by Choi and Schowalter (1975) as well as a linear mixing rule. The idea is that the complex shear modulus originates from the shear moduli of the biphasic phases and also the interface. Therefore, the complex, storage as well as loss moduli are obtained in Equation 1-10, Equation 1-11 and Equation 1-12, respectively.

$$G^*(\omega)=\varphi G_d^*(\omega)+(1-\varphi)G_m^*(\omega)+\varphi G_{\text{int}}^*(\omega) \quad \textbf{Equation 1-10}$$

$$G'(\omega)=G_d'(\omega)+(1-\varphi)G_m'(\omega)+\frac{\eta}{\tau_1}\left(1-\frac{\tau_2}{\tau_1}\right)\left(\frac{\omega^2\tau_1^2}{1+\omega^2\tau_1^2}\right) \quad \textbf{Equation 1-11}$$

$$G''(\omega) = G''_d(\omega) + (1-\varphi)G''_m(\omega) + \frac{\eta}{\tau_1}\left(1-\frac{\tau_2}{\tau_1}\right)\left(\frac{\omega\tau_1}{1+\omega^2\tau_1^2}\right) \quad \textbf{Equation 1-12}$$

Where

$$\eta = \eta_m\left(1+\varphi\frac{5K+2}{2(K+1)}+\varphi^2\frac{5(5K+2)^2}{8(K+1)^2}\right)$$

$$\tau_1 = \frac{(19K+16)(2K+3)}{40(K+1)}\frac{R\eta_m}{\gamma}\times\left(1+\varphi\frac{5(19K+16)}{4(K+1)(2K+3)}\right)$$

$$\tau_2 = \frac{(19K+16)(2K+3)}{40(K+1)}\frac{R\eta_m}{\gamma}\times\left(1+\varphi\frac{3(19K+16)}{4(K+1)(2K+3)}\right)$$

with G', G'_m, and G'_d being the blend, matrix, and dispersed phase storage moduli, respectively, G", G''_m, and G''_d the blend, matrix, and dispersed phase loss moduli, respectively, G^*, G^*_d, G^*_m, and G^*_{int} respectively the complex modulus of the blend, the complex modulus of the dispersed phase, the complex modulus of the matrix, and the complex modulus of the interface. φ is the volume fraction of the dispersed phase, ω is the frequency of oscillation, η, η_m and η_d are the blend, matrix, and dispersed phase zero-shear viscosities, respectively. $K=\eta/\eta_m$ represents the viscosity ratio, ϒ represents the interfacial tension between the phases of the blend, and R represents the average radius of the monodispersed droplets.

1.3.3 Storage moduli

The storage moduli represent the stiffness of the sample, based on which some modeling can be carried out to dig the morphology evolution of the biphasic polymers. The parallel and series modes are indicated in Equation 1-13 and Equation 1-14, respectively (Moly *et al.*, 2006).

$$M_u = M_1\phi_1 + M_2\phi_2 \quad \textbf{Equation 1-13}$$

$$\frac{1}{M_L} = \frac{\phi_1}{M_1} + \frac{\phi_2}{M_2} \quad \textbf{Equation 1-14}$$

where M_i represents the mechanical property of each polymer (mainly reflected in storage modulus); Φ_i represents the volume fractions. M_u represents the upper bound of the blends, while M_L represents the lower bound of the blends. For the parallel model, the components are arranged parallelly. Therefore, the applied stress elongates both of the components as the same extent. For the series model, the components are arranged in series. In this case, the applied stress elongates the components not conventionally as the same extent. The parallel model represents the co-continuous structure, in which both of the two components have a great contribution.

In addition, Coran and Takayanagi proposed the related models evolved from the basic ones. Coran's model is shown in Equation 1-15 (Coran, 1988).

$$M = f\left(M_u - M_L\right) + M_L \quad \textbf{Equation 1-15}$$

Where similarly, M_u represents the upper bound of the blends, while M_L represents the lower bound of the blends. *f* varies between zero and unity for the binary blends, which means the Coran's model is between the upper and lower bounds.

Furthermore, in Takayanagi model is shown in Equation 1-16 (Dickie, 1973).

$$E = (1-\lambda)E_1 + \lambda\left(\frac{1\text{-}\phi}{E_1} + \frac{\phi}{E_2}\right)^{-1} \quad \textbf{Equation 1-16}$$

where λ represents the degree of series-parallel coupling (combination mode), E_1 and E_2 represent the moduli of the matrix and dispersed phase of the blends.

The micromechanical models exhibit a good tool to demonstrate combination mode of the blends, sometimes also representing the degree of co-continuity. However, the drawback is the model lacks the information concerning the interfacial properties, compared with the Palierne or G-M Models. In addition, the micromechanical models are more suitable for the dynamic moduli (Asadinezhad *et al.*, 2005).

1.4 Immiscible blends with water-soluble polymers

Polymer blends containing one soluble sacrificial phase gives the materials possibilities to fabricate more types of products. After the removal of the sacrificial phase, the porous materials or numerous fragmented materials can be obtained and served as potential functional materials, for they own significantly high specific areas. Among the soluble polymers, the water-soluble polymers are playing a more and more important role as sacrificial polymers, for the toxic organic solvents can be avoided. Water-soluble polymers mainly contain hydrophilic functional groups, such as alcohol, pyrrolidone, amide and ether (Halake *et al.*, 2014). There are several available soluble polymers, such as poly (vinyl alcohol) (PVA/PVOH), polyoxyethylene (POE), sulfopolyester (SP).

1.4.1 Poly(vinyl alcohol) (PVA/PVOH)

PVA, as a synthetic and semicrystalline polymer with hydroxyl groups, with a backbone containing only carbon atoms. It possesses an excellent oxygen barrier and dyeing properties, and mechanical strength as well as biodegradable properties in both anaerobic and aerobic environment (Kim *et al.*, 2015; Strecka *et al.*, 2010; Halima, 2016). PVA can be dissolved in water, and its hydrolysis degree influences its water dissolution (Robeson *et al.*, 1994). Hermann and Haehnel in Germany firstly prepared it, in 1924, and it became industrialized using the hydrolysis of polyvinyl acetate (PVAc) (Goodship and Jacobs, 2009). The degree of hydrolysis makes the PVA products varied, mainly divided into two kinds, fully hydrolyzed and partially hydrolyzed ones. The related molecular structures of PVA are displayed in Figure 1-4, and normally the PVA

are copolymers containing vinyl alcohol and vinyl acetate (Patachia *et al.*, 2009). It is used in many fields, such as textile, emulsifier, coating, and adhesives (Jang and Lee, 2003).

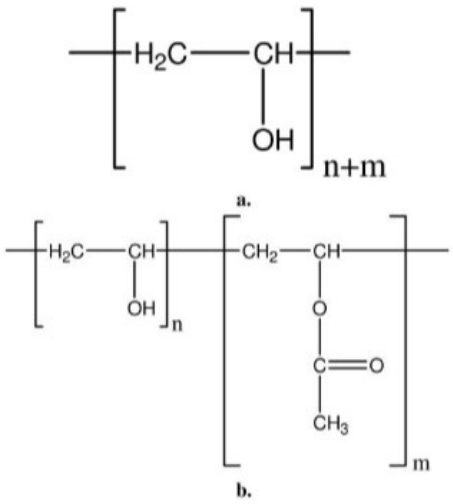

Figure 1-4 Molecular structures of PVA with different degrees of hydrolysis (Patachia *et al.*, 2009).

In most of the cases, PVA is manufactured by wet process dissolved by water. Nowadays, melt processing technology is also employed for PVA manufacturing, in which glycerin, as a plasticizer, is usually added to decrease its melting point. The gas barrier properties of PVA is provided by its small, dense and closely packed "monoclinic" crystallite. Thus, some researchers adopted PVA into the packaging materials to enhance their gas barrier properties and broaden the extensive applications. Jang *et al.* (2004) used PVA to enhance the oxygen barrier property of biaxially oriented PP film over 130 times. The oxygen barrier was enhanced with the increase of the PP viscosity and the draw ratio. Kim *et al.* (2015) also introduced PVA into low-density polyethylene (LDPE) for packaging used to enhance the oxygen barrier. Meanwhile, due to the easy interaction of water vapor with polar hydroxyl groups, the water absorbency of LDPE was greatly enhanced. Therefore, it is more suitable for the packaging the low-moisture goods. Aimed at its biodegradable ability, Brandalise *et al.* blended high recycled density polyethylene (HDPEr) and PVA compatibilized with

maleic anhydride-grafted HDPEr (HDPEr-AM) to discover its potential agricultural film use (Brandalise *et al.*, 2009). The HDPEr crystallization was found to be increased from 56% to over 88% due to the presence of PVA. However, the overall crystallinity was decreased due to the low crystallinity of PVA.

PVA is an important raw material for chemical fibers with good fiber-forming properties, which was commercialized since 1950s (Kim *et al.*, 2016). Segawa *et al.* (1974) investigated the blends of PVA with polyolefins in which the pellets were sheared in an aqueous solution with inorganic salt to prevent the dissolution of PVA, and afterwards formed into papers. Robeson *et al.* (1994) initially removed the PVA phase by water to obtain microfibers.

For the fabrication of polyvinyl alcohol/polypropylene biphasic fibers, Ku and Lin (2005, 2014) had in-depth investigations. The influence of temperature, shear rate and blending ratios on the rheological behaviors of the PVA/PP blends in capillary extrusions was investigated. PP and PVA have similar shear-sensitivity, between which PVA has a higher sensitivity. It is found that the viscosities of the blends are lower than those of the two components. In addition, it is revealed that the non-Newtonian indices as well as the activation energies of the blends are increased compared with those of the neat polymers. When 60 wt.% of PVA is incorporated, the viscosity of blends is more sensitive to temperature rather than the shear rate. With the increment of the shear rate, the impact of the temperature and polymer fractions on flow behavior is weakened. Furthermore, the melt spinning method was utilized to demonstrate the uniaxial elongational flow properties of the PP/PVA blends. It is revealed that the draw and blending ratios are key factors influencing the elongational flow behaviors, while temperature variation has little impact on the related behaviors. The convergence of blending ratio (when the proportion of polymer components in the total amount is close to each other) causes higher elongation rates and lower elongational resistance, which is not beneficial for melt spinning manufacturing.

1.4.2 Polyoxyethylene (POE)

POE is also denoted as polyethylene glycol (PEG), poly(ethylene oxide) PEO, and their nomenclature is usually decided by their molecular weight (MW). The corresponding chemical structures are displayed in Figure 1-5 (Harris, 2013). PEG represents the oligomers and polymers with a MW below 20,000 g/mol, and the polymers with higher values can be labeled as PEOs, both of which can be used as POE. The melting point of POE with a high MW is approximately 65°C. The monomer is ethylene oxide from the oxidation of ethylene by oxygen, and they are polymerized by oxyalkylation to form the polymers (Sheth *et al.*, 1997). It is also a water-soluble polymer with biocompatible, pharmacologically inactive characteristics. It is still an interesting topic to introduce POE into the polyolefin, and Tang and Huang (1994) fabricated PP/PEO blends with a compatibilizer (PP-MA)-g-POE, and POE undergoes fractionated crystallization. The PEO was added into PLLA to modify the mechanical strength, hydrophilicity, degradation rate as well as the crystallization kinetics (do Carmo Rufino and Felisberti, 2016). It is revealed that the PLLA crystal is changed from α'-form to α-form with the increment of POE, and the entrapped POE undergoes the confined fractional crystallization as well. Many bio-sourced materials lack satisfactory mechanical performances. Yu *et al.* (2013) introduced POE into the matrix of plasticized-starch to enhance its mechanical properties, and Young's modulus is elevated. In addition, POE is a common antistatic and dye fixing agent of polyolefinic fabrics (Tang and Huang, 1994). For the melting point of POE is very low, therefore, a large amount of POE is not suitable to be paired with polymer with a high melting point. The reason is that at a high temperature of manufacturing, the viscosity of POE becomes too low and it is difficult to achieve a stable fabrication.

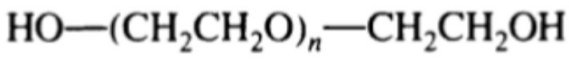

Figure 1-5 Chemical structures of POE (Harris, 2013).

1.4.3 Sulfopolyester (SP)

Polyester is one of the most common thermoplastic resin, and poly(ethylene terephthalate) (PET) is the most important branch, which has been extensively fabricated into clothing fibers and containers, and so on. It has good processability and mechanical properties. PET can behave as both amorphous and semi-crystalline polymer, of which the different cooling rate and the introduction of a nucleating agent causes the difference. After the sulfonation, polyester has the potential to be modified into water-soluble material. Eastman Company has developed a series of sulfonated polyesters, for example, AQ55S (PETi, sulfonated PET, ionic content: 9 mol%, inherent viscosity of ca 0.3 dL/g), AQ48 (sulfopolyester), revealed by the related works of literature (Ghanbari *et al.*, 2013; Soltani and Macosko, 2018; Wang *et al.*, 2016b). The chemical structures are enclosed in Figure 1-6 and Figure 1-7. Ghanbari *et al.* (2013) found that PETi is immiscible with PET, and nanoclay particles have a better affinity with PETi phase, and PETi acts as an exfoliation agent to improve the dispersion of the nanofillers. Wang *et al.* (2016b) used melt blowing technology to manufacture bicomponent islands-in-the-sea nonwovens SP/PBT (70 wt.%/30 wt.%), and then remove SP by water to obtain the multilayer nano-/micro- PBT fiber with an average diameter of 66 nm. Afterwards, Soltani and Macosko (2018) further investigated the related conditions to fabricate hydrophilic PBT and hydrophobic polyvinylidene fluoride (PVDF), and summarized that the island polymer is suggested to have low surface energy coupled with low viscosity, thus the nonwoven fibers after extraction have low average diameter, low bundling and relatively good fiber regularity. The obtained PVDF fibers have an average diameter of 36 nm. Although SP is a potential material as sacrificial phase polymer, it is not a conventional polymer of which the cost needs to be considered.

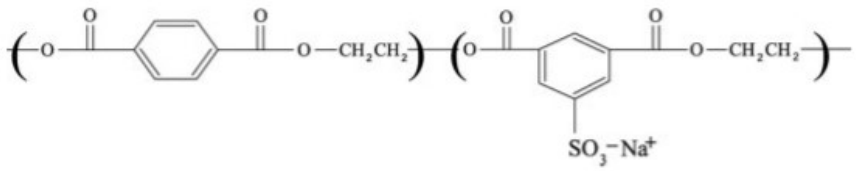

Figure 1-6 Repeat unit of sulfonated PET (AQ55S) (Ghanbari *et al.*, 2013).

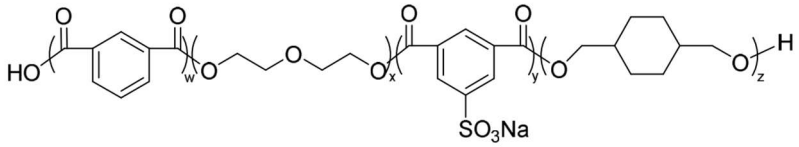

Figure 1-7 Repeat unit of sulfopolyester (AQ48) (Wang *et al.*, 2016b).

1.5 Compatibilization of biphasic blends

Most of the polymer blends exhibit inherent immiscibility, leading to heterogeneous morphology, poor adhesion as well as deterioration of mechanical performance, induced by the interface as a stress concentration point (Bahrami *et al.*, 2017). Therefore, it is of considerable significance to compatibilize the biphasic polymers. Besides, the spinnability of the related fibers may also be enhanced by the compatibilizers.

The compatibilizer can (a) enhance the adhesion between the two phases; (b) decrease the interfacial tension contributing to a finer dispersion; (c) stabilize the morphology against the shear stress during melt processing (Mural *et al.*, 2018).

1.5.1 Traditional compatibilizers

Traditional compatibilizers contain polymeric reagents with long-term development. It has been derived into several sorts, including copolymers (graft, block, random) as well as reactive polymers. The macromolecular compatibilizers can contribute to the decrease of the interfacial tension and the enhancement of interfacial adhesion (Beuguel *et al.*, 2017). Block copolymers (BCPs) are among the most conventional compatibilizers, which plays the role of a coupling agent between the two

polymers generating tremendous effective joints (Brown *et al.*, 1993). Nevertheless, detachment problems can occur, as compatibilizers migrate from the interface at high shear rates. Furthermore, over the critical concentration, block copolymers saturate the interface, aggregate and afterward form micelles towards the bulk phases (Fortelný and Jůza, 2018). In addition, the incorporation of block copolymer of high M_w tends to localize in the bulk phases instead of the biphasic interface (Mural *et al.*, 2018). Furthermore, the traditional compatibilizers are system-specific but not cost-effective to engineering (Si *et al.*, 2006).

1.5.2 (Nano)particles

Compared with plasticizers, the use of inorganic fillers is less explored. With the development of nanotechnology, more and more commercialized and industrialized nanoparticles are being adopted to modify the microstructure of polymer blends. Lipatov (1995) revealed that in ternary systems, the free mixing energy ΔG_m was modified as Equation 1-17.

$$\Delta G_m = \Delta G_{AS} + \Delta G_{BS} + \Delta G_{AB} \quad \textbf{Equation 1-17}$$

where A, B represent the polymer A, B, and S represent the (nano)particles, and the interacting pairs from the components are denoted in the subscripts of free energy ΔG. The addition of the nanofiller can possibly stabilize the binary systems, and the specific surface area of the fillers plays a dominant role, which should be taken into consideration for the selection of fillers (Ray *et al.*, 2004). The rigid core from the particles localized at the biphasic interface exhibits Pickering effect, offering the morphology stability against shearing as well as annealing conditions (Wang *et al.*, 2017b). The incorporation of (nano)particles will unavoidably impact the biphasic morphology, to which the localization of the fillers is a key factor. The resultant change can be refinement, coarsening, irregular shape or co-continuity shift. The scheme of the possible evolution of biphasic morphology influenced by the incorporation of

nanoparticles are displayed in Figure 1-8 (de Luna and Filippone, 2016). As for the particles playing the role as a compatibilizer at the interface, the refinement effect is often expected to occur.

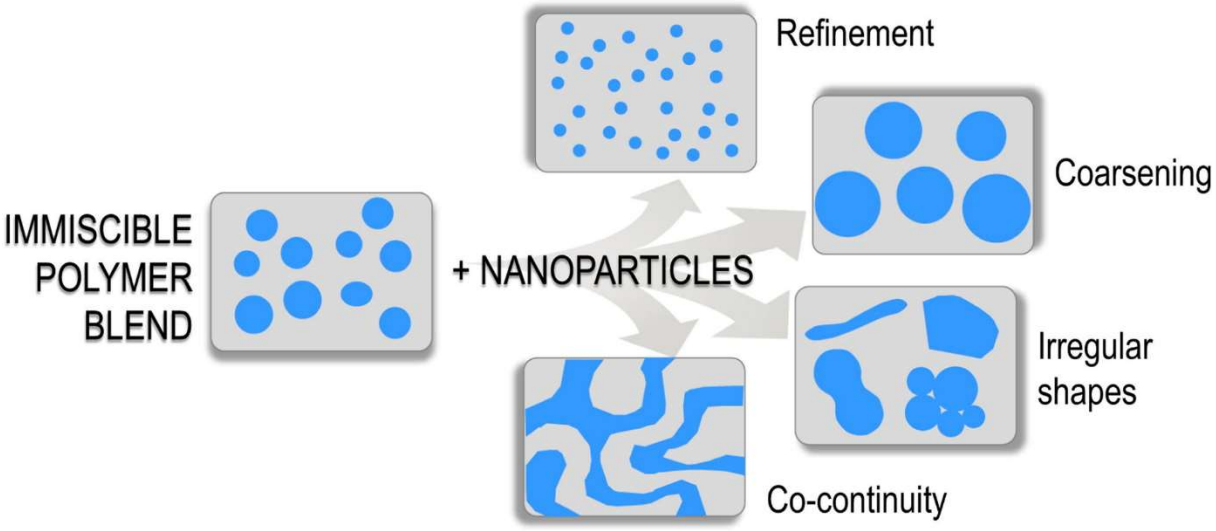

Figure 1-8 Scheme of the possible evolution of biphasic morphology influenced by the incorporation of nanoparticles (de Luna and Filippone, 2016).

Varieties of particles with distinct shapes and dimensions have been tested, such as spherical (silica nanoparticles (Huang *et al.*, 2016), gold nanoparticles (Kwon *et al.*, 2011), TiO2 (Li *et al.*, 2009)), carbon black (Chen *et al.*, 2017a), cage-like (POSS (Kodal, 2016)), patchy (graphene (Tong *et al.*, 2017), clay (Mederic *et al.*, 2018)) as well as one-dimensional (carbon nanotube (CNT) (Chen *et al.*, 2017b) particles. The particles can play the role of not only compatibilizers but also functionalizers. Ginzburg (2010) summarized some examples of the particles and their functionalization, displayed in Table 1-2.

Table 1-2 Various particles and their representative dimensions and functionality**.**

Particle	Shape	Size	Functionality
Silica particles	Sphere	Radius: 5-100 nm	Toughened, flame-retardant
Nanoclays	Platelet	Width: 50-5000 nm; thickness: 1 nm	Hardened, toughened, flame-retardant, gas barrier, electrorheologically sensitive
Carbon black (Primary particles)	Sphere	Radius: 20 nm	Conductive
Carbon nanotubes	Rod	Length: >100 nm ; thickness: 1nm	Conductive
Metal nanoparticles (e.g. Au, Ag, Pt)	Sphere	Radius : 2-100 nm	Sensing, electronic, catalytic

1.5.2.1 Silica nanoparticles

Silica nanoparticles are adopted globally to modify the polymeric materials, and have been successfully utilized to the polymer blends containing polyolefin. Lee *et al.* (2003) adopted different silica nanoparticles to tailor the structure of PP-liquid-crystalline polymer (LCP). It was found that the filler size as well as surface nature impacted the morphology of LCP phase, and the compatibility between the particles and the PP phase influenced the droplet-fibril transition dominantly. Liu and Kontopoulou (2006) and Yang *et al.* (2006, 2007) introduced different silica nanoparticles into the blends of PP and elastomer, and discovered that silica nanoparticles have different influences upon the final shock (impact) properties, due to the varying blend morphology, containing refined dispersed domain or SiO_2-surrounded nodules. Elias *et al.* (2007; 2008a; 2008b) adopted different silica nanoparticles to modify the structure of PP-PS as well as PP-EVA blends. It was found that migration could be detected after the melt manufacturing, mainly due to shear-induced movements and collisions with the dispersed phase.

Accessibility of sacrificial phase is an important parameter in evaluating the porous materials. There are several literatures about the morphology modification via embedding the silica nanoparticles, and distinct localizations lead to varied consequences. For the silica nanoparticles distributed in the bulk polymers, Steinmann *et al.* (2002a) adopted a large quantity of hydrophilic SiO_2-spheres within PS-PMMA (minor phase of PMMA in mass), and the particles were dominantly selective for PMMA. It contributed to a promotion of PMMA accessibility, and the dispersed nodules got more elongated and irregular. Lee *et al.* (2010) adopted hydrophobic silica nanoparticles within the PP-polyolefin elastomer (POE) blends (50/50 in mass ratio). It was found that silica nanoparticles were concentrated within the PP phase, inducing a decrease of POE accessibility. For the nanoparticles localized at the interface, Filippone *et al.* (2011) introduced hydrophobic SiO_2 to tailor the morphology of HDPE-PEO blend (minor phase of PEO in mass), and the interface-located silica particles would weaken the PEO accessibility, because the dimensions of PEO phase are downsized irrespective of the accessibility.

1.5.2.2 Clay particles

Apart from silica particles, the clay particles are also an important branch of industrialized particles from natural materials with low cost, excellent thermal stability, good dispersion properties (Wu *et al.*, 2017). Clay particles possess a layered structure of tetrahedral silica oxide and octahedral Al, Mg or Fe oxide. Clay minerals can be generally classified as two categories, 1:1 and 2:1, which represents the ratio of tetrahedral sheet to octahedral sheet. Kaolin clays are 1:1 phyllosilicates and montmorillonite (e.g. kaolinite, dickite, nacrite and halloysite). Kaolinite is composed of an alumina containing tetrahedral sheet (TS) combined with a silica containing octahedral sheet (OS), of which the formula is $Al_2O_3 \cdot 2SiO_2 \cdot 2H_2O$ (Batistella *et al.*, 2016). The chemical structure of kaolinite is displayed in Figure 1-9 (Weiss *et al.*, 2013). Kaolinite is discovered as anisometric platelets with the aspect ratios of around 20:1-40:1 (Hirsemann *et al.*, 2012). Similar with other clay products, kaolinite is found to

have a good flame-retardant enhancement towards the polymer matrix (Batistella *et al.*, 2013).

Apart from the normal patchy structures, the clays may have other morphologies, for example, imogolite and halloysite. The halloysite exhibit tubular shape with the axis ratio of 20:1, of which the inner lumen can provide the space for containing and releasing the functional chemicals (Lvov *et al.*, 2016).

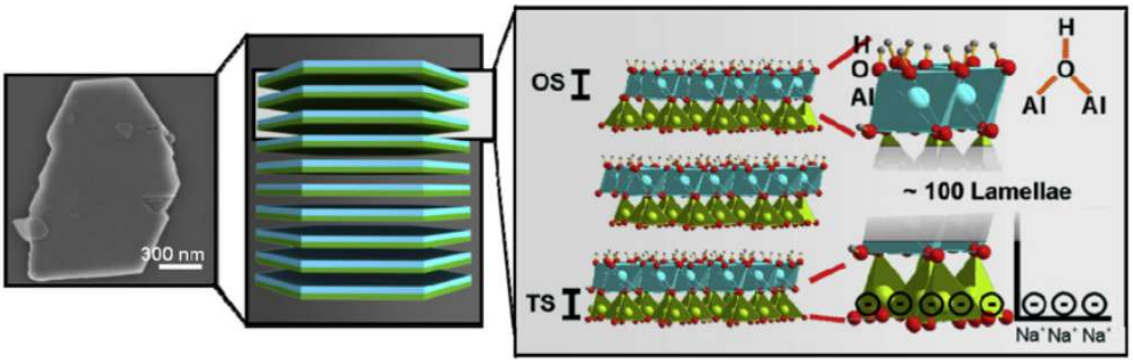

Figure 1-9 SEM images of the top of a typical kaolinite platelet; the scheme of kaolinite platelets; the crystal structure of three lamellae with the special chemical functions at the TS and OS basal (Weiss *et al.*, 2013).

The clay particles in different localizations plays different roles in tailoring the biphasic morphology of the polymers. (1) When the clay particles are dominantly located at the interface, coalescence is inhibited via steric repulsion (Beuguel *et al.*, 2017; Ray *et al.*, 2004; Wu *et al.*, 2017). Apart from the effect, the decrease of interfacial tension can also lead to the size reduction of the dispersed phase; (2) When the clay particles are distributed in the matrix phase, the size of the dispersed phase is also reduced due to the viscosity increment and the barrier effect of the matrix phase; (3) When the clay particles are localized in the dispersed phase, its viscosity enhancement is beneficial for the size increment of the nodules. In practical cases, the localization of the fillers is more complicated, and the effects should be considered comprehensively. Apart from the localization of the fillers, the different exfoliation of clay particles also leads to the different interfacial coverage, thus influencing the

compatibilizing properties. Compared with the spherical structure of silica nanoparticles, its lamellar structure provides more enhanced barrier effect in modifying the biphasic structures.

Similarly, the clay particles can also be added into different systems of polymer pairs, for example, elastomer. Chandran *et al.* (2015) compatilized the PP-elastomer by adding organically modified nanoclay, and the mechanical properties were dramatically increased. It was ascribed to the decrease of the domain size. The particles were dominantly localized at the PP continuous phase as well as the interface.

1.5.2.3 Prediction of the localization of homogenously modified particles

Different homogenously modified particles will localize in different domains of polymers. The localization is controlled by several factors, including kinetic and thermodynamic influences, including mixing sequence (Lee *et al.*, 2003), blend viscosity ratio, mixing time as well as the surface chemistries of the particles, etc. (Plattier *et al.*, 2015; Dai *et al.*, 2007; Elias *et al.*, 2007). When the processing time is long and the shear force is strong enough for equilibrium, the localization of particles is dominantly governed by thermodynamics (Elias *et al.*, 2007). The localization of the homogenously modified particles can be predicted by the Young's model, by the wettability parameter $\omega_{A\text{-}B}$ calculated based on Equation 1-18 (Fenouillot *et al.*, 2009).

$$\omega_{A-B} = \frac{\gamma_{S-B} - \gamma_{S-A}}{\gamma_{A-B}} \quad \textbf{Equation 1-18}$$

where $\gamma_{S\text{-}A}$, $\gamma_{S\text{-}B}$ represent the interfacial tension between the particles S and the polymer A, B, respectively, and $\gamma_{A\text{-}B}$ represents the interfacial tension between the two biphasic polymers.

As for the localization of particles, when $\omega_{A\text{-}B}<-1$, particles will be localized in phase B; when $\omega_{A\text{-}B}>1$, particles will be localized in phase A; and if $\omega_{A\text{-}B}$ is of other values, particles will be localized at the interface between the two polymers.

The measurement of surface tension is normally started with the transformation from the contact angle values. The contact angles of the liquid on the polymer surface enable us to obtain the polar and dispersive contributions to the surface tension of PP and PVA by the method of Owens and Wendt (1969) as in Equation 1-19.

$$\sqrt{\gamma_s^d \gamma_l^d} + \sqrt{\gamma_s^p \gamma_l^p} = 0.5\gamma_l (1 + cos\theta) \quad \textbf{Equation 1-19}$$

Where θ is the contact angle, and γ_l is the liquid surface tension (mN/m), γ_s^d and γ_s^p are the dispersed and polar component of the solid surface (mN/m), γ_l^d and γ_l^p are the dispersed and polar component of the liquid surface tension (mN/m).

However, the surface tensions of polymer and fillers are temperature dependent, and the polymers are melt-manufactured at a high temperature. Therefore, sometimes it would be better to converse the values at the room temperature to that at the melt manufacturing temperature. The relationship of Guggenheim (1945) can be applied to obtain the γ as in Equation 1-20, which is applied for the polymers.

$$\gamma = \gamma_0 (1 - \frac{T}{T_c})^{11/9} \quad \textbf{Equation 1-20}$$

where γ_0 is the surface tension at 0 K; T_c is the critical temperature, which can be consulted in the literatures (Lewin *et al.*, 2005); T is the temperature of the polymers.

After obtaining the values of polar and dispersive contributions of the surface tension of the polymers and fillers, estimation of the interfacial tension can be achieved via Equation 1-21 and Equation 1-22. Equation 1-21 is the geometric average based on Fowkes theory, which is more suitable for filled polymer systems with high differences in surface energy. Equation 1-22 is the harmonic average based on Wu theory, which is more accurate for neat polymer blends with small differences in surface energy (Plattier *et al.*, 2015; Roman *et al.*, 2017).

$$\gamma_{1-2} = \gamma_1 + \gamma_2 - 2\sqrt{\gamma_1^d \gamma_2^d} - 2\sqrt{\gamma_1^p \gamma_2^p} \quad \textbf{Equation 1-21}$$

$$\gamma_{1-2} = \gamma_1 + \gamma_2 - \frac{4\gamma_1^d \gamma_2^d}{\gamma_1^d + \gamma_2^d} - \frac{4\gamma_1^p \gamma_2^p}{\gamma_1^p + \gamma_2^p} \quad \textbf{Equation 1-22}$$

1.5.2.4 Inhomogeneously modified Janus particles

The distribution of nanoparticles is governable by changing their wettability, for the thermodynamical factor often plays a dominant role. Young's model concludes that the particles can only be localized at the interface if the absolute value of the difference between the two interfacial tensions for the nanoparticles with the bulk polymers is weaker than that between the two polymeric phases (Fenouillot *et al.*, 2009). The strict demand needs a relatively precise surface grafting towards the particles, of which the formula conventionally originates from trial-and-error experiments. In addition, the specific surface-modified nanoparticles only fit particularly limited biphasic systems.

In order to overcome the situation, inhomogeneously modified Janus nanoparticles (JNPs) act as a combination of the advantages of particles (Pickering effect) as well as BCPs (amphiphilicity), with two distinct surface natures. The term Janus is a reference to the Roman god, who has two faces towards two opposite directions. The first synthesis of Janus particles was conducted in 1980s by Cho and Lee (1985). Janus nanoparticles can strongly adsorb and orient at the polymer interface. Based on the molecular simulations, it has been demonstrated that the Janus nanoparticles have a higher surface activity, compared with other homogenously modified surfactants (Yang and Loos, 2017). In the beginning, Binks and Fletcher (2001) compared two types of spherical particles in the fluid-fluid interface, of which one is a homogeneous surface of uniform wettabilites and the other is a Janus particle with two surface regions of differing wettabilities. It was found that Janus particles keeps violently more significant surface active for average contact angles near 0 or 180° compared with the other kind

of particles. Although the system is based on the fluid-fluid interface instead of the polymeric interface, it still provides a similar analogy.

Furthermore, JNPs can still work efficiently under high shearing conditions (Walther *et al.*, 2008). So far, the Janus particles have realized various architectures displayed in Figure 1-10 (Walther *et al.*, 2013), from simple spherical structure towards the more complicated shapes, including cylindrical, disc-shaped, dumbbell-shaped particles and even Janus vesicles or capsules.

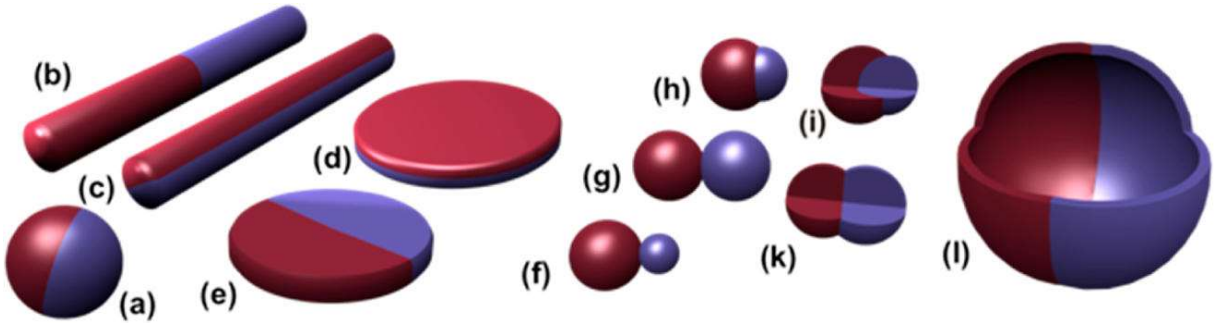

Figure 1-10 Different shapes of Janus particles (a) spherical , (b, c) two types of cylindrical, (d, e) disc-shaped JPs, (f–k) various kinds of dumbbell-shaped JPs with (f) asymmetric or snowman character, (g, k) symmetric appearance, (h) attached nodes, and (i) eccentric encapsulation. (l) Janus vesicles or capsules (Walther *et al.*, 2013).

So far, there have been bursting numbers of reports about the adoption of Janus particles for polymer blends (Bahrami *et al.* (2014, 2017); Bryson *et al.*, 2015; Walther *et al.*, 2008; Wang *et al.*, 2015). The difficulty exists in how to break the symmetry of particles, because the realization of industrialization is hard. One possible method is breaking the symmetry of the particle skeleton. Parpaite *et al.* (2016) fabricated a snowman-like Janus particle, connected with PS and SiO_2, in order to compatibilize the polystyrene (PS)-polyamide-6 (PA6) blend. The related SEM images are displayed in Figure 1-11 (Caro *et al.*, 2017), and the snowman-like structure can be clearly observed. Xu *et al.* (2017) also adopted snowman-like particles with the asymmetrical grafted chains to compatibilize the liquid isoprene rubber-epoxy resin. Nie *et al.* (2018) grafted

synthetic silica nanosheet by PS and polyisoprene (PI) chains for the compatibilization of PS-PI blend.

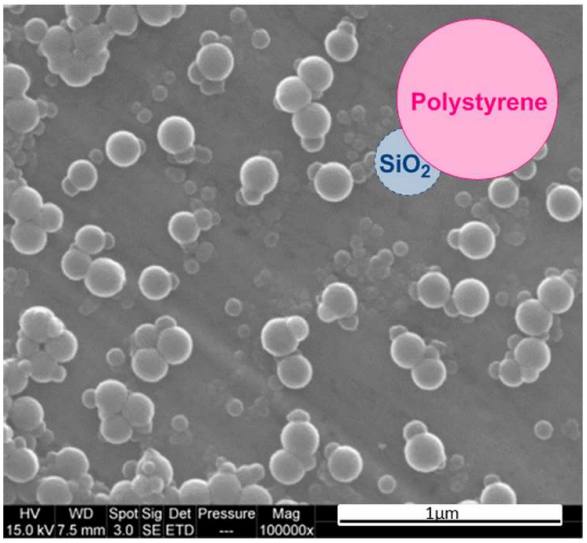

Figure 1-11 SEM images of the snowman-like Janus particles of PS and SiO_2 (Caro *et al.*, 2017).

In fact, some natural fillers exhibit an inherent chemical nature asymmetry which provides the feasibility to tailor regioselectively the surfaces. Most efforts have been made to the high-aspect-ratio clay derivatives, for example, halloysite nanotubes (HNTs) and kaolinite. It is worth noting that not all of the clay derivatives have the inherent Janus properties, and for example, montmorillonites are symmetrical without Janus properties (Weiss *et al.*, 2013). Halloysite nanotube has aluminol groups at the inner surface as well as silanol groups at the outer surface. Sahnoune *et al.* (2017) utilized PS regioselective functionalized halloysite to compatibilize the PS-PA11 blend.

Kaolinite is one sort of phyllosilicate (layered aluminosilicate), with the molecular formula as $Al_2Si_2O_5(OH)_4$. It has dioctahedral 1:1 layered silicate (polar lamellae), which is stacked and held together because of hydrogen bonds. One tetrahedral layer of silica (TS layer, SiO_4) is linked via common apical oxygen atoms with one octahedral layer (OS layer, $AlO_2(OH)_4$) (Sato *et al.*, 2004). Weiss *et al.* (2013) tailored kaolinite via polymer chains in order to fabricate hybrid particles with Janus properties. The

scheme of the modification process is shown in Figure 1-12. The regioselective modifications were achieved for one side by simple cation exchange via poly(2-(dimethylamino)ethyl methacrylate)-block-polystyrene (PDPS) cations, also for the other side by covalent grafting with catechol groups via poly(3-(2,3-dihydroxybenzoyloxy)propyl methacrylate)-stat-(methyl methacrylate) (PCM). Alumina-catechol bonds exhibit much more stability than silica-catechol bonds, contributing to the selective modification of aluminol group with catechol group under the aqueous condition. The Janus kaolinite particles grafted with PS and PMMA were utilized to compatibilize PS-PMMA blend via a solvent casting process. Nevertheless, the treatment of both sides of kaolinite is complicated, which is hard for industrialization.

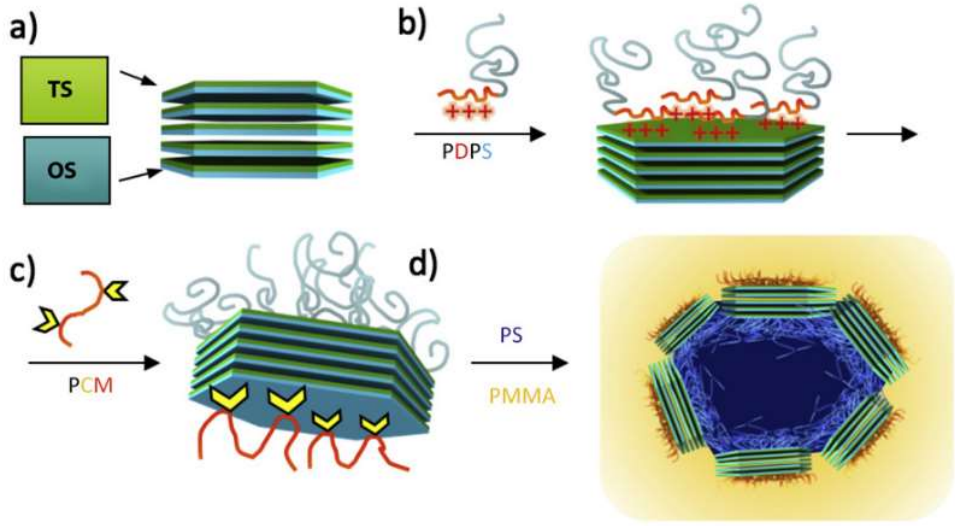

Figure 1-12 Scheme of (a) the pristine kaolinite; (b) the modification of the tetrahedral surface (TS) by PDPS; (c) the modification of the octahedral surface (OS); (d) the incorporation of the modified kaolinite towards the biphasic interface of PS and PMMA (Weiss *et al.*, 2013).

1.6 Melt processing methods

There are varieties of methods to manufacture the polymer materials into different shapes, which can be beneficial for the special use in the distinct areas. One important branch is the melt manufacturing, including melt extrusion, melt spinning, melt electrospinning, etc.

1.6.1 Melt extrusion

Hot melt extrusion (HME) is a standard technology to blend two polymers in the molten state, which can be followed with other downstream melt processing methods (e.g. melt spinning, injection molding). There are mono-screw and twin-screw extruders, of which the latter can provide a fiercer shearing force to reach a more high-efficient blending. The concept of a self-wiping co-rotating twin-screw extruder was invented in the beginning of the 20th century, and the intermeshing co-rotating twin-screw extruder was commercialized since 1939 (White and Bumm, 2011). It has been developed as a very easy technology to be scaled up from the laboratory to the industry, which can reach to as high as 60 tons per hour output (Douroumis, 2012). It is worth noting that prior to the melt compounding procedures, it is suggested to dry the raw materials in advance to avoid the influence of the water evaporation.

The scheme of a co-rotating intermeshing twin-screw extruder was displayed in Figure 1-13. The polymers with additives are fed into the machine, going through several steps, including solid feeding, melting, pumping, and even reaction (Hyun *et al.*, 2011). A melt extruder is consisted of a barrel for heatment, composing one or multiple screws which are responsible for conveying, coumpounding and finally forcing the polymer through a die to form the extrudates. The materials are fed through the feeding port and compounded by the screws rotated by the shaft. The twin-screw is normally divided into several zones, including solid conveying, melting, melt conveying and mixing. As for the materials, they undergo the mixing, grinding, the particle size reducing, venting and kneading (Maniruzzaman, 2015). In the extruder, the polymers are melted in the barrel system via mechanical energy from the rotating

screws as well as heat transfer from the heated barrels (Zhu and Geng, 2002). The flow goes out through the die and the cooling step is needed to solidify the rods, normally by the gas (air, etc.) or the liquid (water, etc.). Finally, the rods are cut by the specific machine into pellets, convenient for the downstream manufacturing.

For the biphasic polymers, the morphology of the minor phase is significantly more influenced by the die rather than by the phenomena occurring before it. The high shear rate near the die wall is in favor of the extended structures. Also the viscosity and elasticity ratios determine the fibrillar formation as well (Favis and Therrien, 1991). The composition also plays a remarkable role in the dispersed phase size, especially at the intermediate concentrations near co-continuity (Favis and Chalifoux, 1988).

Maniruzzaman (2015) summarizes some drawbacks of melt extrusion, which should be taken into consideration. The melt extrusion is a non-ambient processing technique, and it requires a high energy input. The flow properties of the polymers are essential, and the heat sensitive materials cannot be utilized. In addition, the polymers with a lower melting point lead to the softening and agglomeration for the products. For polymers with a higher melting point, the thermal degradation temperature should be considered to prevent the decomposition during melt manufacturing. Generally speaking, the selection of polymers is limited.

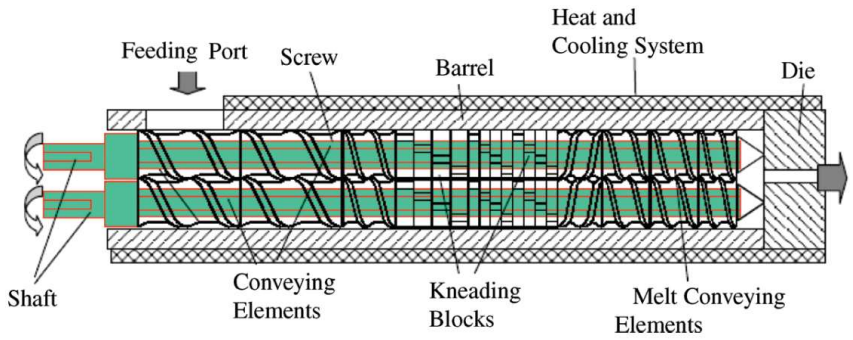

Figure 1-13 Scheme of a co-rotating intermeshing twin-screw extruder (Hyun *et al.*, 2011).

1.6.2 Melt spinning

There are two basic methods to commercially fabricate the synthetic fibers, including melt and solvent fabrication. The melt fabrication is known as melt spinning, while the solvent fabrication can be divided into two branches, wet spinning and dry spinning. The scheme of the three methods of fiber manufacturing is displayed in Figure 1-14 (Imura *et al.*, 2014). Wet spinning is the technique with the longest history. The fiber-forming polymer is dissolved in the solvent. The spinnerets are immersed in the coagulation bath, and fibers are solidified in the solution. Dry spinning is also a solvent fabrication, and the solvent is solidified by evaporating with the aid of hot gas stream, normally air in the evaporating cabinet. For melt spinning, the fibers are manufactured from the melted polymer solidified by cooling, which is the most economical method.

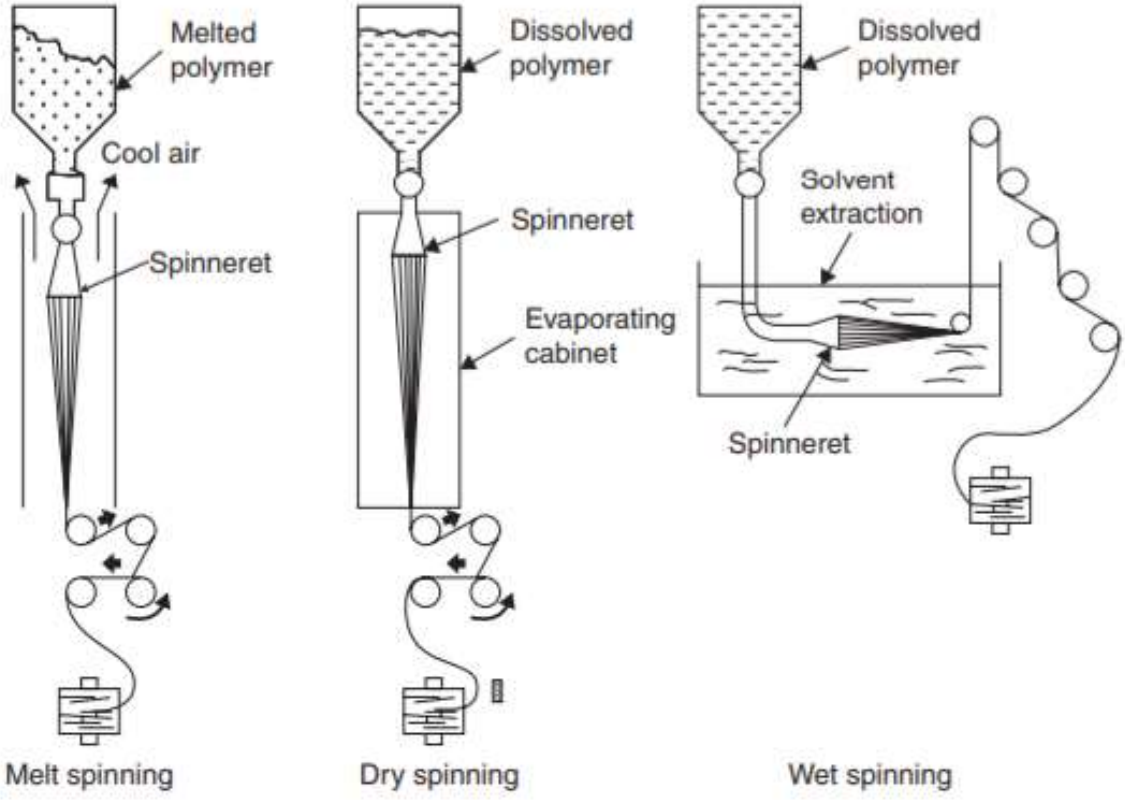

Figure 1-14 Scheme of melt spinning, dry spinning and wet spinning (Imura *et al.*, 2014).

For meltable polymers for which it is difficult to find a suitable solvent, melt

spinning is the most conventional method, for example, polypropylene (PP), polyethylene (PE) and polyethylene terephthalate (PET). Melt spinning can manufacture the yarns, working as a bridge from polymer to textile fields. The polymer pellets are introduced into the hopper with the aid of extruder over the melting temperature of the polymer blend. The heating is divided into several steps to make the polymers better melted. The extruded polymer is pumped through a spinneret and quenched with the cooling air. The as-spun filaments are followed with the further drawing to achieve the alignment of the molecular orientations in the fiber direction. The drawing is conducted over the glass transition temperature of the polymers to ensure that the materials are in the rubbery state. As a result, more satisfactory mechanical properties can be obtained. The draw ratio is the value of the draw roll speed divided by the feed roll speed. In addition, normally the fibers are coated with a specific spin oil in order to achieve better cohesion and lesser electrostatic effects (Didane *et al.*, 2012). In the end, the manufactured multifilament yarns are collected by the bobbins. There are some constraints which should be considered during melt spinning. The drawbacks of melt extrusion are one of the main factors, which has been introduced in the “melt extrusion” part. In addition, the viscosity of the polymer should be controlled within an appropriate range, controlled by the selection of the materials as well as the experimental temperatures. In addition, the high shearing rate and elongation force are the challenges for the fiber spinnability, of which the steady-state conditions are based on the physical balance equation of mass, energy as well as momentum (Rawal and Mukhopadhyay, 2014). For the biphasic polymer spinning, apart from the shearing force, the extensional flow also dominates to transform the minor phase into a more elliptical structure. The isolated droplets are elongated into microfibers, enhanced by the draw ratios.

1.6.3 Melt electrospinning

Apart from the conventional apparatus of polymer manufacturing, the electrospinning is also becoming popular in the current researches since 1990s. It can

be classified into two categories, one is melt electrospinning, and the other is solution electrospinning. Solvent electrospinning is the most common choice among the two categories, for the equipment is simpler and the restriction for the polymers are less strict. However, it brings about the residual or the release of organic solvent, which is not good for the manufacturers' and users' health. Melt electrospinning is a useful strategy to effectively avoid the usage of organic solvent, therefore, it is regarded as a greener method. The devices of the melt and solvent electrospinning are displayed in Figure 1-15 (Lian and Meng, 2017). The commonly used parts are composed of a heating element, a high voltage supplier, a nozzle as well as a collecting plate. The main difference originates from the solidification during the direction process of electrospinning (Detta *et al.*, 2010). For the solution electrospinning, the solidification process is based on the evaporation of a solvent, while for the melt electrospinning, the solidification process is based on the cooling. It determines that the ventilation systems are not needful, and the systems can be sealed. So far, the melt electrospinning still needs in-depth exploration, and for the literature part less than 1% of electrospinning literature is concerning the melt technology. Although compared with solvent electrospinning, the melt electrospinning tends to produce microfibers rather than nanofibers, it provides an alternative strategy to fabricate the fibers in a greener way. In addition, with the assistance of gas, the solidification process can be delayed. As a result, the fibers can be further deformed to achieve a thinner diameter. Zhmayev *et al.* (2010) fabricated the PLA nanofibers by this gas-assisted method.

For the immiscible polymer blends, the most reported manufacturing process is by the solvent electrospinning. For the melt electrospinning, the related reports are still rare. Generally speaking, the electrospinning is of high cost and low producibility, and it should undergo a long-term development for the further scale-up methods in the future. So far, the conventional spinning technology (melt spinning, wet spinning, etc.) is still the mainstream strategy for manufacturing the fibers in the industry.

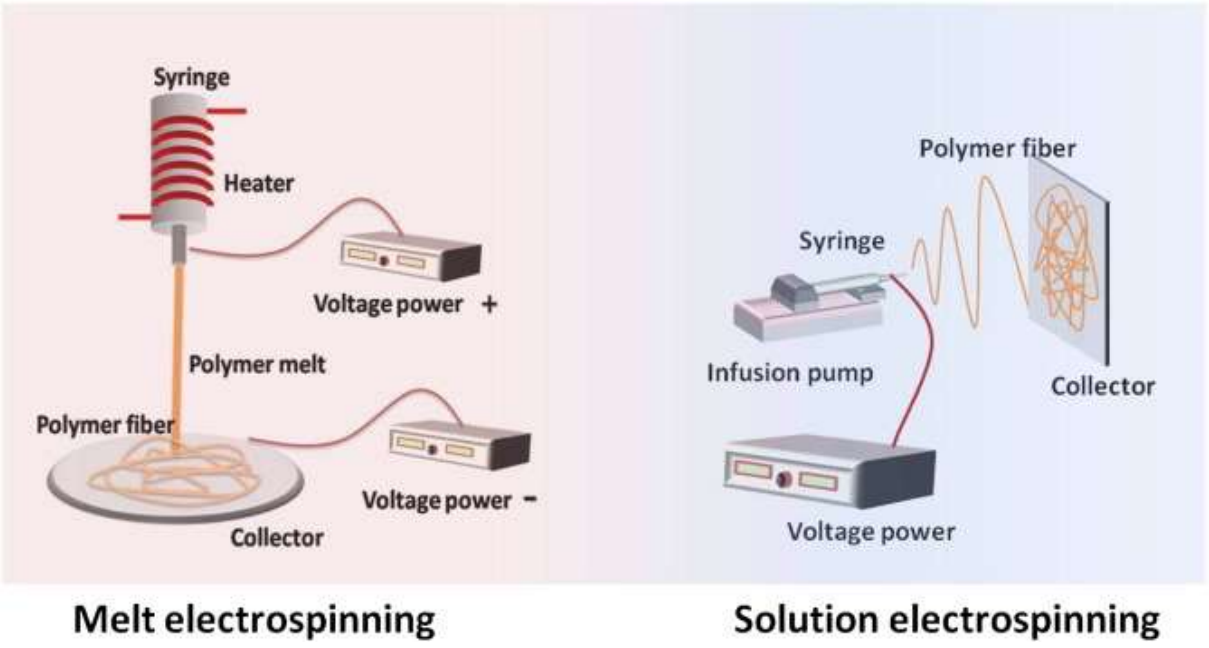

Figure 1-15 Devices of melt electrospinning and solution electrospinning (Lian and Meng, 2017).

1.7 Fabrication of fibers from polymer blends

Polymeric fibers are closely related to people's lives, and have been derived as important subject of the scientific research. The polymer can be manufactured into many forms, among which the fibrous form is attractive due to its high specific areas, which can be utilized in many domains. Similarly, the fabrication of fibers composed of binary polymers has also been vastly investigated. Melt blowing, electrospinning and melt spinning can be adopted. Melt spinning technology, for its high output, is the most conventional strategy.

1.7.1 Melt spinning of binary blends

The binary polymers are melt-extruded with a twin-screw extruder to achieve a better mixing state as an upstream of melt spinning, and the brief introduction of extruder can be found in the previous part 1.6.1. The melt mixing process contributes to the various biphasic morphologies of the immiscible blends, including drop, double emulsion, laminar, fiber, co-continuous or ordered microphases. Every specific

structure has its own characteristics, which signifies the importance of the tailor of biphasic morphology. The scheme of the biphasic morphologies is displayed in Figure 1-16. For example, if a good a barrier property is expected to be realized, the laminar morphology is an optimized selection (Macosko, 2000).

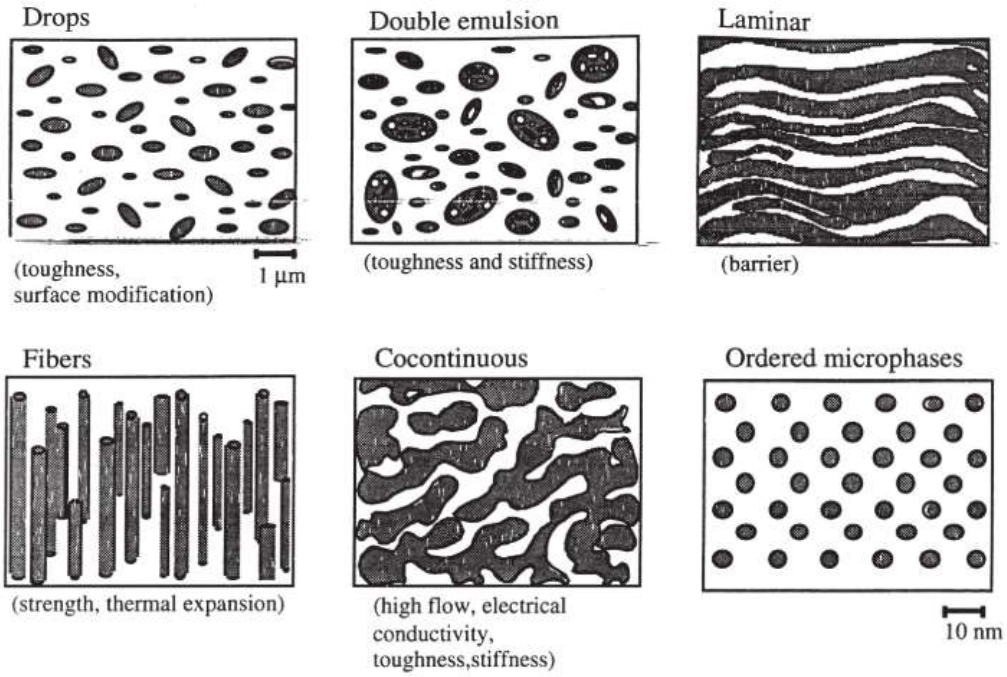

Figure 1-16 Scheme of the biphasic morphologies for specific usages (Macosko, 2000).

Melt spinning is one of the main strategies to manufacture upstream fibers for textile usage, which is rapid, cost-effective and large-scale. When the biphasic polymers are manufactured into fibers with the aid of melt spinning technology, the microstructure undergoes significant changes, which is different from other kinds of processing methods. Wang and Sun (2007) provided a detailed description about the related behaviors. The blend extrudates are fed into the hopper followed by a single screw at a high temperature (over the melting temperature). The minor phase divides in small droplets at this step. Afterwards, the binary mixtures arrive and cross the die inlet, and the polymer undergoes a continuous elongational flow field. Afterwards, the minor

phase is deformed into elliptical shape and transformed into fibrous structures. More internal nodules get connected with the external nodules.

Many researches are dedicated to the fabrication of mixed fibers originating from polymer blends (Li *et al.*, 2015; Muraoka *et al.*, 2001; Wang *et al.*, 2017a). Melt spinning of polymer blends provides the fibers with matrix-fibril morphology (He *et al.*, 2014), and it has already become a practical method to manufacture micro-/nanofibers via the matrix etching. Tran *et al.* (2014a, 2016a, 2016b, 2016c) investigated the impacts of the experimental conditions and demonstrated mathematical simulations concerning the melt spinning of the blends from poly(lactic acid) (PLA) and PVA with the mass ratio of 30wt.%/70wt.%. It was found that the spherical or ellipsoidal dispersed PLA nodules get elongated and coalesced into rod-like or ellipsoidal morphology, while passing through the capillary die. The micromorphology of PLA phase is tailored by the spinning conditions, determined not only by the deformation of the initial sizes, but also by the comprehensive combination of the deformation, coalescence as well as breaking up. The scheme of the fibrillation process in the elongational flow along with the splinnline was also summarized by Tran *et al.* (2014a), displayed in Figure 1-17. It illustrates that the PLA phase is stretched and coalesced as continuous long thin nanofibers. The velocity increases along with the spinnline, rapidly reaching to the maximum and keeping stable. The phase inversion of dispersed phase from short fibers/rod-like morphology towards long thin fibers occurs within the region of the maximum axial velocity gradient. It was found that the increment of velocity and tensile stress within the fiber forming zone is dominant factors influencing the stretching and coalescence of the dispersed phase further into the nanofibers in the matrix phase.

If one of the phases can be removed by the solvent, it gives a possibility of fabricating the porous fibers and microfibers, both of which have a relatively high specific area.

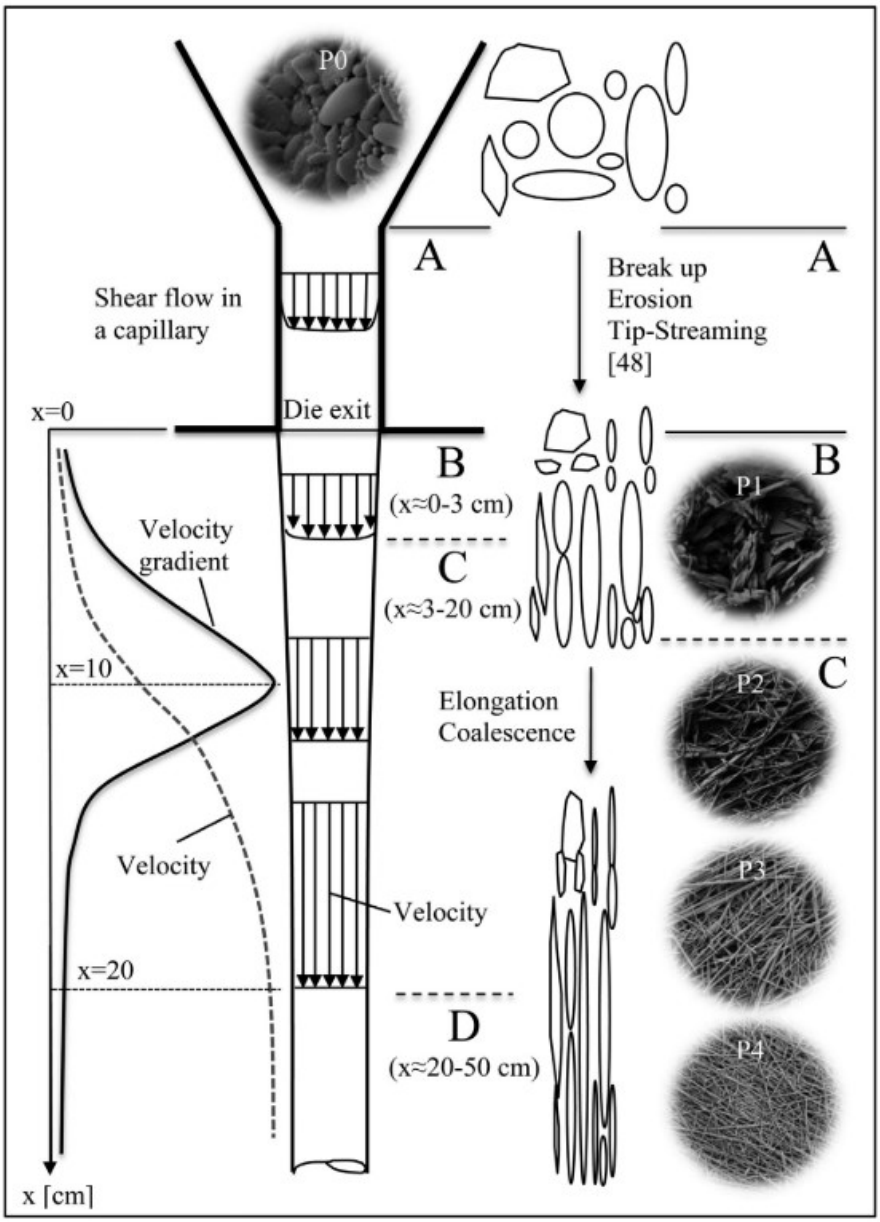

Figure 1-17 Mechanisms of fibrillation process in the elongational flow along with the spinnline in a certain condition (the diameter (D_0)=0.6 mm with aspect ratio (L/D_0) =2 of the capillary hole, volumetric flow rate (V)=0.78 cm^3/min, take-up speed (v)=50 m/min, T=195°C) (Tran *et al.*, 2014a).

1.7.2 Porous structures

Apart from stabilizing the polymers, the nanoparticles can also give materials additional functionality, for example, flame-retardant (Gilman, 2007; Qiu *et al.*, 2003), electrical (Cho *et al.*, 2004; Jiang *et al.*, 2014), antimicrobial (Palza, 2015; Son *et al.*,

2006) and mechanical (Guo *et al.*, 2006; Guo *et al.*, 2016) enhancement.

The porous structure is an attractive design for it provides a high specific area. It has been adopted in many technical fields, such as antimicrobial (Mural *et al.*, 2018; Sun *et al.*, 2016), tissue engineering (Xu *et al.*, 2015; Yao *et al.*, 2006), desalination and protein separation (Mural *et al.*, 2018). There are several approaches to fabricate the porous structures, including phase separation, fiber bonding, particulate leaching, melt bonding and gas foaming (Sarazin *et al.*, 2004; Zhang *et al.*, 2010). Sometimes, the related approaches can be combined to get rid of some drawbacks of a single specific method (Ko *et al.*, 2015; Peng *et al.*, 2016). In many cases, the toxic organic solvents participated the reactions and may remain in the matrix, which is frequently unavoidable. It brings about the damage to the health of the manufacturers and users. Among the approaches, melt blending technology is a cost-effective and non-solvent process, which is carried out in two steps, i.e., (1) sacrificial and target polymers are compounded at melting state free of any solvent, and (2) the sacrificial phase is removed by a solvent to obtain the porous structure.

The introduction of nanofillers can be utilized not only for the binary blend, but also for the porous materials. The porous materials have a very high specific area to embed the nanofillers. Some researchers adopted post-treatment method to endow the porous materials with additional properties. For instance, de Luna *et al.* (2014) immersed the microporous high-density polyethylene (HDPE) into suspension of zinc oxide nanoparticles to functionalize the inner surface. However, it needs an additional step which is inconvenient. Furthermore, a permanent effect is hard to guarantee. Naturally, a single-pot strategy can be proposed: Nanoparticles are incorporated into the polymer blends via melt compounding and located at the interface, and the porous structure with surface-embedded nanofillers is fabricated after the selective phase extraction of the sacrificial phase.

As a matter of fact, some investigators have made efforts in the same direction to produce the porous materials containing nanofillers. Zhang *et al.* (2010b) made a tertiary polymer blend composed of poly(glycolic-co-lactic acid) (PLGA)/ polystyrene

(PS) and hydroxyapatite (HA). The HA particles immigrated from the PS phase towards the PLGA phase during annealing under small-strain oscillatory, and the HA particle within the PLGA phase was over 30wt %. After the removal of PS phase, the porous PLGA with HA particle was obtained. Baklavaridis *et al.* (2014) made a ternary blend from PLGA/Polystyrene (PS) with orgainically modified montmorillonite (Cl15A), followed by the selective phase extraction of PS phase. It has been found that a high content of the clay mineral was inside the matrix of PLGA, which also mechanically reinforced their walls. The porous PLGA porous material is a good candidate for tissue engineering. Mural *et al.* (2014, 2015) compounded PE/PEO blends with modified graphene oxide to produce the antibacterial membranes for the application of water purification. Li *et al.* (2011a) utilized carbon black as well as carbon nanotubes to increase the electric conductivity of porous PP, which is made from the blend of PP and PS by extracting the PS phase by cyclohexane. Zhang *et al.* (2010a) incorporated nanodiamond into porous poly(lactic acid) (PLA) structure from PLA/PS blends. The nanodiamond particles diffuse from PLA towards PS phase during annealing. These nanoparticles are localized in bulk polymeric phases, rather than at the interface of the biphasic polymers.

As for the multifilament yarns, there are a few reports. Reddy *et al.* (2008) mentioned the gradual dissolution of PLA phase from PP/PLA biphasic fibers to produce the porous PP fibers, and this kind of material can be utilized as orthopedic implants. Sumanasinghe *et al.* (2010) fabricated the porous PLA fibers from melt-spun PLA/sulfonated copolyester (SP) blends by selective phase extraction for the tissue engineering applications. The SP content was adjusted as 1, 3, 5 and 10%, and it was found that the size of the porous structure was varied by the SP content.

1.7.3 Microfibers

The application of microfibers includes reinforcement component of composite materials, biomedical uses (e.g. tissue engineering, drug delivery), filter materials, etc. (Fakirov, 2014). There are several conventional methods to fabricate the microfibers,

melt blowing, melt spinning and electrospinning. Melt blowing becomes more and more popular in the current time, but it is only adapted to fabricating the non-woven or webs instead of the multifilament yarns. Electrospinning is also a research hotspot, but its output is very low and limited in the lab scale. With the researchers' efforts, the production rate can be increased by several methods, for example, using multiple nozzles, gas flow, or updating to some specific electrospinning machines without nozzles (Qin, 2010), but its production rate is still not comparable to industrial spinning equipment. In addition, it is not an easy task to handle the spun candidate.

The melt spinning of bicomponent fiber is a possible way as well, which is divided into two different strategies, one is the fabrication of splittable segmented bicomponent fibers (e.g. pie wedge, islands/sea), and the other is the fabrication of melt-blended biphasic fibers. The splittable segmented bicomponent fibers are manufactured by the bicomponent melt-spinning device with special spinneret. In contrast, the fabrication of melt-blended biphasic fibers can be realized by the ordinary melt spinning device, which is more commercialized. For two-phase fibers from melt-spinning, if the sacrificial phase is the matrix phase, the microfibers can be obtained after the selective phase extraction. Also, some polymeric materials which are not suitable for electrospinning gain the feasibility to be manufactured into microfibers. This kind of research was carried out by some Japanese fiber factories since 1970 to fabricate the microfibers for luxury clothing. Min *et al.* (1984) fabricated the polystryrene (PS) and high density polyethylene (PE) blends into fibers and obtained the PE microfibers with the diameter as low as 0.2 μm after the selective phase extraction of PS by toluene, and they attributed the low interfacial tension compared with other polymer pairs to the key to obtaining finer fibers.

In the recent time, Fakirov *et al.* (2007, 2013, 2014, 2018) have conducted extensive research on the spinning of biphasic polymers. Meanwhile, the idea of a "conversion instead of addition concept" has been proposed, as the dispersion problems of nanomaterials can be overcome by transforming the polymer into a nanofibrillar structure during the manufacturing process.

The series of studies was based on the idea of manufacturing microfibrillar composites (MFC) in situ (Evstatiev and Fakirov, 1992), which represents the immiscible blends with dispersed phases in microfibrillar morphology. It offers a feasibility to fabricate the in situ self-reinforced as well as self-toughen materials (Wang and Sun (2007)). The hot treatment temperature should be in between the two melting temperatures of the two polymers. Therefore, the microfibrillar phase can keep their original shape during the melting of the matrix phase. MFC materials conventionally have the polymeric microfibrils with diameters in less than 1 micrometer as well as the length of several hundreds of microns. Similar with other kinds of nanocomposites, the MFC can achieve the enhancement of mechanical properties as about 25%-50% (Schaefer and Justice, 2007).

With the development of the related research, it is then derived from the idea of making autonomous microfibers by extracting the matrix phase, which can then be used in biomedical fields. Wang *et al.* (2007) first adopted PP as a dispersed phase for the manufacture of polypropylene microfibers by melt extrusion, drawing, and selective phase extraction. It was found that the design could further reduce the diameter of the microfibers. In general, the mixing ratio, as well as the draw ratio, are the dominant factors in the determination of microfiber diameters (Zuo *et al.*, 2013). If finer microfibers are expected, a low fraction of dispersed phase and a high draw ratio are preferred.

The selective phase extraction can also be placed after the production of the knitted fabrics from the yarns. Fakirov *et al.* (2014) illustrated a case for the fabricating the fabrics of PET microfibers, as indicated in Figure 1-18. The detailed process is to fabricate the fibers of PP/PET blends of which the mixing ratio is 80 wt.%/20 wt.%. For PP can be well dissolved by the organic solvent xylene at a high temperature, the authors utilized the solvent to remove the PP phase. As a result, the PET fibers were exposed after the removal of PP, and the PET microfibers were successfully prepared.

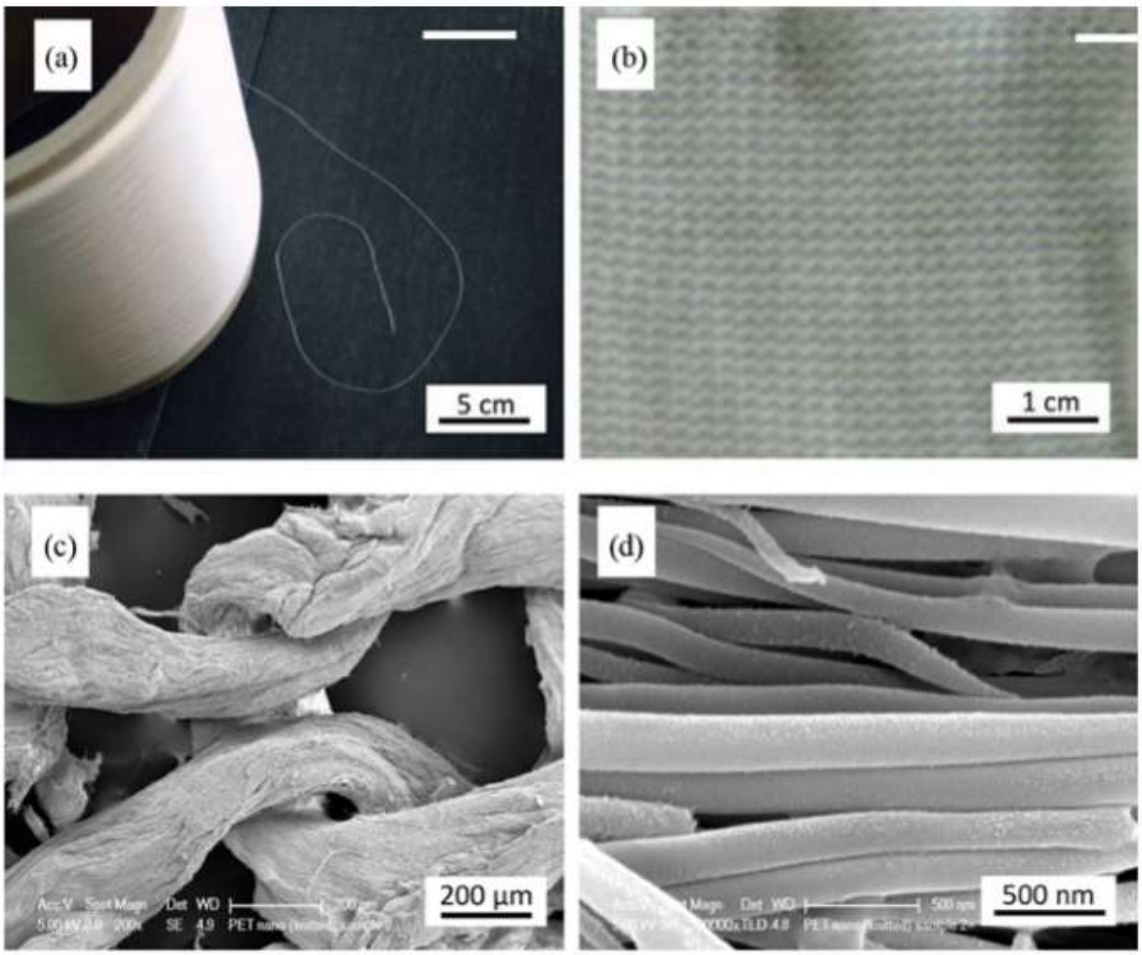

Figure 1-18 Image of (a) the multifilament yarns from polypropylene/poly(ethylene terephthalate) (PP/PET) with the diameters of 30 micrometers; (b) the knitted fabrics from the PP/PET yarns; (c) SEM of the knitted yarns after the selective phase extraction (d) the zoomed image of (c) (Fakirov *et al.*, 2014).

Robeson *et al.* (1994) initially used the polymer-PVA blends to fabricate microfibers. The approach is to blend PVA and the other polymer candidate by melt extrusion followed by post orientation. The microfiber with the diameter of 0.1-5 µm was manufactured, including PP, PVA, polystyrene (PS), polyethylene (PE), poly(vinylindence fuloride) (PVDF), cellulose proprionate, as well as a elastomer from poly(butylene terephthalate)-polytetrahydrofuran block copolymer (Hytrel 4056, DuPont). The recycled polymer scrap (polymer mixtures) was also successfully utilized to fabricate microfibers, while PVA solution was proved that it is also partially

recyclable. PVA was revealed to be an effective material to yield the microfibers. As for PP-PVA blends, the mass ratio of PP and PVA is 50/50, and the SEM images of PP-PVA fibers before and after selective phase extraction are displayed in Figure 1-19. The draw ratio is set as 2.2, and the tenacity of the blend fiber bundle can reach 20900 psi (144 MPa, 13.6 cN/Tex). After the selective extraction, the fibers were obtained and their diameters are about 1 μm (0.03 denier).

Although there have been various literatures concerning the microfiber fabrication by selective phase extraction of biphasic fibers, the reports about incorporation of (nanoparticles) into the strategy are rare.

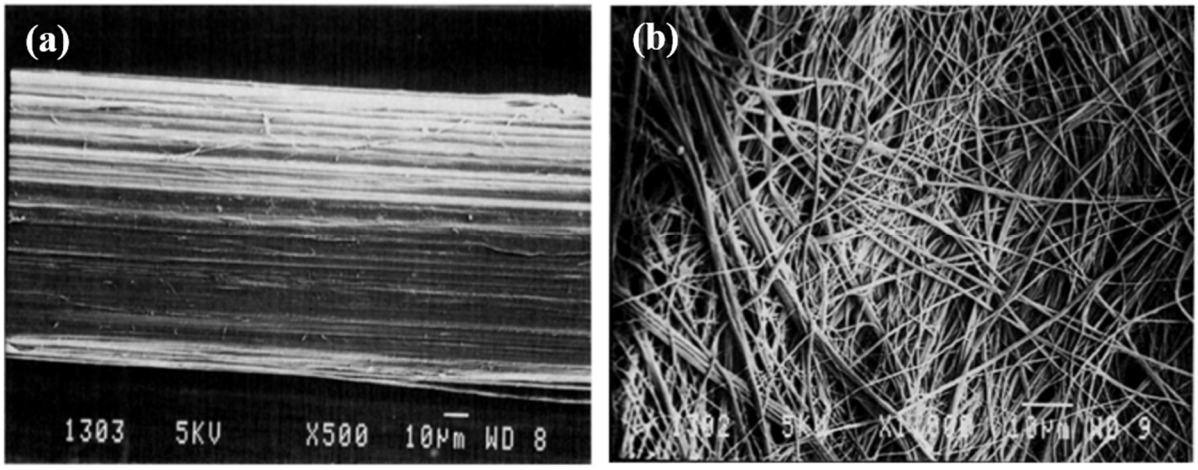

Figure 1-19 SEM images of PP-PVA fibers (50 wt.%/50 wt.%)(a) Before extraction; (b) After selective phase extraction (Robeson *et al.*, 1994).

1.8 Conclusion

Through the literature review, it is found that the importance of polypropylene in polymer industry. In addition, it is revealed that the immiscible polymer blending is a common strategy to fabricate the materials with combined properties. Many factors determine and also provide the feasibility to predict the biphasic morphology, for example, viscosity and elasticity ratios, the surface tension, the storage moduli. The meltable polymers are poly(vinyl alcohol) (PVA/PVOH), polyoxyethylene (POE), sulfopolyester (SP), and so on. There have been many cases to be blended with another

polymer to fabricate the immiscible blends. To increase the interface quality of the polymers, varieties of compatibilizers are incorporated into the systems, started with the traditional compatibilizers and gradually evolved into the (nano)particles. Afterwards, the Janus particles were applied within the biphasic polymer systems with their outstanding selectively absorption properties at the interface. Melt processing methods contain melt extrusion, melt spinning, melt electrospinning, etc. At last, the fabrication of biphasic fibers was introduced, and it gives the feasibility to fabricate the porous fibers as well as the microfibers after the removal of the sacrificial phase.

Some researchers (Strecka *et al.*, 2010; Ku and Lin (2005, 2014)) have made efforts to expand the application of polyolefin-PVA by the melt spinning process. Compared with their research, our study aims to reveal the regularity of the morphology evolution of the biphasic fibers and accompanied changes in the mechanical behaviors, which is still lack of reports to our knowledge. In addition, no study reports the feasibility of manufacturing porous fibers and textiles, taking advantage of the water solubility of PVA. Therefore, our work was began with the discovery of the optimized ratio of PP and PVA to fabricate the porous fibers.

Some researchers (Zhang *et al.*, (2010a, 2010b); Baklavaridis *et al.*, 2014; Mural *et al.*, (2014, 2015); Li *et al.*, 2011a) have made some efforts in this direction to design nanoparticle enhanced porous materials, but these nanoparticles are dispersed in bulk phases rather than at the biphasic interface. In addition, there are hardly any reports concerning the morphological regulation of PP-PVA blends by adding nanofillers. The efforts were made to localize the silica nanoparticles at the interface and produce the surface-tailored porous PP fibers.

Compared with conventional homogenously modified particles, the Janus particles may bring less trial-and-error experiments to be selected for the interfacial localization. Furthermore, there is no study on the application of Janus particles in melt spinning until now. Herein, efforts are made to extend the application of Janus particles into textile areas. Based on the investigations, two kinds of fillers were selected, one kind is homogenously modified silica nanoparticles, the other kind is Janus modified kaolinite

particles.

It is worth noting that the modification of both sides of kaolinite seems complicated and costly, which is not beneficial for industrial production. So far, there are not any reports about the use of single side modified kaolinite for compatibilizing immiscible polymer blends. In the thesis, the single side modified kaolinite was utilized.

In addition, there have been a large number of methods concerning the fabrication of the microfibers, including the melt-blended biphasic fiber manufacturing. However, most of the researches are based on the biphasic system without fillers. Therefore, in the thesis the efforts were made to fabricate the PP microfibers with the Janus kaolinite particles as an exploratory attempt.

Chapter II:

Materials and Experimental Methods

Chapter 2 Materials and Experimental Methods

In this part, the raw materials are described, including the polymeric materials as well as the particles. In addition, the experimental devices and related methods will be introduced in detail.

2.1 Raw materials

2.1.1 Polymeric Materials

Polypropylene (PP) (PPH 9069) was a commercial product from Total Enterprise (France). Its melting temperature is 168°C, with melt flow index (MFI) of 15 g/10min (200°C, 2.16 kg).

Two kinds of polyvinyl alcohol (PVA) were utilized. For the polymer blend with silica nanoparticles, OKS-8112P was utilized in the experiment. It was supplied by Nichigo Gohsei (Japan). Its melting temperature is 179°C, and the MFI is 30 g/10min (200°C, 2.16 kg). For the polymer blend with kaolinite particles, OKS-8042P was chosen, which was purchased from Nichigo Gohsei (Osaka, Japan, spinning grade), with the melting point of 178°C, with MFI of 23 g/10min (200°C, 2.16 kg). To distinguish the differences of the two PVA, OKS-8112P is denoted as PVA, and OKS-8042P is denoted as PVA*.

2.1.2 Inorganic particles

Two kinds of the particles will be used, including silica nanoparticles and kaolinite particles.

Three different silica nanoparticles were utilized in the experiments. The hydrophilic unmodified silica nanoparticles (Sigma-Aldrich® S5505, denoted as Si_{S5505}) with 14 nm of nanoparticle size were purchased from Sigma-Aldrich Company, and its surface area is 200 m^2/g. Meanwhile, two commercialized fumed silica nanoparticles

(Aerosil® R816, Aerosil® R972, denoted as Si_{R816}, Si_{R972}) manufactured by Evonik Company were likewise utilized. Si_{R816} and Si_{R972} were prepared from one kind of unmodified silica via silanization, surface treated with hexadecylsilane and dimethyldichlorosilane, respectively, showing different levels of hydrophobicity. The chemical structures of hexadecylsilane and dimethyldichlorosilane are illustrated in Figure 2-1. Their surface areas are 190 and 110 m^2/g, respectively, and the nanoparticle size 12 nm and 16 nm.

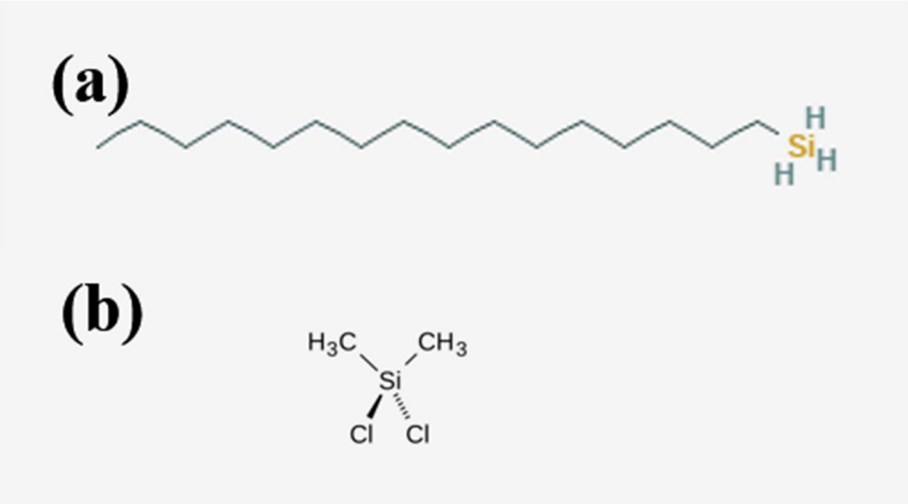

Figure 2-1 The chemical structures of (a) hexadecylsilane; (b) dimethyldichlorosilane (pubchem.ncbi.nlm.nih.gov., 2019; upload.wikimedia.org., 2019).

The kaolinite particles before and after modification were supplied by the collaborator Belkacem Otazaghine in Centre des Matériaux des mines d'Alès (C2MA), IMT, Mines Alès (Yan *et al.*, 2019). There is the detailed information: octadecylphosphonic acid (ODPA) was supplied by Specific Polymers (Montpellier, France). Ethanol and acetone were purchased from Fisher Chemical. Kaolinite (PARALUX®) with a specific surface area (BET) of 12.2 ± 1.5 $m^2.g^{-1}$, an aspect ratio α of 10 and an average primary particle size (d_{el}) of 0.8 μm was kindly supplied by Imerys (Paris, France) and denoted as KL. Surface treatment was carried out as follows: 100 g of kaolinites, 2.5 g of ODPA and 300 ml of an ethanol/water mixture (96/4) were introduced in a 500 ml flask fitted with a condenser. The mixture was then stirred and heated at solvent reflux for 15 h. The mixture was then centrifuged to remove the liquid

phase and washed three times with acetone. Finally, the modified clay was dried under vacuum before characterization. Surface treated kaolinite is referred as KJ. The synthesis of Janus kaolinite particles is schematically represented in Figure 2-2.

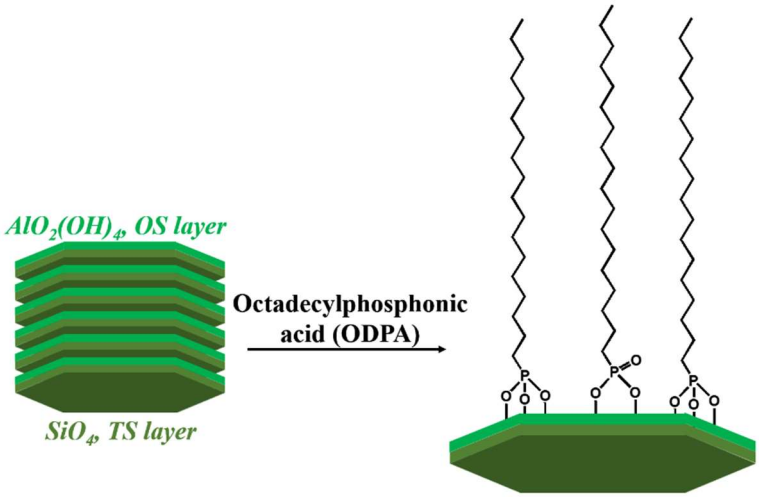

Figure 2-2 Scheme of the synthesis of Janus kaolinite particles.

All of the raw materials were used as received.

2.2 Sample preparation

2.2.1 Melt extrusion of the polymers

All of the materials were melt-mixed into blends by means of a co-rotating intermeshing twin-screw extruder (Thermo Haake, screw diameter=16 mm, L/D=25). The scheme of melt extrusion is displayed in Figure 2-3. The raw materials were dried in the oven at 80°C for at least 12h to get rid of the residual moisture. There are five heating zones near the screw, of which the temperature profiles were 160°C/170°C/180°C/190°C/200°C (T_1/T_2/T_3/T_4/T_5), with the screw rotational speed of 100 rpm. The extruded rods were constantly conveyed by the conveyer belt with the cooling air stream. Finally, the cooled rods were cut by the granulator and collected in the sample bags.

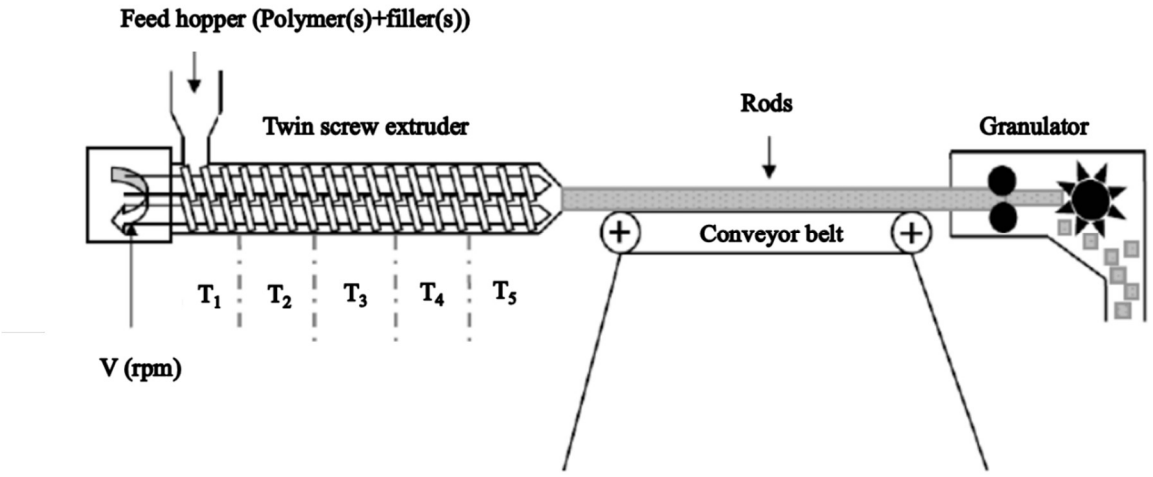

Figure 2-3 Scheme of the extrusion process of the PP-PVA blends without/with fillers.

First of all, in Chapter III, the polymer blends of PP and PVA without fillers were prepared. In order to achieve a high enough interconnectivity (accessibility) of PVA phase as a sacrificial phase, the minimum fraction of PVA is set as 30 wt.%. Different ratios (70/30, 60/40, 50/50 (wt.%/wt.%)) of PP and PVA were prepared. The material in the form of rods was obtained and rapidly cooled down by airstream, followed by cutting pelletization for further characterizations. Depending on the mass ratio differences, the pellet samples are denoted as PP_x-PVA_y, where the mass ratio of PP and PVA is x wt.%/y wt.%. For instance, PP_{60}-PVA_{40} represents the pellets composed of 60 wt.% of PP and 40 wt.% of PVA.

In Chapter IV, in order to explore the effects of different fumed silica nanoparticles, three kinds of silica nanoparticles were introduced into PP-PVA blends, Si_{S5505}, Si_{R816}, Si_{R972}. The same condition of extrusion in processing temperature and screw rotational speed was adopted. The mixing procedures were segregated into two steps (Figure 2-5). Firstly, the silica nanoparticles were precompounded with PP. Secondly, the prepared blends were extruded again with PVA, thus the blended PP-PVA-silica samples were obtained. The mass fraction of silica in the final blends was 1 wt.%, and meanwhile in order to better observe the regulation of the accessibility of PVA by the silica nanoparticles, a relatively lower fraction of PVA was selected. Therefore, the mass ratio of PP and PVA was fixed at 70 wt.%/30 wt.%. Similarly, the samples were cooled down

and cut into pellets. The samples containing hydrophilic Si_{S5505} silica nanoparticles and hydrophobic Si_{R816}, Si_{R972} silica nanoparticles are denoted as PP_{70}-PVA_{30}-Si_{S5505}, PP_{70}-PVA_{30}-Si_{R816} and PP_{70}-PVA_{30}-Si_{R972}. For comparison, the PP blended with silica nanoparticles without PVA for melt spinning were also manufactured. The ratio of PP to silica nanoparticles was set as 99wt.% to 1wt.%. The prepared pellets were denoted as PP-Si_{S5505}, PP-Si_{R816}, and PP-Si_{R972}, respectively.

In Chapter V, the mass ratio of PP and PVA* was fixed at 70/30 (wt.%/wt.%), whereas the weight fraction of particles (KL, KJ) was varied at two different fractions: 1 and 5 wt.% in total. The continuously produced extrudates in the form of rods were transported by a conveyor equipped with the cooling air stream. Afterward, the cooled polymer rods were pelletized, ready for the further melt spinning. For the ternary blends, the melt extrusion procedures were segregated into two steps. Firstly, the kaolinite nanoparticles were pre-compounded with PP. Secondly, the prepared blends were extruded again with PVA* to obtain the PP-PVA*-kaolinite ternary blends. The samples containing unmodified kaolinite (KL) and modified kaolinite (KJ) are denoted as PP_{70}-PVA^*_{30}-KL_x and PP_{70}-PVA^*_{30}-KJ_x, respectively. x represents the wt.% of filler in the polymer blends. The blend without fillers (denoted as PP_{70}-PVA^*_{30}) was compounded by one-step extrusion.

In Chapter VI, the mass ratio of PP and PVA* was reversed as 30/70 (wt.%/wt.%), denoted as PP_{30}-PVA^*_{70}. The weight fraction of particles (KL, KJ) is fixed at 2 wt.%. The blends without fillers were directly compounded. Similarly, the ternary blends were prepared by two steps. Firstly, the kaolinite was blended with PP; Afterwards, the blended PP-kaolinite extrudates were compounded with PVA*. The samples with KL and KJ were denoted as PP_{30}-PVA^*_{70}-KL_2 and PP_{30}-PVA^*_{70}-KJ_2, respectively. The blend without fillers (denoted as PP_{30}-PVA^*_{70}) was compounded by one-step extrusion.

2.2.2 Melt spinning of polymer blends

The obtained extrudates from melt extrusion were melt-spun afterwards, and the melt spinning process is shown in Figure 2-4. Before melt spinning, the related extrudates were dried at 80°C overnight to get rid of the moisture. Multifilament yarns

were made via a melt spinning process using a Busschaert Engineering Spinboy I spinning device (Deerlijk, Belgium). There are five temperature controllable heating zones near the screw, and the temperatures of the spinhead and spinneret are also set up in advance. The polymer blends were melted through the single screw extruder and passed through the filter and two parallel dies containing 40 circular holes (diameter Ø of 1.2 mm) with the aid of a volumetric pump (15rpm, flow rate: 52.5 cm^3), manufacturing 80-monofilament yarns. The as-spun multifilament yarns are cooled down by the fresh air and coated by the spin oil. There are two rolls, draw roll and feed roll, and the stretching of the yarns is achieved due to the difference of the two rolls. The theoretical stretching DR can be calculated by $DR=V_2/V_1$. Finally, the multifilament yarns are collected on the bobbin.

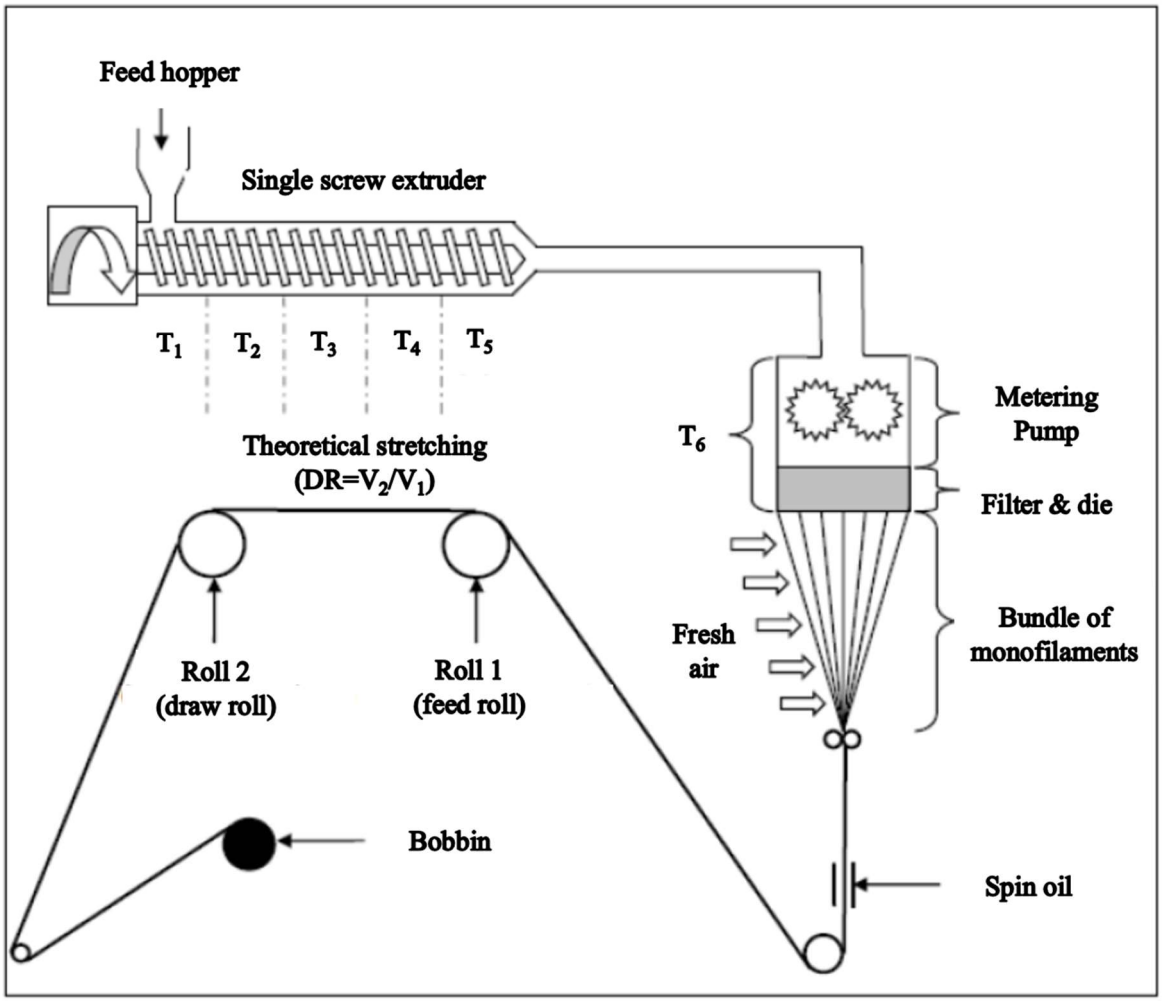

Figure 2-4 Scheme of the melt spinning process of the PP-PVA blends without/with fillers.

In Chapter III, PP/PVA pellets were first introduced into the feeding zone of a single screw extruder and heated gradually from 180 to 215°C using five heating zones. Therefore, yarns of at most 80 monofilaments were obtained and immediately cooled by air, and afterwards drawn by two rolls with the temperature of 60 and 80°C. The two rolls exhibited two distinct speeds and realized the further stretch. The first and second roll speeds were set as 100 and 200/300 rpm, respectively. Therefore, DR was adapted to 2 and 3. The samples are denoted as PP_x-PVA_y-DR_z, where the weight ratio of PP to PVA is x wt.%/y wt.%, and draw ratio is z. In addition, neat PP and PVA were also spun with two draw ratios for comparison, denoted as PP-DR_2, PP-DR_3, PVA-DR_2 and PVA-DR_3.

In Chapter IV, the PP-PVA-Si (Si_{S5505}, Si_{R816}, Si_{R972}) pellets were melt-spun into fibers, of which the related protocol of melt compounding is summarized in Figure 2-5. In the following chapters, the protocol keeps the same for manufacturing the biphasic fibers with fillers. In this chapter, the PP-Si pellets without PVA (PP-Si_{S5505}, PP-Si_{R816}, and PP-Si_{R972}) were also utilized for melt spinning. The polymer blends were first introduced into the feeding zone of a single screw extruder and heated gradually from 180 to 200°C using five heating zones. The yarns were cooled down by airstream and rolled up onto two heated rolls (60°C, 80°C) with two distinct speeds (SR_1=100 rpm, SR_2=200/300 rpm), and the theoretical draw ratio was 2 or 3. Afterwards, the yarns were collected by the winding bobbins with the same speed of SR_2. For the biphasic fibers with silica nanoparticles, the samples are denoted as PP_x-PVA_y-Si_w-DR_z, where the weight ratio of PP to PVA is x/y wt.%, w the kind of silica nanoparticles used, and draw ratio is z. Thus, PP_{70}-PVA_{30}-Si_{R972}-DR_2 represents the Si_{R972}-containing biphasic fiber, with the PP-PVA ratio of 70/30 wt.%, and the draw ratio of 2. Similarly, for the PP fibers with silica nanoparticles, PP-Si_w-DR_z indicates the PP fiber with the kind w of silica nanoparticles with DR=z. The component mass fractions and the melt spinning conditions in Chapter III and IV are summarized in Table 2-1.

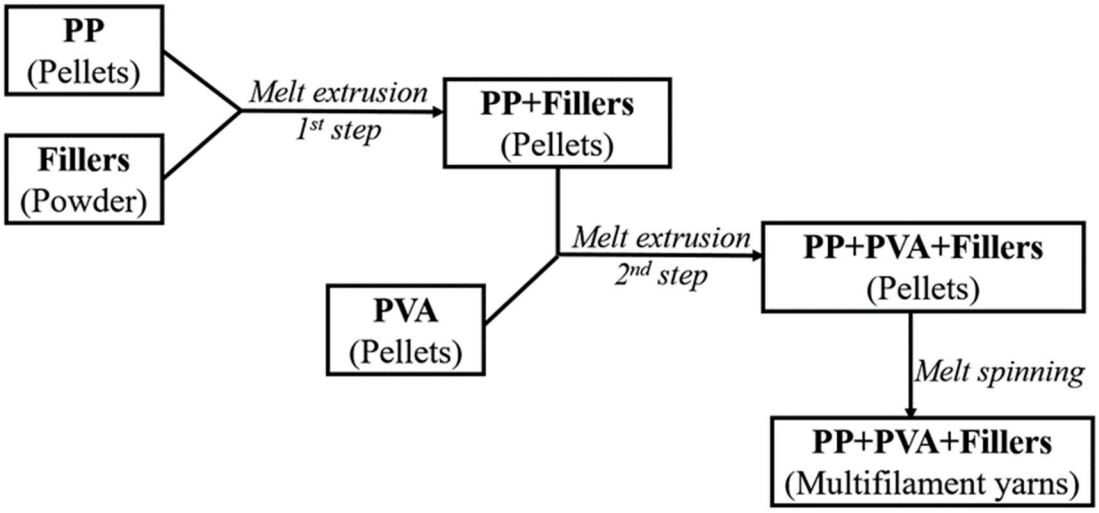

Figure 2-5 The melt extrusion and melt spinning protocol of the polymers and fillers.

Table 2-1 The component fractions and melt spinning conditions in Chapter III and IV.

Chapter	Denotion	Mass fraction (%)			Temperature (°C)		Pump (rpm)	DR
		PP	PVA	Filler	Extruder	Spinhead Spinneret		
III	PP	100	0	0	190/195/200/205/207	207	15	2/3
	PVA	0	100	0	160/170/185/190/195	195	15	2/3
	PP_{70}-PVA_{30}	70	30	0	190/195/200/205/207	207	15	2/3
	PP_{60}-PVA_{40}	60	40	0	190/195/200/205/207	207	15	2
	PP_{50}-PVA_{50}	50	50	0	190/195/200/210/214	215	15	2
IV	PP-Si_{S5505} PP-Si_{R816} PP-Si_{R972}	99	0	1	180/185/190/195/200	200	15	2/3
	PP_{70}-PVA_{30}-Si_{S5505} PP_{70}-PVA_{30}-Si_{R816} PP_{70}-PVA_{30}-Si_{R972}	69.3	29.7	1	180/185/190/195/200	200	15	2/3

In Chapter V and VI, the fillers are changed as kaolinite particles (KL and KJ). In Chapter V, the corresponding multifilament fibers were prepared from the obtained extrudates of PP-PVA(-kaolinite) particles, via the melt-spinning. The temperatures along the barrel were regulated from 180°C to 215°C. Continuously fabricated multifilament yarns (80 monofilaments) were cooled down through the air, followed by the treatment of finishing oil. Afterward, the multifilament fibers were rolled up onto two heated rolls (70-80°C). Two distinct rotational speeds 100 rpm of the first roll and 200 rpm of the second roll were applied to realize a draw for the fibers. The theoretical draw ratio (DR) can be settled as 2.

In Chapter VI, the multifilament fibers were spun from the extrudates. The temperatures along the barrel were set from 175°C to 189°C. Two different rotational speeds 100 rpm of the first roll and 200/400 rpm of the second roll were adopted to achieve the draw. Therefore, the theoretical draw ratio (DR) was set as 2 and 4. The component fractions and melt spinning conditions in Chapter V and VI are summarized in Table 2-2.

Table 2-2 The component fractions and melt spinning conditions in Chapter V and VI.

Chapter	Denotion	Mass fraction (%)			Temperature (°C)		Pump (rpm)	DR
		PP	PVA*	Filler	Extruder	Spinhead Spinneret		
V	PP_{70}-PVA^*_{30}	70	30	0	175/180/185/190/195	190	15	2
	PP_{70}-PVA^*_{30}-KL_1 PP_{70}-PVA^*_{30}-KJ_1	69.3	29.7	1	175/180/185/190/195	190	15	2
	PP_{70}-PVA^*_{30}-KL_5	66.5	28.5	5	175/180/185/190/195	190	15	2
	PP_{70}-PVA^*_{30}-KJ_5	66.5	28.5	5	175/180/190/195/200	195	15	2
VI	PP_{30}-PVA^*_{70}	30	70	0	175/180/185/190/192	187	15	2/4
	PP_{30}-PVA^*_{70}-KL_2 PP_{30}-PVA^*_{70}-KJ_2	29.4	68.6	2	175/180/185/190/194	189	15	2/4

2.2.3 Preparation of the knitted fabrics

In Chapter IV as well as Chapter VII, the multifilament yarns were further knitted. The twisting process can make the yarns more tightened up and harder to be separated, which is beneficial for the knitting process. Therefore, prior to being knitted on a flat knitting machine (Dubied, Couvet, Switzerland) with gauge of 7 (needles/inch), multifilament yarns were twisted (25 twists per meter in Z direction) by using a twisting machine (Twistec, Barcelona, Spain). The texture used during the knitting process was 1x1 Rib stitch (Soyaslan *et al.*, 2010).

2.2.4 Selective phase extraction experiment

In order to obtain the micro(porous) PP material, the selective phase extraction experiment was conducted to remove the sacrificial PVA phase. The porous fiber in Chapter III, IV, V was obtained via the selective phase extraction experiment. Water was selected as the solvent for removing PVA from the polymer blends. In Chapter VI, the PVA was selectively removed to fabricate the PP microfibers. The solvent water is controlled as 80°C. The experimental details can be consulted in 2.3.2.1.

In addition, the knitted fabrics were extracted by water using larger experimental devices by similar approaches.

The suffix -Ex is utilized for the labels of the porous fibers after the selective phase extraction. For example, PP_{70}-PVA_{30}-Si_{R972}-DR_2-Ex refers to the fibers after extraction from PP_{70}-PVA_{30}-Si_{R972}-DR_2.

2.3 Characterization methods

2.3.1 Thermal analyses

To test the thermal stability of the polymeric samples, the thermogravimetric analysis (TGA) was carried out on a TGA/DSC 3+ (Mettler Toledo, Columbus, Ohio, USA) under nitrogen atmosphere at a purge rate of 50 ml/min. For each experiment, a sample of approximately 10 mg was used. A heating rate of 10°C/min was selected, and the temperature was raised from 20 to 600°C. The initial decomposition temperature ($T_{5\%}$) that is measured for 5 wt.% loss during degradation was determined,

as well as the decomposition temperatures at the maximal degradation point and residues at the maximum testing temperature. The maximal degradation points were searched with the aid of software Origin from the derivative thermogravimetry (DTG) curves.

In addition, the thermal stability of the kaolinite particles was tested by TGA analysis as well. In order to get rid of the physisorbed water, an isothermal step with a temperature of 110°C lasted for 10 min prior to conducting the analysis. Afterward, the tested samples were heated to 900°C at a rate of 10°C/min. TGA was carried out under two different atmospheres, nitrogen and air.

The thermal behavior of all the samples was also examined with a differential scanning calorimetry (DSC) with TGA/DSC 3+ as well, under a constant nitrogen flow (50 ml/min). For the fibers, they were first to cut into powder. The sample was placed in a hermetically sealed aluminum pan. In order to erase any previous thermal history in the material, the scanning procedure involved an initial heating from 20°C to 220°C at a rate of 10°C/min, followed by an isothermal step at 220°C for 10 min. The sample was then cooled at a rate of 10°C/min to 20°C, before repeating the temperature scan in the heating and cooling range between 20 and 220°C at 10°C/min as the second cycle, during which the melting endotherm and the crystallization exotherm were investigated. The parameters including melting temperatures (T_m) and corresponding enthalpies (ΔH_m), crystallization temperatures (T_c) and corresponding enthalpies (ΔH_c) were determined.

In order to estimate the crystallinity degree (X_C), Equation 2-1 was utilized:

$$X_c = \frac{\Delta H_f}{\Delta H_f^0} \times 100 \quad \textbf{Equation 2-1}$$

where ΔH_f is the heat of fusion of the tested powders (J/g), and ΔH_f^0 is the reference value that represents the heat of fusion for a perfect 100% crystalline polymer. For the case of PP, ΔH_f^0 can be regarded as 209 J/g (Brandrup and Immergut, 1989).

2.3.2 Morphology analyses

2.3.2.1 PVA accessibility measurement

The determination of PVA accessibility with warm water in the immiscible blends gives a good approximation of the co-continuity extent (Cayla *et al.*, 2012). Approximately 4.0 g of blends (extrudates as well as fibers) and some filter papers were dried for 12h at 50°C and weighed. And then tested blends were immersed in 100 mL of distilled water under magnetic stirring for 5h at 80°C to extract PVA phase. The entire solution was poured onto a filter paper, and the samples were rinsed with warm water to dilute the peripheral PVA solution. The sample with filter paper was dried overnight in the oven at 50°C to get rid of water. The PVA accessibility degree was calculated as the fraction of the removed PVA in the PVA part in the blend. Therefore, the PVA accessibility degree can be calculated by the following Equation 2-2. The values were recorded for at least two times and the average values were taken.

$$\text{PVA accessibility degree}\ (\%) = \frac{W_i - (W_{r+f} - W_f)}{W_i \times \omega_{PVA}} \times 100 \quad \textbf{Equation 2-2}$$

Where W_i represents the initial weight of the dried samples of polymer blends; W_{r+f} indicates the total weight of samples jointed with the filter papers after the selective phase extraction experiment and drying; W_f represents the weight of the dried filter papers prior to use; ω_{PVA} refers to the mass fraction of PVA within the polymer blends.

2.3.2.2 Scanning electron microscopy (SEM) observation

Many SEM experiments towards the extrudates, fibers, plates and the fabrics, were conducted to better understand the morphology evolution as well as the filler localizations. Prior to the SEM experiment, all the samples were sputter-coated with gold.

Extrudates

The extrudates PP-PVA without fillers were dipped into liquid nitrogen to be frozen and fractured by a blade in cross- and longitudinal sections. SEM (Hitachi S4700) was utilized to investigate the cryogenic fracture surfaces. The accelerating voltage is 6.0 kV. The experiment was conducted in PERF laboratory (ENSCL, Lille, France).

The extrudates of PP-PVA with silica nanoparticles were dipped into liquid nitrogen to be frozen and fractured by a razor blade in cross- and longitudinal sections. SEM (Inspect F, FEI, USA) was utilized to investigate the cryogenic fracture surfaces. The accelerating voltage is 20.0 kV. The dispersed PVA particles sizes were determined by ImageJ software, and more than 300 PVA particles were measured in SEM micrographs of longitudinal fracture surfaces. The characterization was carried out in Sichuan University (Chengdu, China).

Form factor (ff) is a measure of the deviation of a finite shape from circularity ($=4\times\pi\times area/perimeter^2$), and the parameter can be a powerful evidence in determining the PVA continuity. When ff is close to 1, it tends to be a perfect circle; when ff is approaching 0, it illustrates that the perimeter is extremely tremendous and the shape is irregular. Herein, in order to observe the evolution of the PVA shape distribution, the PVA nodules were distributed into three classes, spherical ($ff>0.60$), transitional ($0.60>ff>0.15$), fibrous nodules ($ff<0.15$). Among the several hundreds of nodules, the number of spherical, transitional and fibrous nodules are N_s, N_t and N_f, respectively. The diagram of diameter measurement of PVA nodules of different shapes is displayed in Figure 2-6.

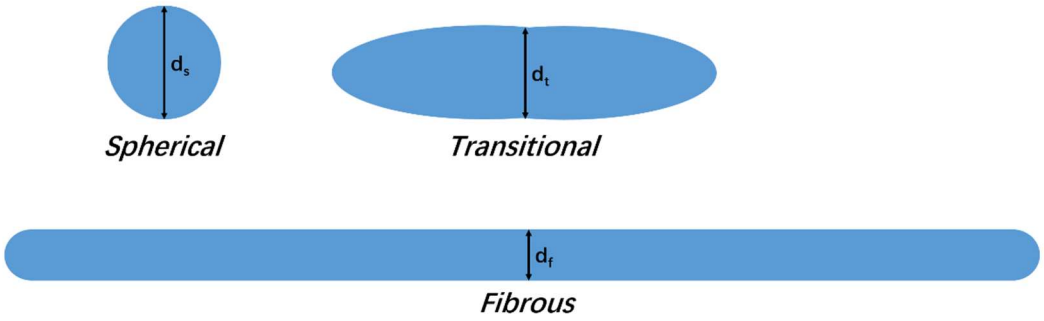

Figure 2-6 Diagram of diameter measurement of PVA nodules of different shapes in PP-PVA blends.

For spherical nodules, the diameter was estimated as $d_{si} = \sqrt{4A_{si}/\pi}$, where A_{si} was the area of the i-th spherical nodule. The volume average diameter of the spherical nodules was calculated by Equation 2-3. In the analysis process, it existed difficulty in observing the spherical nodules with extremely tiny dimension, which deviated the statistical results. Therefore, it is more recommended to use volume average diameter instead of number average diameter for spherical nodules.

$$D_{sv} = \sum_{i=1}^{Ns} d_{si}^{4} / \sum_{i=1}^{Ns} d_{si}^{3} \quad \textbf{Equation 2-3}$$

For transitional nodules, the diameter of the middle part was measured as d_{ti} for the i-th drop. The number average diameter of the transition nodules was evaluated by Equation 2-4.

$$D_{tn} = \sum_{i=1}^{Nt} d_{ti} / N_t \quad \textbf{Equation 2-4}$$

As for the fibrous nodules, the diameter was estimated as $d_{fi} = A_{fi}/L_{fi}$, where A_{fi} and L_{fi} were the area and axial length of the i-th fibrous drop. Similarly, the number average diameter of the fibrous nodules was estimated by Equation 2-5.

$$D_{fn} = \sum_{i=1}^{N_f} d_{fi} / N_f \quad \textbf{Equation 2-5}$$

The micromorphology observation of PP-PVA extrudates with kaolinite particles was conducted via a Scanning Electron Microscope (FEI Quanta 200 ESEM). The sample was put in liquid nitrogen and broken by a hammer blow. The debris was placed on a pad of SEM and then metalized before analysis. The experiment was conducted in Centre des Matériaux des mines d'Alès (C2MA), IMT, Mines Alès (France).

Fibers

The morphology of the fibers before and after selective phase extraction was observed by field emission scanning electron microscopy (SEM) on the machine of Apreo S (ThermoFisher Scientific, USA) with accelerating voltages of 5.0 kV.

In addition, the fibers were cut along the direction of the cross sections, after the treatment by liquid nitrogen. The cross sections were observed by the SEM machine (Inspect F, FEI, USA). The accelerating voltages were 5.0 kV-20.0 kV. The projection areas of PVA nodules on the cross-section were analyzed by ImageJ software, and more than 500 PVA nodules were taken into account. These projections on the cross-section were regarded as perfect circles. Therefore, the diameters were calculated from the areas of the PVA particles.

The external and internal inner surfaces of the porous PP fibers were observed by SEM (Inspect F, FEI, USA). The fibers were cut obliquely with the aid of the liquid nitrogen to expose the internal inner surface. The accelerated voltage was 20.0 kV.

The abovementioned experiments concerning fibers were conducted in Sichuan University (Chengdu, China).

In addition, the morphology of the biphasic fibers (PP_{30}-PVA^{*}_{70}) with kaolinite particles was observed via a Scanning Electron Microscope (FEI Quanta 200 ESEM) in C2MA laboratory, IMT, Mines Alès (France). The accelerated voltage was 12.5 kV.

Plates

The morphology of PP-PVA plate after rheometer measurement was also observed by an SEM apparatus (Inspect F, FEI Company) in Sichuan University (Chengdu, China). The dispersed PVA droplet sizes were determined by ImageJ analysis software (National Institutes of Health (NIH), Bethesda, MD, USA). More than 300 droplets were taken into account to ensure the accuracy. Afterward, Schwartz-Saltikov transformation method was applied to correct the size distributions of the droplets (Saltikov, 1967). The method was operated by dividing the distribution into 7 linear range groups, and the midpoint of each group represents the average value. The 3D particle distribution in volume can be transferred from the 2D particle distribution in area by applying the transformation coefficients.

Fabrics

The knitted fabrics from the PP_{30}-PVA^{*}_{70}-DR_4 before and after selective phase extraction were observed by field emission scanning electron microscopy (SEM) via Apreo S (ThermoFisher Scientific, USA) in Sichuan University (Chengdu, China). The accelerating voltages are from 5.0 kV to 20.0 kV.

2.3.2.3 Transmission electron scanning microscopy (TEM) observation

TEM was performed on the cross-section of the rods in PERF laboratory (ENSCL, Lille, France). The cross-section was obtained by slicing the sample with the aid of liquid nitrogen to the thickness of tens of nanometers. The microstructure of the samples was observed by Philips CM100 transmission electron microscope.

2.3.2.4 Digital camera observation

The images of the fibrous residuals after selective phase extraction experiment as well as the knitted fabrics were acquired by using a digital camera (Huawei P9 EVA-AL00, Shenzhen, China).

2.3.3 Rheometer tests

For the blends without fillers and with silica nanoparticles, the melt rheological behaviors were carried out by a TA rotational rheometer (AR 2000ex, TA Instruments, New Castle, DE, USA) in the mode of oscillatory shear flow. The diameter of the parallel plate was 25 mm and the gap was set at 1.5 mm. The frequency sweep was ranged from 0.01 to 628 rad/s and the strain was 1.0%. All measurements were conducted at 190°C.

For the blends with kaolinite particles, the rheological behaviors were surveyed on the same machine with similar conditions. The only difference is that the frequency sweep was conducted from 100 to 0.01 rad/s, and the ending frequency is relatively low, in order to better observe the gel-like behaviors and remove the plates for the SEM observation.

2.3.4 Melt flow index (MFI)

The MFI value was tightly related to the spinnability of polymers, and it was determined by the Melt Flow Tester (Thermo Haake, USA). Based on the standard ASTM D1238 (ASTM D1238-10, 2010), the piston as well as the tested sample was pre-heated for 4 and 3 minutes respectively. The load was chosen as 2.16 kg and the temperature was set as 190°C. As a result, the melt flow index (MFI) was obtained with the unit (g/10min). The same experiments were conducted twice for the accuracy. For the melt spinning devices in GEMTEX laboratory, the temperature at which the MFI index is 15-30 g/10min is a recommended reference for relatively optimized spinnability.

2.3.5 XRD analysis

The wide-angle X-ray diffraction (WAXD) of the multifilament yarns was taken on an X-ray diffractometer Ultima IV (Rigaku, Japan) in Sichuan University (Chengdu, China). The angle 2θ ranged from 5 to 60°. The radiation was Cu Kα with the wavelength of 1.54 Å. Fibers were manually fixed onto a sample holder. The crystal size was estimated from Scherrer's equation in Equation 2-6 (Alexander, 1969).

$$L = \frac{0.9\lambda}{\beta \cos\theta} \quad \textbf{Equation 2-6}$$

Where L represents the crystallite dimension, β stands for the breadth at half maximum intensity, θ refers to the Bragg angle, and λ is the wavelength.

2.3.6 Mechanical properties

2.3.6.1 Tensile tests

In order to compare the mechanical properties of the yarns, tensile tests were performed on single filaments extracted from the yarns, using a machine named Zwick 1456 (Germany), based on the ISO 5079 standard. The load cell was 10 N, the test length was set as 20 mm and the deformation rate was controlled as 20 mm/min. Tensile tests were conducted in a standard atmosphere (relative humidity: 65±5%; temperature: 20±2°C). The same measurements were conducted for 10 different single fibers from the same yarn to ensure the accuracy. In order to determine the fineness (dTex) of each single fiber before extraction prior to tensile tests, a vibroscope machine (Vibroskop, Lenzing Instruments, Germany) was used according to the NF G 07-306 standard. In addition, the fineness of the filaments after selective phase extraction was confirmed by weighing. The fiber fineness is used to calculate Young's Modulus in MPa and tenacity in cN/Tex. Tenacity is the maximum force of the monofilament fiber divided by the linear mass density. Herein, the unit of mass density is used as Tex, which means the mass in grams per 1000 meters.

The mechanical properties of the knitted fabrics from PP_{70}-PVA_{30}-DR_3 before and after selective phase extraction were tested via an electromechanical universal test system (MTS Criterion Model 43, Eden Prairie, USA) with a load cell of 10 kN. The width of the selected fabrics was near 50 mm, and the gauge length of the sample was fixed at 120 mm, and the deformation rate was 60 mm/min. The mechanical properties of the knitted fabrics from PP-PVA* blends with kaolinite particles were also tested on the same machine. Their widths were near 40 mm. The initial gauge length was adjusted as 60 mm, and the deformation rate was 30 mm/min. The thicknesses of the fabrics were determined by a fabric thickness tester (Sodemat, France).

The abovementioned tensile tests were carried out in a standard atmosphere with the relative humidity of 65±5% and the temperature of 20±2°C.

2.3.6.2 Dynamic mechanical analyses

Dynamic mechanical analyses (DMA) of the neat and blend fibers composed of PP and PVA were carried out by a dynamic mechanical analyzer (Q800, TA instrument, USA) with a frequency of 3.5 Hz and a strain amplitude of 0.8%. The stress is in tension mode. A bundle of multifilaments was fixed onto the clamp, and the temperature was increased from room temperature to 120°C at a heating rate of 3°C/min.

The dynamic mechanical properties are between the lower-bound series model and upper-bound parallel model. The related properties in parallel and series modes can be calculated by the means of Equation 1-13 and Equation 1-14.

In the part “State of the Art”, the Coran’s model is also introduced. In Coran’s model, the formula can be expressed below as Equation 1-15, and f can vary between zero and unity for the fibers.

2.3.7 Air permeability

The air permeability of textile fabrics is determined by the rate of flow of air passing perpendicularly through a given area of fabric by measuring at a given pressure its difference across the fabric test area over a given time period. Transverse air permeability was measured with a “Permeabilimetre à l’air” (Emi Développement,

Bréviandes, France) with a pressure applied of 100 Pa and a test area of 20 cm^2, according to ISO 9237 (ISO, 1995). Air permeability tests were conducted in a standard atmosphere (relative humidity: 65±5%; temperature: 20±2°C). The data results were recorded for more than two times and the average values were taken for the accuracy.

2.3.8 Surface tension measurement

There is a tight relationship between the surface tension and contact angle of materials. The contact angles between probe liquids and polymers were monitored by a sessile drop apparatus named "Digidrop" manufactured by GBX. In order to ensure a smooth surface for contact angle tests, hot pressing technology was utilized to make moulded plates. Neat PP or PVA pellets were placed between Teflon plates with heating over their melting temperatures without pressure. And then a high pressure between the two plates (40 bars) was offered and lasted for some time. Afterwards, the pressure was maintained and the plates were water-cooled to the room temperature. After the stress reliever of the plates, the neat polymer plates with smooth surfaces were generated for contact angle measurement.

By Equation 1-19, the surface tension was carried out, where two probe liquids were utilized, one apolar liquid (diiodomethane, γ=50.8 mN/m, γ^p=2.3 mN/m, γ^d=48.5 mN/m) and one polar liquid (distilled water, γ=72.8 mN/m, γ^p=51.0 mN/m, γ^d=21.8 mN/m) (Salaün *et al.*, 2009).

Chapter III:

Microstructure Evolution of Immiscible PP-PVA Blends Tuned by Polymer Ratio and Its Transformation into Fibers

Chapter 3 Microstructure Evolution of Immiscible PP-PVA Blends Tuned by Polymer Ratio and Its Transformation into Fibers

The dual-phase continuity can be strongly affected by the ratio of the two polymers (Chuai *et al.*, 2001). In this study, PVA is selected as the minority phase, and the fraction of PVA ranges from 30 wt.% to 50 wt.%. An appropriate ratio of PP to PVA is beneficial for constructing a favorable scaffold microstructure. The polymer blends were prepared by melt extrusion, followed by the melt spinning process to fabricate the biphasic fibers. The microstructure investigations concerning the whole process were carried out to reveal the relationship between the blend ratio and obtained morphology. Main objective is to find out an appropriate ratio for melt spinning from PP-PVA blends and keeping the fiber form after the selective phase extraction.

3.1 Polymeric compounds

3.1.1 Thermal properties of the blends

In order to demonstrate how the PVA influences the thermal stability of PP-PVA blends, TGA and DSC analyses were conducted for the polymer blend extrudates in the N_2 atmosphere. TGA curves of the neat and blend polymers of PP and PVA are shown in Figure 3-1 and the results are summarized in Table 3-1. PP has one weight-loss peak in the derivative thermogravimetric (DTG) curve, and shows superior thermal stability with $T_{5\%}$ of 393°C. Its temperature at the maximum decomposition rate is 454°C. PP is thermally decomposed into volatile products through a radical chain process due to carbon-carbon bond scission (Batistella *et al.*, 2016). PP decomposes completely at approximately 480°C. PVA displays two weight-loss peaks, and the initial decomposition temperature of PVA at 5% weight loss is 295°C, which is far higher than the melting temperature 179°C. This illustrates that there is a broad thermal range

for PVA processing. Typically, the elimination of volatile products often occurs from the side groups (e.g., OH groups) approximately below 260°C (Alexy *et al.*, 2002). However, the elimination peak is postponed towards 321°C attributed to the modification of the multi-hydroxyl structure (Tran *et al.*, 2014b). The second degradation stage containing T_{dmax2} (437°C) is ascribed to the chemical degradation from C-C bond scission.

For the PP-PVA blends, the initial decomposition temperatures at 5% weight loss are between those of neat PP and PVA, which signifies that near the melt manufacturing temperatures (approximately 200°C), the neat polymers as well as their blends exhibit excellent thermal stability and do not have noticeable degradation within a certain time. The (derivative thermogravimetric) DTG curves of the biphasic blends are split into two peaks distinctly as well, one close to PVA and the other approaching to PP, which is the feature of immiscible polymers (Bikales, 1971). Note that the T_{dmax2} is significantly increased, which originates from the breakage of carbon-carbon, compared to the raw polymers.

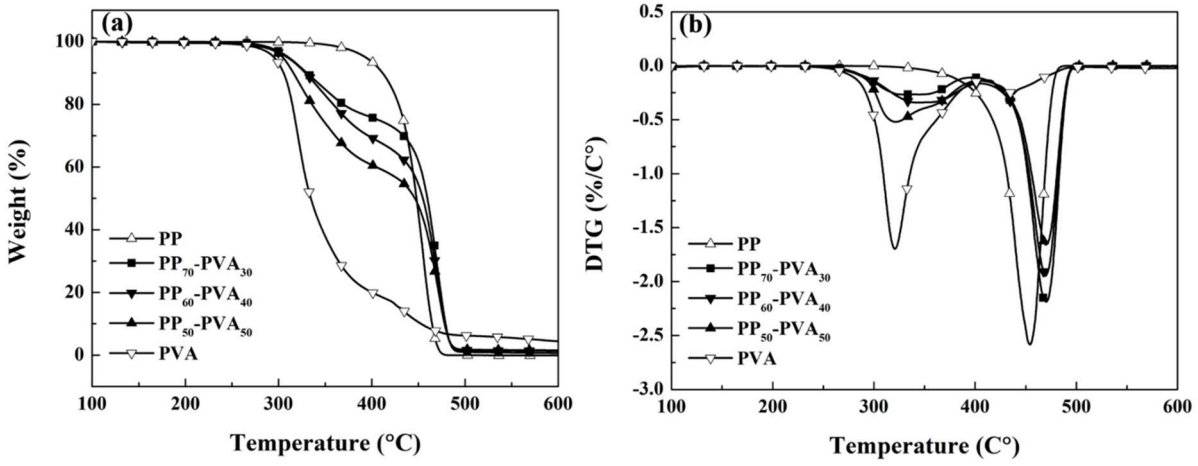

Figure 3-1 TGA results of neat and blend polymers of PP and PVA in N_2 atmosphere (a) TGA curves; (b) DTG curves.

Table 3-1 TG data of PP and PVA in N_2 atmosphere.

Pellets	$T_{5\%}$ (°C)	T_{dmax1} (°C)	T_{dmax2} (°C)	Residue at 600°C (%)
PP	393.1	-	454.4	0.0
PP_{70}-PVA_{30}	310.4	329.3	470.1	0.65
PP_{60}-PVA_{40}	309.2	342.4	469.5	1.34
PP_{50}-PVA_{50}	304.4	321.3	470.0	1.53
PVA	295.1	320.6	437.1	4.39

The melting and crystallization behaviors in DSC measurement are illustrated in Figure 3-2, and the related thermal parameters are listed in Table 3-2. Figure 3-2(a) demonstrates that the polymers exhibit only one single melting peak, regardless of the components of PP and PVA. This results from the fact that the melting temperature of PP (171°C) and PVA (179°C) are too close. The crystallization peaks of the samples are shown in Figure 3-2(b). The crystallization peak of PVA is located at 125°C, and PP appears at a lower position of 107°C, of which the differences can be distinguished. The binary blends have three peaks, assigned to the crystallization peak of PVA component (T_{c1}, near 130°C), bulk crystallization peak of PP (T_{c2}, near 110°C) and fractionated crystallization peak of PP (T_{c3}, near 80°C) from high to low temperature, respectively. The bulk crystallization is ascribed to the heterogeneous nucleation, and the fractionated crystallization is due to homogenous nucleation induced by the confined PP phase (Li *et al.*, 2013; Santana and Müller, 1994). The bulk crystallization temperature of PP in the blends is near that of pure PP one (107°C). For PP_{70}-PVA_{30}, the bulk crystallization peak predominates compared with the fractionated peak. With the increment of PVA fraction, fractionated crystallization behaviors are strengthened, which indicates that the dispersion of PP is enhanced (Santana and Müller, 1994). The fractionated peak of PP_{60}-PVA_{40} is the most compelling, which corresponds well with the phase inversion of PP and PVA phase.

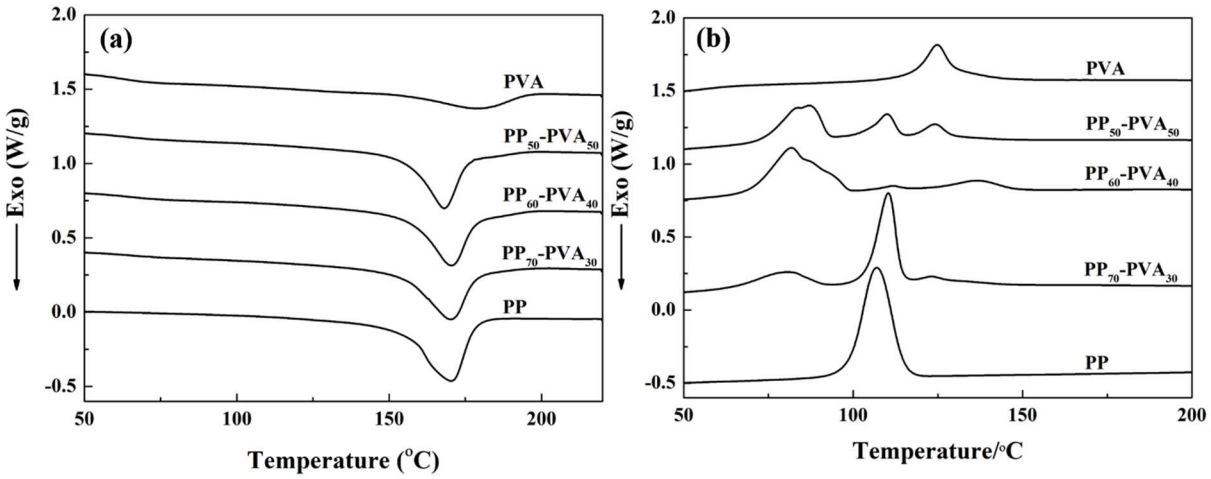

Figure 3-2 DSC analyses of neat and blend polymers of PP and PVA (a) melting process in the 2nd cycle; (b) crystallization process in the 2nd cycle.

Table 3-2 Thermal parameters of neat and blend PP-PVA materials.

Pellets	T_m	ΔH_m	T_c (°C)			ΔH_c (J/g)			ΔH_{cT}
	(°C)	(J/g)	1	2	3	1	2	3	(J/g)
PP	170.5	39.05	-	107.0	-	-	46.87	-	46.87
PP_{70}-PVA_{30}	170.3	34.10	123.1	110.5	80.2	0.13	23.19	9.25	32.57
PP_{60}-PVA_{40}	170.3	36.13	136.9	111.6	81.7	4.88	0.80	30.34	36.02
PP_{50}-PVA_{50}	168.2	33.44	124.3	110.0	86.8	1.47	5.81	17.57	24.85
PVA	179.3	13.45	124.9	-	-	18.13	-	-	18.13

3.1.2 Morphology of the polymer blends

The selective phase extraction experiment provides a facile method to evaluate the co-continuity extent of the polymer blends. Figure 3-3 graphically indicates the PVA accessibility degree of the PP-PVA blends with different mass ratios. For PP_{70}-PVA_{30}, the PVA accessibility is 50.5±3.0 %, which indicates that only half of PVA can be removed. With the content of the PVA increasing, the PVA accessibility degree increases violently, resulted from the change of the microstructure of PP-PVA.

In order to intuitively observe the evolution of the biphasic microstructure, SEM observation was also given. Cross-sections of the extrudates perpendicular to extrusion direction have been observed, all the projections of PVA nodules presents circular. Thus, the longitudinal section of the extrudates can well render the information of their biphasic morphology. Figure 3-4 is the SEM images of the longitudinal section of the pellets after melt extrusion with different mass ratios (70 wt.%/30 wt.%; 60 wt.%/40 wt.%; 50 wt.%/50 wt.%) of PP and PVA. In order to distinguish PP and PVA, a backscattered electron detector (BSE) was applied. The light part in the SEM images is PVA and the dark part is PP. Figure 3-4(a) is the longitudinal direction observation of PP_{70}-PVA_{30} pellets. PVA forms isolated ellipsoidal and spherical droplets inside the PP matrix. Apart from shear stress, some extensional stress also exists during the extrusion process, it leads to the elongation of the PVA nodules. As the content of PVA increases, some PVA forms an interconnected structure instead of isolated droplets, which gives the evidence that its morphology is approaching co-continuous structure. Its high PVA accessibility (84.6±6.5%) also gives the same imply. Furthermore, their sizes and shapes diverse a lot. With the content of PVA further increasing, the PVA accessibility is even higher (91.5±1.4%), and it can be assumed that nearly all of PVA becomes approachable. Based on the SEM image of PP_{50}-PVA_{50}, it illustrates that the roles of PP and PVA phases are reversed. PVA phase becomes highly continuous and PP phase is fenced off by PVA phase. It gives an inference that the structure was evolved from PP matrix-PVA dispersed structure to PVA matrix-PP dispersed structure, which experienced a phase inversion.

By altering the PVA content, the microstructure of PP-PVA blends experiences a significant change. The SEM observation fits well with the PVA accessibility results. Thus, the ratio tailoring upon PP-PVA blends dominantly governs the biphasic microstructure.

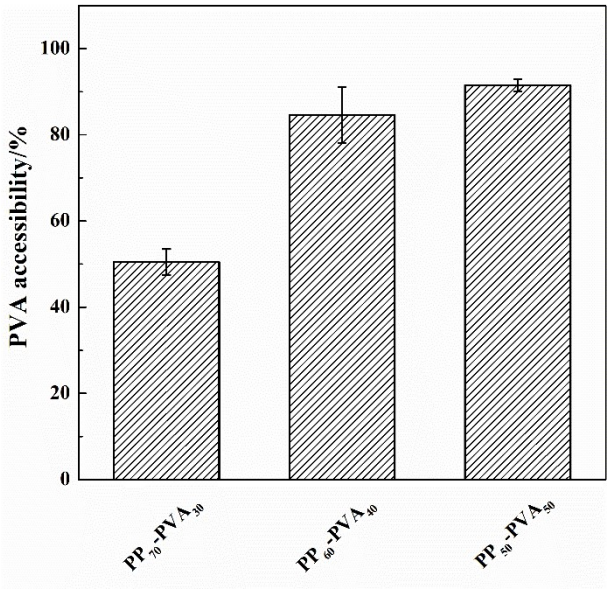

Figure 3-3 PVA accessibility degree of the PP-PVA blends with different mass ratios of polymers.

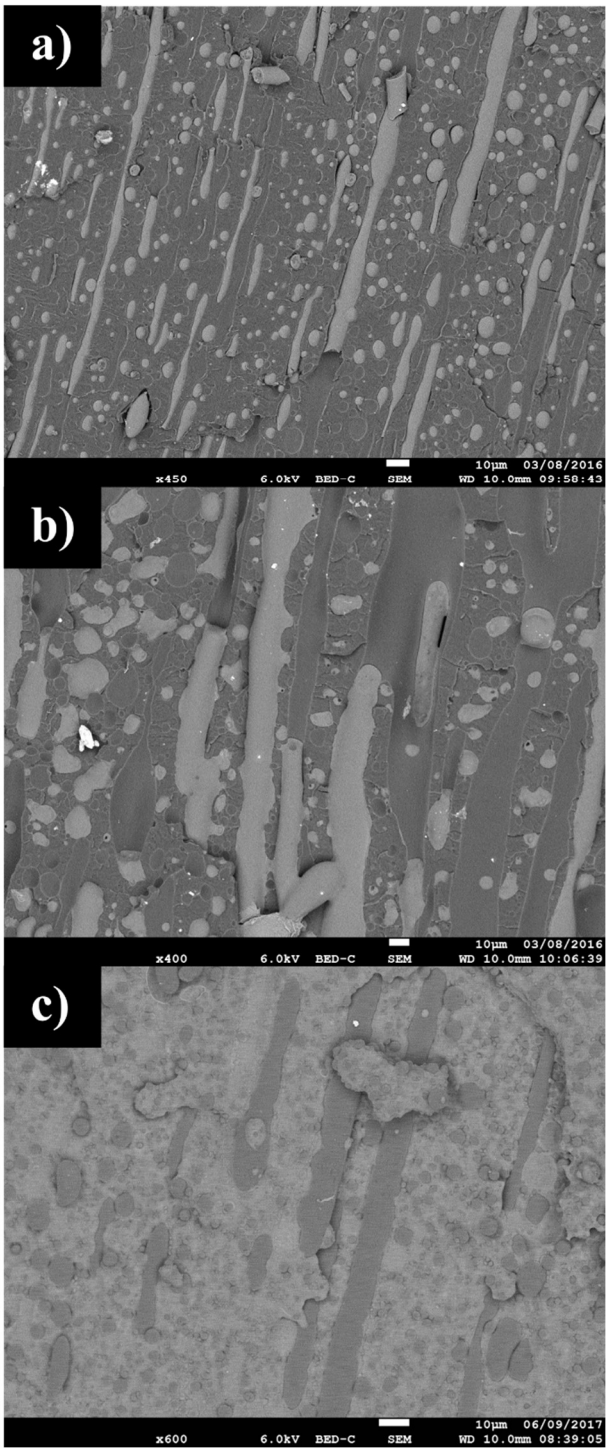

Figure 3-4 SEM images of the pellets after melt extrusion with different mass ratios in longitudinal direction (a) PP_{70}-PVA_{30}; (b) PP_{60}-PVA_{40}; (c) PP_{50}-PVA_{50} (PP: dark part; PVA: light part).

3.1.3 Rheometer tests

Rheological behaviors of polymer blends are tightly relevant to the microstructure evolution of biphasic polymers (Caro *et al.*, 2017; Zhang *et al.*, 2012). Steinmann *et al.* (2002b) considered that the rheological evaluation sometimes is even more suitable for the determination of phase inversion concentration than morphological evaluation, for it reflects the three-dimensional bulk properties rather than the two-dimensional images. It also provides a plain way to discover the characteristic of polymers, from the perspective of the shape relaxation of the dispersed phase. The viscoelastic behaviors of neat polymers and their blends were measured, and the storage modulus and complex viscosity are illustrated in Figure 3-5. Aimed at quantitatively obtaining the trends of these curves, the local slope of the storage modulus, $\alpha(\omega)$ ($= \left.\frac{\partial \log G'}{\partial \log \omega}\right|_{\omega}$) was also calculated and shown in the lower right corner of Figure 3-5(a), where G' represents the storage modulus and ω represents the angular frequency. α values of any materials are between 0 and 2, and the lower limit 0 represents the response of a purely elastic solid and the upper limit 2 stands for the terminal behavior of a Maxwellian fluid (Filippone *et al.*, 2011). At the low frequency (0.025 rad/s) the value of α_{PVA} and α_{PP} are about 0.6 and 1.4, respectively. PP behaves like Maxwellian fluid, while PVA demonstrates more distinct features of elastic solid. It is worth noting that there is a Newtonian plateau of complex viscosity in PP, while there is no such phenomenon in PVA, and instead there is a sharp slope. The solid-like behavior may be resulted from the existence of dynamic hydrogen bonds between PVA molecules, which played the role of dynamic physical crosslinking points, thus the relaxation of PVA molecules is limited (Wang *et al.*, 2013).

For PP_{60}-PVA_{40} and PP_{50}-PVA_{50}, the storage modules are even higher than that of sole PVA and PP, which gives an evidence that the cause is not only led from the bulk polymers. The extra part of storage modulus is also owing to the shape relaxation of the dispersed phase. In detail, the secondary plateau is dominantly led by the size and the amount of dispersed phase, and its width is related to the size distribution of the drops (Graebling *et al.*, 1993). When the fraction of PVA increases from 40 wt.% to 50 wt.%,

the storage modulus decreases slightly, even though PVA has a more excellent solid-like properties. It is due to the phase inversion of PP and PVA, proving that the existence of co-continuous structure lies in the blends, in which the PVA content is near 40-50 wt.%. The evolution has been observed by SEM measurement. In addition, as for the complex viscosity, there are no Newtonian plateaus in PP_{60}-PVA_{40} and PP_{50}-PVA_{50}, mainly resulted from the enormous amount of continuous PVA.

In terms of the α values, the rheology behavior of PP_{70}-PVA_{30} verges upon that of PP, and the $\alpha_{PP70\text{-}PVA30}$ is reduced slightly to 1.2. For PP_{60}-PVA_{40} and PP_{50}-PVA_{50} blends, the α values are lower with the values of 0.5 and 0.7. The slope of storage modulus (α) is sensitive to the degree of interconnectivity in materials with network structure (Winter and Chambon, 1986). The solid-like behavior of PP_{60}-PVA_{40} is even more evident than PVA, although the fraction of PVA is only 40 wt.%. The further enhanced elasticity is due to the biphasic structure approaching co-continuous structures (Graebling *et al.*, 1993).

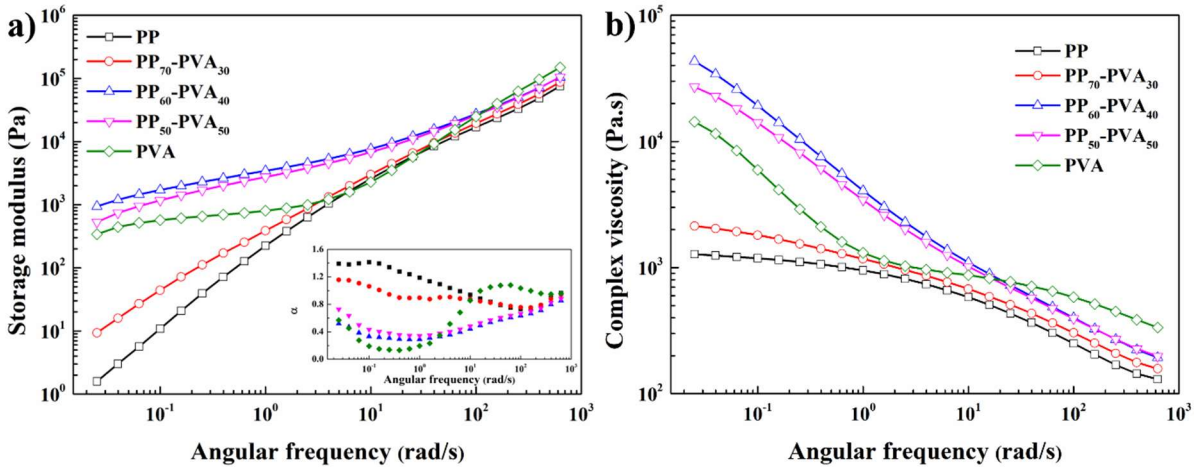

Figure 3-5 Rheological behaviours of neat PP, PP_{70}-PVA_{30}, PP_{60}-PVA_{40}, PP_{50}-PVA_{50} and neat PVA at 190 °C. (a) Storage modulus and the slope of the storage modulus α(ω); (b) Complex viscosity.

3.1.4 Melt flow index (MFI)

Herein, polymeric fibers from PP-PVA were made through melt spinning technology. Before this, in order to investigate the fluidity of the polymer blends, melt flow index measurements were carried out. It spreads direct information about the viscosity at specific temperatures, which is a critical factor for melt spinning process. Melt flow indexes (MFI) of PP, PVA, and PP-PVA blends with the three different ratios at 190°C were tested, and the corresponding results are shown in Figure 3-6. The MFI of PP and PVA are respectively 11.8±0.6 and 21.6±0.0 g/10 min, and PVA shows a higher fluidity than PP. For PP with the addition of PVA, the MFI values are significantly increased, even higher than that of PVA. PP-PVA blends show a positive deviation in MFI, and negative deviation in viscosity, which is ascribed to the weak interactions between the two components. The MFI values of PP_{70}-PVA_{30}, PP_{60}-PVA_{40} and PP_{50}-PVA_{50} are 27.6±0.3, 48.2±4.8 and 62.8±2.3 g/10 min, respectively, exhibiting decreasing viscosity, and it implies an increasing area of incompatible interphases of polymer blends (Ku and Lin, 2005). The MFI value of 15-30 g/10 min is the most suitable area for the melt spinning device that was used. It indicates that for PP_{70}-PVA_{30}, the temperature for melt spinning is suggested to be set at 190°C. The spinning temperature for PP_{60}-PVA_{40} and PP_{50}-PVA_{50} may be adapted at a lower temperature.

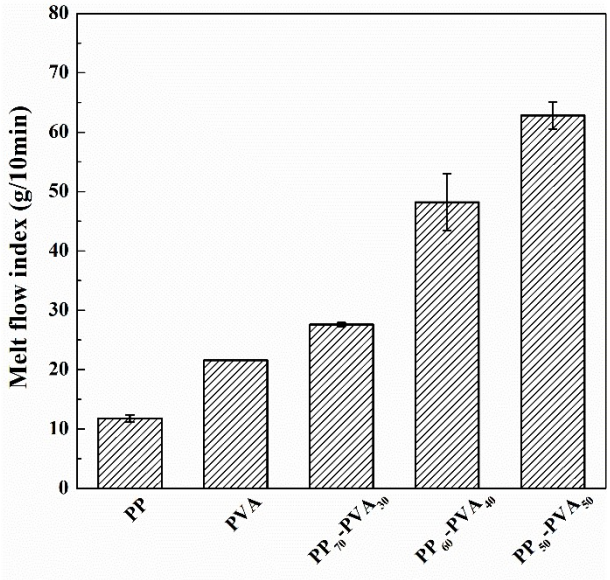

Figure 3-6 Melt flow index (190°C, 2.16 kg) of neat and blend polymers of PP/PVA.

3.2 Polymeric fibers

3.2.1 Spinnability and morphology

The spinning condition has been described in detail in Section 2.3, under which the multifilament fibers were successfully obtained for each sample. However, the spinning process could not realize the stable production of the PP_{50}-PVA_{50} and PP_{60}-PVA_{40} fibers, often concomitant with broken threads, and the maximum draw ratio (DR) only reached 2. For PP_{70}-PVA_{30} blends, the spinning process was stable and ceaseless, even if the DR was further increased to 3.

The melt-spun fibers were selectively extracted with warm water, to obtain the porous fibers. PVA accessibility degree was also calculated according to Equation 2-2, and the related results are displayed in Figure 3-7. A higher PVA accessibility signifies that more PVA can be removed and even reused. For the extrudates, it has been found that with the increase of the PVA fraction, PVA accessibility increases significantly, approaching co-continuous structure. However, the microstructure will be changed a great deal after melt spinning. PP_{70}-PVA_{30}-DR_2 possesses a high PVA accessibility degree of 64.9±0.6%, and PVA accessibility is diminished with the increase of PVA fraction, which is not beneficial for obtaining porous materials. Also, increasing the DR to 3 increases the PVA accessibility degree of the fibers from PP_{70}-PVA_{30} to 78.7±1.1%. For PP_{70}-PVA_{30} polymer blends, the increase of DR elevates the PVA accessibility obviously, due to the enhanced interconnectivity of PVA nodules and enlarged specific areas of the biphasic fibers under the elongational flow.

Figure 3-7 shows the residual morphology of the fibers with DR=2 after selective phase extraction as well. Unfortunately, for PP_{60}-PVA_{40}-DR_2 and PP_{50}-PVA_{50}-DR_2, the fiber morphology was damaged and collapsed in a heap. By contrast, the fiber shape of PP_{70}-PVA_{30}-DR_2 was maintained, and the fibers with DR=3 also behaved well. Mechanically robust material is the goal of our research, and PP_{70}-PVA_{30} is the suitable candidate.

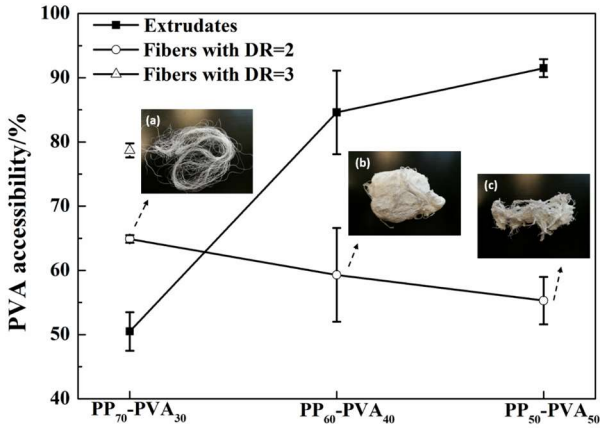

Figure 3-7 PVA accessibility degree of polymer blends and digital photos of extracted fibers from (a) PP_{70}-PVA_{30}-DR_2; (b) PP_{60}-PVA_{40}-DR_2; (c) PP_{50}-PVA_{50}-DR_2.

The cross-section of all the blend fibers is circular based on the optical microscopy observation, which is decided by the spinneret hole shape in melt spinning. In order to further confirm the morphology of the fibers, the SEM observation is shown in Figure 3-8. There are different degrees of wrinkles on the surface of the fibers, among which PP_{60}-PVA_{40}-DR_2 is the most significant, even accompanied with some detached fibrous phase. It hints that the unsatisfactory spinnability of PP_{60}-PVA_{40} originates from the immiscibility of the polymer blends. After the selective phase extraction, there emerge long and narrow holes in parallel on the fiber surface from PP_{70}-PVA_{30}-DR_2-Ex, which offers solvent access to the inner part of the fibers. With the increase of draw ratio, the holes are further elongated with a higher density due to the transformation of extracted PVA phase. The cross-sections of the PP_{70}-PVA_{30} fibers are also revealed in Figure 3-8 (i)(j). The diameters of the fibers are not uniform, which often occurs for the biphasic fibers. Furthermore, it demonstrates that there are numerous submicron-scale holes generated by sample cutting in the inner part of the fibers, which proves the porous structures. For the low temperature induced by liquid nitrogen and the immiscibility of biphasic polymers, the PVA nodules were detached from the fiber cross-section revealing the biphasic morphology within the fibers. With the increment of draw ratio, the diameters of the fibers as well as those of the pores are decreased. In contrast, the fibrous matrix is evolved towards bundle-like microfibers for PP_{60}-PVA_{40} and PP_{50}-

PVA_{50} with some short, detached and large-size nodules. With a higher magnification, it is found that the microfibers are not completely isolated, and instead they are partially interconnected. It further proves that the phase inversion lies near the fractions, which gives rise to the difficulty in melt spinning.

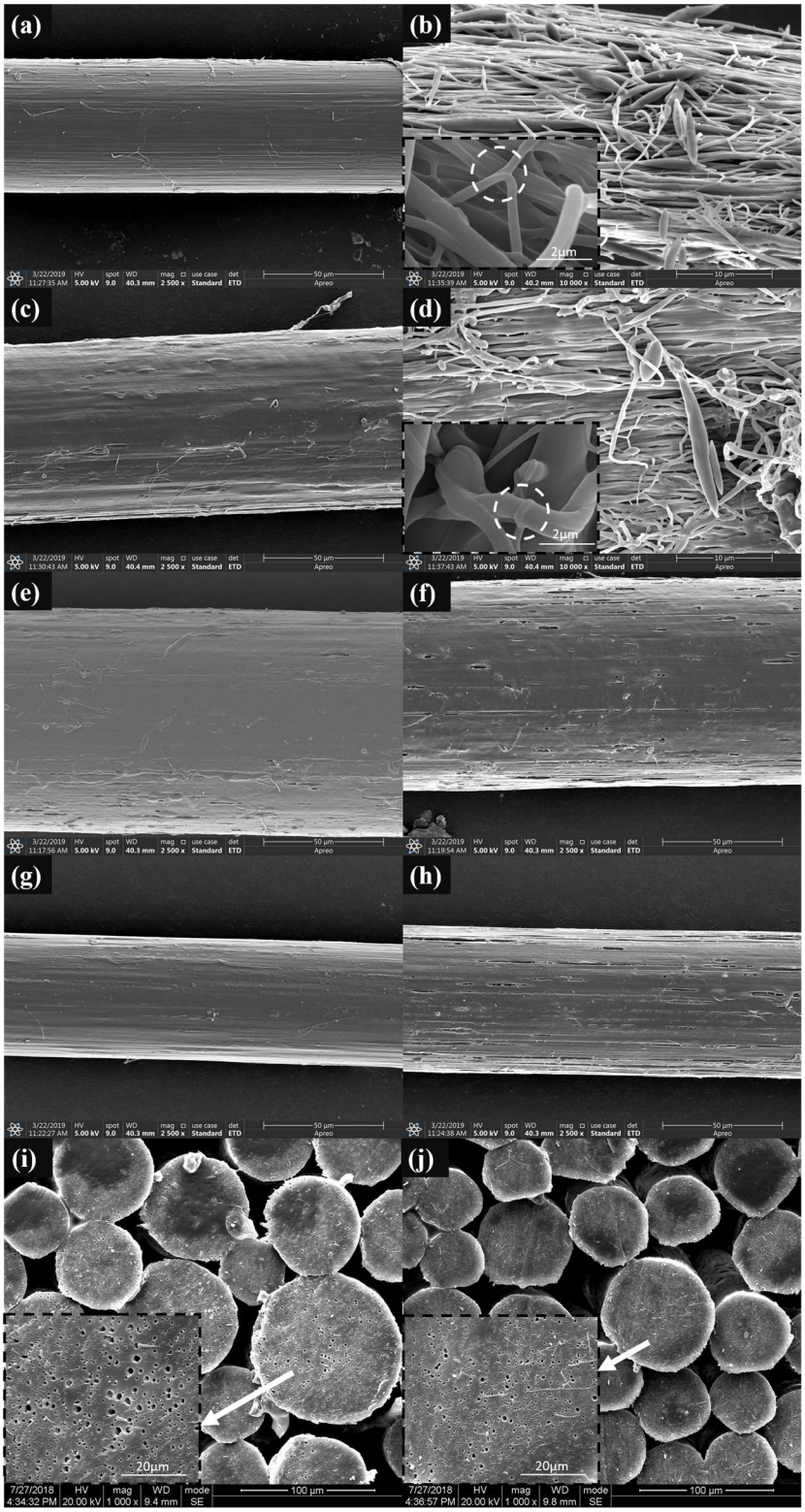

Figure 3-8 SEM observation of PP-PVA blend fibers before and after extraction (a) PP_{50}-PVA_{50}-DR_2; (b) PP_{50}-PVA_{50}-DR_2-Ex; (c) PP_{60}-PVA_{40}-DR_2; (d) PP_{60}-PVA_{40}-DR_2-Ex; (e) PP_{70}-PVA_{30}-DR_2; (f) PP_{70}-PVA_{30}-DR_2-Ex; (g) PP_{70}-PVA_{30}-DR_3; (h) PP_{70}-PVA_{30}-DR_3-Ex; (i) the cross-sections of PP_{70}-PVA_{30}-DR_2 fibers; (j) the cross-sections of PP_{70}-PVA_{30}-DR_3 fibers.

Apart from the surface topography, XRD patterns of the neat PP and PVA fibers and the related blend fibers are illustrated in Figure 3-9(a) and (b), respectively. As for PP, the α-crystalline form dominates, in which the peaks of 14.3, 17.1, 18.7 and 25.7° belong to the (110), (040), (130) and (060) planes of the α phase (Li *et al.*, 2011b), and 21.8° refers to the (131) and (041) planes of the α phase (Gradys *et al.*, 2005).The XRD peak data are illustrated in Table 3-3, with parameter specifics about (110) and (040) planes of PP to investigate its crystallite size. In contrast, the XRD pattern of PVA shows a single peak at 19.6°, corresponding to the PVA crystalline phase (Roy and Bysakh, 2011). With the DR increment of PP and PVA fibers, the XRD pattern is not changed significantly, indicating that the crystallinity is not altered strongly, resulting from the restriction on the stretched chains at high draw ratios (Zhang *et al.*, 2004).

For the blends of PP and PVA, it tends to be a combination of the XRD patterns of PP and PVA, including the positions of the related peaks. It means that the crystal form of the PP is not influenced by the addition of PVA. The peak of PVA is overlapped with that of the (130) planes of PP. With the increment of draw ratios of PP and PP_{70}-PVA_{30} fibers, the (110) (040) crystallite sizes are decreased, for the crystal was shortened in the direction perpendicular to the drawing direction (Wang *et al.*, 2017a). The improvement of the draw ratio upon PP_{70}-PVA_{30} increases the crystallinity degree. Although the PVA fraction is low in PP_{50}-PVA_{50}-DR_2, the intensity of the peaks is strong, indicating that the crystallization of PP phase in PP_{50}-PVA_{50} is improved. It is suggested that the PVA promotes the crystallization of the PP phase. Furthermore, the crystal grain size of PP (perpendicular to the drawing direction) is slightly increased due to the introduction of PVA.

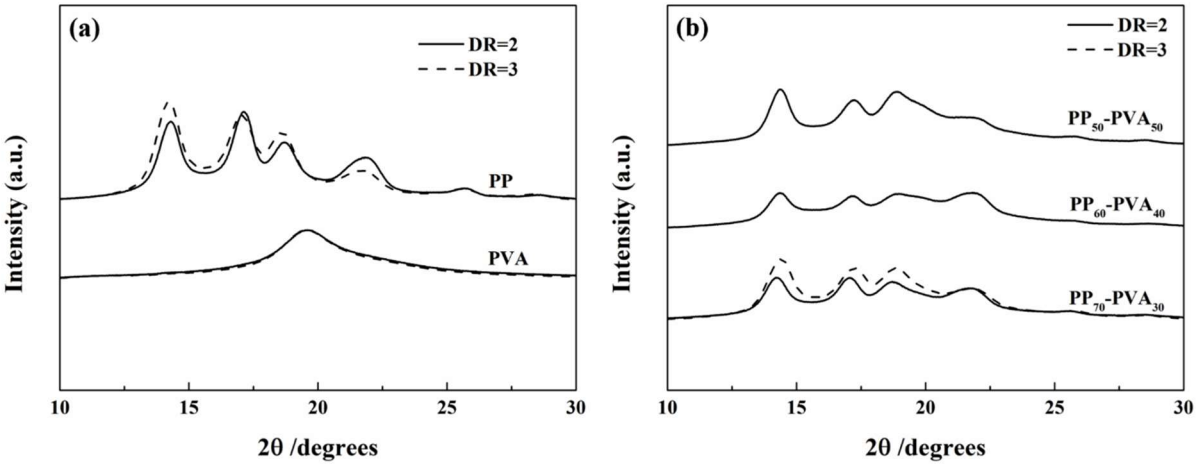

Figure 3-9 XRD spectra of (a) PP and PVA fibers with different draw ratios; (b) PP-PVA blend fibers with different fractions and draw ratios.

Table 3-3 XRD peak data of PP-containing fibers.

Fibers	2 θ(110)	FWHM1 10	D110 (Å)	2 θ (040)	FWHM04 0	D040 (Å)	2 θ (130)	2 θ (131)/(041)	2 θ (060)
PP-DR_2	14.3°	0.763	104.9	17.1°	0.695	115.5	18.7°	21.8°	25.7°
PP-DR_3	14.2°	0.824	97.1	17.0°	0.750	107.1	18.6°	21.7°	25.6°
PP_{70}-PVA_{30}-DR_2	14.2°	0.785	101.9	17.1°	0.694	115.7	18.7°	21.6°	-
PP_{70}-PVA_{30}-DR_3	14.4°	0.850	94.2	17.3°	0.765	105.0	18.8°	21.8°	-
PP_{60}-PVA_{40}-DR_2	14.4°	0.750	106.7	17.1°	0.646	124.3	19.0°	21.8°	-
PP_{50}-PVA_{50}-DR_2	14.4°	0.751	106.6	17.2°	0.691	116.2	18.9°	-	-

3.2.2 Mechanical properties

3.2.2.1 Tensile test

The tensile test for a single fiber from multifilament yarns was conducted, and the corresponding results of mechanical properties of PP-PVA blends with different ratios are displayed in Table 3-4. In order to compare the mechanical performance with that of the neat fibers, the related information of the PP and PVA fibers is also illustrated in the same table. Meanwhile, the stress-strain curves of PP-PVA fibers before and after

selective phase extraction are shown in Figure 3-10(b)(c). Similarly, the stress-strain curves of PP and PVA fibers are shown in Figure 3-10(a). From the stress-strain curves, PP fibers show ductile behaviors with high tensile toughness (breaking elongation>300%), while PVA fibers show brittle behaviors with low tensile toughness (breaking elongation<50%). The ductile behaviors are still maintained after the addition of a small quantity of PVA. However, when the fraction of PVA is increased to 50 wt.%, brittle behaviors emerge within the biphasic fibers. The behavior is related to the phase inversion of PP and PVA. It illustrates that the mechanical properties of PP_{60}-PVA_{40}-DR_2 are the weakest, which shows the worst spinnability as well. It implies that the morphological approach of a co-continuous structure leads to difficulties in melt spinning (Afshari *et al.*, 2002), due to the lack of adhesion between the two polymers. Among the three biphasic fibers with DR=2, the breaking elongation of PP_{70}-PVA_{30} shows the highest, which signifies the excellent tensile toughness of pure PP fibers is not dominantly influenced. It also possesses relatively high Young's modulus and tenacity, slightly weaker than those of the pure PP fibers.

The draw ratio can be adjusted to a higher value towards 3 for PP_{70}-PVA_{30}, and it can also keep a robust scaffold after the selective phase extraction. The impact of draw ratio on the mechanical properties was examined. With the draw ratio increase, Young's modulus and tenacity are enhanced, and the breaking elongation as well as tensile toughness are decreased, for neat PP and PVA fibers as well as PP_{70}-PVA_{30} fibers. Only PP_{70}-PVA_{30} fibers provide complete porous scaffolds, of which the mechanical properties were also tested. After the selective phase extraction experiment, the stress-strain curves indicate that the porous PP fibers exhibit ductile behaviors similar as neat PP fibers. In addition, Young's modulus was decreased for the removal of PVA. Meanwhile, the tenacity and breaking elongation (tensile toughness) was increased. Hence, the ratio of PP to PVA can be adjusted to 70 wt.%/30 wt.%, of which the polymer blend manufactures into robust multifilaments. The draw ratio is suggested be a higher value if better mechanical performance is required.

Table 3-4 Mechanical properties of blend fibers of PP and PVA with different ratios.

Fibers	Before extraction			After extraction		
	Young's modulus (MPa)	**Tenacity (cN/Tex)**	**Breaking elongation (%)**	**Young's modulus (MPa)**	**Tenacity (cN/Tex)**	**Breaking elongation (%)**
PP-DR_2	2174±238	17.9±2.2	516±66	-	-	-
PP-DR_3	2951±322	24.2±2.1	302±100	-	-	-
PVA-DR_2	3379±507	7.1±1.0	45±11	-	-	-
PVA-DR_3	3792±1224	11.2±2.0	28±7	-	-	-
PP_{70}-PVA_{30}-DR_2	1853±249	12.3±1.7	449±51	1570±389	13.1±2.9	547±65
PP_{70}-PVA_{30}-DR_3	2871±617	16.7±2.6	256±108	2012±220	20.9±2.5	371±74
PP_{60}-PVA_{40}-DR_2	1426±486	6.5±0.7	229±176	-	-	-
PP_{50}-PVA_{50}-DR_2	1962±394	13.2±2.4	24±9	-	-	-

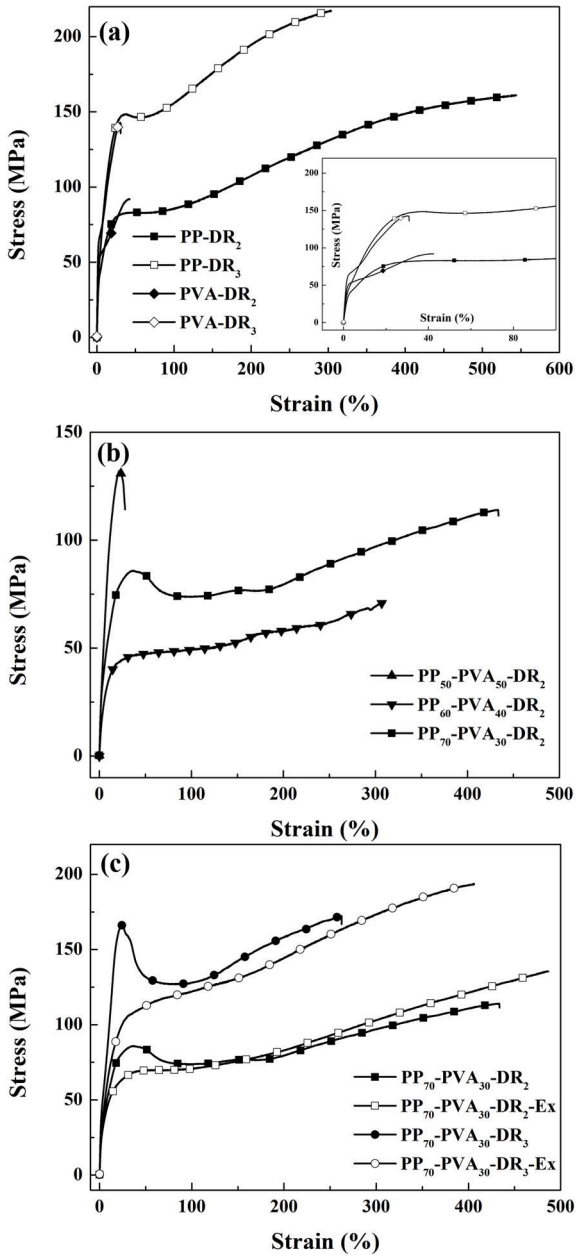

Figure 3-10 Stress-strain curves of (a) neat fibers from PP or PVA with a DR value of 2 or 3 with the zoomed figure; (b) PP-PVA fibers of different fractions with a DR value of 2; (c) PP_{70}-PVA_{30} with different DR values before and after selective phase extraction.

3.2.2.2 Dynamic mechanical analyses (DMA)

The storage modulus versus temperature plot of neat and blend fibers from PP and PVA are shown in Figure 3-11(a). The storage modulus conveys the elastic response of the viscoelastic material, indicating its stiffness and the energy conserved under an

applied load (Rizvi and D'Souza, 2016). It shows that the storage modulus of all the polymers decreases with the increment of the temperature, resulting from the increased segmental mobility (Omonov *et al.*, 2007). The change of PVA shows the most dramatic, evolved from a glassy towards a rubbery state. At a lower temperature, the storage modulus of PVA is significantly higher than that of the other fibers, showing a distinct difference. The results of tan δ of PVA and PP-PVA fibers are presented in Figure 3-11(b). The glass transition temperature of neat PVA is 80°C, and after the addition of PP, it shows no distinct variation, related on the immiscibility between PP and PVA phases.

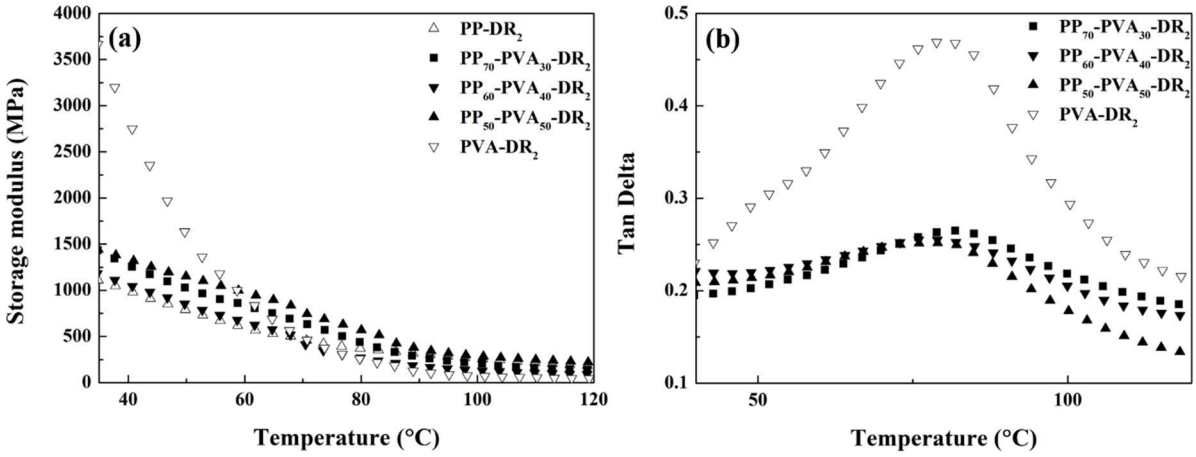

Figure 3-11 (a) Storage moduli of PP-PVA fibers with different fractions; (b) Tan δ of PP-PVA fibers with different fractions.

DMA is also a useful method to determine the PVA continuity (Wu *et al.*, 2010). For the PP-PVA, the storage moduli are affected by the crystallinity and orientation of the polymers (Zhang *et al.*, 2016). The draw ratio of the multifilament is low, and it does not experience a post-drawing process (Wang *et al.*, 2016a). Irrespective of the effects, the storage modulus of the components is regarded as invariable under the same spinning conditions (e.g., draw ratio). Therefore, it can be regarded as a semiquantitative measurement.

There are two extreme modes of the combination of biphasic polymers: parallel mode as the upper bound and series mode as the lower bound. For parallel mode, the

stress applies directly to the two components; for series mode, there exists indirect stress. When the case is converted into the biphasic microstructure, the upper bound can be regarded as the co-continuity structure, and the lower bound can be seen as the matrix-dispersed structure.

The parallel and series modes have been introduced in the part "State of the Art" in Equation 1-13 and Equation 1-14, respectively (Moly *et al.*, 2006). Herein, the mechanical property M refers to the storage modulus.

After examining the storage modulus of the two components PP and PVA, the lower and upper bound are simulated by Equation 1-13 and Equation 1-14. The storage modulus of the blends varies with the increment of PVA content. The experimental and theoretical results of PP-PVA fiber as a function of PVA weight fraction near room temperature (35°C) are illustrated in Figure 3-12. It indicates that the experimental storage moduli are more relevant to the curve of the lower bound series model (solid line, from Equation 1-14). Therefore, these fibrous blends are not highly co-continuous, and interconnectivity of PVA nodules has not been drastically constructed.

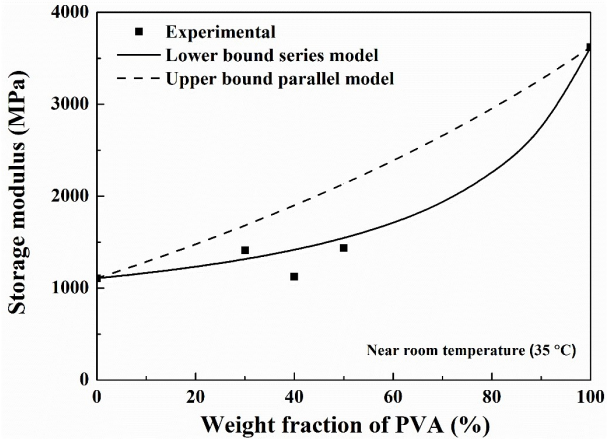

Figure 3-12 Experimental values and simulated curves of storage moduli of PP-PVA fibers as a function of PVA weight fraction near room temperature.

3.2.3 Textile creation by knitting technology

In order to check the feasibility of fabric knitting from the blend fibers, the knitting technology was attempted for the materials. It was found that the thickness of the yarns is required. Unfortunately, the fibers with a draw ratio of 2 were too difficult to be

knitted due its low fineness (high thickness), and their high elasticity and low tenacity are also unfavorable factors for the knitting fabrication. The only candidate is PP_{70}-PVA_{30}, of which the draw ratio can be further increased to 3. The mechanical properties and air permeability of the knitted fabrics from PP_{70}-PVA_{30}-DR_3 fibers are displayed in Table 3-5, denoted as PP_{70}-PVA_{30}-DR_3-Knit and PP_{70}-PVA_{30}-DR_3-Knit-Ex (after selective phase extraction). The average stress-strain curves of the two kinds of fabrics are also displayed in Figure 3-13, accompanied with the digital photos, which indicates that the shrinkage of the fabric is not obvious after the selective phase extraction. The air permeability of the PP_{70}-PVA_{30}-DR_3-Knit is 1906±44 mm/s, and after the removal of PVA, its air permeability is almost no change as 1951±149 mm/s. Because of the selective phase extraction, the thickness and areal density are decreased. The mechanical properties of the fabrics behave well with high values of maximum stress δ_{max} of 9.1±0.9 MPa and related elongation of 113.9±19.8%, performing as a brittle behavior in the stress-strain curve. After the selective phase extraction process, the maximum stress gets slightly higher as 10.2±0.2 MPa, and the elongation at δ_{max} is prolonged to 224.2±14.6%, exhibiting a more ductile behavior. It is caused by the original mechanical properties of PP materials, due to the extraction of PVA phase.

Table 3-5 Mechanical properties and air permeability of the fabrics knitted from PP_{70}-PVA_{30}-DR_3 fibers.

Fabrics	**Thickness (mm)**	**Areal density (g/m^2)**	**σ_{max} (MPa)**	**Elongation at σ_{max} (%)**	**Air permeability (mm/s)**
PP_{70}-PVA_{30}-DR_3-Knit	3.129	711.5	9.1±0.9	114±20	1906±44
PP_{70}-PVA_{30}-DR_3-Knit-Ex	2.725	552.8	10.2±0.2	224±15	1951±149

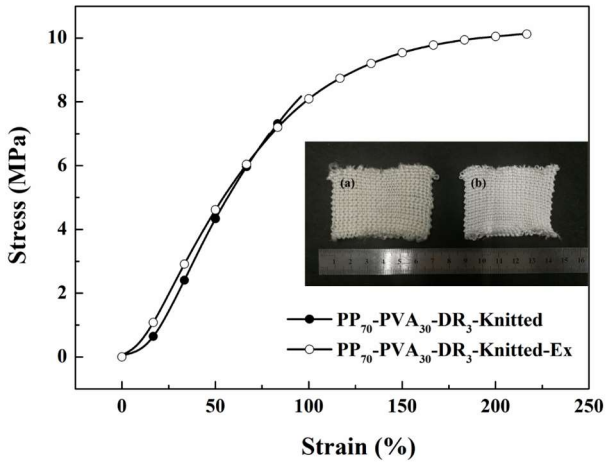

Figure 3-13 Stress-strain curves of the knitted fabrics from PP_{70}-PVA_{30}-DR_3 before and after selective phase extraction.

3.3 Conclusion

This chapter reports on a simple method to fabricate porous PP fibers from PP-PVA blends. The microstructure of PP-PVA was tailored by different ratios. Three different ratios were employed for melt spinning, and the fraction of PVA is increased from 30 wt.% to 50 wt.%. The motivation is to explore the ideal ratio of PP and PVA to spin the biphasic multifilament fibers with good performance as porous fibers.

For the polymer compounds, the PP-PVA blend shows excellent thermal stability, which favors the stable melt processing, and the crystallization behavior of PP is influenced by the state of its dispersion. It is revealed that the biphasic microstructure experiences a significant change by altering the PVA content. The structure was evolved from PP matrix-PVA dispersed structure (PP_{60}-PVA_{40}) towards PVA matrix-PP dispersed structure (PP_{50}-PVA_{50}). For rheological analysis, the variation in storage modulus of blends also provides an evidence for the phase inversion.

The MFI result indicates that there is a negative deviation in viscosity, due to the weak interactions between the two polymers. PP_{70}-PVA_{30} performs an excellent spinnability during melt spinning, along with good mechanical properties. Furthermore, it is inspiring that although PP_{70}-PVA_{30} extrudates own a large quantity of isolated PVA nodules, the drawing during melt spinning makes the PVA interconnected, exhibiting an outstanding value of PVA accessibility. The extraction of dominant PVA leaves

complete porous fibrous shapes, maintaining good mechanical performance. In addition, a higher draw ratio is suggested to be adopted, which contributes to higher PVA accessibility and mechanical properties. Furthermore, thanks to the higher draw ability, the PP_{70}-PVA_{30}-DR_3 fibers were successfully knitted into fabrics for extending the potential textile use, and the porous PP fabric was also obtained. Conversely, a higher PVA fraction offers a worse spinnability with more fragile mechanical behavior and even lower PVA accessibility. What's more, it cannot provide porous fibrous scaffold after selective phase extraction.

Results verify the feasibility and find out the most suitable ratios of PP and PVA (70 wt.%/30 wt.%), to fabricate porous PP fibers and related fabrics with a dominant PVA removal and ideal mechanical properties.

Chapter IV:

Microstructure Evolution of Immiscible PP-PVA Blends Incorporated with Silica Nanoparticles and Its Transformation into Fibers

Chapter 4 Microstructure Evolution of Immiscible PP-PVA Blends Incorporated with Silica Nanoparticles and Its Transformation into Fibers

The incorporation of nanoparticles can endow the bulk polymers with additional properties. They also play an important role in tailoring the microstructure of the biphasic materials. Apart from tailoring the ratio of PP and PVA, this chapter will take silica nanoparticles for example to discover the microstructure diversification of PP-PVA blends. The mass ratio of PP to PVA is kept at 70 wt.% to 30 wt.%, and 1wt.% (overall) of fumed silica nanoparticles are introduced into the blends. Three typical silica nanoparticles with different wettability are hydrophilic Si_{S5505}, partially hydrophobic Si_{R816} and highly hydrophobic Si_{R972}. Afterwards, the extrudates were further manufactured into fibers.

4.1 Polymeric compounds

4.1.1 Prediction and confirmation of silica localization

The localization of the fumed silica nanoparticles can be predicted by the Young's model (Fenouillot *et al.*, 2009), as Equation 1-18 in the "State of the Art" part. The obtained wettability parameter $\omega_{A\text{-}B}$ plays the role of important judgment basis.

As for the localization of silica nanoparticles, when $\omega_{A\text{-}B}<-1$, silica nanoparticles will be localized in phase B; when $\omega_{A\text{-}B}>1$, silica nanoparticles will be localized in phase A; and if $\omega_{A\text{-}B}$ is of other values, silica nanoparticles will be localized at the interface between the two polymers.

The surface tensions of polymers and fumed silicas at 25°C and 200°C are illustrated in Table 4-1. The related results were normally conducted at room temperature (25°C). However, the surface tension is temperature dependent, and the pellets were extruded at a high temperature (160°C-200°C). Therefore, it would be

better to carry out the values at the extrusion temperature. For the tested polymers, the relationship of Guggenheim (1945) was applied to obtain the γ at 200°C in Equation 1-20.

For the fumed silicas, the γ value is cited from the related representative literatures. It is worth noting that the surface energy of Si_{S5505} is derived by the related contact angles of one kind of typical bare fumed silica. Elias *et al.* (2008b) proposed that for silica particles, the surface tension can be estimated by using the constant rate $d\gamma/dT$ as -0.1 mN m^{-1} K^{-1}.

Yan *et al.* (2000) found that although Si_{R816} has been modified with hexadecylsilane, it can also be easily dispersed into water, still behaving relatively hydrophilic, which is reflected in its surface energy. It shows increasing hydrophobicity followed by Si_{S5505}, Si_{R816} and Si_{R972} silica nanoparticles.

Table 4-1 Surface tension of polymers and fumed silicas.

	Surface tension (mN/m)						γ_0	**Tc (K)** [a]	$-d\gamma/dT$ (mN m^{-1} K^{-1})
	25°C			**200°C**					
	γ	γ^d	γ^p	γ	γ^d	γ^p			
PP	24.7	24.5	0.2	16.4	16.3	0.1	40.0	914	-
PVA	60.2	32.6	27.6	41.0	22.2	18.8	95.5	948	-
Si_{S5505} [b]	91.1	0.7	90.4	73.6	0.6	73.0	-	-	0.1
Si_{R816} [b]	88.5	0.4	88.1	71.0	0.3	70.7	-	-	0.1
Si_{R972} [c]	32	30	2	14.5	13.6	0.9	-	-	0.1

a. Related critical temperatures are cited from (Lewin *et al.*, 2005);

b. Values calculated from the contact angles of water and toluene with the silica nanoparticles (Yan *et al.*, 2000);

c. Values cited from (Fenouillot *et al.*, 2009).

For the systems at 200°C, estimation of the interfacial tension can be achieved via Equation 1-21 and Equation 1-22. Both geometric and harmonic averages of interfacial energy between polymers and silica nanoparticles are listed in the Table 4-2.

Table 4-2 Interfacial energy between different components (silica with polymer, polymer with polymer) using geometric and harmonic mean equations.

	Interfacial energy with PP (mJ/m^2)		**Interfacial energy with PVA (mJ/m^2)**	
	Geometric mean	**Harmonic mean**	**Geometric mean**	**Harmonic mean**
Si_{S5505}	78.3	87.3	33.2	52.5
Si_{R816}	77.7	85.8	33.9	51.4
Si_{R972}	0.5	0.9	12.5	18.3
PP	-	-	16.6	19.4

The wetting parameters $\omega_{PP\text{-}PVA}$ can be obtained by Equation 1-18. Regarding PP as phase A and PVA as phase B, both of the geometric and harmonic averages of $\omega_{PP\text{-}PVA}$ were calculated and shown in Table 4-3. ω is calculated less than -1 for both PP-PVA-Si_{S5505} and PP-PVA-Si_{R816} samples, which predicts that at thermodynamic equilibrium, the fumed silicas will be preferentially located inside the PVA phase. As for PP-PVA-Si_{R972}, the value of $\omega_{PP\text{-}PVA}$ is 0.72 in geometric mean and 0.90 in harmonic mean, of which both indicate that Si_{R972} silica tends to be limited at the interface of PP. While extrusion, complete thermodynamic equilibrium may be hard to achieve, because the processing time is short (Elias *et al.*, 2007). However, due to the high shear force of the twin screws in the extrusion machine, the thermodynamical prediction still offers a strong preference to predict the tendency of the nanofiller migration.

Table 4-3 Wetting parameters $\omega_{PP\text{-}PVA}$ calculated with geometric and harmonic data and the localization predictions of silica nanoparticles.

Silica nanoparticle	Wetting parameter (geometric mean)	Wetting parameter (harmonic mean)	Prediction
Si_{S5505}	-2.72	-1.79	PVA phase
Si_{R816}	-2.64	-1.77	PVA phase
Si_{R972}	0.72	0.90	interface

In order to confirm the localizations of different silica nanoparticles, the TEM observation of the cross-section of the extrudates was carried out. The definite localizations of nanoparticles are summarized in Table 4-4. Representative TEM images of three blends are enclosed in Figure 4-1. Due to the lower fraction of PVA, spherical PVA domains can be distinguished in the PP matrix. Hydrophilic unmodified Si_{S5505} silica nanoparticles are trapped in the PVA domains, because of the strong affinity between Si_{S5505} and PVA. The definite distribution of Si_{S5505} silica nanoparticles is identical with the prediction. Si_{R816} nanoparticles are predicted to be localized within the PVA nodules, however, the silica nanoparticles are found not only in the PVA phase, but also at the interface of PP and PVA. The blending procedure is decided as pre-blending silica particles in PP matrix and blending PVA and the silica-filling PP pellets. Therefore, owing to the kinetics of the silica particles, Si_{R816} transferred from less preferred PP phase to the PVA phase, passing through the interface, and a tiny number of silica nanoparticles appear at the interface.

The hydrophobic Si_{R972} silica is localized exclusively at the biphasic interface, while a small amount of Si_{R972} silica nanoparticles can also be found within the bulk phases. Given the wetting parameter $\omega_{PP\text{-}PVA}$ (near 1) of Si_{R972} and the kinetic factors, it is not difficult to explain why the silica nanoparticles are also distributed in the PP phase. As for the silica nanoparticles with PVA phase, perhaps it may be resulted from the modification inhomogeneity of Si_{R972} silica nanoparticles. Nevertheless, it is

inspiring that a large quantity of silica nanoparticles is distributed at the interface and form a partial thin layer, although only 1 wt.% of silica nanoparticles are involved in the blends. It can be expected that if a higher quantity of Si_{R972} silica nanoparticles are incorporated, the interface enrichment behavior of silica nanoparticles would be enhanced. If PVA is removed afterwards, surface-modified PP can be obtained.

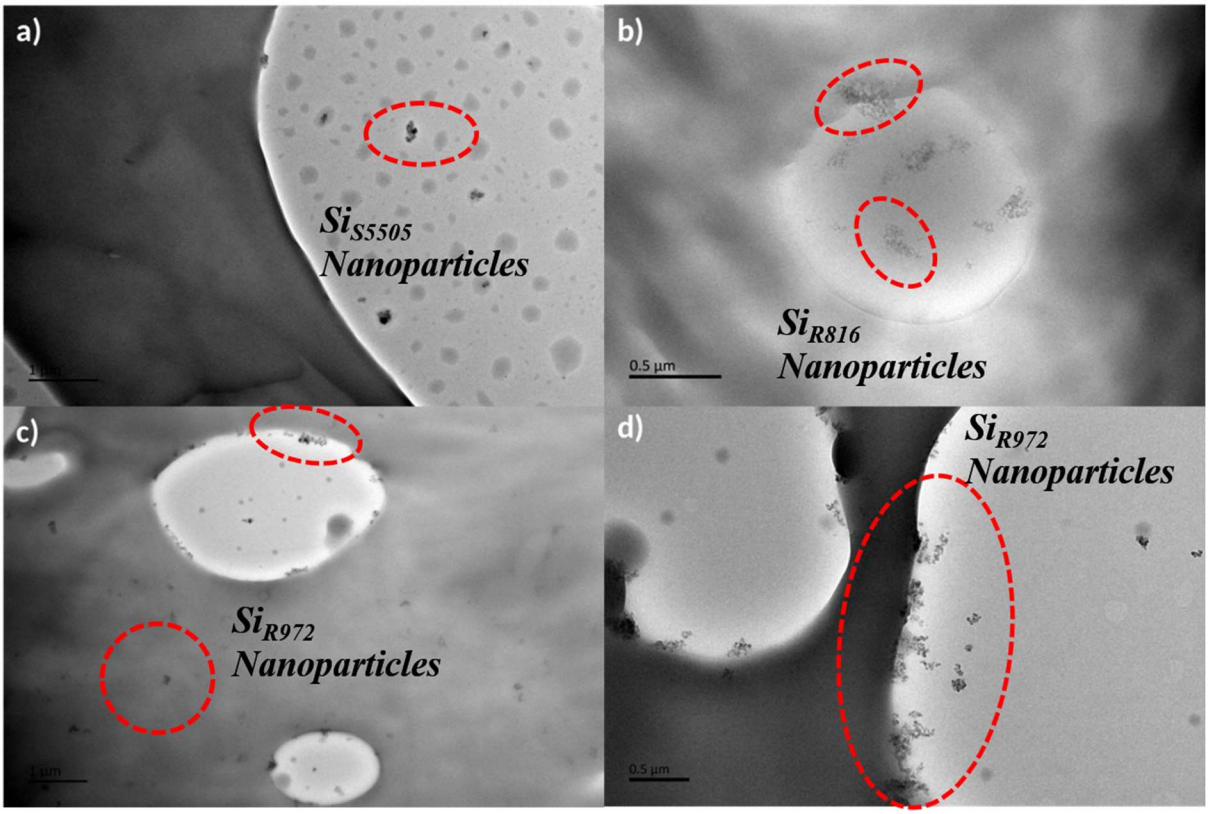

Figure 4-1 TEM observation of the PP-PVA blends with silica nanoparticles. (a) PP_{70}-PVA_{30}-Si_{S5505}; (b) PP_{70}-PVA_{30}-Si_{R816}; (c) PP_{70}-PVA_{30}-Si_{R972}; (d) PP_{70}-PVA_{30}-Si_{R972} (higher magnification).

Table 4-4 Confirmation of the localization of nanoparticles in PP-PVA blends from TEM images.

Silica nanoparticle	Confirmation
Si_{S5505}	PVA phase
Si_{R816}	PVA phase, interface
Si_{R972}	PP phase, interface, PVA phase

4.1.2 Morphology of the polymer blends

As we know, the heterogeneously distributed nanoparticles will affect the morphology evolution. Thus, the biphasic morphology investigation of the three blends is concentrated on. First of all, the polymer blends were selectively extracted by water to test the PVA accessibility degree, and the results are displayed in Figure 4-2. The PVA accessibility degree of PP_{70}-PVA_{30} is 50.5±3.0%, and it maintains below 60% with the addition of silica nanoparticles, implying that PP and PVA still perform matrix-dispersed structure. However, the PVA accessibility ranges a lot, which indicates that the addition of silica nanoparticles will affect the interconnection of PVA significantly. After introduction of Si_{S5505} nanoparticles, the PVA accessibility degree increases slightly to 58.8±1.4%. If the modified silica nanoparticles Si_{R816} and Si_{R972} are incorporated into the blends, the PVA accessibility will decrease to 41.7±2.9% and 26.5±1.7%, respectively. It is mainly ascribed to the different localization of the fumed silicas.

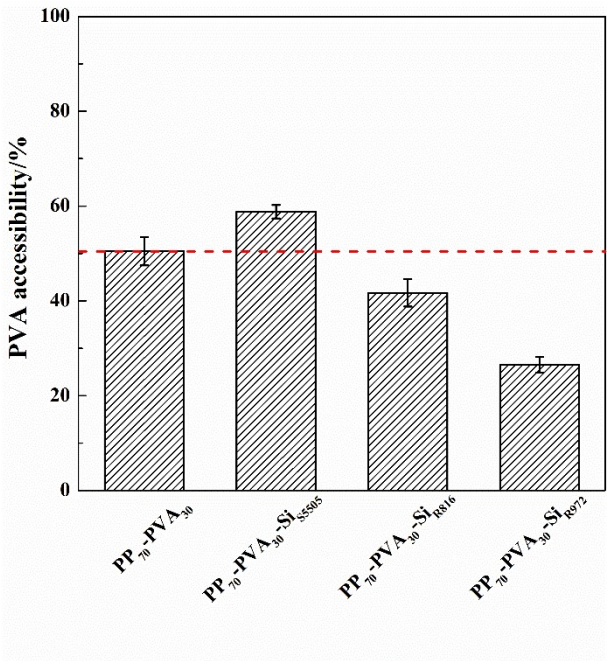

Figure 4-2 PVA accessibility degree of the PP-PVA blends with 1 wt.% of silica nanoparticles with different hydrophobicity (the red dotted line represents the value of PP_{70}-PVA_{30}).

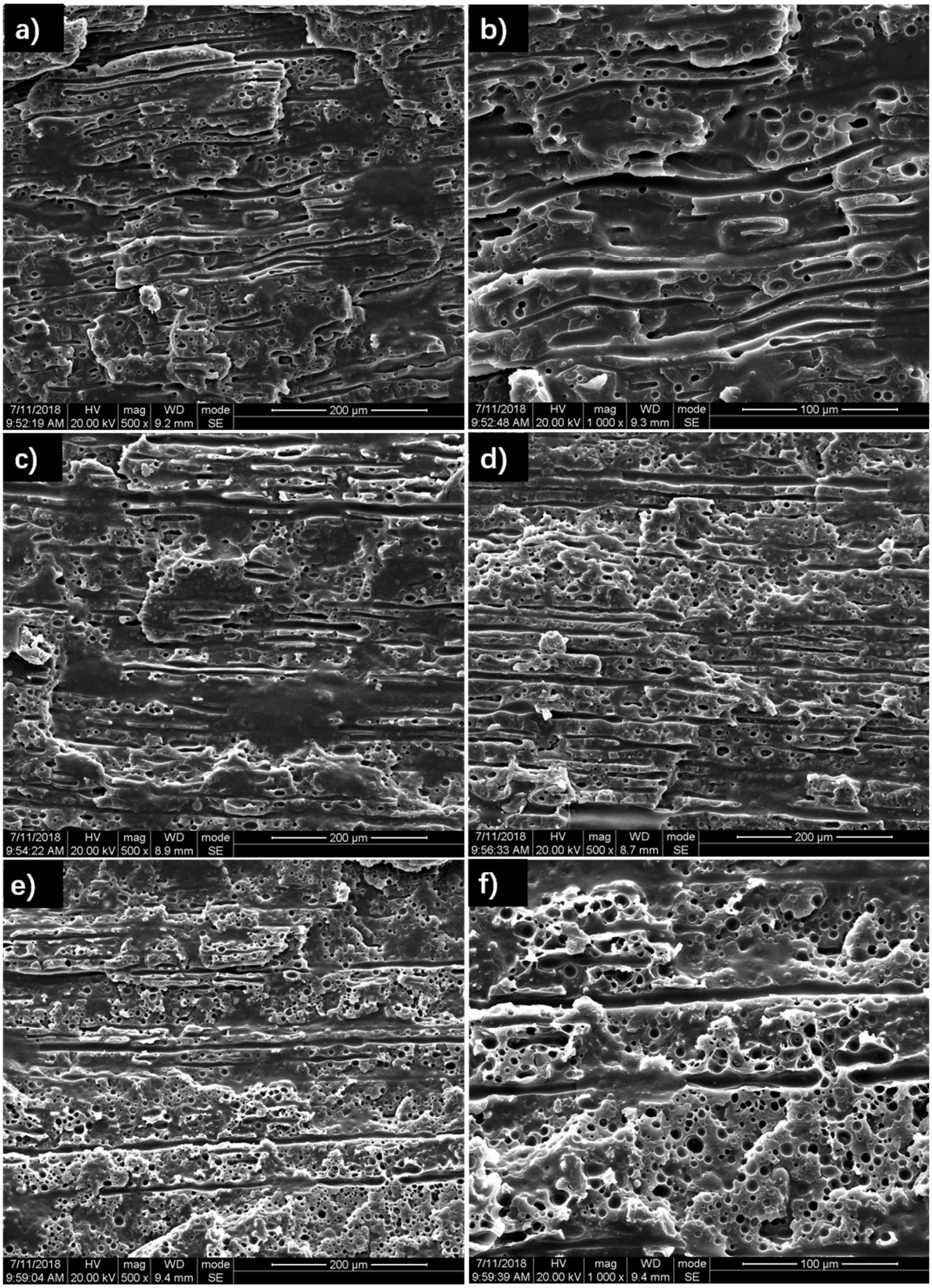

Figure 4-3 SEM images of the longitudinal section of the extrudates. (a)(b) PP_{70}-PVA_{30}; (c) PP_{70}-PVA_{30}-Si_{S5505}; (d) PP_{70}-PVA_{30}-Si_{R816}; (e)(f) PP_{70}-PVA_{30}-Si_{R972}.

Table 4-5 Characteristics of the microstructure of extrudates from PP-PVA blends.

Sample	Spherical PVA		Transitional PVA		Fibrous PVA	
	D_{sv} (μm)	Projection fraction (%)	D_{tn} (μm)	Projection fraction (%)	D_{fn} (μm)	Projection fraction (%)
PP_{70}-PVA_{30}	10.0	22.1	6.4	41.9	5.3	36.0
PP_{70}-PVA_{30}-Si_{S5505}	11.8	20.6	8.5	36.0	9.2	43.4
PP_{70}-PVA_{30}-Si_{R816}	11.4	29.3	7.1	33.0	8.1	37.7
PP_{70}-PVA_{30}-Si_{R972}	8.3	40.0	4.7	15.0	6.4	45.0

To systematically investigate the morphology evolution of the blend extrudates, the SEM observation was carried out. The shapes of the PVA nodules from the cross-section are identical as circles, of which the SEM results are not presented in consequence. The SEM images of the longitudinal section of PP_{70}-PVA_{30} extrudates with and without fillers are shown in Figure 4-3. The PVA nodules are classified into 3 kinds, spherical, transitional and fibrous, and the average diameters of the three kinds of PVA nodules were counted. The methodology of measurement has been stated in 2.2. The fiercely deformed nodules (transitional and fibrous) determine the PVA accessibility of the blends, which make the PVA interconnected. In addition, the volume of one nodule can be viewed as the integral of the tremendous projections of every layer, thus the projection fraction of the classified PVA nodules was totaled, and it can represent the proportion of the three components to some extent. The average diameter and projection fractions are illustrated in Table 4-5.

For PP_{70}-PVA_{30} blend, transitional PVA is the major component in the PVA nodules (41.9 %). The dominant fraction goes to the fibrous structure, and the diameter of fibrous PVA is elevated after the addition of nanofillers. It suggests that the addition of fillers will help the formation of fibrous PVA. For the spherical and transitional PVA, the localization of the silica nanoparticles makes the diameter and fraction quite varied. For Si_{S5505} silica nanoparticles, it centralizes within the PVA phase. As a result, the diameter of spherical and transitional PVA increases. More spherical and transitional

PVA will transform into fibrous PVA. The elongation and irregularity will contribute to the increment of the PVA accessibility. It may be caused by the slowdown of destructive processes like fibril breakup by filling (Steinmann *et al.*,2002a).

For hydrophobic Si_{R972} silica nanoparticles, the dominant position of silica nanoparticles goes to the interface. The enlarged SEM images of PP_{70}-PVA_{30} and PP_{70}-PVA_{30}-Si_{R972} are enclosed in Figure 4-3(b) and (f), respectively. It can be seen clearly that there are more spherical nodules instead of transformed ones. From Table 4-5, the fraction of transitional PVA is reduced from 41.9% to 15.0 % and instead the fraction of spherical PVA is increased from 22.1% to 40.0 %. What's more, the Si_{R972} silica nanoparticles lead to a significant reduction of diameter of spherical and transitional PVA. It can be ascribed that these interface-located silica nanoparticles can act as steric hindrance or exert surface energy effects, preventing the coalescence of PVA nodules (Elias *et al.*, 2007).

As for Si_{R816} silica nanoparticles, the TEM observation has illustrated that the silica nanoparticles are located within the PVA phase and at the interface. Although the silica nanoparticles inside the PVA phase can contribute to the increment of PVA accessibility, the prevention effect of interface-located silica nanoparticles in PVA coalescence cannot be ignored. As a result, the diameter of spherical and transitional PVA increases, while more transitional PVA is transformed into spherical PVA. As a result, it gives rise to the slight reduction of PVA accessibility. Silica nanoparticles with different localizations endow PVA accessibility with diversities by tuning the biphasic morphology. Conversely, PVA accessibility also gives evidences about the silica localizations.

4.1.3 Rheometer tests

The linear viscoelastic behavior of the blends was examined by the rheological analyses. The results are illustrated in Figure 4-4. Storage modulus and $\alpha(\omega)$ curves are respectively displayed in Figure 4-4(a), and the complex viscosities of the polymers are given Figure 4-4(b). For the additional fraction of silica is only 1 wt.%, G' curves of the blends with silica nanoparticles are not changed obviously. However, the G' curves

present subtle differences, which can still offer some evidence about the evolution of microstructure. Among the blends, their high frequency response is almost the same, which is only controlled by the relaxation process of the polymer chains, while for the low frequency area the storage modulus shows some differences. Upon the addition of silica nanoparticles, all of the α(ω) values at the low frequency are almost decreased. The extra elasticity should be confirmed by many factors, and different localizations of nanoparticles make a different contribution. For PP_{70}-PVA_{30}-Si_{S5505}, it may be resulted from the increasing interconnectivity of the PVA nodules; while for PP_{70}-PVA_{30}-Si_{R816} and PP_{70}-PVA_{30}-Si_{R972}, although the shapes and sizes are refined leading to a decrease of elasticity, the solid character of the interface filled with silica nanoparticles gives a stronger contribution. It leads to an even lower α(ω) value at the low frequency area compared with PP_{70}-PVA_{30} blend. The addition of silica nanoparticles has a certain effect upon the complex viscosities of the blends. After the addition of Si_{S5505} or Si_{R816}, the complex viscosity will be enhanced; after the introduction of Si_{R972}, its complex viscosity will be weakened. The alteration may be influenced by the biphasic morphology, which is determined by the localization of silica nanoparticles.

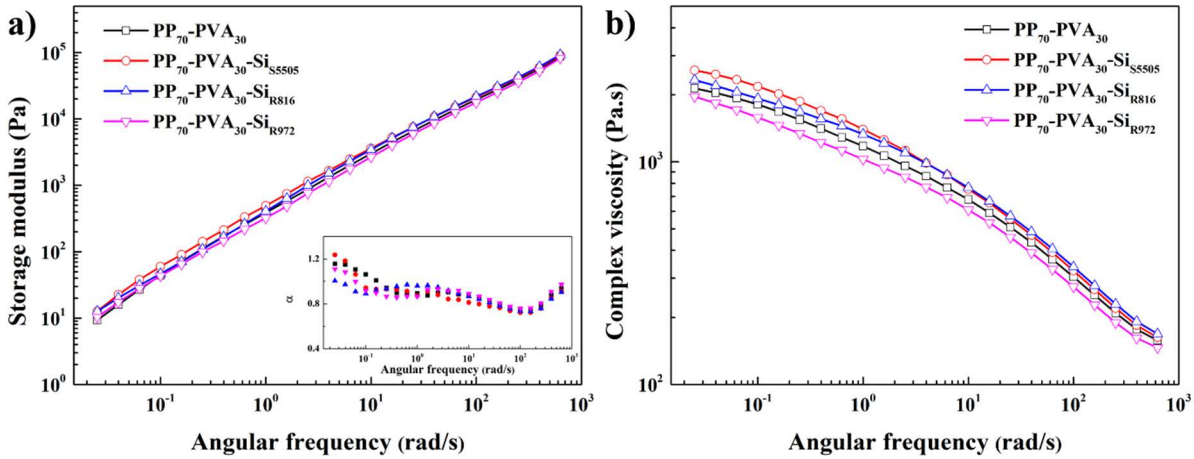

Figure 4-4 Rheological behaviours of PP_{70}-PVA_{30}, PP_{70}-PVA_{30}-Si_{S5505}, PP_{70}-PVA_{30}-Si_{R816} and PP_{70}-PVA_{30}-Si_{R972} at 190 °C. (a) Storage modulus and α(ω); (b) Complex viscosity.

4.1.4 Melt flow index (MFI)

Prior to melt spinning, MFI measurement is an effective and global technology for testing the fluidity of polymers, for the determination of the processing temperature. The melt flow indexes of PP_{70}-PVA_{30} extrudates with and without fillers at 190°C are shown in Figure 4-5. For the polymer blends from PP_{70}-PVA_{30}, all the MFI values are centralized from 15 to 30 g/10 min as the spinnable zone (Cayla *et al.*, 2016), signifying that 190°C may be appropriate for the melt spinning. The MFI of PP_{70}-PVA_{30} is 27.6±0.3 g/10 min, and the blend with Si_{S5505} nanoparticles keeps constant in MFI index. After the introduction of Si_{R816} and Si_{R972}, the values go down mildly with 25.4±0.3 and 24.6±0.8 g/10 min, respectively. In general, a small amount of silica nanoparticles slightly alters the viscosity. Based on the details of the localizations, it is confirmed that there are an increasing fraction of silica nanoparticles distributed at the interface between PP and PVA, with the increment of the hydrophobicity (Si_{R972}>Si_{R816}>Si_{S5505}) of the fillers. It leads to the enhancement of interactions between the two components, reflected in the decreasing MFI values and increasing viscosity.

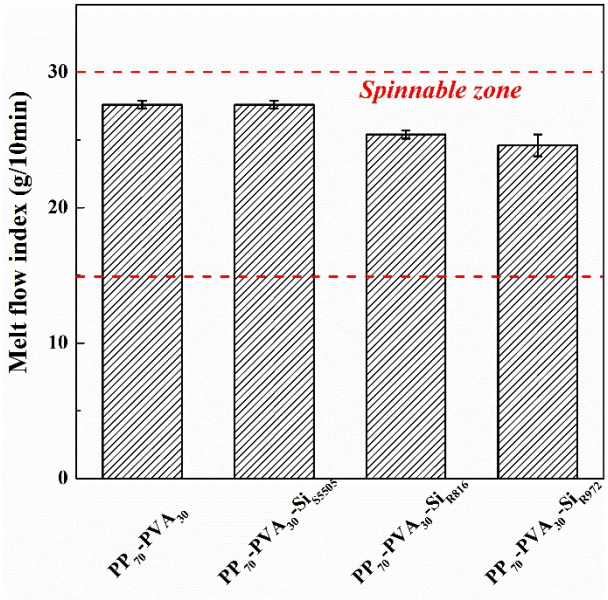

Figure 4-5 Melt flow index (190°C, 2.16 kg) of PP_{70}-PVA_{30} without/with different silica nanoparticles (the range between the two red dotted lines represents the spinnable zone).

4.2 Polymeric fibers

Controlling the dispersion and location of nanoparticles in polymeric matrices is necessary to fully exploit the desired properties. Thus, the selective distribution of particles is linked to their wettability by polymers provided that thermodynamic equilibrium is reached. It was found that depending on their surface properties, i.e., hydrophilic (Si_{S5505}), partially hydrophobic (Si_{R816}) and hydrophobic (Si_{R972}), nanosilica particles were distributed:

(1) in the PVA phase for Si_{S5505};

(2) partially at the interface and in the PVA phase for Si_{R816};

(3) dominantly at the interface, and a small amount in bulk polymers for Si_{R972}.

It is of great interest to explore the fibrous morphology evolution and concomitant changes in mechanical properties in function of different silica nanoparticles.

The spinning of PP_{70}-PVA_{30} performs well without any broken threads, and the spinnability is maintained as well after the addition of 1 wt.% of different silica nanoparticles, without any broken fibers during the manufacturing process. The draw ratios were successfully adjusted to 2 and 3, which were relatively more stable conditions for melt spinning, and the low draw ratios can better serve an investigation of the transition from extrudates to yarns.

4.2.1 Localization of silica nanoparticles within the fibers

To illustrate the localization of the silica nanoparticles within the biphasic fibers, the microscopic methods were attempted. As the transmission electron scanning microscopy (TEM) was not a feasible method due to the difficult preparation of sliced fibers even with the aid of epoxy resin, scanning electron microscopy (SEM) was conducted upon the PP_{70}-PVA_{30}-Si_{R972}-DR_3-Ex porous fibers. Some of the PVA phases are on the surface of the PP-PVA composite fibers, exposing some of the external inner surface after selective phase extraction, which can be directly observed. For the internal inner surfaces are unexposed inside the porous fibers, the fibers were cut obliquely with

the aid of liquid nitrogen, as illustrated in Figure 4-6(a)(b). Therefore, the unexposed internal inner surface could also be investigated. The other SEM images perform the observation of the internal and external inner surfaces of the biphasic fibers with the higher draw ratio with 3. The agglomerated silica nanoparticles can be clearly detected, of which the dimension is on the order of hundreds of nanometers, identical with the TEM observation towards the extrudates. Almost no Si_{S5505} silica nanoparticles remain on the inner surface of the porous fibers of PP_{70}-PVA_{30}-Si_{S5505}-DR_3-Ex. Most of the Si_{S5505} have been removed with the help of the solvent water. Due to the strong agglomeration of Si_{S5505} silica nanoparticles for their hydrophilicity, there are still some residual particles with a large dimension inside the holes. A small quantity of Si_{R816} silica nanoparticles are embedded on the inner surface of the porous PP fibers of PP_{70}-PVA_{30}-Si_{R816}-DR_3-Ex. Furthermore, if Si_{R972} silica nanoparticles are incorporated within the fibers, more nanoparticles are localized on the inner surface, also confirming the preponderant localization of fillers at the biphasic interface of PP_{70}-PVA_{30}-Si_{R972}-DR_3 fibers. All of the SEM observations of the porous fibers correspond well with the TEM results of the extrudates. It proves that the relative localization of silica nanoparticles has been basically fixed during the extrusion process, for the thermodynamic equilibrium has been achieved.

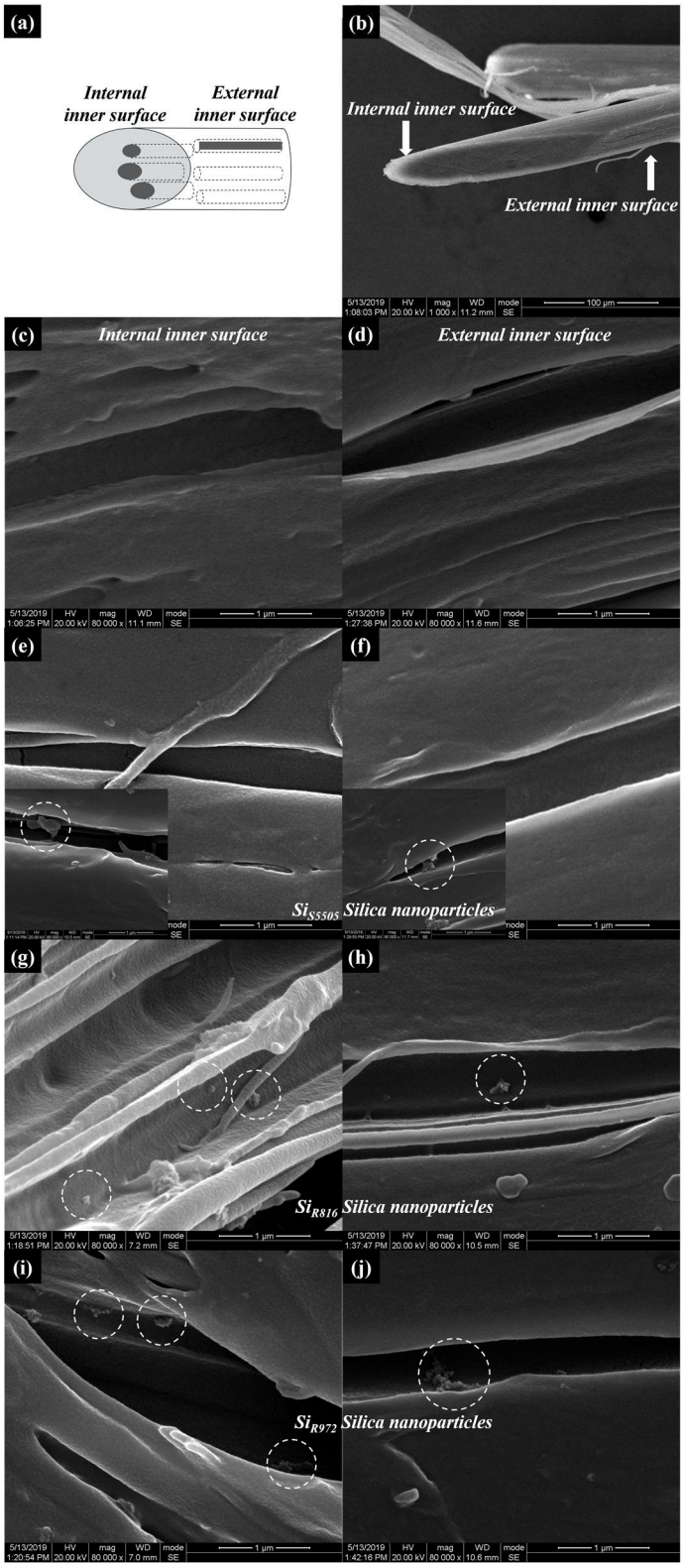

Figure 4-6 (a) Schematic figure of SEM sample preparation; (b) SEM image of an obliquely cut fiber from PP_{70}-PVA_{30}-DR_3-Ex; Internal and external inner surfaces of (c)(d) PP_{70}-PVA_{30}-DR_3-Ex; (e)(f) PP_{70}-PVA_{30}-Si_{S5505}-DR_3-Ex; (g)(h) PP_{70}-PVA_{30}-Si_{R816}-DR_3-Ex; (i)(j) PP_{70}-PVA_{30}-Si_{R972}-DR_3-Ex.

4.2.2 Morphology of the fibers

The localization of silica nanoparticles was confirmed again within the melt-spun yarns. To investigate the morphology of the fibers, PVA cross-sectional dimensions and its accessibility as well as PP crystalline structure were analyzed, respectively. The silica sorts and draw ratios play differentiated roles in the morphology evolution, to be discussed as two variables in the following section.

4.2.2.1 PVA cross-sectional dimensions

To observe the biphasic morphology of the fibers and estimate the biphasic specific interface area, the SEM images of the cross-section of blend fibers (before extraction) were taken. SEM images of the cross-section of the representative fibers are shown in Figure 4-7. Due to the low temperature induced by liquid nitrogen and the biphasic immiscibility, the PVA nodules were detached from the cross-section and formed tremendous porous structure. Therefore, the pores existing on the cross-section stand for the traces of PVA fibrous droplets. It should be noted that the diameters of the multifilament fibers are not uniform, which has a significant impact on the diameter distribution of PVA nodules.

In order to exclude impact, all the comparisons were made between fibers with a mean diameter close to 68.1 μm (the mean diameter of PP_{70}-PVA_{30}-DR_2 related fibers) and 56.4 μm (PP_{70}-PVA_{30}-DR_3). The figure legend about the acquisition of the cross-section of the biphasic fibers is illustrated in Figure 4-7(e), to determine the specific surface area (per unit mass of the blend fiber). A thin layer was observed in the calculation, and tiny PVA cylinders can be studied. Equation 4-1 expressed the specific interface area A of this layer.

$$A = \frac{\sum_{i=1}^{N_S} \pi d_i \delta_H}{\sum_{i=1}^{N_S} \pi (\frac{d_i}{2})^2 \delta_H \rho_{PVA} (1/w_{PVA})} = \frac{4 w_{PVA}}{\rho_{PVA}} \frac{\sum_{i=1}^{N_S} d_i}{\sum_{i=1}^{N_S} {d_i}^2} \quad \textbf{Equation 4-1}$$

Where N_s is the number of the PVA cylinders, d_i is the bottom areas of the i-th PVA cylinder, δ_H is the thickness of the layer (close to zero), which will be eliminated in the final formula, ρ_{PVA} is the density of PVA, and w_{PVA} is the mass fraction of PVA. The mean diameter $d_s = \frac{\sum_{i=1}^{N_s} {d_i}^2}{\sum_{i=1}^{N_s} d_i}$ can be defined to study the change of the specific interface area, which shows a negative correlation.

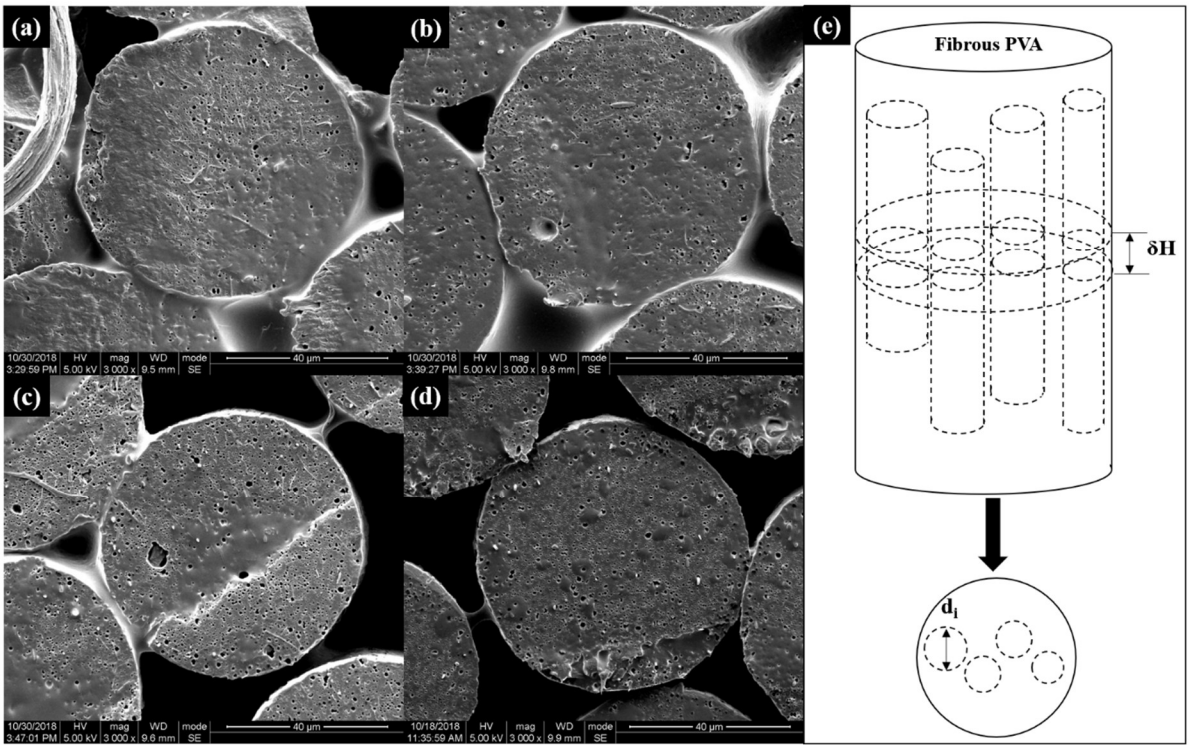

Figure 4-7 SEM images of the fiber cross-sections without/with different silica nanoparticles (a) PP_{70}-PVA_{30}-DR_2; (b) PP_{70}-PVA_{30}-Si_{S5505}-DR_2; (c) PP_{70}-PVA_{30}-Si_{R816}-DR_2; (d) PP_{70}-PVA_{30}-Si_{R972}-DR_2. (e) schematic diagram about the thin layer acquired from a biphasic fiber.

(a) The impact of silica nanoparticles

The diameters of the examined fibers and the mean diameters of the PVA filament (pores) are shown in Table 4-6. Note that the diameter of the monofilament is too hard to be fixed at a certain value. Therefore, only semi-quantitative conclusion can be drawn, for the diameter differences of the monofilament fiber. Nevertheless, it is found that the addition of the silica nanoparticles in small amounts does not give a significant change

in mean diameter of PVA nodules. What's more, there is a tight relationship between the mean diameter of PVA nodules and specific interface area. It is concluded that the specific interface area is not influenced drastically either by the silica nanoparticles.

(b) The impact of draw ratios

The main influence upon the PVA diameters originates from draw ratios. The mean diameter of PVA phases is 0.29 μm for PP_{70}-PVA_{30}-DR_2, and the specific interface area is 3.2 m^2/g based on Equation 4-1. Therefore, the fibers provide a suitable scaffold to embed nanofillers. With the increase in the draw ratio, the pore diameter decreases to 0.26 μm, related to the decrease in the fiber diameter. Similarly, the specific interface surface area of PP_{70}-PVA_{30}-DR_3 was estimated at 3.6 m^2/g, exhibiting an increase with the draw ratio. For the silica-containing fibers, a high draw ratio also has an enhancement towards the specific interface area.

Table 4-6 Diameter of the pores inside the representative fibers.

Fibers	DR=2			DR=3		
	Diameter of fiber (μm)	**Mean diameter of PVA nodules (μm)**	**Estimated specific interface area (m^2/g)**	**Diameter of fiber (μm)**	**Mean diameter of PVA nodules(μm)**	**Estimated specific interface area (m^2/g)**
PP_{70}-PVA_{30}	69.8	0.29	3.2	58.7	0.26	3.6
PP_{70}-PVA_{30}-Si_{S5505}	68.6	0.29	3.2	59.4	0.25	3.7
PP_{70}-PVA_{30}-Si_{R816}	64.9	0.33	2.8	54.6	0.23	4.0
PP_{70}-PVA_{30}-Si_{R972}	68.0	0.27	3.4	55.8	0.23	4.0

4.2.2.2 PVA accessibility degree

It has been demonstrated that specific interface area of the biphasic fibers is maintained after the introduction of silica nanoparticles. As we know, the PVA accessibility degree represents the fraction of removable PVA, of which a low value is not conducive to manufacturing porous materials. Therefore, the PVA accessibility was also confirmed as a precondition of obtaining plentiful pores. It was revealed that the PVA accessibility degrees of extrudates were highly varied after the addition of silica nanoparticles. It is essential to observe the evolution of PVA accessibility degree of the polymer blends from extrudates to multifilament yarns. Thus, the PVA accessibility of PP_{70}-PVA_{30} extrudates and fibers with different types of silica nanoparticles as a function of draw ratio (DR) is shown in Figure 4-8.

(a) The impact of silica nanoparticles

For the extrudates, after the addition of hydrophilic Si_{S5505} nanoparticles, the accessibility degree of PVA is increased slightly; the incorporation of partially hydrophobic Si_{R816} and highly hydrophobic Si_{R972} cripples the PVA accessibility. For the multifilament with DR=2, the PVA accessibility of the PP_{70}-PVA_{30}-DR_2 fibers is 64.9%±0.6%, with that elevated by the silica nanoparticles incorporated, showing 79.2%±0.6%, 85.3%±0.4% and 85.4%±1.3% for samples containing Si_{S5505}, Si_{R816} and Si_{R972}, respectively. The incorporation of any kind of silica nanoparticles has an enhancement of PVA accessibility degree, compared with the neat samples.

(b) The impact of draw ratios

The accessibility of PVA phases for PP_{70}-PVA_{30} extrudates without loads is 50.5±3.0%, and melt-spinning from extrudates to multifilaments leads to a higher PVA accessibility degree. It indicates that the dominant fraction of isolated PVA has obtained the interconnectivity to be accessed with solvent. It is mainly caused by the extensional force during melt spinning. The similar evolution occurs in the silica-containing samples, and the most significant difference is the one from Si_{R972}-based mixture, during the extrusion stage it was 26.5±1.7% to reach more than 85%, even better than

that of Si_{S5505}-containing multifilaments. It proves that the elongation field plays a decisive role in the PVA interconnectivity. It also hints that the refinement effect makes PVA droplets isolated in extrudates, but it is beneficial for PVA interconnectivity forming under the elongation field.

Furthermore, the draw ratio from 2 to 3 also has an enhancing effect as well on the PVA accessibility of PP_{70}-PVA_{30} fibers. It has been discovered that the PVA accessibility has a significant increment of 13.8%. The increment in the draw ratio from 2 to 3 allows an increase in the degree of accessibility as well, in the case of mixtures containing the nanoparticles Si_{S5505} and Si_{R972}, by 4.4 and 3%, respectively. However, in the case of mixing with Si_{R816} fillers, changing the draw ratio has no effect. When a draw ratio of 3 is applied, the difference in the PVA accessibility between different samples becomes less obvious. It implies that draw ratio is also a key factor in deciding the PVA accessibility degree.

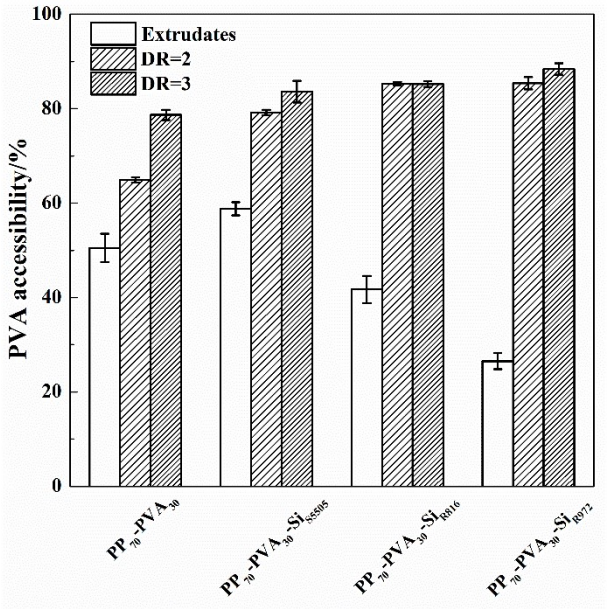

Figure 4-8 PVA accessibility of PP_{70}-PVA_{30} without/with different silica nanoparticles in the form of extrudates and multifilament fibers with different draw ratios.

4.2.2.3 Crystalline structure

PP is the scaffold component from the PP_{70}-PVA_{30} biphasic fibers, which has the dominant fraction of 70 wt.% in the polymers. The crystalline structures of each multifilament sample were investigated by X-ray diffraction (XRD) analysis. Figure 4-9 shows the XRD patterns of PP_{70}-PVA_{30} fibers without/with silica nanoparticles for the two tested draw ratios, and the related data are listed in Table 4-7. The efforts were made to make deconvolution of the XRD patterns, but found that the fitted results were not unique due to the two different amorphous peaks from PP and PVA.

(a) The impact of silica nanoparticles

The positions of the 2θ of planes (110) (040) (130) (131)/(041) are maintained compared with PP_{70}-PVA_{30} fibers, indicating that the crystal forms of PP are kept regardless of the incorporation of silica nanoparticles. However, the intensity of the XRD peaks is varied corresponding to the PP crystallinity, which is decreased with PP_{70}-PVA_{30}-Si_{R972}-DR_2, increased with PP_{70}-PVA_{30}-Si_{S5505}-DR_2 and unchanged with PP_{70}-PVA_{30}-Si_{R816}-DR_2. Thereinto, crystallite sizes of PP in PP_{70}-PVA_{30}-Si_{R972}-DR_2 are decreased as well. It proves that the interface-located Si_{R972} nanoparticles act as a block to the growth of PP crystallites during cooling. In addition, applied with the high draw ratio of 3, no matter which kind of silica nanoparticles are added, there is no positive enhancement in the PP crystallinity.

(b) The impact of draw ratios

For the PP_{70}-PVA_{30} fibers, it is concluded that the increment of draw ratio is beneficial for increasing the crystallinity of PP. For the composite fibers containing Si_{R972} and Si_{R816}, high draw ratio has also an enhancing effect on the PP crystallinity. However, in contrast, high draw ratio has a negative effect on the PP crystallinity for the PP_{70}-PVA_{30}-Si_{S5505}. The distinct impacts of draw ratios on the PP crystallinity lie in the different localization of the silica nanoparticles. Si_{S5505} is confined in the PVA phase, and it can be estimated that the mass fraction of Si_{S5505} is as high as 3.3% in the PVA

droplets with silica nanoparticles. What's more, for the hydrophilic properties of Si_{S5505}, a certain degree of agglomeration is unavoidable. These factors with Si_{S5505}-based blends are not beneficial for applying a high draw ratio, leading to a crystallinity reduction. It has been found that for PP_{70}-PVA_{30} fibers without fillers, high draw ratio leads to the decrease of (110) (040) crystallite sizes, due to the shortage in the direction perpendicular to the draw ratio. After the introduction of Si_{S5505} and Si_{R816} silica nanoparticles, the crystallite sizes are also reduced with the increment of draw ratios. However, for PP_{70}-PVA_{30}-Si_{R972} fibers, the increment of draw ratio is beneficial for crystal growth, which may be induced by the Si_{R972} silica nanoparticles. Therefore, the Si_{R972} played different roles in PP crystallinity during different stages of melt spinning.

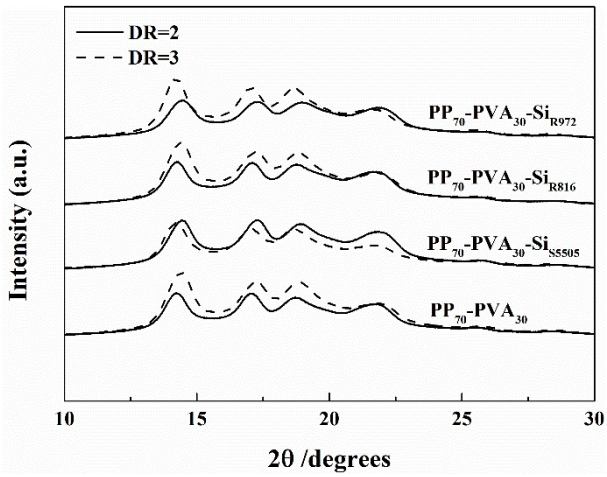

Figure 4-9 XRD spectra of PP_{70}-PVA_{30} fibers without/with silica nanoparticles with the two tested draw ratios.

Table 4-7 XRD data of PP_{70}-PVA_{30} fibers with silica nanoparticles with DR=2 and 3.

Fibers	$2\theta_{(110)}$	$FWHM_{110}$	D_{110} (Å)	$2\theta_{(040)}$	$FWHM_{040}$	D_{040} (Å)	$2\theta_{(130)}$	$2\theta_{(131)/(041)}$
PP_{70}-PVA_{30}-DR_2	14.2°	0.785	101.9	17.1°	0.694	115.7	18.7°	21.6°
PP_{70}-PVA_{30}-DR_3	14.4°	0.850	94.2	17.3°	0.765	105.0	18.8°	21.8°
PP_{70}-PVA_{30}-Si_{S5505}-DR_2	14.4°	0.800	100.1	17.3°	0.725	110.8	18.9°	21.8°
PP_{70}-PVA_{30}-Si_{S5505}-DR_3	14.2°	0.810	98.8	17.1°	0.727	110.5	18.7°	21.8°
PP_{70}-PVA_{30}-Si_{R816}-DR_2	14.3°	0.768	104.2	17.1°	0.671	119.7	18.7°	21.6°
PP_{70}-PVA_{30}-Si_{R816}-DR_3	14.4°	0.848	94.4	17.2°	0.766	104.8	18.9°	21.7°
PP_{70}-PVA_{30}-Si_{R972}-DR_2	14.5°	0.851	94.1	17.4°	0.776	103.5	19.0°	21.8°
PP_{70}-PVA_{30}-Si_{R972}-DR_3	14.2°	0.778	102.9	17.0°	0.697	115.2	18.7°	21.7°

4.2.3 Mechanical properties of the fibers

To determine the influence of silica nanoparticles and draw ratios upon the mechanical performance of the fibers, tensile tests were carried out. A good mechanical performance gives the fibers potential to be industrialized. Furthermore, dynamical mechanical analysis was also conducted to reveal its relationship with the biphasic morphology evolution within the multifilament fibers.

4.2.3.1 Tensile tests

The introduction of silica nanoparticles inevitably influences the mechanical behaviors of the fibers. First of all, in order to make in-depth investigations, the PP with silica nanoparticles without PVA was also melt-spun. The strain-stress curves of the fibers were illustrated in Figure 4-10, and the mechanical properties were listed in Table 4-8. The introduction of the silica nanoparticles weakens the mechanical behaviors of the PP fibers with DR=2 in different degrees, among which hydrophobic Si_{R972} silica nanoparticles has the slightest influence. Moreover, if the draw ratio is elevated to 3, the introduction of Si_{R972} even has a further enhancement for the PP fibers. It gives a strong evidence that the dispersion of Si_{R972} within PP is very excellent.

Table 4-8 Mechanical properties of PP fibers without/with silica nanoparticles.

Fibers	DR=2			DR=3		
	Young's modulus (MPa)	Tenacity (cN/Tex)	Breaking elongation (%)	Young's modulus (MPa)	Tenacity (cN/Tex)	Breaking elongation (%)
PP	2174±238	17.9±2.2	516±66	2951±322	24.2±2.1	302±100
PP-Si_{S5505}	1759±188	15.3±1.5	436±71	2376±148	21.5±0.9	301±26
PP-Si_{R816}	1657±366	14.2±3.4	507±84	2552±349	23.4±2.6	227±32
PP-Si_{R972}	1819±295	17.0±1.5	433±43	2750±243	25.4±1.6	226±21

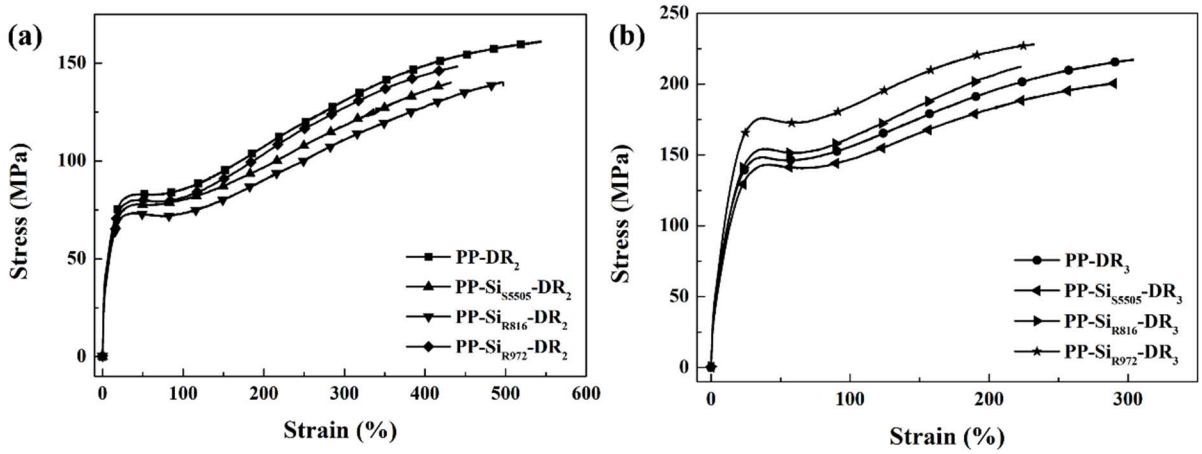

Figure 4-10 Stress-strain curves of PP fibers without/with different silica nanoparticles (a) DR=2; (b) DR=3.

The mechanical properties of the PP-PVA fibers with the nanoparticles were measured via tensile tests, displayed in Table 4-9. Additionally, the stress-strain curves of the representative samples for the two different draw ratios before and after selective phase extraction are illustrated in Figure 4-11.

All the fibers with a draw ratio of 2 exhibit ductile behaviors in stress-strain curves, with a high breaking elongation of more than 370%. The mechanical properties of Si_{R972} nanoparticles containing fibers are least affected, and the stress-strain curves of PP_{70}-PVA_{30} and PP_{70}-PVA_{30}-Si_{R972} are almost identical. It indicates that the interface localization of the Si_{R972} silica nanoparticles leaves the slightest damage to the

mechanical properties. The other two silica nanoparticles, Si_{R816} and Si_{S5505} are localized in the PVA phase as well, and it leads to more evident influence upon the mechanical properties, reflected in a lower Young's modulus and tenacity, as well as breaking elongation.

The draw ratio from 2 to 3 generally gives a significant enhancement to the mechanical properties, reflected in Young's modulus and tenacity. Note that the Young's modulus of PP_{70}-PVA_{30}-Si_{S5505}-DR_3 only has a faint increment, which corresponds well to its weakened crystallinity of PP phase due to the rise of draw ratio. Furthermore, the breaking elongation is decreased with the increment of draw ratio due to enhanced stiffness. Compared with the fibers with DR=2, the introduction of silica nanoparticles has a more remarkable impact upon the mechanical properties of the fibers of DR=3. With this draw ratio, the mechanical performance is obviously weakened by the addition of Si_{S5505} nanoparticles. PP_{70}-PVA_{30}-Si_{R816}-DR_3 fibers show a quasi-brittle behavior instead of ductile behaviors, and Young's modulus is enhanced after the addition of Si_{R816}. As for surface-localized Si_{R972} nanoparticles, the mechanical properties show no distinct difference. The silica nanoparticles do not improve the mechanical performance of the fibers significantly, but the interface-localized fillers give the least negative effects.

All the porous PP fibers after the removal of PVA perform ductile behaviors, which is due to the nature of PP material. Young's modulus gets weakened, and the breaking elongation is significantly increased, revealing that the stiffness of the composite fiber is decreased. Meanwhile, the tenacity remains almost the same. It has the capacity of providing robust enough mechanical performance. For the interface-located silica nanoparticles Si_{R972}, it provides porous PP fibers with Young's modulus of 1238±185 MPa, tenacity of 13.9±2.0 cN/Tex and breaking elongation of 349±66%, applied with draw ratio of 3.

Table 4-9 Mechanical properties of PP_{70}-PVA_{30} fibers with different silica nanoparticles with DR=2 and 3.

Fibers	Before extraction			After extraction		
	Young's modulus (MPa)	Tenacity (cN/Tex)	Breaking elongation (%)	Young's modulus (MPa)	Tenacity (cN/Tex)	Breaking elongation (%)
PP_{70}-PVA_{30}-DR_2	1853±249	12.3±1.7	449±51	1570±389	13.1±2.9	547±65
PP_{70}-PVA_{30}-DR_3	2871±617	16.7±2.6	256±108	2012±220	20.9±2.5	371±74
PP_{70}-PVA_{30}-Si_{S5505}-DR_2	1658±236	8.5±1.5	372±58	1265±205	10.7±1.7	575±66
PP_{70}-PVA_{30}-Si_{S5505}-DR_3	1796±182	13.8±0.8	224±25	1564±227	15.2±1.8	373±99
PP_{70}-PVA_{30}-Si_{R816}-DR_2	1638±135	9.6±0.9	375±23	1109±327	9.8±2.8	497±66
PP_{70}-PVA_{30}-Si_{R816}-DR_3	3350±394	17.3±1.7	111±83	1891±226	16.9±2.8	299±89
PP_{70}-PVA_{30}-Si_{R972}-DR_2	1851±167	11.4±0.8	443±68	1207±195	10.9±1.9	643±118
PP_{70}-PVA_{30}-Si_{R972}-DR_3	2839±561	16.2±3.5	211±127	1238±185	13.9±2.0	349±66

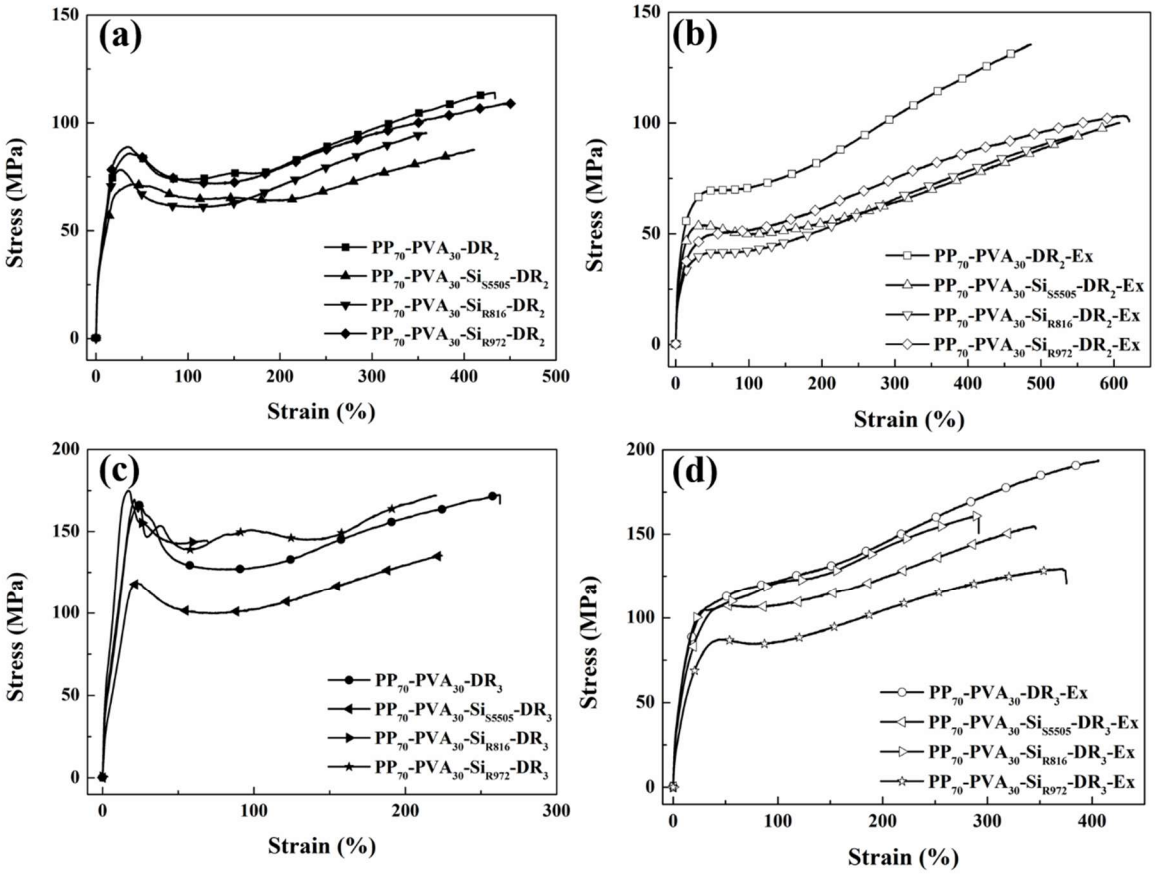

Figure 4-11 Stress-strain curves of PP_{70}-PVA_{30} fibers without/with different silica nanoparticles (a) DR=2, before extraction; (b) DR=2, after extraction; (c) DR=3, before extraction; (d) DR=3, after extraction.

4.2.3.2 DMA results

The dynamic mechanical properties were tested for the composite fibers with silica nanoparticles. The glass transition temperature was also investigated via observing the peak of mechanical loss factor of the materials in Figure **4-12**(b)(d). It is found that the addition of silica nanoparticles has no noticeable impact upon the glassy temperature, possibly due to the low addition fraction (1 Phr).

The storage moduli of PP_{70}-PVA_{30} fibers with different silica nanoparticles are shown in Figure 4-12(a)(c). The additive amount is too small to influence the storage modulus, but it impacts the PVA morphology within the blends. The storage moduli of the blends are mainly attributed to the evolution of the combination mode of the two polymers. Therefore, the evolution of the storage moduli is of great interest to be

investigated. It is discovered that no matter which draw ratios are selected, the storage modulus of fibers is further increased after the addition of silica nanoparticles. It hints that the components have a greater contribution to the storage modulus once the silica nanoparticles are added.

Based on Coran's model (Equation 1-15), the fitting result of storage modulus of PP_{70}-PVA_{30} with silica nanoparticles near room temperature (35°C), accompanied with the f values, is illustrated in Figure 4-13. The f value of PP_{70}-PVA_{30}-DR_2 fiber is 0.26. After the incorporation of silica nanoparticles, the f values were increased significantly to 0.82, 0.70 and 0.85, respectively. f can be a reference for the degree of PVA continuity. When the draw ratio is increased to 3, the incorporation of silica nanoparticles also leads to the increment of f values. When the draw ratio is high, the crystallinity and mechanical properties of fibers were significantly varied, which implies that the simulated components would have a nonnegligible deviation with the neat reference polymer. Therefore, it should be noticed that the precision is limited if a high draw ratio is adopted, which cannot replace the selective phase extraction experiment to determine the PVA accessibility.

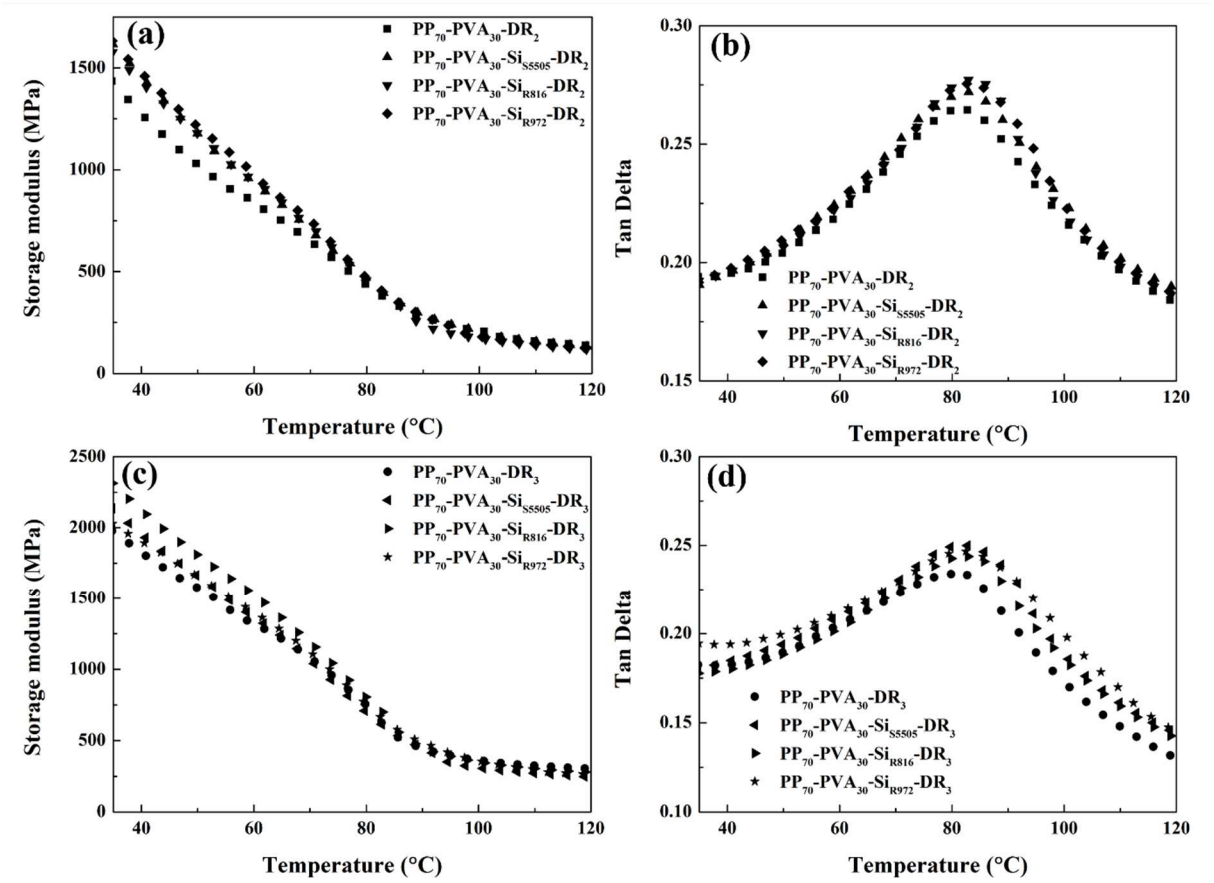

Figure 4-12 (a)(c) Storage modulus of PP_{70}-PVA_{30} fibers without/with different silica nanoparticles with DR=2, 3; (b)(d) Tan delta of PP_{70}-PVA_{30} fibers without/with different silica nanoparticles with DR=2, 3.

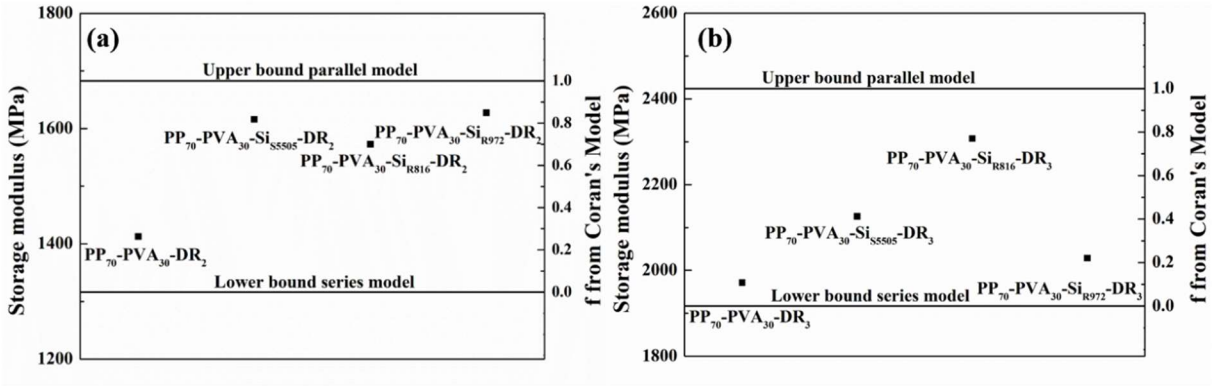

Figure 4-13 Fitting of storage modulus of PP_{70}-PVA_{30} fiber containing different silica nanoparticles with different DR by Coran's model (a) DR=2; (b) DR=3.

4.3 Conclusion

Silica nanoparticles with different surface chemistries were incorporated into PP_{70}-PVA_{30} blends aimed at manufacturing surface functionalized porous PP fibers via melt spinning technology.

For the extrudates, hydrophilic Si_{S5505} and partially hydrophobic Si_{R816} were predicted to be localized in PVA phase. The prediction about Si_{S5505} was confirmed, however, Si_{R816} was found to distribute also at the interface. Si_{R972} was forecasted to be concentrated at the interface. The dominant localization at the interface was verified, although there was still a small amount existing within the bulk phases. The definite localizations are basically consistent with thermodynamical prediction. The different localization gave rise to the significantly distinctive biphasic morphology of PP-PVA. Si_{S5505} conduces to the increment of PVA size and its fraction in fibrous form, which is beneficial for elevation of PVA accessibility. Si_{R972} is in favor of forming spherical PVA nodules in the polymer blends and refining the sizes of PVA, which leads to the reduction of PVA accessibility. Si_{R816} is localized within PVA and at the interface, and synthetically impacts the biphasic morphology.

The spinnability of the fibers with 1wt.% of silica nanoparticles remains outstanding. Si_{R972} silica nanoparticles maintain the most remarkable interfacial localization during the fiber stage due to the thermodynamic equilibrium. The biphasic fibers provide a high specific interface area with the PVA mean diameters of hundreds of nanometers as well as a good mechanical property, upon which silica nanoparticles has no significant enhancement. However, silica nanoparticles have a positive contribution to the PVA accessibility, especially with a low draw ratio of 2. The dominant localization of Si_{R972} at the biphasic interface has limited negative influence in the aggregation structure of the fibers, as well as their mechanical properties. In addition, the increment of draw ratio generally has a positive impact on the specific interface area, PVA accessibility, PP crystallinity and mechanical properties of the biphasic fibers. The silica nanoparticles contribute to the shift towards a parallel model in DMA results, as another indicator of the PVA continuity.

The chapter demonstrates the feasibility of fabricating the surface-funtionalized porous fibers with silica nanoparticles. The PVA accessibility of PP_{70}-PVA_{30}-Si_{R972}-DR_3 reaches as high as 88.4%, and the tenacity of the fibers reaches to 16.2 cN/Tex and retained as 13.9 cN/Tex after selective phase extraction. Their good mechanical properties provide the precondition for further textile implementation.

Chapter V:

Polypropylene/Poly(vinyl alcohol) Blends Compatibilized with Kaolinite Janus Hybrid Particles and Their Transformation into Fibers

Chapter 5 Polypropylene/Poly(vinyl alcohol) Blends Compatibilized with Kaolinite Janus Hybrid Particles and Their Transformation into Fibers

In the previous chapter, the homogeneously modified silica nanoparticles were utilized. In this chapter, Janus particles-modified kaolinite hybrid particles are further adopted for the biphasic PP-PVA systems. Different from silica nanoparticles, the kaolinite particles are patchy and with a larger dimension. Apart from the choice of particles, another PVA material was also used, denoted as PVA*, which is commercialized for melt spinning. It can offer a more satisfactory accessibility by the water possibly due to the differential rheological properties (viscosity etc.), to better expose the PP porous structure.

5.1 Polymeric compounds

5.1.1 Heat resistance properties of kaolinites and blends

The excellent thermal stability of the nanofillers at the processing temperature is an essential precondition for melt manufacturing. The initial decomposition temperature can give a valuable reference. For both KL (unmodified kaolinite particles) and KJ (Janus kaolinite particles) particles, the initial decomposition temperature is around 500°C at either nitrogen or air atmosphere (Figure 5-1(a) and Figure 5-1(c) respectively). The DTG curves are observable in Figure 5-1(b) and (d). It is clearly shown that there is even no subtle decomposition below 200°C. The melt extrusion and spinning were both conducted below 200°C. The excellent thermal stability of KL and KJ particles ensures that it can be a stable additive for the polymer blends. These analyses show also a higher weight loss for modified kaolinite which correspond to the degradation of the grafted ODPA. The weight loss when KJ is analyzed under air atmosphere (which corresponds to a total decomposition of the grafted organic part) gives a grafting rate of about 1.4 wt.%.

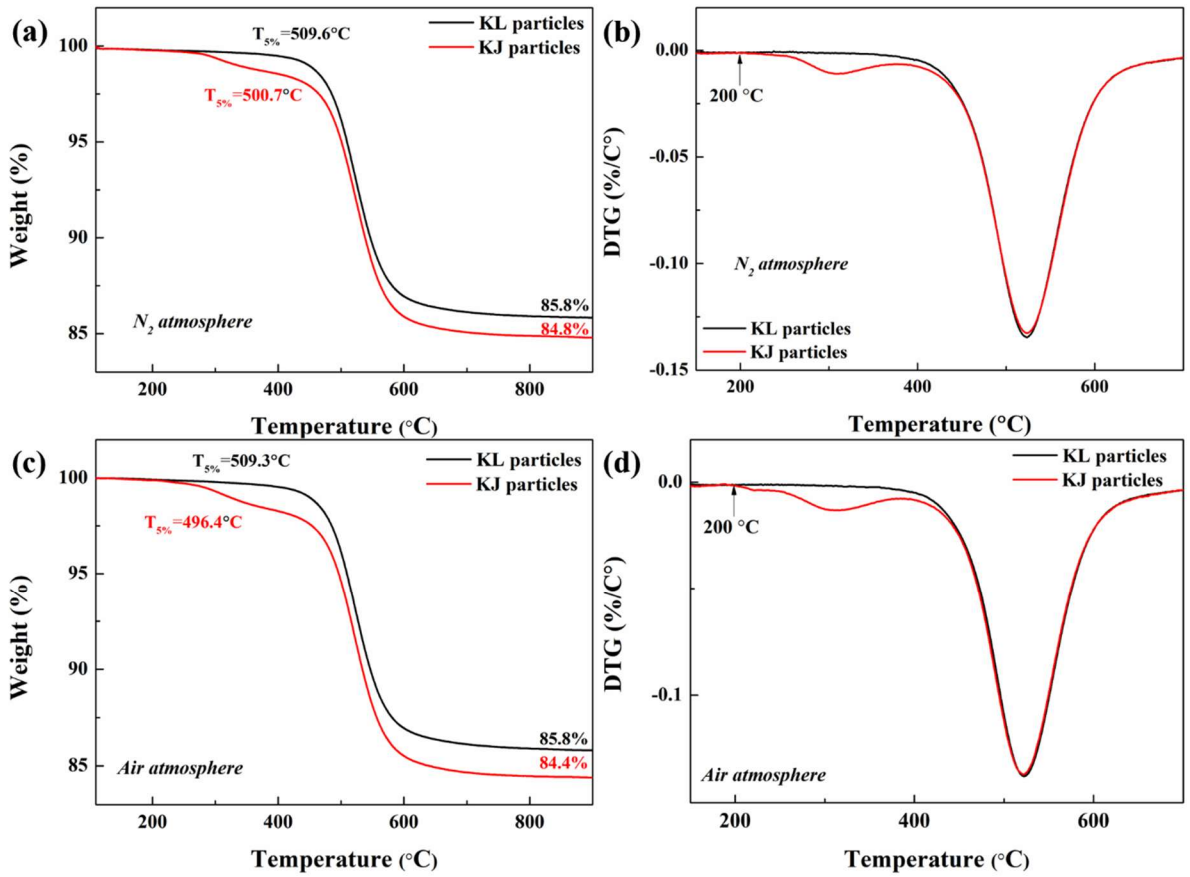

Figure 5-1 TG and DTG curves of KL and KJ particles in nitrogen and air atmosphere. (a) TG curves in a nitrogen atmosphere; (b) DTG curves in a nitrogen atmosphere; (c) TG curves in an air atmosphere; (d) DTG curves in an air atmosphere.

5.1.2 Morphology of the nanocomposites

The median grain size (d_{50}) of kaolinite can reach as large as 800nm, which can provide enough pixels for detection by SEM. Figure 5-2 shows the SEM images of the fractured samples of PP_{70}-PVA^{*}_{30} blends containing the different kaolinites. Combined with the BSE images of the SEM, the morphology of PP-PVA blends can be easily distinguished. The light part stands for the PVA phase, and the dark part represents the PP phase. An additional EDS mapping has been conducted and it has been found that the white dots are the kaolinite particles, with the detection of Si and Al element.

It can be observed that the shape of the PVA nodules is governed by continuous structure instead of the spherical structure, which is beneficial for the PVA connectivity in the matrix. It can be distinguished that unmodified kaolinite KL particles are localized within the PVA phase, while Janus-modified kaolinite KJ particles are

distributed at the biphasic interface. It can be concluded that the images show a location of a dominantly more substantial portion of kaolinite at the PP-PVA interface when it is modified.

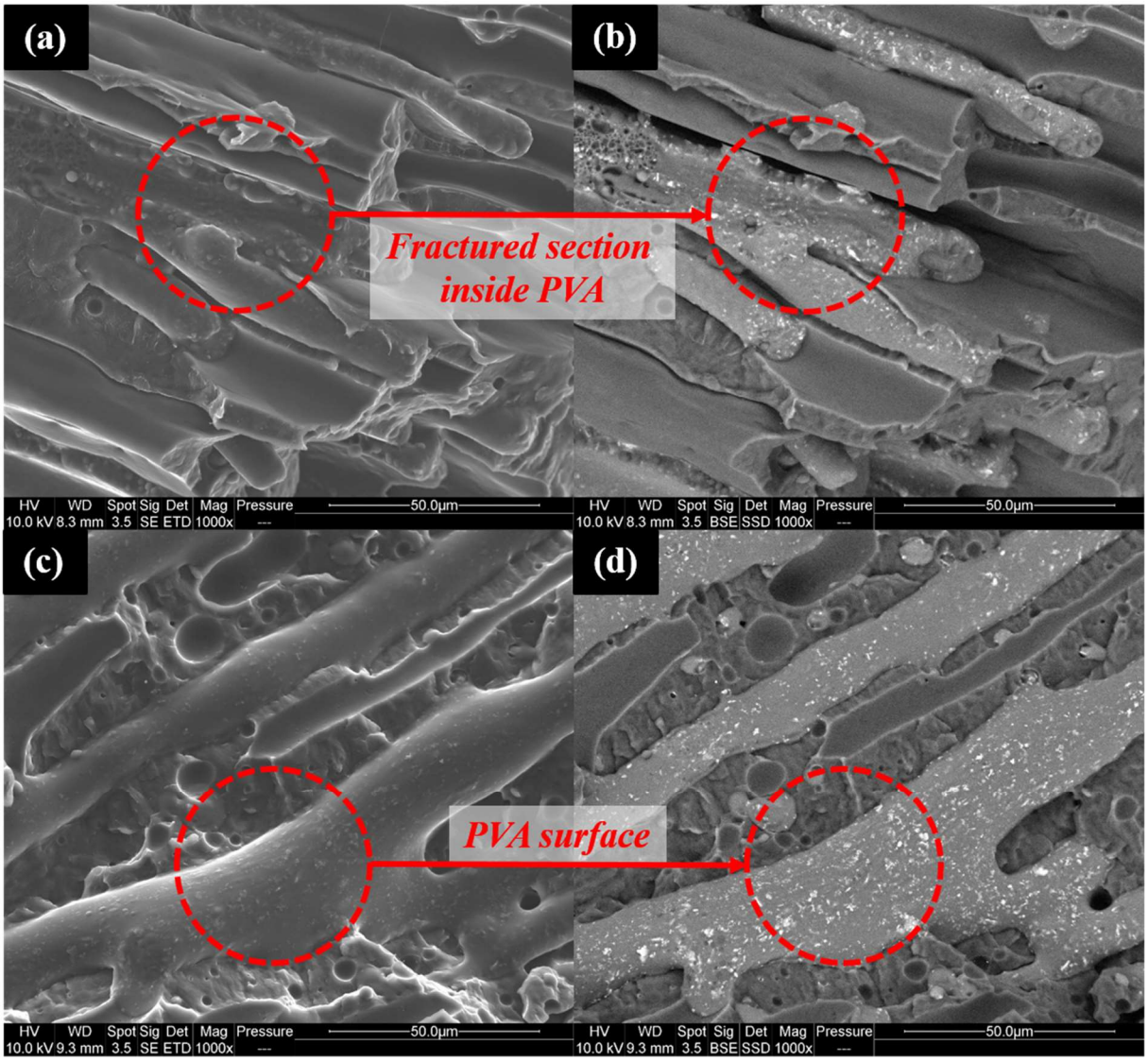

Figure 5-2 SEM images of PP_{70}-PVA^{*}_{30} blends with pristine and modified kaolinites (samples were cryo-fractured after treatment in liquid nitrogen). (a) PP_{70}-PVA^{*}_{30}-KL_5; (b) PP_{70}-PVA^{*}_{30}- KL_5 (BSE); (c) PP_{70}-PVA^{*}_{30}-KJ_5; (d) PP_{70}-PVA^{*}_{30}- KJ_5 (BSE) (BSE images: PP: dark part; PVA: light part; kaolinite particles: white dots).

The PVA accessibility degree of PP_{70}-PVA^{*}_{30} blends with two different kaolinites are illustrated in Figure 5-3. After the introduction of KL kaolinite nanoparticles, the

PVA accessibility is not altered significantly and slightly enhanced by the addition of 5 wt.% KL particles. As for the modified kaolinite, the addition leads to the dramatic decrease of PVA accessibility, which is related to the presence of the Janus kaolinite particles at the polymers interface. In our previous research, similar behaviors were investigated. It has been found that the PVA accessibility degrees are tightly relevant to the silica nanoparticles localization within the biphasic polymers, and the accessibility degree of the dispersed phase can even provide a route to predict the localization of the particles. The filling of the unmodified kaolinite in the dispersed phase may slow down the effect of the destructive process, e.g. fibril breakup (Steinmann *et al.*,2002a), leading to the increment of PVA accessibility. As for the interface-located kaolinite, the effecting function is changed into steric hindrance or surfactants (Zhang *et al.*, 2012), to prevent the coalescence of PVA phase.

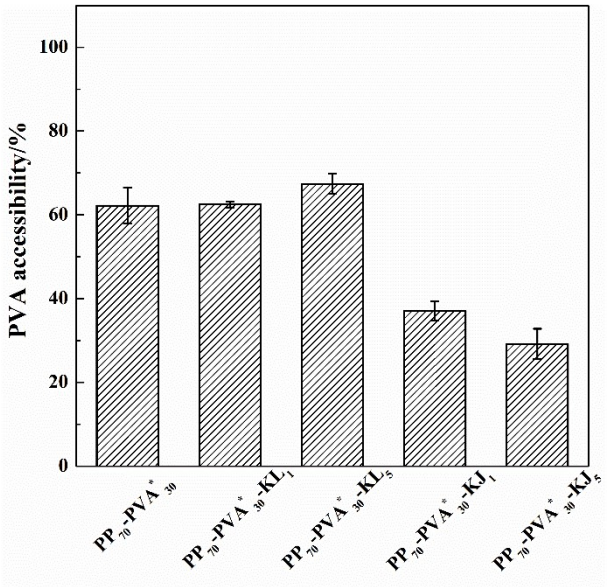

Figure 5-3 PVA accessibility degree of PP_{70}-PVA_{30} extrudates with pristine and modified kaolinites at 1 or 5 wt.%.

In order to investigate the effect of kaolinite upon the size distribution of PVA nodules of the PP-PVA composites, SEM images of the cross-section of the plates after rheological tests are shown in Figure 5-4. The volume average diameter of PVA

nodules within PP_{70}-PVA^{*}_{30} is 73.3 μm. The PVA nodules perform bimodal distribution, resulting from the annealing of initial spherical and elongated PVA nodules (Parpaite *et al.*, 2016). The initial elongated nodules were relaxed into the spherical PVA nodules with a high diameter value during the rheology test. After a long relaxation time, the deformed droplets evolve to recover the original spherical shapes (Wu *et al.*, 2012). The characteristic relaxation time of a slightly deformed droplet can be depicted by a concluded formula from Ultracki *et al.* (Kong *et al.*, 2011; Luciani *et al.*, 1997).

$$\tau_d = \frac{(2p+3)(19p+16)\eta_m}{40(p+1)}\frac{R_0}{\sigma} \quad \textbf{Equation 5-1}$$

Where p is viscosity ratio of dispersed phase to matrix phase, η_m represents the viscosity of the matrix, R_0 represents the radius of a droplet, σ is the interfacial tension of the blends.

Equation 5-1 indicates that the retraction dynamics depends largely on the viscosity ratio, the interfacial tension and droplet radius at equilibrium (Kong *et al.*, 2011). From the SEM observation of the cross-sections, the PVA nodules within the blend samples without fillers can be reverted to spherical shapes after the rheology tests, demonstrating a complete relaxation. However, for the KL-containing PP-PVA blends, it cannot be completely changed into spherical shapes and keeps spheroidicity instead. Combined with the localization of KL inside PVA phase, it can be concluded that the increment of the relaxation time is due to the enhancement of the viscosity. What's more, there is also an increment of the size of the PVA nodules with the diameter of 126.1 μm, and a dominant fraction of PVA nodules over 170 μm, which also needs a longer relaxation time, based on Equation 5-1. It is worth noting that for the PP_{70}-PVA_{30}-KL_5 sample, the distribution of PVA nodules is too diverse, thus, the Schwartz-Saltikov transformation cannot be carried out due to the difficulty in statistics. Nevertheless, it can be clearly concluded that the PVA size is further increased with a higher amount of KL.

In contrast, it can be observed that the addition of modified kaolinite KJ leads to the refinement of PVA nodules. When 1 wt. % of KJ particles are incorporated, the average diameter of PVA nodules is shifted to a lower value of 51.2 μm, a wide peak appears under 80 μm representing the majority volume fraction. It has been found that the PVA accessibility of KJ-containing extrudates is low, proving the PVA nodules haven't formed a highly interconnected structure. In addition, it does not require a long relaxation time because of the small diameter of the PVA droplets. As a result, the PVA droplets also exhibit spherical shapes after the addition of Janus particles. After the addition of 5 wt.% of KJ, the size of PVA nodules is significantly reduced, and fused into one double peak under 30 μm. The volume average diameter is 13.6 μm for PP_{70}-PVA^{*}_{30}-KJ_5, presenting only 19% of the diameter of samples without nanoparticles. The refinement effect of KJ particles leads to a higher fraction of isolated PVA nodules in the extrudates, bringing about the drastic decrease of the PVA accessibility degree.

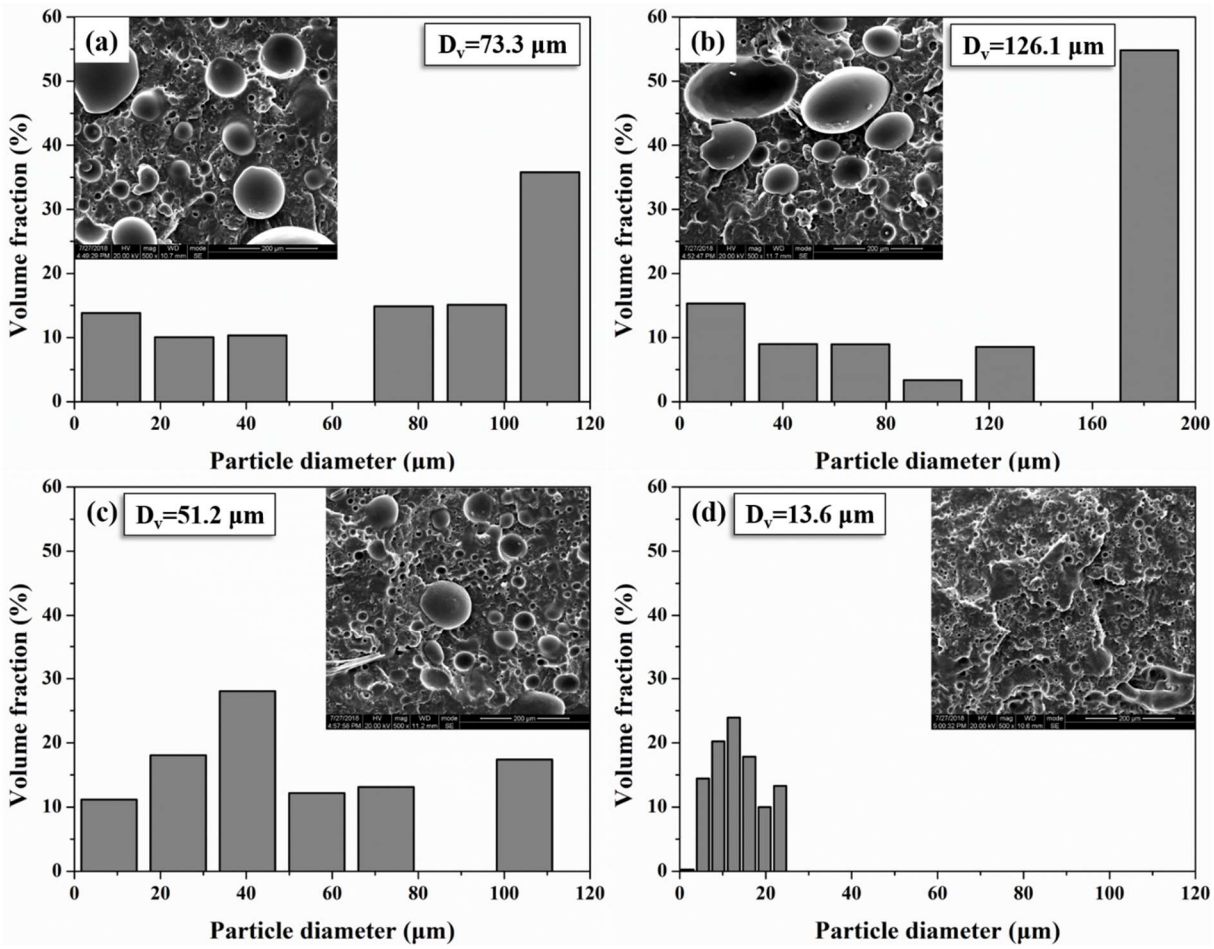

Figure 5-4 Particle diameter distribution and the SEM images of the PVA nodules inside PP matrix after the rheometer measurement (a) PP_{70}-PVA^*_{30} (b) PP_{70}-PVA^*_{30}-KL_1 (c) PP_{70}-PVA^*_{30}-KJ_1 (d) PP_{70}-PVA^*_{30}-KJ_5.

5.1.3 Rheometer tests

The rheological results of PP_{70}-PVA^*_{30} blends with different kaolinites are displayed in Figure 5-5(a)(b). After the introduction of small amount of KL kaolinite particles, there is no distinct difference only leading to a slight enhancement of storage modulus and complex viscosity. For the unmodified kaolinite particles, when the adding amount is increased to 5 wt.%, the enhancement effect is not elevated significantly. However, the storage modulus and complex viscosity of PP_{70}-PVA^*_{30}-KJ_5 blend are significantly varied, reflected in the sudden and fierce increment in the low frequency, which proves that a gel-like (yield stress) behavior emerges. In order to demonstrate this phenomenon in depth, the pure polymer component was also tested

for the rheological behaviors. PP exhibits a Newtonian plateau of complex viscosity at low shear rates, and instead PVA exhibits a distinctive behavior replaced by a sharp slope, resulting from the existence of dynamic hydrogen bonds between PVA molecules. However, it is worth noting that the storage modulus of the blends is higher than that of PVA component, although PVA is only a minor phase inside the blends. What's more, the other filler-filling samples have no obvious gel-like behaviors. Related literatures revealed that this phenomenon is also attributed to the formation of a solid network of nanofillers (percolation) through the material (Parpaite *et al.*, 2016). Generally speaking, the gel-like phenomenon of the blends originates from the joint effects of the biphasic percolation and hydrogen bonds inside PVA phase.

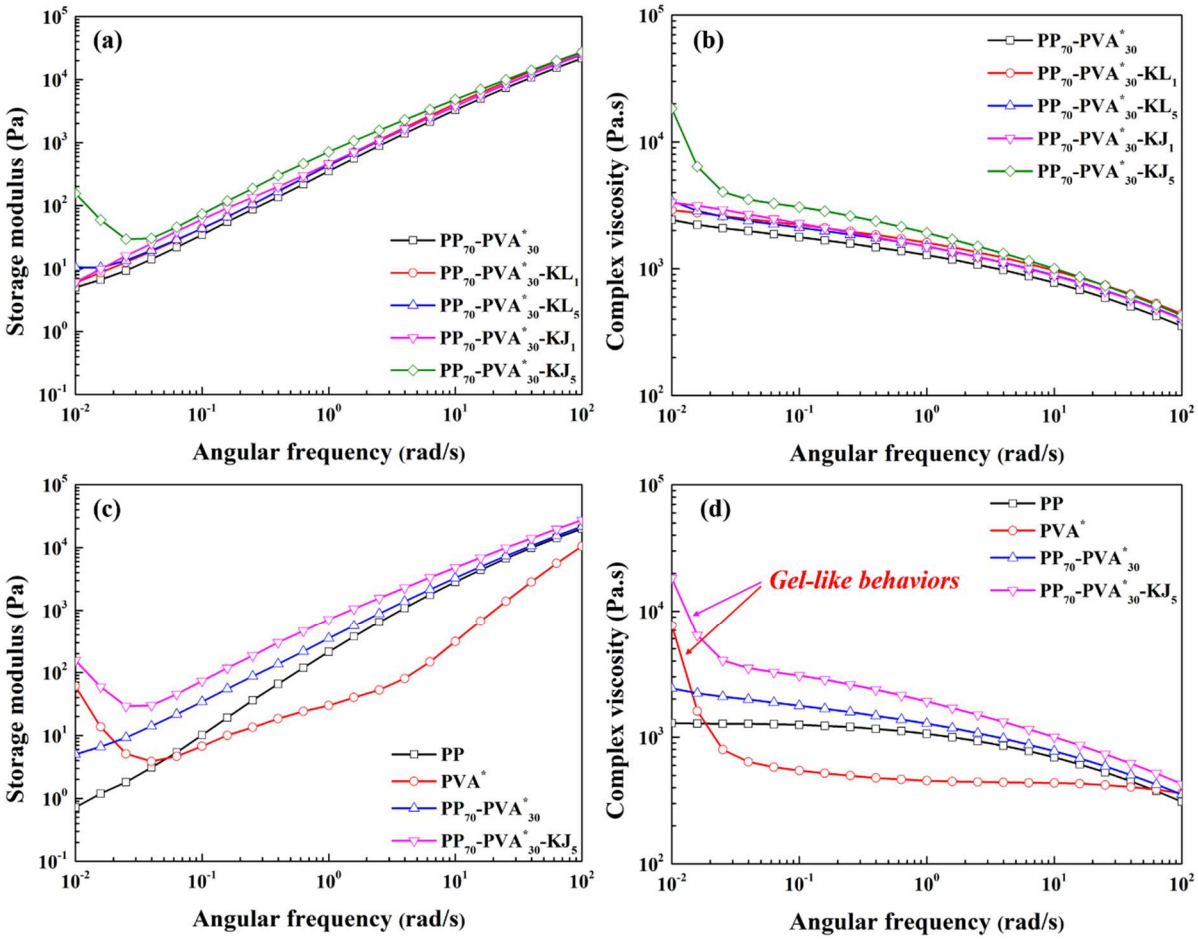

Figure 5-5 Rheological results of PP_{70}-PVA^*_{30} blends and pure components at 190 °C (a)(b) storage moduli and complex viscosities of PP_{70}-PVA^*_{30} blends without/with kaolinite particles (c)(d) storage moduli and complex viscosities of PP, PVA, PP_{70}-PVA^*_{30} blends without/with 5 wt.% of KJ Janus particles.

5.1.4 Melt flow index (MFI)

Values of the melt flow indices (MFI) for PP_{70}-PVA^*_{30} blends with unmodified and modified kaolinites are listed in Figure 5-6. The MFI values related to the fluidity of the polymer composites are very significant reference for the determination of melt spinning temperature, among which from 15 to 30 g/10min the spinning process can be well-optimized. It can be found that the PP_{70}-PVA^*_{30} blends perform as the positive correlation compared with the pure components, with an MFI value of 30±1.1 g/10min (respectively 11.8±0.6 g/10min for PP, and 19.3±0.3 g/10min for PVA^*). After the

introduction of unmodified KL kaolinite particles, the MFI values are not altered obviously. It is ascribed to the particle localization within the dispersed PVA phase and the slight influence upon area of incompatible interphases (PVA accessibility) (Ku and Lin, 2005). However, it is not the same case with the incorporation of KJ Janus particles. The KJ particles can effectively decrease the fluidity (MFI index) of the blends (28.1±1.0 g/10min and 22.2±0.3 g/10min with 1 wt.%/ 5 wt.% respectively) and so increase their viscosity. It is due to the interfacial localization of KL particles and the decreased area of incompatible interphase (decreased PVA accessibility). In the practical spinning, it was found that the temperature profiles had to be adjusted to a higher value to guarantee the success of melt spinning process.

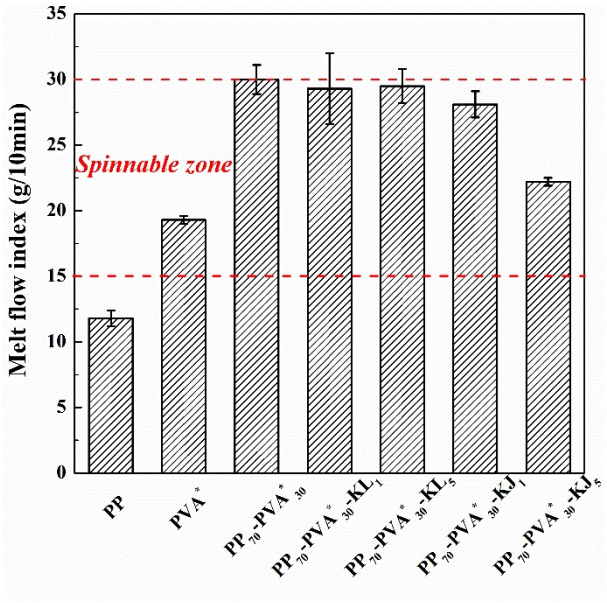

Figure 5-6 Melt flow index (190°C, 2.16 kg) of PP_{70}-PVA_{30} blends with different kaolinite particles.

5.2 Polymeric fibers

5.2.1 PVA accessibility of the fibers

PVA accessibility for PP_{70}-PVA^*_{30} fibers with KL and KJ is shown in Figure 5-7. Although the PVA accessibility of PP-PVA* blends is low (lower than 70%), especially for the blends with KJ Janus particles, the PVA accessibility degree can be elevated

significantly due to melt spinning process. It is inspiring that the PVA accessibility degree can always be over 90 % for PP_{70}-PVA^{*}_{30} fibers even in presence of kaolinite particles. All the PVA phase can be removed after the selective phase extraction step, indicating that the PVA nodules are dominantly deformed and interconnected. A highly available PVA makes an excellent contribution to obtain a porous material, endowed the multifilament yarns a high extraction efficiency towards the sacrificial phase.

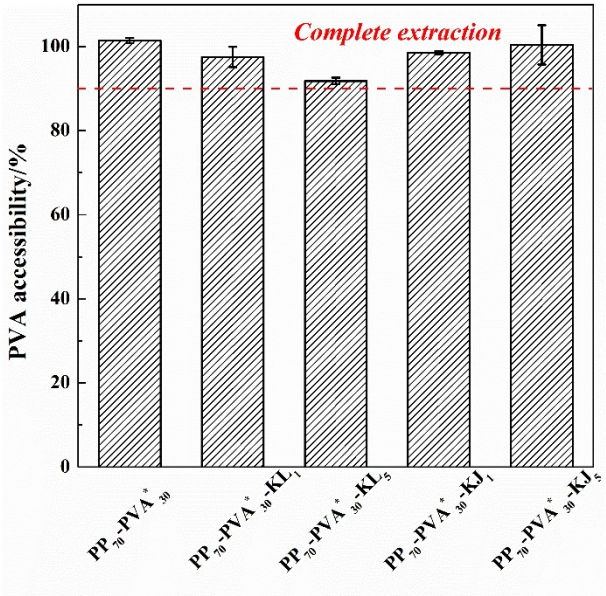

Figure 5-7 PVA accessibility of PP_{70}-PVA_{30} fibers with pristine and modified kaolinites.

5.2.2 Mechanical properties of the fibers

In order to investigate the influence of kaolinite particles upon the mechanical properties of the multifilament yarns, tensile tests were conducted and the related data are illustrated in Table 5-1. Moreover, the stress-strain curves are also displayed in Figure 5-8. The biphasic PP_{70}-PVA^{*}_{30} fibers exhibit good mechanical properties, with the Young's modulus of 1417±136 MPa, tenacity of 11.4±0.6 cN/tex and elongation at break of 440±39%. With the treatment of selective phase extraction, the Young's modulus and tenacity keep unchanged, with a significant increment of elongation at break to 632±41%. The related stress-strain curves are displayed in Figure 5-8(a). The

shape of the curve for PP is similar with that of selectively extracted PP_{70}-PVA^{*}_{30}-Ex fibers, attributed to the component PP.

Figure 5-8(b)(c) illustrates the stress-strain curves of the filaments without/with kaolinite particles, before and after selective phase extraction. After the introduction of KL particles, the mechanical properties are gradually weakened. The tenacity and breaking elongation are decreased, and Young's modulus is kept stable. After the introduction of 1wt.% of KJ particles into the blends, the tenacity and breaking elongation is decreased slightly and value of the Young's modulus is slightly increased. However, if 5wt.% of KJ is introduced, the Young's modulus is increased fiercely from 1417±136 MPa for unfilled blends towards 2227±370 MPa, with a sharp 57% increment. Meanwhile, its tenacity is slightly enhanced with a decrease of elongation at break. It proves that the introduction of the Janus particles significantly enhances the Young's modulus of the fibers, with a strengthening of the interface due to the particular localization of the kaolinite particles. The decrease in the breaking elongation also gives the evidence of the interfacial localization of the fillers. So Janus-modified particles can also be utilized in melt spinning technology fields, to offer a remedy and enhancement strategy for the weakening effect in mechanical properties of melt-spun fibers.

Meanwhile, after selective phase extraction, the breaking elongation is increased due to the removal of PVA. The tenacity has no significant change after the extraction. The Young's modulus is decreased at a different degree, and that of PP_{70}-PVA^{*}_{30}-KJ_5 is recovered near that of the filaments without fillers. It hints that the great mechanical contribution of the filaments with Janus particles mainly originates from PVA phase.

Table 5-1 Mechanical properties of PP_{70}-PVA^{*}_{30} fibers containing kaolinite particles and neat PP fibers.

Fibers	Before extraction			After extraction		
	Young's modulus (MPa)	**Tenacity (cN/Tex)**	**Elongation at break (%)**	**Young's modulus (MPa)**	**Tenacity (cN/Tex)**	**Elongation at break (%)**
PP_{70}-PVA^{*}_{30}	1417±136	11.4±0.6	440±39	1453±316	12.2±2.5	632±41
PP_{70}-PVA^{*}_{30}-KL_1	1401±96	10.2±0.7	421±40	1248±195	11.2±1.7	503±54
PP_{70}-PVA^{*}_{30}-KL_5	1485±248	9.5±1.7	327±74	1189±294	8.4±2.3	428±76
PP_{70}-PVA^{*}_{30}-KJ_1	1657±303	10.2±1.0	408±21	1413±290	11.8±2.0	604±52
PP_{70}-PVA^{*}_{30}-KJ_5	2227±370	12.2±1.6	299±82	1447±395	11.7±3.4	488±80
PP	2174±238	17.9±2.2	516±66	-	-	-

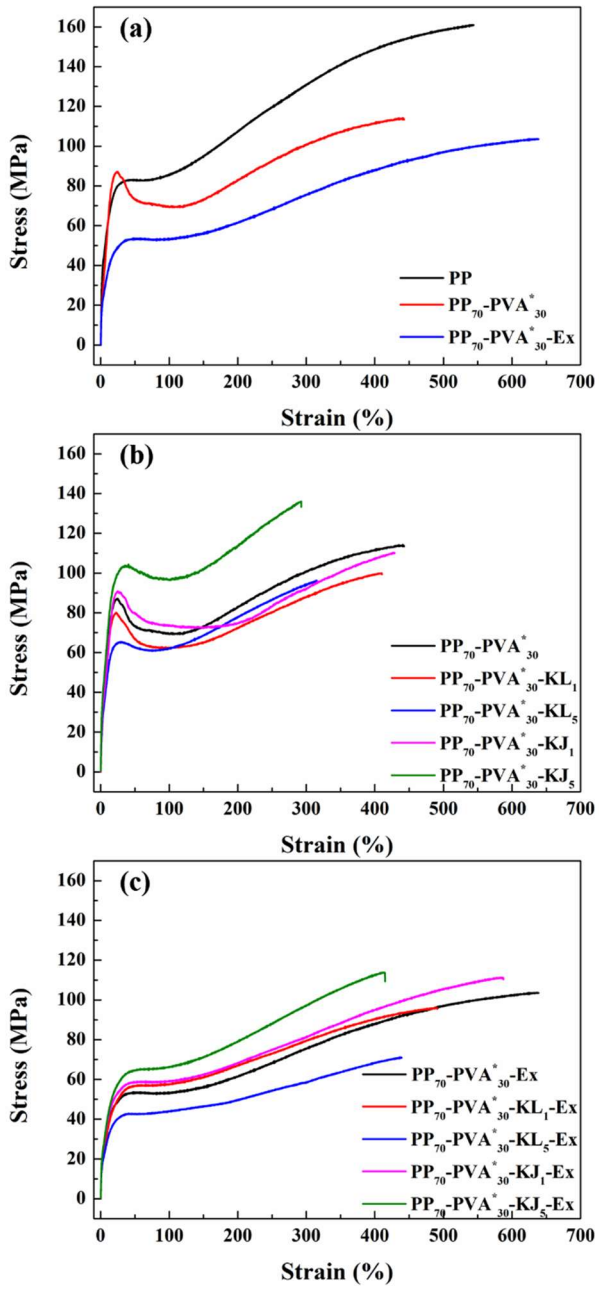

Figure 5-8 Stress-strain curves of PP_{70}-PVA^{*}_{30} fibers with pristine and modified kaolinite particles (a) before extraction; (b) after extraction; (c) neat PP fibers.

5.2.3 Thermal properties of the porous fibers

Melting points of PP and PVA are very close, which complicates the analysis of their crystallization transition. However, it is still of great interest to dig the related information of the PP porous fibers obtained after PVA extraction. Therefore, the DSC spectra of PP and PP_{70}-PVA^{*}_{30}-Ex fibers (after selective phase extraction) are shown in

Figure 5-9(a), with data details in Table 5-2.

Figure 5-9(a) shows that there is one peak around 167°C for neat PP fibers. For PP_{70}-PVA^{*}_{30}-Ex fibers, the shape of the DSC spectra is similar with the adjacent melting point of 166°C, while the crystallinity degree is decreased. It is one of the reasons that the mechanical properties of PP_{70}-PVA^{*}_{30}-Ex fibers are weaker. It is also due to the generated porous structures form tremendous stress concentration points. To investigate the influence of kaolinite particles to the crystallization of PP porous fibers, the DSC spectra of the composite fibers after extraction are shown in

Figure 5-9(b) with details in Table 5-2 as well. The PP_{70}-PVA^{*}_{30}-Ex fibers show a single melting peak during heating, and the crystallinity degree is not altered obviously after the addition of the clay. However, fibers obtained using kaolinite exhibit two endothermic maxima instead of a single peak. Compared with unmodified kaolinite, the impact of Janus particles to the DSC peak splitting is more significant. The peak splitting is associated with a degree of perfection of the crystals, of which the high-temperature endotherm is caused by the recrystallization due to more thermal energy (Cho *et al.*, 2010; Torre *et al.*, 2004). It indicates that the perfection of the crystals is enhanced by the addition of the kaolinite particles, especially the Janus-modified ones.

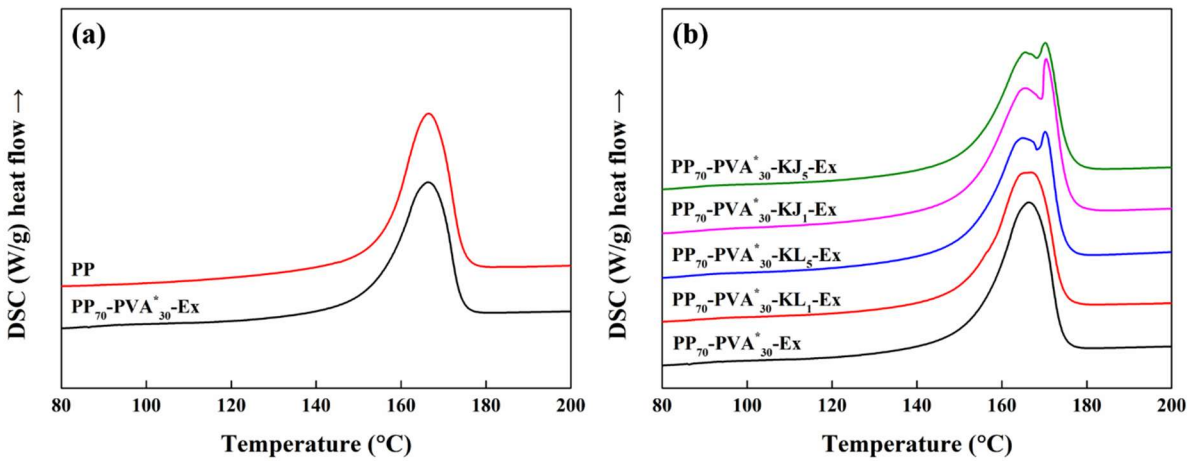

Figure 5-9 DSC spectra of (a) neat PP and PP_{70}-PVA^{*}_{30}-Ex (b) PP_{70}-PVA^{*}_{30} without/with kaolinite particles after selective phase extraction.

Table 5-2 Thermal properties of neat PP and PP_{70}-PVA_{30} fibers after extraction.

	Enthalpy (J/g)	X_c (%)	$T_{Peak\ 1}$ (°C)	$T_{Peak\ 2}$ (°C)
PP	83.34	39.9	166.5	-
PP_{70}-PVA^*_{30}-Ex	75.60	36.2	166.3	-
PP_{70}-PVA^*_{30}-KL_1-Ex	72.77	34.8	166.8	-
PP_{70}-PVA^*_{30}-KL_5-Ex	71.69	34.3	164.9	170.2
PP_{70}-PVA^*_{30}-KJ_1-Ex	80.26	38.4	165.5	170.4
PP_{70}-PVA^*_{30}-KJ_5-Ex	72.67	34.8	165.5	170.3

5.3 Conclusion

Janus particles are originally introduced into melt spinning systems, with hybrid kaolinite as an example. The Janus particles are proved to be successfully grafted, and they localize at the PP-PVA interface and significantly enhance the polymer compatibility. By contrast, the original kaolinite particles are distributed within the PVA phase. The kaolinite particles influence the morphology of the extrudates, reflected in the differentiated PVA accessibility. KL particles slightly enhance the PVA accessibility, while Janus KJ particles dramatically decrease the PVA accessibility, which originates from their refinement effect. For the plates after rheological tests, 5 wt.% of KJ particles can bring about significant PVA diameter reduction towards 19%. Rheological characterizations show a gel-like behavior for 5 wt.% of KJ, originating from the PVA and from a percolation effect due to the interfacial localization of the Janus particles.

The KJ-containing samples also exhibit lower melt flow indices. Therefore, the temperature profiles of melt spinning are suggested to be slightly increased. The new PVA can endow with the polymer blends with a very high PVA accessibility even in presence of kaolinite particles. All the PVA phase can be removed by the selective phase extraction, which is beneficial for obtaining a porous material. The obtained melt-spun yarns from PP_{70}-PVA^*_{30} are mechanically improved, of which the Young's modulus is significantly increased with a sharp 57% increment. Furthermore, the PP

crystallinity degree slightly decreases with the addition of the kaolinite particles even if the perfection of the crystals is improved.

Briefly speaking, apart from homogeneously modified particles, Janus particles provide an alternative method to fabricate the modified porous fibers. Their strong trend towards the interface may bring about less trial-and-error experiments and more excellent mechanical properties.

Chapter VI:

Melt Spinning of Polypropylene (Dispersed)/Poly(vinyl alcohol) (Matrix) Blends Compatibilized with Kaolinite Janus Hybrid Particles and Fabrication of PP Microfibers

Chapter 6 Melt Spinning of Polypropylene (Dispersed)/Poly(vinyl alcohol) (Matrix) Blends Compatibilized with Kaolinite Janus Hybrid Particles and Fabrication of PP Microfibers

It has been found that the ratio of 70 wt.%/30 wt.% in PP and PVA allows the manufacture of the PP porous fibers. Many kinds of inorganic particles can endow them with potential functionalities, of which the feasibility has been validated in the previous chapters. As the last chapter of the thesis, the efforts are made to reverse the ratio of the polymer blends to give the material more potentiality. Therefore, the ratios of PP and PVA are changed as 30 wt.%/70 wt.%. Our objective is to fabricate the PP microfibers also with a high specific area. Also, Janus kaolinite particles are added into the blends. It is worth noting that the blending procedure goes first with the compounding of PP and particles. In order to prevent the possible agglomeration of the kaolinite particles in the PP matrix impacting the morphology evolution, the fraction of particles in PP-PVA* blends is reduced from 5 wt.% to 2 wt.%, for the PP phase is shifted from majority to minority in the PP_{30}-PVA^*_{70} blends instead of PP_{70}-PVA^*_{30} blends.

6.1 Polymeric compounds

6.1.1 Rheometer tests

The rheological results of the polymer blends are illustrated in Figure 6-1. PP behavior is as a Newtonian plateau at low shear rates, while there appears a sharp slope in the PVA curves, due to the dynamic hydrogen bonds of PVA. For the polymer blend PP_{30}-PVA^*_{70}, the complex viscosity, as well as storage modulus, is even more significant. It results from the contribution of the interface of PP and PVA to the storage modulus. The introduction of a small amount of kaolinite particles has a slight influence

on the rheological behaviors of the PP_{30}-PVA^*_{70} blends. The differences are related to the presence of PP nodules having various sizes, caused by the different localizations of kaolinite particles. KL particles have a higher tendency to be localized in the PVA phase. It can be due to the hydrophilicity of the unmodified kaolinite particles. The Janus kaolinite particles, KJ, seem to be distributed at the biphasic interface. Commonly, the dimension of PP domains should be reduced when the particles are dispersed in the PVA matrix or at the interface. The use of the Janus particles allows for enhancing this effect. Therefore, the elasticity is decreased at the low-frequency area, with the presence of the Janus particles.

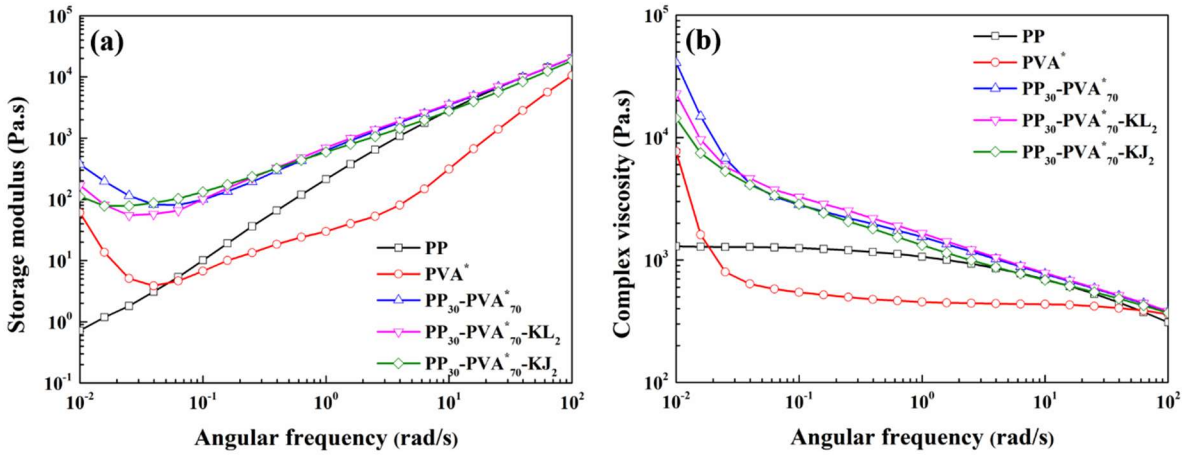

Figure 6-1 Rheological results of PP_{30}-PVA^*_{70} blends with/without kaolinite particles at 190 °C (a) storage modulus; (b) complex viscosity.

6.1.2 Melt flow index (MFI)

The melt flow index of neat polymers and their blends from PP and PVA^* at 190°C is shown in Figure 6-2. The melt flow index of PP is 11.8 g/10min, while that of PVA^* is 19.3 g/10 min. After the blending of the polymers, the melt flow index increases up to 41.6 g/10 min. The negative deviations in viscosity result from the weak interaction of the two components of the polymer blends (Ku and Lin, 2005). The addition of the kaolinite particles decreases the melt flow index. For the addition amount of the particles is low, the MFI index is not altered significantly.

KL particles are supposed to localized in the matrix PVA phase, which has a more noticeable impact upon the fluidity compared with the KJ particles at the biphasic interface. The PP_{30}-PVA^{*}_{70}-KL_2 exhibits the lowest value as 37.2 g/10min among the polymer blends. The melt spinning temperature should be adjusted below 190°C.

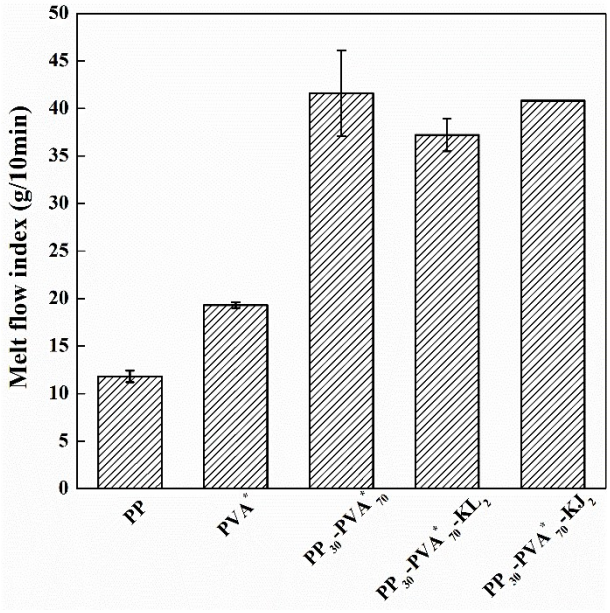

Figure 6-2 Melt flow index (190°C, 2.16 kg) of PP, PVA^{*} and the blends with/without kaolinite particles.

6.2 Polymeric fibers

6.2.1 Thermal stability of the microfibers

The melt spinnability of the biphasic polymers without and with the kaolinite particles behaves well. Also, for the pellets and the obtained fibers, it was found that the PVA is completely removed during the selective phase extraction experiment with hot water (the accessibility is close to 100%). In order to investigate if some kaolinite particles retain on the PP microfibers, an indirect method was carried out using the thermogravimetric analysis (TGA). The related figures are displayed in Figure 6-3. Besides, the TGA analyses of kaolinite particles have been done in the last chapter, and the corresponding figures can be found in Figure 5-1. Based on the TGA data, the residues at 700°C are shown in Table 6-1.

The kaolinite particles are slightly decomposed at a high temperature, and their residues are approximately about 85%-86%, of which the modified kaolinite exhibits a higher weight loss for the degradation of the grafted ODPA. The residue of PP microfibers without fillers at 700°C is 0%, but the residue of the PP microfibers with fillers is over 2.7% in any circumstances. The fraction of the kaolinite particles is only 2% of the total mass. Thus, the introduction of kaolinite particles enhances the thermal stability of the PP microfibers. Also, it signifies that kaolinite particles retain with the PP microfibers, no matter which particles are utilized. Both KL and KJ particles can be embedded with the PP microfibers.

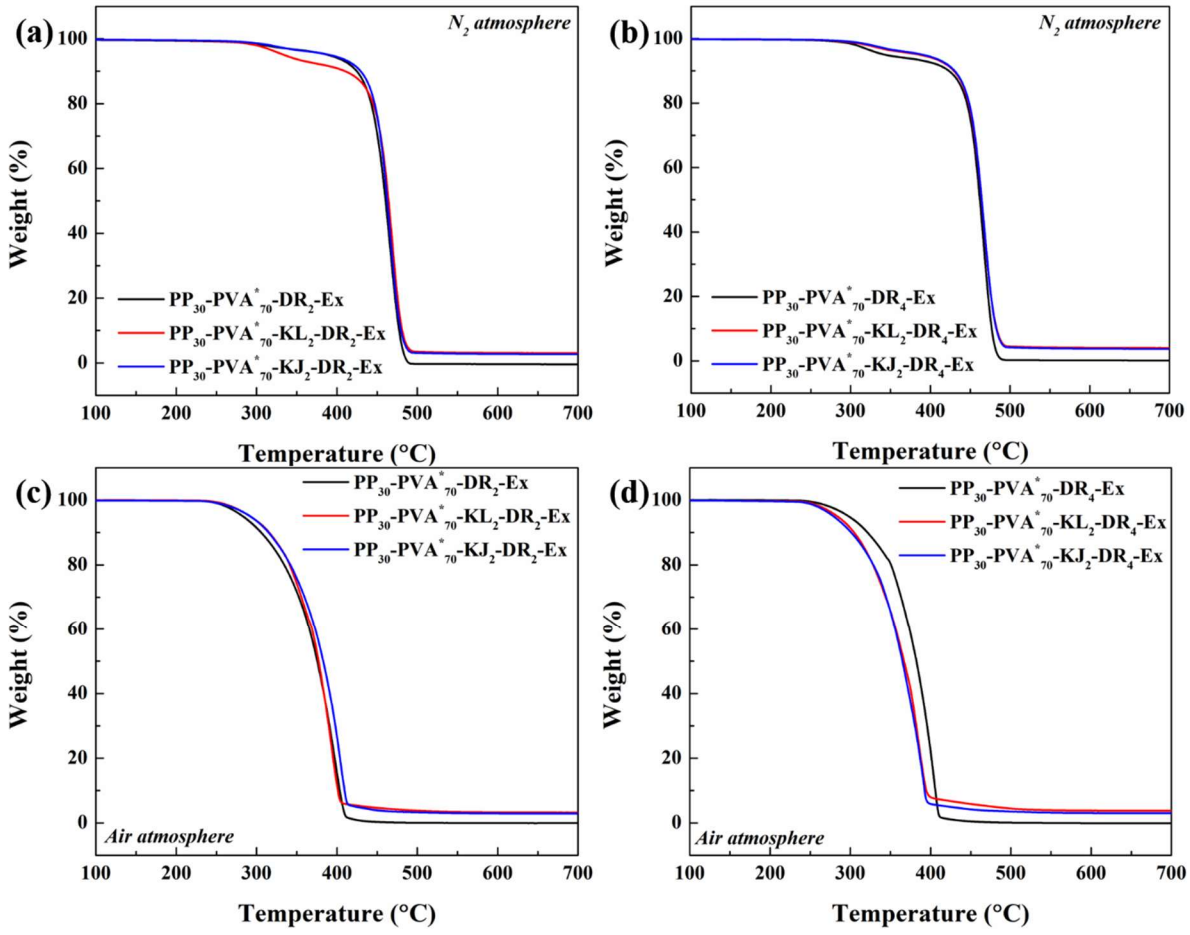

Figure 6-3 TGA results of the PP microfibers extracted from PP-PVA^* blend fibers.

Table 6-1 Residues (700°C) of PP microfibers extracted from PP-PVA* blend fibers.

PP microfibers	Residue in N_2 atmosphere (%)	Residue in air atmosphere (%)
KL particles	86.1	86.1
KJ particles	85.1	84.7
PP_{30}-PVA^*_{70}-DR_2	0	0
PP_{30}-PVA^*_{70}-KL_2-DR_2	3.0	3.3
PP_{30}-PVA^*_{70}-KJ_2-DR_2	2.7	2.9
PP_{30}-PVA^*_{70}-DR_4	0.1	0
PP_{30}-PVA^*_{70}-KL_2-DR_4	4.0	3.8
PP_{30}-PVA^*_{70}-KJ_2-DR_4	3.7	3.0

6.2.2 Morphology of the biphasic fibers

The fiber yarns were twisted to allow the knitting process. Afterward, the knitted fabrics were selectively extracted to remove the PVA phase. Therefore, the PP microfibers were released after the removal of PVA, and at the same time, the microfiber fabrics were obtained as well. SEM observations were conducted to observe the morphology of the knitted fabrics before and after extraction (Figure 6-4). Figure 6-4(a)(c)(e) illustrate that the morphology of the fabric before selective phase extraction, among which (a) reveals the knitting structure of the fabrics and (c)(e) demonstrates that the surface of the biphasic fiber is rough due to the immiscibility of the blends. After the selective phase extraction in hot water, the knitting structure still maintains, which can be distinguished in Figure 6-4(b). Also, many microfibers emerge after the removal of the PVA phase (Figure 6-4(d)(f)).

In order to observe the structures better, a higher magnification for the SEM observation was used in Figure 6-5. The mean diameters are about many hundreds of nanometers, representing a high specific area. Furthermore, from Figure 6-5(d), it can be distinguished that the microfibers are not entirely isolated, although the PP mass fraction is only about 30 wt.% in the blends. Instead, the microfibers are interconnected,

which is also the reason for the well maintaining of the knitting structure. Quantitative calculation of PP microfiber diameter is difficult to be carried out in the case of the diameter deviations of the multifilament PP_{30}-PVA^{*}_{70}-DR_4 fibers.

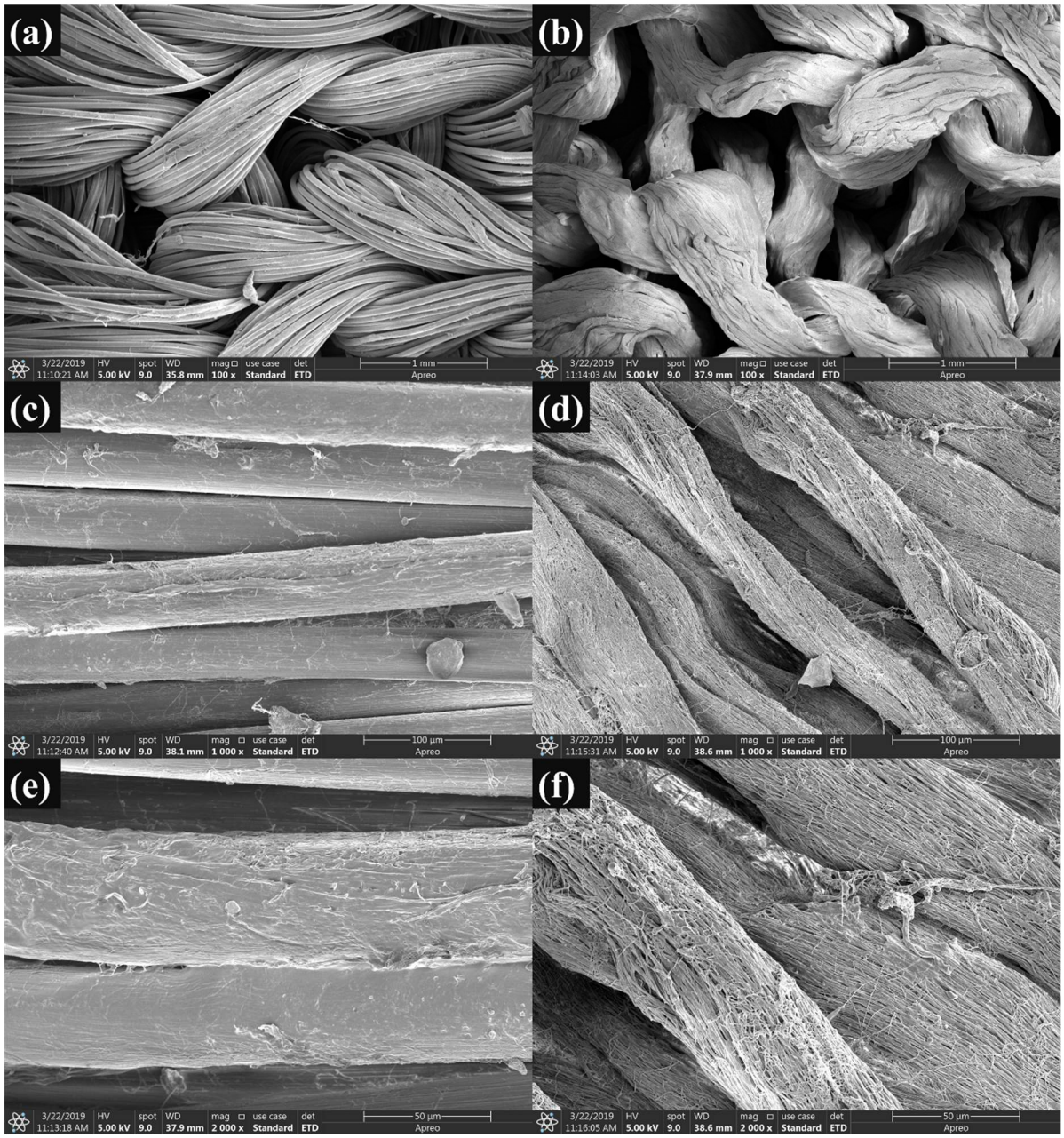

Figure 6-4 SEM images of knitted PP_{30}-PVA^{*}_{70}-DR_4 fabrics before and after selective phase extraction at various magnifications.

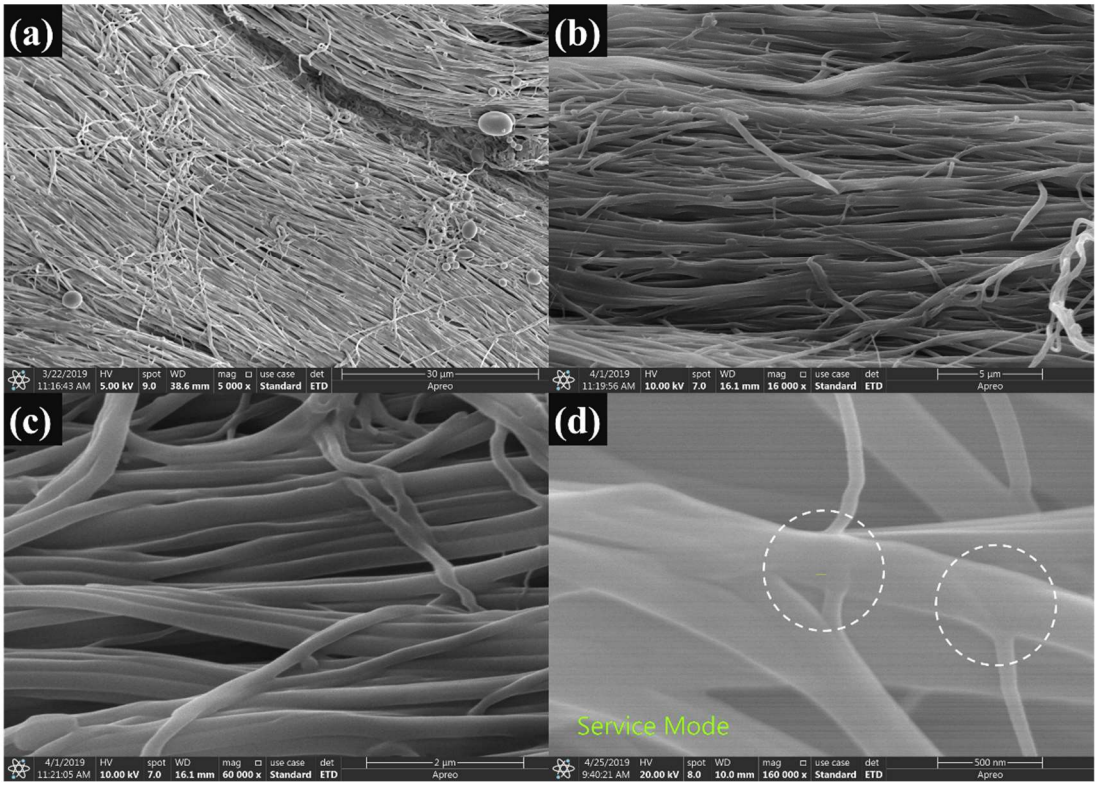

Figure 6-5 Further zoomed figures of knitted PP_{30}-PVA^{*}_{70}-DR_4 fabrics after selective phase extraction.

The SEM images of the biphasic fibers after the incorporation of kaolinite particles are displayed in Figure 6-6. The white dots are the kaolinite particles on the BSE images. The dimension of the KL particles is more significant than that of the KJ particles, mainly due to the more significant agglomeration of the KL particles. In general, both of the two kinds of particles can be dispersed well within the PP-PVA blends. The further demonstration of the biphasic fibers with kaolinite particles will be carried out in future work. It is beneficial for understanding the different localization and arrangement of kaolinite particles with the PP microfibers.

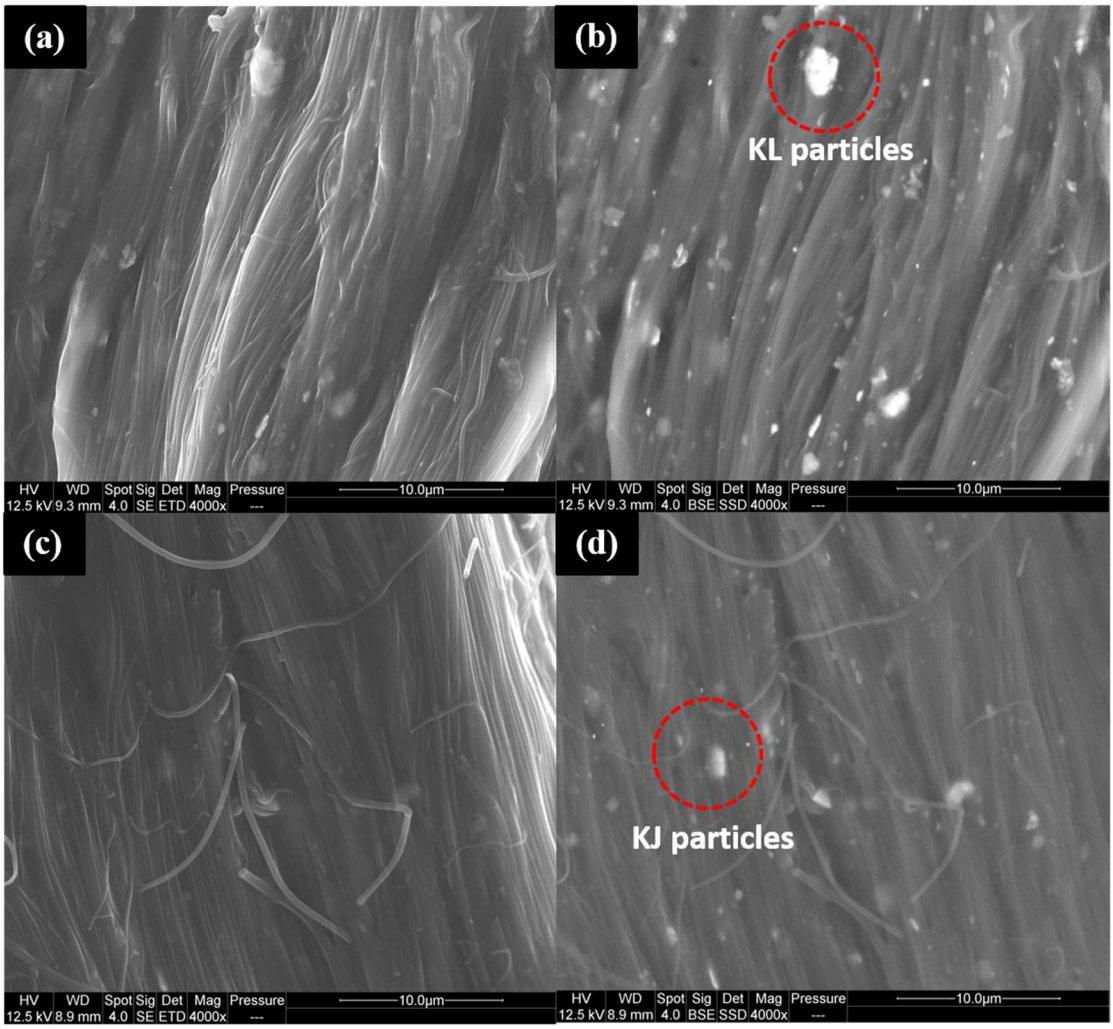

Figure 6-6 SEM images of (a) PP_{30}-PVA^{*}_{70}-KL_2-DR_4 fibers; (b) BSE of (a); (c) PP_{30}-PVA^{*}_{70}-KJ_2-DR_4 fibers; (d) BSE of (c).

6.2.3 Mechanical tests of the fibers

In order to investigate the mechanical performance of the composite fibers from PP_{30}-PVA^{*}_{70}, the tensile tests were realized on the fibers extracted from the yarns. The mechanical properties of the composite fibers from PP_{30}-PVA^{*}_{70}, with and without kaolinite particles, and their stress-strain curves are shown in Table 6-2 and Figure 6-7, respectively. When the draw ratio is low, the mechanical properties of the fibers are fragile. The adding of kaolinite particles in the polymer blend significantly enhances Young's modulus. Meanwhile, the breaking elongation is slightly decreased, even if the particles enhance the interfacial adhesion between the polymers. With the increment of the draw ratio, the mechanical properties are significantly enhanced due to alignment

of macromolecular chains in fiber direction. In detail, Young's modulus is increased sharply from 842±124 MPa to 2916±431 MPa, while the tenacity increases from 5.8±1.0 cN/Tex to 19.4±1.9 cN/Tex. Thus, a high draw ratio results in better mechanical properties. For a draw ratio of 4, the incorporation of kaolinite particles is detrimental to Young's modulus as well as the tenacity. It is interesting that based on the stress-strain curves, it can be observed that within a certain degree of strain, the stress is enhanced due to the kaolinite particles. However, the particles as stress concentration points lead to the advance of breakage, which is the cause of the negative influence of mechanical properties.

Table 6-2 Mechanical properties of the composite fibers from PP_{30}-PVA^*_{70} with/without kaolinite particles.

Fibers	Young's modulus (MPa)	Tenacity (cN/Tex)	Breaking elongation (%)
PP_{30}-PVA^*_{70}-DR_2	842±124	5.8±1.0	47±14
PP_{30}-PVA^*_{70}-KL_2-DR_2	1638±446	7.0±1.0	35±13
PP_{30}-PVA^*_{70}-KJ_2-DR_2	1810±674	7.3±1.4	34±9
PP_{30}-PVA^*_{70}-DR_4	2916±431	19.4±1.9	21±3
PP_{30}-PVA^*_{70}-KL_2-DR_4	1987±209	18.6±1.8	17±2
PP_{30}-PVA^*_{70}-KJ_2-DR_4	2165±225	15.8±3.7	13±3

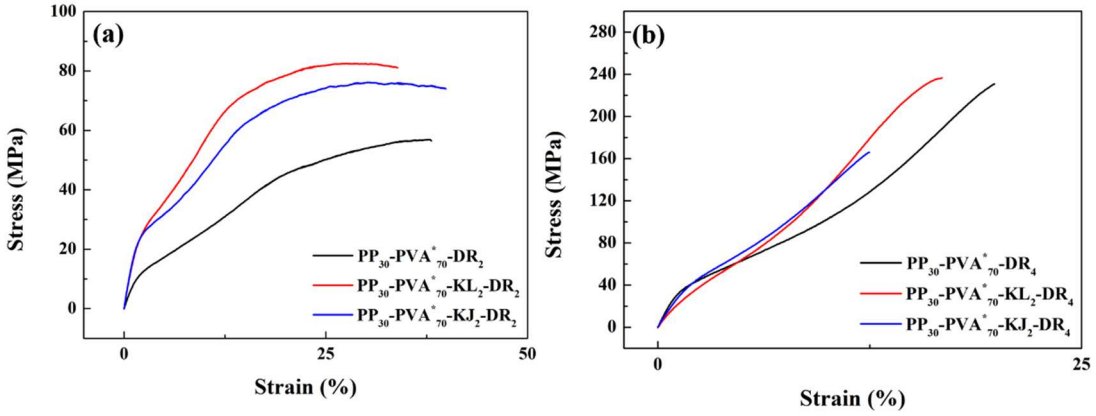

Figure 6-7 Stress-strain curves of (a) PP_{30}-PVA^*_{70} fibers with/without kaolinites with DR=2; (b) PP_{30}-PVA^*_{70} fibers with/without kaolinites with DR=4.

6.2.4 Mechanical tests of the knitted fabrics

As an important branch of downstream processes in textile industry, the fibers can be further twisted and knitted into fabrics. In this case, the higher draw ratio leads to significantly better mechanical properties. Also, it is beneficial for manufacturing the fibers with a reduced thickness, which may be used during the knitting process. Therefore, the fibers with DR=4 was chosen for further manufacturing into knitted fabrics. Qualified mechanical performance of the knitted fabrics is also required to satisfy the potential industrial usage. Therefore, the tensile tests of the knitted fabrics before and after selective phase extraction were also done. The mechanical properties, as well as the air permeability of the knitted fabrics from PP_{30}-PVA^*_{70} fibers before and after selective phase extraction, are illustrated in Table 6-3. For better comparison, the stress-strain curves of knitted fabrics from PP_{30}-PVA^*_{70} fibers are displayed in Figure 6-8. The elongation at δ_{max} (maximum force) of the fabrics is 86.3±3.5 %. The addition of kaolinite particles weakens the elongation, especially when the Janus particles KJ particles are adopted. Meanwhile, the maximum stress can be slightly enhanced due to the introduction of the kaolinite particles. The related stress-strain curves are illustrated in Figure 6-8(a), in which the mechanical enhancement by the kaolinite particles can be clearly observed.

The thicknesses of the fabrics, as well as their specific weights, are decreased after the selective phase extraction. Furthermore, the air permeability is slightly increased. The most visible increment appears in the samples with Janus kaolinite particles. It may result from the decrease of the mean diameters of the PP microfibers. As for the mechanical properties, the maximum stress is decreased, and the corresponding elongation is significantly increased. The drastic increase in elongation at the maximum stress is due to the good extensibility of PP material as well as the sliding effect of obtained PP microfibers between loops. Although the PVA phase has been removed, the mechanical enhancement of the kaolinite particles still exists. Thus, the mechanical enhancement mechanism towards the PP-PVA blends may lie in not only the better interfacial adhesion but also an optimized aggregate structure of the PP phase. In conclusion, while imparting surface modification to the microfiber fabrics, the kaolinite particles also endow them with better mechanical properties.

Table 6-3 Mechanical properties of the knitted fabrics from PP_{30}-PVA^{*}_{70} fibers.

Fabrics	Thickness (mm)	Width (mm)	Cross-section (mm^2)	Areal density (g/m^2)	δ_{max} (MPa)	Elongation at δ_{max} (%)	Air permeability (mm/s)
PP_{30}-PVA^{*}_{70}-DR_4-Knit	2.451	42	102.942	838.7	8.6±0.2	86.3±3.5	2532±45
PP_{30}-PVA^{*}_{70}-KL_2-DR_4-Knit	2.359	42	99.078	825.4	10.8±0.8	87.8±3.9	2780±109
PP_{30}-PVA^{*}_{70}-KJ_2-DR_4-Knit	2.353	41	96.473	824.9	11.3±0.1	67.8±1.5	2780±109
PP_{30}-PVA^{*}_{70}-DR_4-Knit-Ex	1.840	41	75.44	319.3	5.8±0.5	153.9±14.3	2571±187
PP_{30}-PVA^{*}_{70}-KL_2-DR_4-Knit-Ex	1.715	42	72.03	307.3	5.3±0.1	111.5±14.0	2634±98
PP_{30}-PVA^{*}_{70}-KJ_2-DR_4-Knit-Ex	1.825	42	76.65	302.0	6.8±0.6	148.2±21.7	2991±190

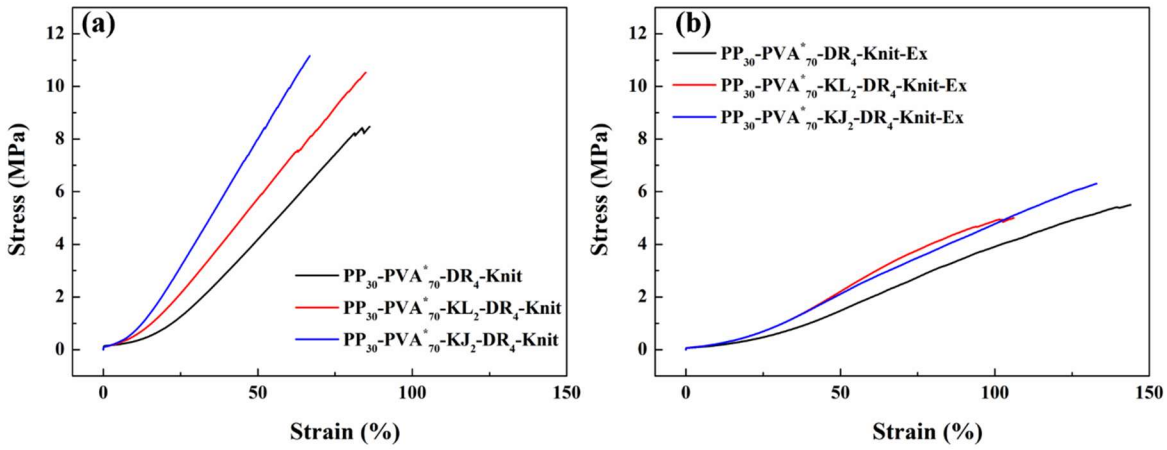

Figure 6-8 Stress-strain curves of knitted fabrics from PP_{30}-PVA^*_{70} fibers (a) before selective phase extraction; (b) after selective phase extraction.

6.2.5 Thermal properties of the PP microfibers

The DSC measurement was carried out to investigate the thermal properties of the obtained PP microfibers. The DSC spectra are displayed in Figure 6-9, and related details are summarized in Table 6-4. There is a single peak for the PP microfibers when the draw ratio is 2. In addition, the introduction of the Janus kaolinite increases the melting point, but there is no significant alteration of the crystallinity degree. When the draw ratio is elevated to 4, the crystallinity degree is increased from 30.4% to 32.1%, and the melting point is also increased from 165°C to 168°C. The incorporation of Janus kaolinite particles gives rise to the further increment of crystallinity degree towards 33.4%. However, their impact on the melting point becomes negligible. Generally speaking, the increment of draw ratio and the incorporation of kaolinite particles have slight enhancement upon the crystallinity degree of the PP microfibers.

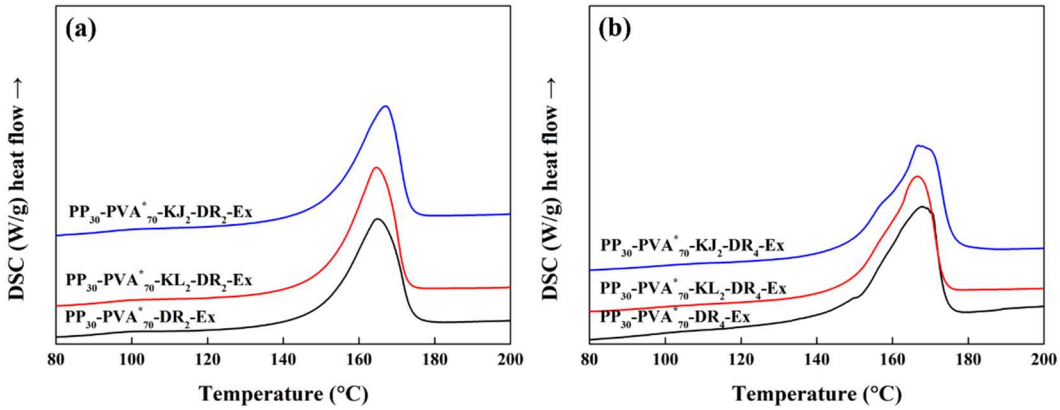

Figure 6-9 DSC spectra of PP microfibers (a) extracted from PP_{30}-PVA^{*}_{70} with/without kaolinite particles with DR=2; (b) extracted from PP_{30}-PVA^{*}_{70} with/without kaolinite particles with DR=4.

Table 6-4 Thermal properties of PP microfibers extracted from PP_{30}-PVA^{*}_{70} with/without kaolinite particles with different draw ratios.

	Enthalpy (J/g)	**X_c (%)**	**T_{Peak} (°C)**
PP_{30}-PVA^{*}_{70}-DR_2-Ex	63.48	30.4	164.8
PP_{30}-PVA^{*}_{70}-KL_2-DR_2-Ex	67.94	32.5	164.6
PP_{30}-PVA^{*}_{70}-KJ_2-DR_2-Ex	62.94	30.1	167.1
PP_{30}-PVA^{*}_{70}-DR_4-Ex	67.10	32.1	167.9
PP_{30}-PVA^{*}_{70}-KL_2-DR_4-Ex	67.81	32.4	166.5
PP_{30}-PVA^{*}_{70}-KJ_2-DR_4-Ex	69.91	33.4	166.6

6.3 Conclusion

In this chapter, the ratio of PP and PVA blends is reversed as 30 wt.%/70 wt.% for manufacturing the PP-PVA composite fibers, in which PP microfibers are arranged in the PVA matrix phase. Therefore, with the aid of water, the PP microfibers can be finally obtained with the removal of PVA.

Meanwhile, kaolinite particles are incorporated into the PP_{30}-PVA^{*}_{70} blends. The measurement of the thermal stability of PP microfibers demonstrates that some kaolinite particles are embedded with the PP phase. The elasticity in rheometer tests is varied due to the introduction of different kaolinite particles, influenced by their different affinities to the polymer blends. The kaolinite particles also decrease the melt flow index as an indication of the fluidity. Based on the MFI values, the melt spinning is suggested to be below 190°C. The knitting technology is adopted to create textile products followed with selective phase extraction. As a result, numerous PP microfibers with the diameters of hundreds of nanometers are obtained, and the knitting structure still maintains due to the interconnectivity of the microfibers. A high draw ratio is preferred with the aim of better mechanical performance as well as the accessibility of knitting. The introduction of kaolinite particles may bring about more stress concentration points in the biphasic fibers; however, the enhancement effects still exist for the knitted fabrics, especially for the Janus particles even after the selective phase extraction.

It demonstrates that adjusting the ratios of PP and PVA provides more diversity of PP products. The surface-tailored products with a high specific area are not limited to porous fibers, and the PP microfibers can also be explored. The chapter sets an example for the potential future development.

General Conclusions and Prospects

The textile products are expected to behave good surface effects with more added values. Instead of the conventional chemical treatment, thermodynamic control can also be achieved to make the nanoparticles towards the interfacial localization of biphasic blends. The nanoparticles can have or be endowed with additional properties afterward.

The purpose of the thesis dissertation is to make efforts to apply the related application into the textile field, mainly depending on the melt spinning technology. The detailed protocol is divided into two steps: (1) Localize the filler at the biphasic interface; (2) Remove the water-soluble PVA phase and expose the PP phase with the embedded particles. Therefore, in order to demonstrate the feasibility, the experimental sections were divided into **four stages**.

The **first stage (Chapter 3)** is to reveal the most appropriate ratio of PP and PVA blends to manufacture the biphasic fibers. PP-PVA blend favors stable melt processing due to its good thermal stability. The biphasic microstructure experiences a significant change by altering the PVA content, during which phase inversion may occur. There is a negative deviation in viscosity due to the weak interactions between the two polymers. PP_{70}-PVA_{30} performs an excellent spinnability during melt spinning, along with good mechanical properties. The drawing during melt spinning makes the PVA interconnected, exhibiting an outstanding value of PVA accessibility. This is a good certificate that the morphology undergoes extreme evolution during the melt spinning process. The extraction of dominant PVA leaves complete porous fibrous shapes, maintaining good mechanical performance. In addition, a higher draw ratio is suggested to be adopted, which contributes to higher PVA accessibility and mechanical properties. Furthermore, the knitting technology is also tried, and a finer diameter caused by the high draw ratio can also do a favor. The requirement of the PVA fraction is strict, for a higher fraction may lead to the failure with worse spinnability with fragile mechanical behavior and even lower PVA accessibility. Furthermore, it cannot provide a porous fibrous scaffold after selective phase extraction.

In the **following stages (Chapter 4, Chapter 5)**, the ratio of the blends is always fixed for the following stages for manufacturing PP porous fibers. As for **conventional homogenously modified particles (Chapter 4)**, silica nanoparticles with different surface chemistries were incorporated into PP_{70}-PVA_{30} blends aimed at manufacturing surface-functionalized porous PP fibers via melt spinning technology. Different silica nanoparticles exhibit different localizations. Si_{R972} and Si_{R816} are confirmed to be partially localized at the interface. The definite localizations are basically consistent with thermodynamical prediction. As a result, the different localization gave rise to the significantly distinctive biphasic morphology of PP-PVA, about which the in-depth investigations have been done. The spinnability of the fibers with 1 wt.% of silica nanoparticles remains outstanding. Si_{R972} silica nanoparticles maintain the most remarkable interfacial localization during the fiber stage due to the thermodynamic equilibrium. The biphasic fibers provide a high specific interface area with the PVA mean diameters of hundreds of nanometers as well as a good mechanical property, upon which the silica nanoparticles have no significant enhancement. Nevertheless, Si_{R972} has the least negative influence in the aggregation structure as well as the mechanical performance, thanks to the interfacial localization. A high draw ratio is proved again to be an advantage condition for manufacturing the biphasic fibers even when particles are incorporated.

As the research progressed, a new PVA is tried that is more suitable and commercialized for melt spinning. The new PVA can endow the polymer blends with a very high PVA accessibility, even in the presence of kaolinite particles. All the PVA phase can be removed by the selective phase extraction, which is beneficial for obtaining a porous material. Apart from the homogenously modified particles, efforts are also made to introduce the **Janus particles (Chapter 5)** into the melt spinning systems to prevent redundant trial-and-error experiments. They localize at the biphasic interface and significantly enhance the polymer compatibility, violently influencing the morphology of the blends. Rheological characterizations show a gel-like behavior for 5 wt.% of Janus particles, partially originating from a percolation effect due to the

interfacial localization of the Janus particles. The obtained melt-spun yarns from PP_{70}-PVA^{*}_{30} are mechanically improved, of which Young's modulus is significantly increased with a sharp 57% increment. It proves that the introduction of particles even has the potential to enhance rather than weaken the mechanical properties of fibers.

Apart from manufacturing the porous fibers, the **microfibers** can also be obtained by increasing the amount of PVA. In the **last stage (Chapter 6)**, the ratio of PP and PVA blends is reversed as 30 wt.%/70 wt.% for manufacturing the PP-PVA composite fibers. Meanwhile, Janus kaolinite particles are incorporated into the PP_{30}-PVA^{*}_{70} blends. The knitting technology is adopted to create textile products followed with selective phase extraction. Numerous PP microfibers with the diameters of hundreds of nanometers are obtained, and the knitting structure still maintains due to the interconnectivity of the microfibers. The Janus particles can enhance the knitted fabrics even after the selective phase extraction, which the conventional chemical treatment cannot bring about. For biphasic polymers, melt spinning temperature is a key factor in determining the feasibility, of which the MFI values are important parameters. A high draw ratio is also preferred with the aim of better mechanical performance as well as the accessibility of knitting.

In summary, a methodology is demonstrated to fabricate the high-specific-area textile products (porous/microfibers) with surface-modified particles, not only by the homogenously modified particles but also by the Janus particles. The thesis as basic research is mainly concerning the morphology evolution, and accompanied thermal and mechanical properties, standing at the perspective of textiles. The melt spinning temperature is a key parameter, of which MFI index should be considered. The fraction of two polymers is also very important determining the melt spinnability, of which some can lead to the failure. The melt spinning of PP_{70}-PVA_{30} and PP_{30}-PVA_{70} behaves well, even with the incorporation of fillers. The morphology of the composite fibers differs drastically from the extrudates to the multifilament yarns. Apart from the direct microscopy observation, PVA accessibility measurement is a facile test to indirectly observe the morphology evolution, and DMA measurement can be a supplementary

method to test the PVA continuity. Rheometer tests are also a powerful tool to distinguish the morphology evolution and filler localizations. It is found that the mean diameter of dispersed phase (PVA or PP) within the biphasic fiber is about hundreds of nanometers, and it tends to be slightly interconnected although the fraction is only 30 wt.%, which gives support to a thoroughly removal of sacrificial phase (porous fibers) or a maintaining of downstream textile structure (microfibers). The surface-localized fillers have the least negative effects upon the mechanical properties, even bring about the enhancement in the case of Janus particles. In addition, a high draw ratio is always preferred to reach a better mechanical performance. As for the fibers not reaching the co-continuous morphology, a high draw ratio is also beneficial for enhancing the PVA accessibility. In addition, it's also beneficial for reaching a lower thickness better adapted to the knitting technology. It can be a reference to guide the researchers to manufacture the related textile products without or even with customized functions.

Based on the practical experience in the completed research, there are some suggestions for further developing this topic, which can be taken into consideration in the future work. It can be divided into three aspects, nanoparticles, polymers and fabrication technology.

Nanoparticles:

- This is a basic research focusing on the morphology evolution of the materials. As an important extension, the nanoparticles with specific functionality can be incorporated into the biphasic polymer systems in the future work, for example, with the conductive, catalytic or flame-retardant properties;
- The fraction range of the nanoparticles can be further extended. For the current research, the maximum fraction is 5 wt.%. A higher amount can be further attempted, for it sometimes requires a high amount to reach a certain functionality, and unavoidably it will bring about different influence upon the morphology;
- Different kinds nanoparticles can be utilized, including different shapes, sizes.

It is of great interest to discover the impact of the different dimensional parameters to the morphology evolution of the polymer blends including the biphasic fibers;

- More than two nanoparticles can be attempted to added simultaneously to reach the synergistic effect, for example, targeting the morphology control, mechanical enhancement or specific functionality enhancement. In addition, simultaneously adding the conventional compatibilizer (e.g. copolymers) with nanoparticles can be also a strategy. So far, the reactive compatibilization is also a very popular direction, providing an additional idea for researchers.

Polymers:

- The selection of the polymers can be also extended. The fiber matrix PP can be replaced by other polymers, for example, biocompatible materials, e.g. PLA. Also, the sacrificial polymer PVA can be also replaced by others, for example, sulfonated PET (SP). For a certain macromolecule kind, it is also very significant to discuss about the influence brought about by the distinct monomer composition, molecular weight, etc.;
- The melt spinning of ternary phase polymers can be also an interesting topic, combined with the concept of selective phase extraction;

Fabrication technology:

- Discussion on the spinning mechanism can also be carried out, based on a series of related experiments, including the extensional rheometer test;
- The recycling process of sacrificial phase can be developed. In many cases, the number of recycling of certain polymer is limited;
- The energy-consumption issue can be also considered. For example, in the thesis, the maximum compounding times are 3 (2 for melt extrusion, 1 for melt spinning), leading to a lot of energy consumption, which can be optimized in the future work. Also, the solvent temperature and extraction time during the

selective phase extraction can be optimized.

- Apart from knitting technology, other textile fabrication technology can be also attempted, such as weaving technology.

References

AFSHARI, M., KOTEK, R., KISH, M.H., DAST, H.N. and GUPTA, B.S., 2002. Effect of blend ratio on bulk properties and matrix–fibril morphology of polypropylene/nylon 6 polyblend fibers. *Polymer*, 43(4), pp.1331-1341. Available at: http://dx.doi.org/10.1016/s0032-3861(01)00689-9.

ALEXANDER LE. *X-Ray Diffraction Methods in Polymer Science*. New York: Wiley, 1969.

ALEXY, P., KÁCHOVÁ, D., KRŠIAK, M., BAKOŠ, D. and ŠIMKOVÁ, B., 2002. Poly (vinyl alcohol) stabilisation in thermoplastic processing. *Polymer Degradation and stability*, 78(3), pp.413-421. Available at: http://dx.doi.org/10.1016/s0141-3910(02)00177-5.

ASADINEZHAD, A., YAVARI, A., JAFARI, S.H., Khonakdar, H.A. and BÖHME, F., 2005. Description of the dynamic moduli of poly (trimethylene terephthalate)/polyamide-12 blends in molten state. *Polymer Engineering & Science*, 45(10), pp.1401-1407. Available at: http://dx.doi.org/10.1002/pen.20413.

ASTM D1238-10 *Standard Test Method for Melt Flow Rates of Thermoplastics by Extrusion Plastometer.*

AVGEROPOULOS, G.N., WEISSERT, F.C., BIDDISON, P.H. and BOHM, G.G.A., 1976. Heterogeneous Blends of Polymers. Rheology and Morphology. *Rubber Chemistry and Technology*, 49(1), pp.93–104. Available at: http://dx.doi.org/10.5254/1.3534954.

BAHRAMI, R., LÖBLING, T.I., GRÖSCHEL, A.H., SCHMALZ, H., MÜLLER, A.H. and ALTSTÄDT, V., 2014. The impact of Janus nanoparticles on the compatibilization of immiscible polymer blends under technologically relevant conditions. *ACS Nano*, 8(10), pp.10048-10056. Available at: http://dx.doi.org/10.1021/nn502662p.

BAHRAMI, R., LÖBLING, T.I., SCHMALZ, H., MÜLLER, A.H. and ALTSTÄDT, V., 2017. Synergistic effects of Janus particles and triblock terpolymers on toughness of immiscible polymer blends. *Polymer*, 109, pp.229-237. Available at: http://dx.doi.org/10.1016/j.polymer.2016.12.044.

BAKLAVARIDIS, A., ZUBURTIKUDIS, I. and PANAYIOTOU, C., 2014. Porous composite structures derived from multiphase polymer blends. *Polymer Engineering & Science*, 55(8), pp.1856-1863. Available at: http://dx.doi.org/10.1002/pen.24025.

BATISTELLA, M., OTAZAGHINE, B., SONNIER, R., CARO-BRETELLE, A.S., PETTER, C. and LOPEZ-CUESTA, J.M., 2014. Fire retardancy of ethylene vinyl acetate/ultrafine kaolinite composites. *Polymer Degradation and Stability*, 100, pp.54-62. Available at: http://dx.doi.org/10.1016/j.polymdegradstab.2013.12.026.

BATISTELLA, M., OTAZAGHINE, B., SONNIER, R., PETTER, C. and LOPEZ-CUESTA, J.M., 2016. Fire retardancy of polypropylene/kaolinite composites. *Polymer Degradation and Stability*, 129, pp.260-267. Available at: http://dx.doi.org/10.1016/j.polymdegradstab.2016.05.003.

BENTLEY, B.J. and LEAL, L.G., 1986. An experimental investigation of drop deformation and breakup in steady, two-dimensional linear flows. *Journal of Fluid Mechanics,* 167(-1), p.241. Available at: http://dx.doi.org/10.1017/s0022112086002811.

BEUGUEL, Q., VILLE, J., CREPIN-LEBLOND, J., MEDERIC, P. and AUBRY, T., 2017. Influence of clay mineral structure and polyamide polarity on the structural and morphological properties of clay polypropylene/polyamide nanocomposites. *Applied Clay Science*, 135, pp.253-259. Available at: http://dx.doi.org/10.1016/j.clay.2016.09.034.

BIKALES, N. M. *Characterization of Polymers*; Wiley-Inter- science: New York, 1971.

BINKS, B.P. and FLETCHER, P.D.I., 2001. Particles adsorbed at the oil− water interface: A theoretical comparison between spheres of uniform wettability and "Janus" particles. *Langmuir*, 17(16), pp.4708-4710. Available at: http://dx.doi.org/10.1021/la0103315.

BOURRY, D. and FAVIS, B.D., 1998. Cocontinuity and phase inversion in HDPE/PS blends: influence of interfacial modification and elasticity. *Journal of Polymer Science Part B: Polymer Physics*, 36(11), pp.1889-1899. Available at: https://doi.org/10.1002/(SICI)1099-0488(199808)36:11<1889::AID-POLB10>3.0.CO;2-3.

BOUSMINA, M., 1999. Rheology of polymer blends: linear model for viscoelastic emulsions. *Rheologica Acta*, 38(1), pp.73–83. Available at: http://dx.doi.org/10.1007/s003970050157.

BRANDALISE, R.N., ZENI, M., MARTINS, J.D. and FORTE, M.M., 2009. Morphology, mechanical and dynamic mechanical properties of recycled high density polyethylene and poly (vinyl alcohol) blends. *Polymer Bulletin*, 62(1), pp.33-43. Available at: http://dx.doi.org/10.1007/s00289-008-0989-4.

BRANDRUP, J. and IMMERGUT, E.H. *Polymer Handbook, 3rd ed.,* Wiley Interscience, New York (1989)

BROWN, H.R., CHAR, K., DELINE, V.R. and GREEN, P.F., 1993. Effects of a diblock copolymer on adhesion between immiscible polymers. 1. Polystyrene (PS)-PMMA copolymer between PS and PMMA. *Macromolecules*, 26(16), pp.4155-4163. Available at: http://dx.doi.org/10.1021/ma00068a014.

BRYSON, K.C., LÖBLING, T.I., MÜLLER, A.H., RUSSELL, T.P. and HAYWARD, R.C., 2015. Using Janus nanoparticles to trap polymer blend morphologies during solvent-evaporation-induced demixing. *Macromolecules*, 48(12), pp.4220-4227. Available at: http://dx.doi.org/10.1021/acs.macromol.5b00640.

CARO, A.S., PARPAITE, T., OTAZAGHINE, B., TAGUET, A. and LOPEZ-CUESTA, J.M., 2017. Viscoelastic properties of polystyrene/polyamide-6 blend compatibilized with silica/polystyrene Janus hybrid nanoparticles. *Journal of Rheology,* 61(2), pp.305-310. Available at: http://dx.doi.org/10.1122/1.4975334.

CAYLA, A., CAMPAGNE, C., ROCHERY, M. and DEVAUX, E., 2012. Melt spun multifilament yarns of carbon nanotubes-based polymeric blends: Electrical, mechanical and thermal properties. *Synthetic Metals,* 162(9-10), pp.759-767. Available at: http://dx.doi.org/10.1016/j.synthmet.2012.03.021.

CAYLA, A., RAULT, F., GIRAUD, S., SALAÜN, F., FIERRO, V. and CELZARD, A., 2016. PLA with intumescent system containing lignin and ammonium polyphosphate for flame retardant textile. *Polymers,* 8(9), p.331. Available at: http://dx.doi.org/10.3390/polym8090331.

CHANDRAN, N., CHANDRAN, S., MARIA, H.J. and THOMAS, S., 2015. Compatibilizing action and localization of clay in a polypropylene/natural rubber

(PP/NR) blend. *RSC Advances*, 5(105), pp.86265-86273. Available at: http://dx.doi.org/10.1039/c5ra14352g.

CHEN, G.X., KIM, H.S., KIM, E.S. and YOON, J.S., 2005. Compatibilization-like effect of reactive organoclay on the poly (L-lactide)/poly (butylene succinate) blends. *Polymer*, 46(25), pp.11829-11836. Available at: http://dx.doi.org/10.1016/j.polymer.2005.10.056.

CHEN, J., CUI, X., SUI, K., ZHU, Y. and JIANG, W., 2017a. Balance the electrical properties and mechanical properties of carbon black filled immiscible polymer blends with a double percolation structure. *Composites Science and Technology,* 140, pp.99-105. Available at: http://dx.doi.org/10.1016/j.compscitech.2016.12.029.

CHEN, J., CUI, X., ZHU, Y., JIANG, W. and SUI, K., 2017b. Design of superior conductive polymer composite with precisely controlling carbon nanotubes at the interface of a co-continuous polymer blend via a balance of π-π interactions and dipole-dipole interactions. *Carbon*, 114, pp.441-448. Available at: http://dx.doi.org/10.1016/j.carbon.2016.12.048.

CHO, D., ZHOU, H., CHO, Y., AUDUS, D. and JOO, Y.L., 2010. Structural properties and superhydrophobicity of electrospun polypropylene fibers from solution and melt. *Polymer,* 51(25), pp.6005-6012. Available at: http://dx.doi.org/10.1016/j.polymer.2010.10.028.

CHO, I. and LEE, K.W., 1985. Morphology of latex particles formed by poly (methyl methacrylate)-seeded emulsion polymerization of styrene. *Journal of Applied Polymer Science,* 30(5), pp.1903-1926. Available at: http://dx.doi.org/10.1002/app.1985.070300510.

CHO, M.S., PARK, S.Y., HWANG, J.Y. and CHOI, H.J., 2004. Synthesis and electrical properties of polymer composites with polyaniline nanoparticles. *Materials Science and Engineering: C*, 24(1-2), pp.15-18. Available at: http://dx.doi.org/10.1016/j.msec.2003.09.003.

CHOI, S.J. and SCHOWALTER, W.R., 1975. Rheological properties of nondilute suspensions of deformable particles. *The Physics of Fluids*, 18(4), pp.420-427. Available at: http://dx.doi.org/10.1063/1.861167.

CHUAI, C.Z., ALMDAL, K., JOHANNSEN, I. and LYNGAAE-JØRGENSEN, J., 2001. Morphology evolution of polycarbonate–polystyrene blends during compounding. *Polymer*, 42(19), pp.8217-8223. Available at: http://dx.doi.org/10.1016/s0032-3861(01)00309-3.

COOK, J.G., 1968. *Handbook of Textile Fibres. 2.: Man-made Fibres.* Watford: Merrow Publishing.

CORAN, A.Y., 1988. *Handbook of Elastomers.* Marcel & Dekker, New York, p.249.

DAI, K., XU, X.B. and LI, Z.M., 2007. Electrically conductive carbon black (CB) filled in situ microfibrillar poly (ethylene terephthalate)(PET)/polyethylene (PE) composite with a selective CB distribution. *Polymer*, 48(3), pp.849-859. Available at: http://dx.doi.org/10.1016/j.polymer.2006.12.026.

DE LUNA, M.S. and FILIPPONE, G., 2016. Effects of nanoparticles on the morphology of immiscible polymer blends–challenges and opportunities. *European Polymer Journal*, 79, pp.198-218. Available at: http://dx.doi.org/10.1016/j.eurpolymj.2016.02.023.

DE LUNA, M.S., GALIZIA, M., WOJNAROWICZ, J., ROSA, R., LOJKOWSKI, W., LEONELLI, C., ACIERNO, D. and FILIPPONE, G., 2014. Dispersing hydrophilic nanoparticles in hydrophobic polymers: HDPE/ZnO nanocomposites by a novel template-based approach. *Express Polymer Letters*, 8(5), pp.362–372. Available at: http://dx.doi.org/10.3144/expresspolymlett.2014.40.

DETTA, N., BROWN, T.D., EDIN, F.K., ALBRECHT, K., CHIELLINI, F., CHIELLINI, E., DALTON, P.D. and HUTMACHER, D.W., 2010. Melt electrospinning of polycaprolactone and its blends with poly (ethylene glycol). *Polymer International*, 59(11), pp.1558-1562. Available at: http://dx.doi.org/10.1002/pi.2954.

DICKIE, R.A., 1973. Heterogeneous polymer–polymer composites. I. Theory of viscoelastic properties and equivalent mechanical models. *Journal of Applied Polymer Science*, 17(1), pp.45-63. Available at: http://dx.doi.org/10.1002/app.1973.070170104.

DIDANE, N., GIRAUD, S. and DEVAUX, E., 2012. Fire performances comparison of back coating and melt spinning approaches for PET covering textiles. *Polymer Degradation and Stability*, 97(7), pp.1083-1089. Available at: http://dx.doi.org/10.1016/j.polymdegradstab.2012.04.010.

DO CARMO RUFINO, T. and FELISBERTI, M.I., 2016. Confined PEO crystallisation in immiscible PEO/PLLA blends. *RSC Advances*, 6(37), pp.30937-30950. Available at: http://dx.doi.org/10.1039/c6ra02406h.

DOUROUMIS, D., 2012. *Hot-melt Extrusion: Pharmaceutical Applications*. Chichester: Wiley.

ELIAS, L., FENOUILLOT, F., MAJESTÉ, J.C. and CASSAGNAU, P., 2007. Morphology and rheology of immiscible polymer blends filled with silica nanoparticles.

Polymer, 48(20), pp.6029-6040. Available at: http://dx.doi.org/10.1016/j.polymer.2007.07.061.

ELIAS, L., FENOUILLOT, F., MAJESTÉ, J.C., ALCOUFFE, P. and CASSAGNAU, P., 2008a. Immiscible polymer blends stabilized with nano-silica particles: Rheology and effective interfacial tension. *Polymer*, 49(20), pp.4378-4385. Available at: http://dx.doi.org/10.1016/j.polymer.2008.07.018.

ELIAS, L., FENOUILLOT, F., MAJESTÉ, J.C., MARTIN, G. and CASSAGNAU, P., 2008b. Migration of nanosilica particles in polymer blends. *Journal of Polymer Science Part B: Polymer Physics*, 46(18), pp.1976-1983. Available at: http://dx.doi.org/10.1002/polb.21534.

EVSTATIEV, M. and FAKIROV, S., 1992. Microfibrillar reinforcement of polymer blends. *Polymer*, 33(4), pp.877-880. Available at: http://dx.doi.org/10.1016/0032-3861(92)90354-y.

FAKIROV, S., 2013. Nano-/microfibrillar polymer–polymer and single polymer composites: The converting instead of adding concept. *Composites Science and Technology*, 89, pp.211-225. Available at: http://dx.doi.org/10.1016/j.compscitech.2013.10.007.

FAKIROV, S., 2018. Nanofibrillar polymer–polymer and single polymer composites via the "converting instead of adding" concept – Examples of true polymer nanocomposite. *Advanced Industrial and Engineering Polymer Research*, 1(1), pp.40–47. Available at: http://dx.doi.org/10.1016/j.aiepr.2018.02.001.

FAKIROV, S., BHATTACHARYYA, D. and PANAMOOTTIL, S.M., 2014. Converting of bulk polymers into nanosized materials with controlled nanomorphology.

International Journal of Polymeric Materials and Polymeric Biomaterials, 63(15), pp.777-793. Available at: http://dx.doi.org/10.1080/00914037.2014.886214.

FAKIROV, S., BHATTACHARYYA, D., LIN, R.J.T., FUCHS, C. and FRIEDRICH, K., 2007. Contribution of coalescence to microfibril formation in polymer blends during cold drawing. *Journal of Macromolecular Science*, Part B: Physics, 46(1), pp.183-194. Available at: http://dx.doi.org/10.1080/00222340601044375.

FAVIS, B.D. and CHALIFOUX, J.P., 1988. Influence of composition on the morphology of polypropylene/polycarbonate blends. *Polymer*, 29(10), pp.1761-1767. Available at: http://dx.doi.org/10.1016/0032-3861(88)90388-6.

FAVIS, B.D. and THERRIEN, D., 1991. Factors influencing structure formation and phase size in an immiscible polymer blend of polycarbonate and polypropylene prepared by twin-screw extrusion. *Polymer,* 32(8), pp.1474-1481. Available at: http://dx.doi.org/10.1016/0032-3861(91)90429-m.

FENOUILLOT, F., CASSAGNAU, P. and MAJESTÉ, J.C., 2009. Uneven distribution of nanoparticles in immiscible fluids: Morphology development in polymer blends. *Polymer*, 50(6), pp.1333-1350. Available at: http://dx.doi.org/10.1016/j.polymer.2008.12.029.

FILIPPONE, G., ROMEO, G. and ACIERNO, D., 2011. Role of Interface Rheology in Altering the Onset of Co-Continuity in Nanoparticle-Filled Polymer Blends. *Macromolecular Materials and Engineering*, 296(7), pp.658-665. Available at: http://dx.doi.org/10.1002/mame.201000343.

FORTELNÝ, I. and JŮZA, J., 2018. Analysis of the effect of block copolymers on interfacial tension in immiscible polymer blends. *Polymer*, 150, pp.380-390. Available at: http://dx.doi.org/10.1016/j.polymer.2018.07.041.

GALANTI, A.V. and MANTELL, C.L., 1965. *Polypropylene Fibers and Films*. Available at: http://dx.doi.org/10.1007/978-1-4899-2822-1.

GHANBARI, A., HEUZEY, M.C., CARREAU, P.J. and TON-THAT, M.T., 2013. Morphology and properties of polymer/organoclay nanocomposites based on poly (ethylene terephthalate) and sulfopolyester blends. *Polymer International*, 62(3), pp.439-448. Available at: http://dx.doi.org/10.1002/pi.4331.

GILMAN, J.W., 2007. Flame retardant mechanism of polymer-clay nanocomposites. *Flame Retardant Polymer Nanocomposites*, pp.67-87. Available at: http://dx.doi.org/10.1002/9780470109038.ch3.

GINZBURG, V.V., 2010. Nanoparticle/polymer blends: theory and modeling. *Encyclopedia of Polymer Blends*, pp.233-268.

GOODSHIP, V. and JACOBS, D., 2009. Polyvinyl alcohol: materials, processing and applications. *Rapra Review Reports*. Shrewsbury Rapra Technology.

GOWNDER, M. and NGUYEN, J., 2006. *Syndiotactic Polypropylene Fibers*. U.S. Patent Application 11/317,813.

GRADYS, A., SAJKIEWICZ, P., MINAKOV, A.A., ADAMOVSKY, S., SCHICK, C., HASHIMOTO, T. and SAIJO, K., 2005. Crystallization of polypropylene at various cooling rates. *Materials Science and Engineering: A*, 413, pp.442-446. Available at: http://dx.doi.org/10.1016/j.msea.2005.08.167.

GRAEBLING, D., MULLER, R. and PALIERNE, J.F., 1993. Linear viscoelastic behavior of some incompatible polymer blends in the melt. Interpretation of data with a model of emulsion of viscoelastic liquids. *Macromolecules*, 26(2), pp.320-329. Available at: http://dx.doi.org/10.1021/ma00054a011.

GRAMESPACHER, H. and MEISSNER, J., 1992. Interfacial tension between polymer melts measured by shear oscillations of their blends. *Journal of Rheology*, 36(6), pp.1127-1141. Available at: http://dx.doi.org/10.1122/1.550304.

GUGGENHEIM, E.A., 1945. The Principle of Corresponding States. *The Journal of Chemical Physics*, 13(7), pp.253–261. Available at: http://dx.doi.org/10.1063/1.1724033.

GUO, Y., HE, S., YANG, K., XUE, Y., ZUO, X., YU, Y., LIU, Y., CHANG, C.C. and RAFAILOVICH, M.H., 2016. Enhancing the mechanical properties of biodegradable polymer blends using tubular nanoparticle stitching of the interfaces. *ACS Applied Materials & Interfaces*, 8(27), pp.17565-17573. Available at: http://dx.doi.org/10.1021/acsami.6b05698.

GUO, Z., PEREIRA, T., CHOI, O., WANG, Y. and HAHN, H.T., 2006. Surface functionalized alumina nanoparticle filled polymeric nanocomposites with enhanced mechanical properties. *Journal of Materials Chemistry*, 16(27), pp.2800-2808. Available at: http://dx.doi.org/10.1039/b603020c.

HALAKE, K., BIRAJDAR, M., KIM, B.S., BAE, H., LEE, C., KIM, Y.J., KIM, S., KIM, H.J., AHN, S., AN, S.Y. and LEE, J., 2014. Recent application developments of water-soluble synthetic polymers. *Journal of Industrial and Engineering Chemistry*, 20(6), pp.3913-3918. Available at: http://dx.doi.org/10.1016/j.jiec.2014.01.006.

HALIMA, N.B., 2016. Poly (vinyl alcohol): review of its promising applications and insights into biodegradation. *RSC Advances*, 6(46), pp.39823-39832. Available at: http://dx.doi.org/10.1039/c6ra05742j.

HARRIS, J.M., 2013. *Poly (ethylene glycol) Chemistry: Biotechnical and Biomedical Applications.* Springer Science & Business Media.

HE, H., CHEN, L., ZHANG, Y., HONG, S., ZHOU, Y. and ZHU, M., 2014. Studies on melt spinning of sea-island fibers. I. morphology evolution of polypropylene/polystyrene blend fibers. *Fibers and Polymers*, 15(9), pp.1941-1949. Available at: http://dx.doi.org/10.1007/s12221-014-1941-x.

HIRSEMANN, D., SHYLESH, S., DE SOUZA, R.A., DIAR-BAKERLY, B., BIERSACK, B., MUELLER, D.N., MARTIN, M., SCHOBERT, R. and BREU, J., 2012. Large-Scale, Low-Cost Fabrication of Janus-Type Emulsifiers by Selective Decoration of Natural Kaolinite Platelets. *Angewandte Chemie International Edition*, 51(6), pp.1348-1352. Available at: http://dx.doi.org/10.1002/anie.201106710.

HUANG, S., BAI, L., TRIFKOVIC, M., CHENG, X. and MACOSKO, C.W., 2016. Controlling the morphology of immiscible cocontinuous polymer blends via silica nanoparticles jammed at the interface. *Macromolecules*, 49(10), pp.3911-3918. Available at: http://dx.doi.org/10.1021/acs.macromol.6b00212.

HYUN, K.S., GOGOS, C.G. and KIM, M.H., 2011. Extrusion technology for manufacturing polymer blends. *Encyclopedia of Polymer Blends*, pp.207-262.

IMURA, Y., HOGAN, R.M.C. and JAFFE, M., 2014. Dry spinning of synthetic polymer fibers. *Advances in Filament Yarn Spinning of Textiles and Polymers*, pp. 187-202. Woodhead Publishing.

JANG, J. and LEE, D.K., 2003. Plasticizer effect on the melting and crystallization behavior of polyvinyl alcohol. *Polymer*, 44(26), pp.8139-8146. Available at: http://dx.doi.org/10.1016/j.polymer.2003.10.015.

JANG, J. and LEE, D.K., 2004. Oxygen barrier properties of biaxially oriented polypropylene/polyvinyl alcohol blend films. *Polymer*, 45(5), pp.1599-1607. Available at: http://dx.doi.org/10.1016/s0032-3861(03)01207-2.

JIANG, W.R., BAO, R.Y., YANG, W., LIU, Z.Y., XIE, B.H. and YANG, M.B., 2014. Morphology, interfacial and mechanical properties of polylactide/poly (ethylene terephthalate glycol) blends compatibilized by polylactide-g-maleic anhydride. *Materials & Design*, 59, pp.524-531. Available at: http://dx.doi.org/10.1016/j.matdes.2014.03.016.

KARGER-KOCSIS, J. and BÁRÁNY, T., 2019. *Polypropylene Handbook: Morphology, Blends and Composites.* Springer.

KIM, D., JUNG, J., PARK, S.I. and SEO, J., 2015. Preparation and characterization of LDPE/PVA blend films filled with glycerin-plasticized polyvinyl alcohol. *Journal of Applied Polymer Science*, 132(22). Available at: http://dx.doi.org/10.1002/app.41985.

KIM, J.H., LEE, H., JATOI, A.W., IM, S.S., LEE, J.S. and KIM, I.S., 2016. Juniperus chinensis extracts loaded PVA nanofiber: Enhanced antibacterial activity. *Materials Letters*, 181, pp.367-370. Available at: http://dx.doi.org/10.1016/j.matlet.2016.05.164.

KO, J., KAN, D. and JUN, M.B., 2015. Combining melt electrospinning and particulate leaching for fabrication of porous microfibers. *Manufacturing Letters*, 3, pp.5-8. Available at: http://dx.doi.org/10.1016/j.mfglet.2014.11.001.

KODAL, M., 2016. Polypropylene/polyamide 6/POSS ternary nanocomposites: Effects of POSS nanoparticles on the compatibility. *Polymer*, 105, pp.43-50. Available at: http://dx.doi.org/10.1016/j.polymer.2016.10.021.

KONG, M., HUANG, Y., CHEN, G., YANG, Q. and LI, G., 2011. Retarded relaxation and breakup of deformed PA6 droplets filled with nanosilica in PS matrix during annealing. *Polymer*, 52(22), pp.5231-5236. Available at: http://dx.doi.org/10.1016/j.polymer.2011.08.052.

KRASSIG, H.A., 1984. *Fiber Technology: from Film to Fiber*. CRC Press.

KU, T.H. and LIN, C.A., 2005. Rheological properties of thermoplastic polyvinyl alcohol and polypropylene blend melts in capillary extrusions. *Journal of Polymer Research*, 12(1), pp.23-29. Available at: http://dx.doi.org/10.1007/s10965-004-0985-9.

KU, T.H. and LIN, C.A., 2014. Elongational flow properties of thermoplastic polyvinyl alcohol/polypropylene from the melt spinning method. *Textile Research Journal*, 84(9), pp.932-940. Available at: http://dx.doi.org/10.1177/0040517513499433.

KWON, T., KIM, T., ALI, F.B., KANG, D.J., YOO, M., BANG, J., LEE, W. and KIM, B.J., 2011. Size-controlled polymer-coated nanoparticles as efficient compatibilizers for polymer blends. *Macromolecules*, 44(24), pp.9852-9862. Available at: http://dx.doi.org/10.1021/ma2020134.

LEE, M.W., HU, X., LI, L., YUE, C.Y. and TAM, K.C., 2003. Flow behaviour and microstructure evolution in novel SiO_2/PP/LCP ternary composites: effects of filler properties and mixing sequence. *Polymer international*, 52(2), pp.276-284. Available at: http://dx.doi.org/10.1002/pi.1098.

LEE, S.H., KONTOPOULOU, M. and PARK, C.B., 2010. Effect of nanosilica on the co-continuous morphology of polypropylene/polyolefin elastomer blends. *Polymer*, 51(5), pp.1147-1155. Available at: http://dx.doi.org/10.1016/j.polymer.2010.01.018.

LEWIN, M., MEY-MAROM, A. and FRANK, R., 2005. Surface free energies of polymeric materials, additives and minerals. *Polymers for Advanced Technologies*, 16(6), pp.429-441. Available at: http://dx.doi.org/10.1002/pat.605.

LI, L., HUANG, W., WANG, B., WEI, W., GU, Q. and CHEN, P., 2015. Properties and structure of polylactide/poly (3-hydroxybutyrate-co-3-hydroxyvalerate) (PLA/PHBV) blend fibers. *Polymer*, 68, pp.183-194. Available at: http://dx.doi.org/10.1016/j.polymer.2015.05.024.

LI, M., ZHANG, W., WANG, C. and WANG, H., 2011a, January. Fabrication of Conductive Porous Structure Loaded with Carbon black and/or Carbon Nanotube. *ASME 2011 International Mechanical Engineering Congress and Exposition* (pp. 317-322). American Society of Mechanical Engineers. Available at: http://dx.doi.org/10.1115/imece2011-65122.

LI, P., HUANG, Y., KONG, M., LV, Y., LUO, Y., YANG, Q. and LI, G., 2013. Fractionated crystallization and morphology of PP/PS blends in the presence of silica nanoparticles with different surface chemistries. *Colloid and Polymer Science*, 291(7), pp.1693-1704. Available at: http://dx.doi.org/10.1007/s00396-013-2904-2.

LI, W., KARGER-KOCSIS, J. and THOMANN, R., 2009. Compatibilization effect of TiO2 nanoparticles on the phase structure of PET/PP/TiO2 nanocomposites. *Journal of Polymer Science Part B: Polymer Physics*, 47(16), pp.1616-1624. Available at: http://dx.doi.org/10.1002/polb.21752.

LI, Y., ZHU, J., WEI, S., RYU, J., WANG, Q., SUN, L. and GUO, Z., 2011b. Poly (propylene) nanocomposites containing various carbon nanostructures. *Macromolecular Chemistry and Physics*, 212(22), pp.2429-2438. Available at: http://dx.doi.org/10.1002/macp.201100364.

LIAN, H. and MENG, Z., 2017. Melt electrospinning vs. solution electrospinning: a comparative study of drug-loaded poly (ε-caprolactone) fibres. *Materials Science and Engineering: C*, 74, pp.117-123. Available at: http://dx.doi.org/10.1016/j.msec.2017.02.024.

LIPATOV, Y.S., 1995. *Polymer reinforcement*. Toronto, Canada: ChemTec Publishing.

LIU, Y. and KONTOPOULOU, M., 2006. The structure and physical properties of polypropylene and thermoplastic olefin nanocomposites containing nanosilica. *Polymer*, 47(22), pp.7731-7739. Available at: http://dx.doi.org/10.1016/j.polymer.2006.09.014.

LUCIANI, A., CHAMPAGNE, M.F. and UTRACKI, L.A., 1997. Interfacial tension coefficient from the retraction of ellipsoidal drops. *Journal of Polymer Science Part B: Polymer Physics*, 35(9), pp.1393-1403. Available at: http://dx.doi.org/10.1002/(SICI)1099-0488(19970715)35:9<1393::AID-POLB9>3.0.CO;2-N.

LVOV, Y., WANG, W., ZHANG, L. and FAKHRULLIN, R., 2016. Halloysite clay nanotubes for loading and sustained release of functional compounds. *Advanced Materials*, 28(6), pp.1227-1250. Available at: http://dx.doi.org/10.1002/adma.201502341.

MACOSKO, C.W., 2000, January. Morphology development and control in immiscible polymer blends. *Macromolecular Symposia*, Vol. 149, No. 1, pp. 171-184. Weinheim: WILEY-VCH Verlag. Available at: https://doi.org/10.1002/1521-3900(200001)149:1<171::aid-masy171>3.0.co;2-8.

MADDAH, H.A., 2016. Polypropylene as a promising plastic: A review. American *Journal of Polymer Science*, 6(1), pp.1-11. Available at: http:// dx.doi.org/10.5923/j.ajps.20160601.01.

MEDERIC, P., FNEICH, F., VILLE, J. and AUBRY, T., 2018. Migration of clay and its role in droplet morphology establishment during melt mixing of clay polyethylene/polyamide nanocomposites. *Applied Clay Science*, 165, pp.257-263. Available at: http://dx.doi.org/10.1016/j.clay.2018.08.024.

MEKHILEF, N. and VERHOOGT, H., 1996. Phase inversion and dual-phase continuity in polymer blends: theoretical predictions and experimental results. *Polymer*, 37(18), pp.4069–4077. Available at: http://dx.doi.org/10.1016/0032-3861(96)00254-6.

METELKIN, V.I. and BLEKHT, V.S., 1984. Formation of a continuous phase in heterogeneous polymer mixtures. *Colloid Journal of the USSR*, 46(3), pp.425-429.

MILES, I.S. and ZUREK, A., 1988. Preparation, structure, and properties of two-phase co-continuous polymer blends. *Polymer Engineering and Science*, 28(12), pp.796–805. Available at: http://dx.doi.org/10.1002/pen.760281205.

MIN, K., WHITE, J.L. and FELLERS, J.F., 1984. High density polyethylene/polystyrene blends: Phase distribution morphology, rheological measurements, extrusion, and melt spinning behavior. *Journal of Applied Polymer Science*, 29(6), pp.2117-2142. Available at: http://dx.doi.org/10.1002/app.1984.070290619.

MANIRUZZAMAN, M., 2015. Practical guide to hot-melt extrusion: continuous manufacturing and scale-up. *Smithers Rapra Technology*.

MOLY, K.A., BHAGAWAN, S.S., GROENINCKX, G. and THOMAS, S., 2006. Correlation between the morphology and dynamic mechanical properties of ethylene vinyl acetate/linear low-density polyethylene blends: Effects of the blend ratio and compatibilization. *Journal of Applied Polymer Science*, 100(6), pp.4526-4538. Available at: http://dx.doi.org/10.1002/app.22466.

MURAL, P.K.S., BANERJEE, A., RANA, M.S., SHUKLA, A., PADMANABHAN, B., BHADRA, S., MADRAS, G. and BOSE, S., 2014. Polyolefin based antibacterial membranes derived from PE/PEO blends compatibilized with amine terminated graphene oxide and maleated PE. *Journal of Materials Chemistry A*, 2(41), pp.17635-17648. Available at: http://dx.doi.org/10.1039/c4ta03997a.

MURAL, P.K.S., MADRAS, G. and BOSE, S., 2018. Polymeric membranes derived from immiscible blends with hierarchical porous structures, tailored bio-interfaces and enhanced flux: Potential and key challenges. *Nano-structures & Nano-objects*, 14, pp.149-165. Available at: http://dx.doi.org/10.1016/j.nanoso.2018.02.002.

MURAL, P.K.S., SHARMA, M., SHUKLA, A., BHADRA, S., PADMANABHAN, B., MADRAS, G. and BOSE, S., 2015. Porous membranes designed from bi-phasic polymeric blends containing silver decorated reduced graphene oxide synthesized via

a facile one-pot approach. *RSC Advances*, 5(41), pp.32441-32451. Available at: http://dx.doi.org/10.1039/c5ra01656h.

MURAOKA, Y., FUJIWARA, T., SANO, Y., YASUDA, T. and KANBARA, H., 2001. Properties of polymer alloy fibers of polypropylene and cationic dyeable poly (ethylene terephthalate) prepared with an in-situ generated compatibilizer. *Textile Research Journal*, 71(12), pp.1053-1056. Available at: http://dx.doi.org/10.1177/004051750107101203.

NIE, H., LIANG, X. and HE, A., 2018. Enthalpy-Enhanced Janus Nanosheets for Trapping Nonequilibrium Morphology of Immiscible Polymer Blends. *Macromolecules*, 51(7), pp.2615-2620. Available at: http://dx.doi.org/10.1021/acs.macromol.8b00039.

OMNEXUS.SPECIALCHEM.COM., 2019. Maintenace - SpecialChem. Available at: https://omnexus.specialchem.com/_/media/selection-guides/omnexus/polymer-profiles/polypropylene/polypropylene-molecular-stucture.jpg?h=142&w=421&la=en [Accessed 10 Oct. 2019].

OMONOV, T.S., HARRATS, C., MOLDENAERS, P. and GROENINCKX, G., 2007. Phase continuity detection and phase inversion phenomena in immiscible polypropylene/polystyrene blends with different viscosity ratios. *Polymer*, 48(20), pp.5917-5927. Available at: http://dx.doi.org/10.1016/j.polymer.2007.08.012.

OWENS, D.K. and WENDT, R.C., 1969. Estimation of the surface free energy of polymers. *Journal of Applied Polymer Science*, 13(8), pp.1741-1747. Available at: http://dx.doi.org/10.1002/app.1969.070130815.

PALIERNE, J.F., 1990. Linear rheology of viscoelastic emulsions with interfacial tension. *Rheologica Acta*, 29(3), pp.204-214. Available at: http://dx.doi.org/10.1007/bf01331356.

PALZA, H., 2015. Antimicrobial polymers with metal nanoparticles. *International Journal of Molecular Sciences,* 16(1), pp.2099-2116. Available at: http://dx.doi.org/10.3390/ijms16012099.

PARPAITE, T., OTAZAGHINE, B., CARO, A.S., TAGUET, A., SONNIER, R. and LOPEZ-CUESTA, J.M., 2016. Janus hybrid silica/polymer nanoparticles as effective compatibilizing agents for polystyrene/polyamide-6 melted blends. *Polymer*, 90, pp.34-44. Available at: http://dx.doi.org/10.1016/j.polymer.2016.02.044.

PATACHIA, S., VALENTE, A.J.M, PAPANCEAA A., Lobo, V.M.M, 2009. *Poly (Vinyl Alcohol) PVA-Based Polymer Membranes.* Nova Science Publishers, Inc. New York.

PENG, X.F., MI, H.Y., JING, X., YU, P., QU, J.P. and CHEN, B.Y., 2016. Preparation of highly porous interconnected poly (lactic acid) scaffolds based on a novel dynamic elongational flow procedure. *Materials & Design*, 101, pp.285-293. Available at: http://dx.doi.org/10.1016/j.matdes.2016.03.156.

PLATTIER, J., BENYAHIA, L., DORGET, M., NIEPCERON, F. and TASSIN, J.F., 2015. Viscosity-induced filler localisation in immiscible polymer blends. *Polymer*, 59, pp.260-269. Available at: http://dx.doi.org/10.1016/j.polymer.2014.12.044.

PÖTSCHKE, P. and PAUL, D.R., 2003. Formation of Co-continuous Structures in Melt-Mixed Immiscible Polymer Blends. *Journal of Macromolecular Science, Part C: Polymer Reviews*, 43(1), pp.87–141. Available at: http://dx.doi.org/10.1081/mc-120018022.

PRITCHARD, M.; SARSBY, R. W. and ANAND, S. C. *Handbook of Technical Textiles*; 2000; ISBN 9781855733855.

PUBCHEM.NCBI.NLM.NIH.GOV., 2019. Available at: https://pubchem.ncbi.nlm.nih.gov/image/imgsrv.fcgi?cid=101244783&t=l [Accessed 7 Oct. 2019].

QIN, Y., 2010. *Micromanufacturing Engineering and Technology.* William Andrew.

QIU, L., XIE, R., DING, P. and QU, B., 2003. Preparation and characterization of Mg (OH) 2 nanoparticles and flame-retardant property of its nanocomposites with EVA. *Composite Structures*, 62(3-4), pp.391-395. Available at: http://dx.doi.org/10.1016/j.compstruct.2003.09.010.

RAWAL, A. and MUKHOPADHYAY, S., 2014. Melt spinning of synthetic polymeric filaments. *Advances in Filament Yarn Spinning of Textiles and Polymers*, pp. 75-99. Woodhead Publishing.

RAY, S.S., POULIOT, S., BOUSMINA, M. and UTRACKI, L.A., 2004. Role of organically modified layered silicate as an active interfacial modifier in immiscible polystyrene/polypropylene blends. *Polymer*, 45(25), pp.8403-8413. Available at: http://dx.doi.org/10.1016/j.polymer.2004.10.009.

REDDY, N., NAMA, D. and YANG, Y., 2008. Polylactic acid/polypropylene polyblend fibers for better resistance to degradation. *Polymer Degradation and Stability*, 93(1), pp.233-241. Available at: http://dx.doi.org/10.1016/j.polymdegradstab.2007.09.005.

RIZVI, H.R. and D'SOUZA, N., 2016. Design of a Multifunctional Porous Coaxial Electrospun Mesh Using Polycaprolactone (PCL) and Poly Butylene Adipate-CO-Terephthalate (PBAT). *Volume 3: Biomedical and Biotechnology Engineering*. Available at: http://dx.doi.org/10.1115/imece2016-67534.

ROBESON, L.M., AXELROD, R.J., VRATSANOS, M.S. and KITTEK, M.R., 1994. Microfiber formation: immiscible polymer blends involving thermoplastic poly (vinyl alcohol) as an extractable matrix. *Journal of Applied Polymer Science*, 52(13), pp.1837-1846. Available at: http://dx.doi.org/10.1002/app.1994.070521301.

ROMAN, C., GARCÍA-MORALES, M., GUPTA, J. and MCNALLY, T., 2017. On the phase affinity of multi-walled carbon nanotubes in PMMA: LDPE immiscible polymer blends. *Polymer*, 118, pp.1-11. Available at: http://dx.doi.org/10.1016/j.polymer.2017.04.050.

ROY, S. and BYSAKH, S., 2011. Ultrafine PZT based ceramics synthesized by auto-ignition of metal–polymer gel: enhanced sinterablity and higher remnant polarization. *Materials Chemistry and Physics*, 126(3), pp.948-954. Available at: http://dx.doi.org/10.1016/j.matchemphys.2010.11.059.

SAHNOUNE, M., TAGUET, A., OTAZAGHINE, B., KACI, M. and LOPEZ-CUESTA, J.M., 2017. Inner surface modification of halloysite nanotubes and its influence on morphology and thermal properties of polystyrene/polyamide-11 blends. *Polymer International*, 66(2), pp.300-312. Available at: http://dx.doi.org/10.1002/pi.5266.

SALAÜN, F., BEDEK, G., DEVAUX, E., DUPONT, D. and DERANTON, D., 2009. Investigation of water absorption and diffusion in microparticles containing xylitol to provide a cooling effect by thermal analysis. *International Journal of Thermophysics*, 30(4), pp.1242-1256. Available at: http://dx.doi.org/10.1007/s10765-009-0649-4.

SALTIKOV, S.A., 1967. The determination of the size distribution of particles in an opaque material from a measurement of the size distribution of their sections. *Stereology*, pp. 163-173. Springer, Berlin, Heidelberg. Available at: http://dx.doi.org/10.1007/978-3-642-88260-9_31.

SANTANA, O.O. and MÜLLER, A.J., 1994. Homogeneous nucleation of the dispersed crystallisable component of immiscible polymer blends. *Polymer Bulletin*, 32(4), pp.471-477. Available at: http://dx.doi.org/10.1007/bf00587890.

SARAZIN, P., ROY, X. and FAVIS, B.D., 2004. Controlled preparation and properties of porous poly (L-lactide) obtained from a co-continuous blend of two biodegradable polymers. *Biomaterials*, 25(28), pp.5965-5978. Available at: http://dx.doi.org/10.1016/j.biomaterials.2004.01.065.

SATO, H., ONO, K., JOHNSTON, C.T. and YAMAGISHI, A., 2004. First-principle study of polytype structures of 1: 1 dioctahedral phyllosilicates. *American Mineralogist*, 89(11-12), pp.1581-1585. Available at: http://dx.doi.org/10.2138/am-2004-11-1201.

SCHAEFER, D.W. and JUSTICE, R.S., 2007. How nano are nanocomposites?. *Macromolecules*, 40(24), pp.8501-8517. Available at: http://dx.doi.org/10.1021/ma070356w.

SCHMIDT, D., SHAH, D. and GIANNELIS, E.P., 2002. New advances in polymer/layered silicate nanocomposites. *Current Opinion in Solid State and Materials Science*, 6(3), pp.205-212. Available at: http://dx.doi.org/10.1016/s1359-0286(02)00049-9.

SEGAWA, H. *et al.*, *Showa 49-26519*, March 9, 1974. Kuraray Co.

SHETH, M., KUMAR, R.A., DAVÉ, V., GROSS, R.A. and MCCARTHY, S.P., 1997. Biodegradable polymer blends of poly (lactic acid) and poly (ethylene glycol). *Journal of Applied Polymer Science*, 66(8), pp.1495-1505. Available at: https://dx.doi.org/10.1002/(SICI)1097-4628(19971121)66:8<1495::AID-APP10>3.0.CO;2-3.

SI, M., ARAKI, T., ADE, H., KILCOYNE, A.L.D., FISHER, R., SOKOLOV, J.C. and RAFAILOVICH, M.H., 2006. Compatibilizing bulk polymer blends by using organoclays. *Macromolecules*, 39(14), pp.4793-4801. Available at: http://dx.doi.org/10.1021/ma060125

SOLTANI, I. and MACOSKO, C.W., 2018. Influence of rheology and surface properties on morphology of nanofibers derived from islands-in-the-sea meltblown nonwovens. *Polymer*, 145, pp.21-30. Available at: http://dx.doi.org/10.1016/j.polymer.2018.04.051.

SON, W.K., YOUK, J.H. and PARK, W.H., 2006. Antimicrobial cellulose acetate nanofibers containing silver nanoparticles. *Carbohydrate Polymers*, 65(4), pp.430-434. Available at: http://dx.doi.org/10.1016/j.carbpol.2006.01.037.

SOYASLAN, D., ÇÖMLEKÇI, S. and GÖKTEPE, Ö., 2010. Determination of electromagnetic shielding performance of plain knitting and 1X1 rib structures with coaxial test fixture relating to ASTM D4935. *The Journal of the Textile Institute*, 101(10), pp.890-897. Available at: http://dx.doi.org/10.1080/00405000902945360.

STEINMANN, S., GRONSKI, W. and FRIEDRICH, C., 2002a. Influence of selective filling on rheological properties and phase inversion of two-phase polymer blends. *Polymer*, 43(16), pp.4467-4477. Available at: http://dx.doi.org/10.1016/s0032-3861(02)00271-9.

STEINMANN, S., GRONSKI, W. and FRIEDRICH, C., 2002b. Quantitative rheological evaluation of phase inversion in two-phase polymer blends with cocontinuous morphology. *Rheologica Acta*, 41(1-2), pp.77-86. Available at: http://dx.doi.org/10.1007/s003970200007.

STRECKA, Z., UJHELYIOVA, A., BOLHOVA, E., ALEXY, P. and BORSIG, E., 2010. Polypropylene fibers modified by polyvinyl alcohol and montmorillonite. *The Journal of the Textile Institute*, 101(4), pp.315-323. Available at: http://dx.doi.org/10.1080/00405000802399551.

SUMANASINGHE, R.D., HASLAUER, C.M., POURDEYHIMI, B. and LOBOA, E.G., 2010. Melt spun microporous fibers using poly (lactic acid) and sulfonated copolyester blends for tissue engineering applications. *Journal of Applied Polymer Science*, 117(6), pp.3350-3361. Available at: http://dx.doi.org/10.1002/app.32025.

SUN, Z., FAN, C., TANG, X., ZHAO, J., SONG, Y., SHAO, Z. and XU, L., 2016. Characterization and antibacterial properties of porous fibers containing silver ions. *Applied Surface Science*, 387, pp.828-838. Available at: http://dx.doi.org/10.1016/j.apsusc.2016.07.015.

TANG, T. and HUANG, B., 1994. Compatibilization of polypropylene/poly (ethylene oxide) blends and crystallization behavior of the blends. *Journal of Polymer Science Part B: Polymer Physics*, 32(12), pp.1991-1998. Available at: http://dx.doi.org/10.1002/polb.1994.090321205.

THOMAS, S., GROHENS, Y. and JYOTISHKUMAR, P., 2014. *Characterization of Polymer Blends: Miscibility, Morphology and Interfaces*. John Wiley & Sons.

TOMOTIKA, S., 1935. On the instability of a cylindrical thread of a viscous liquid surrounded by another viscous fluid. Proceedings of the Royal Society of London. *Series A-Mathematical and Physical Sciences*, 150(870), pp.322-337. Available at: http://dx.doi.org/10.1098/rspa.1935.0104.

TONG, J., HUANG, H.X. and WU, M., 2017. Promoting compatibilization effect of graphene oxide on immiscible PS/PVDF blend via water-assisted mixing extrusion. *Composites Science and Technology*, 149, pp.286-293. Available at: http://dx.doi.org/10.1016/j.compscitech.2017.07.005.

TORRE, J., CORTAZAR, M., GOMEZ, M., ELLIS, G. and MARCO, C., 2004. Melting behavior in blends of isotactic polypropylene and a liquid crystalline polymer. *Journal of Polymer Science Part B: Polymer Physics*, 42(10), pp.1949-1959. Available at: http://dx.doi.org/10.1002/polb.20062.

TRAN, N.H.A., BRÜNIG, H. and HEINRICH, G., 2016a. Controlling micro-and nanofibrillar morphology of polymer blends in low-speed melt spinning process. Part I. Profiles of PLA/PVA-filament parameters along the spinline. *Journal of Applied Polymer Science*, 133(47). Available at: http://dx.doi.org/10.1002/app.44258.

TRAN, N.H.A., BRÜNIG, H., AUF DER LANDWEHR, M. and HEINRICH, G., 2016b. Controlling micro-and nanofibrillar morphology of polymer blends in low-speed melt spinning process. Part III: Fibrillation mechanism of PLA/PVA blends along the spinline. *Journal of Applied Polymer Science*, 133(48). Available at: http://dx.doi.org/10.1002/app.44259.

TRAN, N.H.A., BRÜNIG, H., AUF DER LANDWEHR, M., VOGEL, R., PIONTECK, J. and HEINRICH, G., 2016c. Controlling micro-and nanofibrillar morphology of polymer blends in low-speed melt spinning process. Part II: Influences of extrusion rate

on morphological changes of a PLA/PVA blend through a capillary die. *Journal of Applied Polymer Science*, 133(47). Available at: http://dx.doi.org/10.1002/app.44257.

TRAN, N.H.A., BRÜNIG, H., BOLDT, R. and HEINRICH, G., 2014a. Morphology development from rod-like to nanofibrillar structures of dispersed poly (lactic acid) phase in a binary blend with poly (vinyl alcohol) matrix along the spinline. *Polymer*, 55(24), pp.6354-6363. Available at: http://dx.doi.org/10.1016/j.polymer.2014.10.002.

TRAN, N.H.A, BRÜNIG, H., HINÜBER, C. and HEINRICH, G., 2014b. Melt spinning of biodegradable nanofibrillary structures from poly (lactic acid) and poly (vinyl alcohol) blends. *Macromolecular Materials and Engineering*, 299(2), pp.219-227. Available at: http://dx.doi.org/10.1002/mame.201300125.

TSEBRENKO, M.V., REZANOVA, N.M. and VINOGRADOV, G.V., 1980. Rheology of molten blends of polyoxymethylene and ethylene-vinyl acetate copolymer and the microstructure of extrudates as a function of their melt viscosities. *Polymer Engineering and Science*, 20(15), pp.1023–1028. Available at: http://dx.doi.org/10.1002/pen.760201507.

UGBOLUE, S.C., 2017. *Polyolefin Fibres: Structure, Properties and Industrial Applications*. Woodhead Publishing.

UPLOAD.WIKIMEDIA.ORG., 2019. Available at: https://upload.wikimedia.org/wikipedia/commons/thumb/9/99/Dichlorodimethylsilane.svg/1280px-Dichlorodimethylsilane.svg.png [Accessed 7 Oct. 2019].

WALTHER, A., MATUSSEK, K. and MULLER, A.H., 2008. Engineering nanostructured polymer blends with controlled nanoparticle location using Janus particles. *ACS Nano*, 2(6), pp.1167-1178. Available at: http://dx.doi.org/10.1021/nn800108y.

WALTHER, A. and MULLER, A.H., 2013. Janus particles: synthesis, self-assembly, physical properties, and applications. *Chemical Reviews*, 113(7), pp.5194-5261. Available at: http://dx.doi.org/10.1021/cr300089t.

WANG, B., WANG, Q. and LI, L., 2013. Morphology and properties of highly talc-and CaCO3-filled poly (vinyl alcohol) composites prepared by melt processing. *Journal of Applied Polymer Science*, 130(5), pp.3050-3057. Available at: http://dx.doi.org/10.1002/app.39557.

WANG, D. and SUN, G., 2007. Formation and morphology of cellulose acetate butyrate (CAB)/polyolefin and CAB/polyester in situ microfibrillar and lamellar hybrid blends. *European Polymer Journal*, 43(8), pp.3587-3596. Available at: http://dx.doi.org/10.1016/j.eurpolymj.2007.05.018.

WANG, F., LIU, L., XUE, P. and JIA, M., 2017a. Crystal structure evolution of UHMWPE/HDPE blend fibers prepared by melt spinning. *Polymers*, 9(3), p.96. Available at: http://dx.doi.org/10.3390/polym9030096.

WANG, H., DONG, W. and LI, Y., 2015. Compatibilization of immiscible polymer blends using in situ formed janus nanomicelles by reactive blending. *ACS Macro Letters*, 4(12), pp.1398-1403. Available at: http://dx.doi.org/10.1021/acsmacrolett.5b00763.

WANG, H., FU, Z., ZHAO, X., LI, Y. and LI, J., 2017b. Reactive nanoparticles compatibilized immiscible polymer blends: synthesis of reactive SiO_2 with long poly (methyl methacrylate) chains and the in situ formation of janus SiO_2 nanoparticles anchored exclusively at the interface. *ACS Applied Materials & Interfaces*, 9(16), pp.14358-14370. Available at: http://dx.doi.org/10.1021/acsami.7b01728.

WANG, Y., ZHAO, W., WANG, X. and WU, D., 2016a. Preparation, mechanical properties and microstructure of polyoxymethylene fiber through melt spinning and hot drawing by using injection-molding grade resins. *Fibers and Polymers*, 17(9), pp.1464-1474. Available at: http://dx.doi.org/10.1007/s12221-016-6586-5.

WANG, Z., LIU, X., MACOSKO, C.W. and BATES, F.S., 2016b. Nanofibers from water-extractable melt-blown immiscible polymer blends. *Polymer*, 101, pp.269-273. Available at: http://dx.doi.org/10.1016/j.polymer.2016.08.058.

WEISS, S., HIRSEMANN, D., BIERSACK, B., ZIADEH, M., MÜLLER, A.H. and BREU, J., 2013. Hybrid Janus particles based on polymer-modified kaolinite. *Polymer*, 54(4), pp.1388-1396. Available at: http://dx.doi.org/10.1016/j.polymer.2012.12.041.

WHITE, J.L. and Bumm, S.H., 2011. Polymer blend compounding and processing. *Encyclopedia of Polymer Blends*, 2, pp.1-26.

WHITE, J.L. and MIN, K., 1985. Processing and Phase Morphology of Incompatible Polymer Blends. *Polymer Blends and Mixtures*, pp.413–428. Available at: http://dx.doi.org/10.1007/978-94-009-5101-3_22.

WILLEMSE, R.C., DE BOER, A.P., VAN DAM, J. and GOTSIS, A.D., 1999. Co-continuous morphologies in polymer blends: the influence of the interfacial tension. *Polymer*, 40(4), pp.827-834. Available at: http://dx.doi.org/10.1016/s0032-3861(98)00307-3.

WINTER, H.H. and CHAMBON, F., 1986. Analysis of linear viscoelasticity of a crosslinking polymer at the gel point. *Journal of Rheology*, 30(2), pp.367-382. Available at: http://dx.doi.org/10.1122/1.549853.

WU, D., YUAN, L., LAREDO, E., ZHANG, M. and ZHOU, W., 2012. Interfacial properties, viscoelasticity, and thermal behaviors of poly (butylene succinate)/polylactide blend. *Industrial & Engineering Chemistry Research*, 51(5), pp.2290-2298. Available at: http://dx.doi.org/10.1021/ie2022288.

WU, G., XU, H. and ZHOU, T., 2010. Morphology evolution, crystalline orientation, and thermal expansion of PA6/SEBS blends with nanolayer networks. *Polymer*, 51(15), pp.3560-3567. Available at: http://dx.doi.org/10.1016/j.polymer.2010.05.058.

WU, T., YUAN, D., QIU, F., CHEN, R.Y., ZHANG, G.Z. and QU, J.P., 2017. Polypropylene/polystyrene/clay blends prepared by an innovative eccentric rotor extruder based on continuous elongational flow: Analysis of morphology, rheology property, and crystallization behavior. *Polymer Testing*, 63, pp.73-83. Available at: http://dx.doi.org/10.1016/j.polymertesting.2017.07.012.

XU, T., MISZUK, J.M., ZHAO, Y., SUN, H. and FONG, H., 2015. Bone Tissue Engineering: Electrospun Polycaprolactone 3D Nanofibrous Scaffold with Interconnected and Hierarchically Structured Pores for Bone Tissue Engineering (Adv. Healthcare Mater. 15/2015). *Advanced Healthcare Materials*, 4(15), pp.2237. Available at: http://dx.doi.org/10.1002/adhm.201570089.

XU, W., CHEN, J., CHEN, S., CHEN, Q., LIN, J. and LIU, H., 2017. Study on the Compatibilizing Effect of Janus Particles on Liquid Isoprene Rubber/Epoxy Resin Composite Materials. *Industrial & Engineering Chemistry Research*, 56(47), pp.14060-14068. Available at: http://dx.doi.org/10.1021/acs.iecr.7b03200.

YAN, N., MAHAM, Y., MASLIYAH, J.H., GRAY, M.R. and MATHER, A.E., 2000. Measurement of contact angles for fumed silica nanospheres using enthalpy of

immersion data. *Journal of Colloid and Interface Science*, 228(1), pp.1-6. Available at: http://dx.doi.org/10.1006/jcis.2000.6856.

YAN, X., CAYLA, A., DEVAUX, E., OTAZAGHINE, B. and SALAÜN, F., 2019. Polypropylene/poly (vinyl alcohol) blends compatibilized with kaolinite Janus hybrid particles and their transformation into fibers. *Industrial & Engineering Chemistry Research*, 58(25), pp.10931-10940. Available at: http://dx.doi.org/10.1021/acs.iecr.9b01990.

YANG, H., ZHANG, Q., GUO, M., WANG, C., DU, R. and FU, Q., 2006. Study on the phase structures and toughening mechanism in PP/EPDM/SiO2 ternary composites. *Polymer*, 47(6), pp.2106-2115. Available at: http://dx.doi.org/10.1016/j.polymer.2006.01.076.

YANG, H., ZHANG, X., QU, C., LI, B., ZHANG, L., ZHANG, Q. and FU, Q., 2007. Largely improved toughness of PP/EPDM blends by adding nano-SiO2 particles. *Polymer*, 48(3), pp.860-869. Available at: http://dx.doi.org/10.1016/j.polymer.2006.12.022.

YANG, Q. and LOOS, K., 2017. Janus nanoparticles inside polymeric materials: interfacial arrangement toward functional hybrid materials. *Polymer Chemistry*, 8(4), pp.641-654. Available at: http://dx.doi.org/10.1039/c6py01795a.

YAO, D., SMITH, A., NAGARAJAN, P., VASQUEZ, A., DANG, L. and CHAUDHRY, G.R., 2006. Fabrication of polycaprolactone scaffolds using a sacrificial compression-molding process. *Journal of Biomedical Materials Research Part B: Applied Biomaterials*, 77(2), pp.287-295. Available at: http://dx.doi.org/10.1002/jbm.b.30419.

YU, F., PRASHANTHA, K., SOULESTIN, J., LACRAMPE, M.F. and KRAWCZAK, P., 2013. Plasticized-starch/poly (ethylene oxide) blends prepared by extrusion. *Carbohydrate Polymers*, 91(1), pp.253-261. Available at: http://dx.doi.org/10.1016/j.carbpol.2012.08.008.

YU, W., BOUSMINA, M., GRMELA, M. and ZHOU, C., 2002. Modeling of oscillatory shear flow of emulsions under small and large deformation fields. *Journal of Rheology*, 46(6), pp.1401-1418. Available at: http://dx.doi.org/10.1122/1.1517303.

ZHANG, K., JIANG, L. and WU, G., 2016. Co-continuity and thermal expansion of injection-molded EPDM/PP blends with heterogeneous dispersion of nanoparticles. *Composites Science and Technology*, 125, pp.123-131. Available at: http://dx.doi.org/10.1016/j.compscitech.2016.01.024.

ZHANG, M., HUANG, Y., KONG, M., ZHU, H., CHEN, G. and YANG, Q., 2012. Morphology and rheology of poly (l-lactide)/polystyrene blends filled with silica nanoparticles. *Journal of Materials Science*, 47(3), pp.1339-1347. Available at: http://dx.doi.org/10.1007/s10853-011-5908-7.

ZHANG, W., WYATT, T., YAO, D., ZHANG, Q. and ZHOU, J.G., 2010a, January. Processing of Nanodiamond Loaded Poly (Lactic Acid) Co-Continuous Porous Structures. *ASME 2010 International Manufacturing Science and Engineering Conference*, pp. 1-6. American Society of Mechanical Engineers. Available at: http://dx.doi.org/10.1115/msec2010-34181.

ZHANG, W., YAO, D., ZHANG, Q., ZHOU, J.G. and LELKES, P.I., 2010b. Fabrication of interconnected microporous biomaterials with high hydroxyapatite nanoparticle loading. *Biofabrication*, 2(3), p.035006. Available at: http://dx.doi.org/10.1088/1758-5082/2/3/035006.

ZHANG, X., YANG, M., ZHAO, Y., ZHANG, S., DONG, X., LIU, X., WANG, D. and XU, D., 2004. Polypropylene/montmorillonite composites and their application in hybrid fiber preparation by melt-spinning. *Journal of Applied Polymer Science*, 92(1), pp.552-558. Available at: http://dx.doi.org/10.1002/app.20039.

ZHMAYEV, E., CHO, D. and JOO, Y.L., 2010. Nanofibers from gas-assisted polymer melt electrospinning. *Polymer*, 51(18), pp.4140-4144. Available at: http://dx.doi.org/10.1016/j.polymer.2010.06.058.

ZHONG, G., WANG, K., ZHANG, L., LI, Z.M., FONG, H. and ZHU, L., 2011. Nanodroplet formation and exclusive homogenously nucleated crystallization in confined electrospun immiscible polymer blend fibers of polystyrene and poly (ethylene oxide). *Polymer*, 52(24), pp.5397-5402. Available at: http://dx.doi.org/10.1016/j.polymer.2011.09.045.

ZHU, L. and GENG, X., 2002. Experimental investigation of polymer pellets melting mechanisms in corotating twin‐screw extrusion. *Advances in Polymer Technology: Journal of the Polymer Processing Institute*, 21(3), pp.188-200. Available at: http://dx.doi.org/10.1002/adv.10021.

ZUO, F., TAN, D.H., WANG, Z., JEUNG, S., MACOSKO, C.W. and BATES, F.S., 2013. Nanofibers from melt blown fiber-in-fiber polymer blends. *ACS Macro Letters*, 2(4), pp.301-305. Available at: http://dx.doi.org/10.1021/mz400053n.

Appendix: Publications and Conferences

Publications:

[1] **Yan X***, Cayla A, Devaux E, Salaün F. Microstructure Evolution of Immiscible PP-PVA Blends Tuned by Polymer Ratio and Silica Nanoparticles. *Polymers*. MDPI AG; 2018 Sep 17;10(9):1031. Available at: http://dx.doi.org/10.3390/polym10091031.

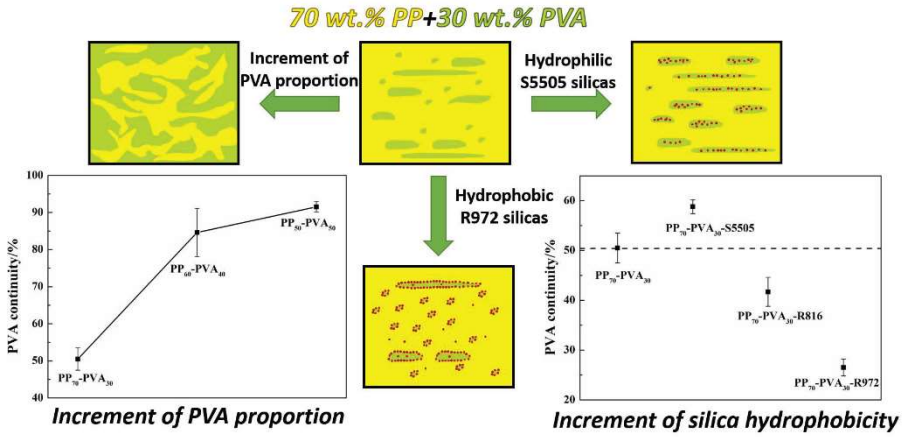

Graphic abstract

[2] **Yan X***, Cayla A, Devaux E, Otazaghine B, Salaün F. Polypropylene/Poly(vinyl alcohol) Blends Compatibilized with Kaolinite Janus Hybrid Particles and Their Transformation into Fibers. *Industrial & Engineering Chemistry Research*. American Chemical Society (ACS); 2019 Jun 4;58(25):10931–40. Available at: http://dx.doi.org/10.1021/acs.iecr.9b01990.

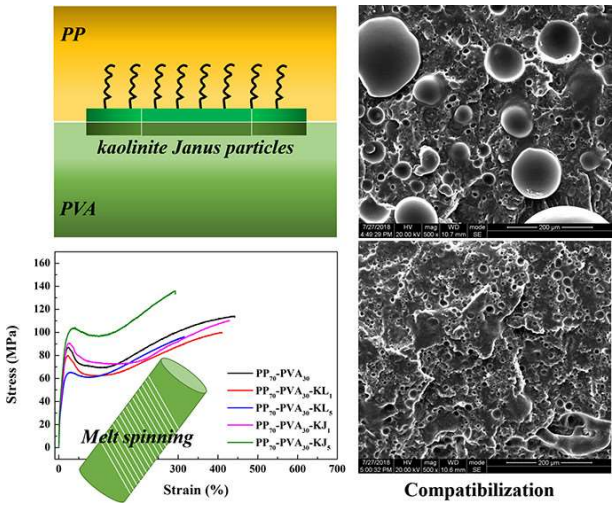

Graphic abstract

[3] **Yan X***, Cayla A, Salaün F, Devaux E, Liu P, Huang T. A green method to fabricate porous polypropylene fibers: development toward textile products and mechanical evaluation. *Textile Research Journal*. SAGE Publications; 2019 Aug 28. Available at: http://dx.doi.org/10.1177/0040517519871944.

[4] **Yan X***, Cayla A, Salaün F, Devaux E, Liu P, Mao J, Huang T. Porous fibers surface decorated with nanofillers: From melt-spun PP/PVA blend fibers with silica nanoparticles. *Journal of Applied Polymer Science*. Wiley; 2019 Sep 4;48470. Available at: http://dx.doi.org/10.1002/app.48470.

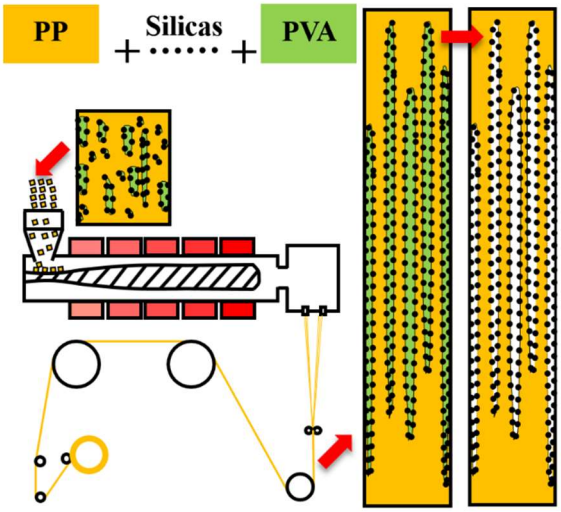

Graphic abstract

Conferences:

[1] 45ème Journées d'Etudes des Polymères JEPO'17. 1-6 Octobre 2017, Graveline, France. *(**Oral Presentation**: Design of biphasic PP/PVA fibres filled with silicas to obtain the surface modified fibres.)*

[2] Polymers: Design, Function and Application. 21-23 March 2018, Barcelona, Spain. *(**Poster**: Microstructure evolution of immiscible PP/PVA blends tuned by polymer ratio and silica nanoparticles.)*

[3] 19th World Textile Conference (AUTEX-Textile at the Crossroads). 11-15 June 2019, Ghent, Belgium. (***Oral Presentation*** *and* ***conference paper****: Fabrication of porous polypropylene fibers embedded with nanosilica based on immiscible polymers blend by melt spinning and selective extraction.*)

[4] 48th International Colloquium of GFP (Groupe Français d'études et d'applications des Polymères). 25-29 November 2019, Mulhouse, France. *(**Oral Presentation**:*

Fabrication of PP microfiber fabrics with potential surface functionality from melt-spun PP-PVA fibers.)

Abstract

The work aims to make the functional porous polypropylene (PP) fibers as well as PP microfibers, by the melt spinning of PP-poly(vinyl alcohol) (PVA) blends followed with the selective phase extraction of PVA. The objective is to first find out the optimal ratio of PP and PVA for fabrication of multifilament yarns by melt spinning, and to localize the filler at the biphasic interface. The fillers include not only the homogenously modified silica nanoparticles, but also the kaolinite Janus particles. The concomitant morphology evolution of the extrudates and fibers were observed. The work mainly discusses about the fabrication of porous fibers, but also makes an exploratory experiment to reverse the ratio to fabricate the microfibers. It was found that the ratio of two polymers as 70 wt.%/30 wt.% is an ideal formula for fabricating the porous fibers. Both of the two fillers are successfully tailored at the biphasic interface. The localization of silica nanoparticles within the biphasic can be fixed by the thermodynamic control, and one of the sorts has been dominantly localized at the biphasic interface. In addition, the Janus particles provide an alternative way to have the interface localization, which even helps the mechanical enhancement. The feasibility of microfiber production with the embedment of the fillers was also demonstrated.

Keywords: Biphasic; Polymeric fiber; melt-spinning; nanoparticles; interface.

Résumé

Le but de ce travail est de développer des filaments fonctionnels de polypropylène (PP) poreuses mais aussi des microfibres de PP par filage voie fondu de mélange de polymères immiscibles PP/Poly(vinyl-alcool) (PVA) après extraction sélective de la phase de PVA. Le premier objectif est de déterminer le ratio optimal entre le PP et le PVA afin d'obtenir la filabilité du mélange et de localiser les charges à l'interface du mélange biphasique. Les charges utilisées sont à la fois des nanoparticules de silices modifiées ainsi que des particules Janus à base de kaolinite, favorisant la localisation à l'interface. Les morphologies et les localisations des charges ont été analysées à la fois sur des joncs extrudés ainsi que sur des fibres. Le travail s'est concentré principalement sur des ratios de polymères permettant d'obtenir des fibres de PP poreuses, mais un travail exploratoire a permis de déterminer les conditions d'obtention de microfibres de PP. Le ratio PP/PVA avec 70 % de PP et 30 % de PVA en masse est la formulation idéale pour fabriquer ces fibres poreuses. La localisation des nanocharges de silice dans le mélange biphasique est principalement contrôlée par la thermodynamique du mélange, et en fonction des tensions de surface des nanosilices, la localisation à l'interface a pu être obtenue. De plus, les particules Janus permettent une voie alternative afin d'obtenir une localisation à l'interface, qui apportent un renforcement mécanique de la formulation. La faisabilité de la production de microfibres via l'inversion de phase PVA/PP avec l'ajout de nanocharges a été démontrée.

Mots clés: biphasique; fibre polymère; filage en voie fondue; nanoparticules; interface.